

**THE USE OF PATIENT-SPECIFIC PLURIPOTENT
STEM CELLS TO STUDY HUMAN NEURAL
DISEASE**

TAN, THONG TECK


(B.Sc. (Hons.), University of Queensland)

**A THESIS SUBMITTED
FOR THE DEGREE OF DOCTOR OF PHILOSOPHY
DEPARTMENT OF BIOCHEMISTRY
NATIONAL UNIVERSITY OF SINGAPORE
2014**

Declaration

I hereby declare that this thesis is my original work and it has been written by me in its entirety. I have duly acknowledged all the sources of information which have been used in the thesis.

This thesis has also not been submitted for any degree in any university previously.



Tan Thong Teck

29 Dec 2014

Acknowledgements

I would like to express my deepest gratitude to the many people who made this thesis possible: Dr. Alan Colman for his invaluable guidance, advice, support and his belief in me. His mentorship encouraged independence, creativity, and allowed me the freedom to grow and develop. Dr Sherry Wang Xueying and Dr Bruno Reversade who both played very big roles towards this thesis. Without their help, it would have been impossible. My thesis advisory committee, A/Prof Gavin Dawe and A/Prof Peter Droge for their helpful advice throughout this period. Dr Oz Pomp who has been extremely helpful to me and has assisted in all aspects of this work.

I would also like to thank my fellow lab-mates, past and present, for their assistance in my research work and for making this journey an enjoyable one, especially to members of AC and BR Labs.

I would like to thank the Institute of Medical Biology for providing the scholarship and environment to carry out my research work. I also thank NUS Department of Biochemistry for this opportunity to do a PhD.

I would also like to thank the examiners for going through the thesis and for their comments which has been very useful to me.

Lastly, I would like to thank my family for their support during this period.

Table of contents

Declaration page	ii
Acknowledgements	iii
Table of contents	iv
Summary	xii
List of Tables	xiii
List of Figures	xv
List of Abbreviations	xviii
Chapter 1: Introduction	
1.1 Rett Syndrome	
1.1.1 Introduction to Rett Syndrome	1
1.1.2 Stages of the disease and clinical manifestations	1
1.1.3 Brain pathology of RTT patients	3
1.1.4 RTT is caused by mutation in the <i>MeCP2</i> gene	3
1.1.5 <i>MeCP2</i> gene location and transcript variants	4
1.1.6 MeCP2 protein structure and function	5
1.1.7 <i>MeCP2</i> mutations	7
1.1.8 <i>MeCP2</i> mutations in males	8

1.1.9	Duplication of MeCP2	9
1.1.10	Knockout mouse models of RTT	10
1.1.11	Mutant mouse models of RTT	11
1.1.12	Rescue of mouse RTT models	13
1.2	Stem cells	
1.2.1	Introduction to human embryonic stem cells	16
1.2.2	The advent of induced pluripotent stem cells	19
1.2.3	The reprogramming process	14
1.2.4	Advantages of iPSCs	21
1.3	Neural cells	
1.3.1	Neural Stem Cells	22
1.3.2	Astrocytes	23
1.3.3	Microglia	24
 Chapter 2: Background and outline of thesis		
2.1	Background of thesis	26
2.2	Outline of thesis	27
 Chapter 3: Materials and Methods		
3.1	Cell culture medium	29
3.2	Cell culture	30
3.3	Teratoma formation	32
3.4	Karyotyping	33
3.5	Plasmids	33

3.6	Virus preparation	34
3.7	Immunocytochemistry	34
3.8	Flow cytometry	35
3.9	Live-cell flow cytometry	36
3.10	Luminex	36
3.11	Glucose uptake assay	36
3.12	Glutamate determination assay	37
3.13	WST-1 proliferation assay	37
3.14	TNFα detection assay	37
3.15	Phagocytosis assay	38
3.16	Migration assay	38
3.17	Synapse quantification	39
3.18	RNA isolation	39
3.19	Reverse transcription	39
3.20	Reverse Transcription-PCR (RT-PCR)	39
3.21	Quantitative RT-PCR (qRT-PCR)	41
3.22	Sequencing	43
3.23	Microarray experiments	43
3.24	Statistical Analysis	45
Chapter 4: Reprogramming of RTT patients' fibroblast		
4.1	Introduction	46
4.2	Hypotheses and Aims	47

4.3 Results	48
4.3.1 RTT patients' background	48
4.3.2 Reprogramming of fibroblast through retroviral induction	49
4.3.3 hTert can overcome skewing of reprogramming	51
4.3.4 Pluripotent marker expression and transgene silencing	53
4.3.5 <i>In vitro</i> differentiation of iPSCs	55
4.3.6 <i>In vivo</i> differentiation of iPSCs	58
4.3.7 Karyotypic analysis of iPSCs	60
4.3.8 Detection of MeCP2 in iPSCs	60
4.4 Discussion	62
4.4.1 The role of Tert in reprogramming	62
4.4.2 Characterisation of iPSCs	64
4.5 Conclusions	65
4.6 Limitations	65
4.6.1 Characterisation of more patients' iPSCs	65
4.6.2 Retroviral-based reprogrammning	65
4.6.3 MeCP2 expression in iPSCs	66
Chapter 5: Investigating the role of NPCs in RTT using iPSCs	
5.1. Introduction	67
5.2 Hypothesies and Aims	68
5.3 Results	69
5.3.1 Derivation of NPCs from iPSCs	69

5.3.2	Comparison of NPCs proliferation rate	73
5.3.3	iPSC-derived NPC showed defect in cell migration	73
5.3.4	Non-cell autonomous effect of NPCs	76
5.3.5	Gene expression array of NPCs	78
5.3.6	Neuronal differentiation of NPCs	81
5.4	Discussion	83
5.4.1	iPSCs from RTT patients can be induced into NPCs	83
5.4.2	MT NPCs showing migratory defects	83
5.4.3	Gene expression study revealed several genes differentially regulated in MT NPCs	86
5.4.4	MT neurons have reduced synapse numbers	88
5.5	Conclusions	88
5.6	Limitations	88
5.6.1	More patients' samples needed	88
5.6.2	Rescue of migration phenotype	89
5.6.3	Non-cell autonomous effect of NPCs	89
 Chapter 6: Investigating the role of astrocytes in RTT using iPSCs		
6.1	Introduction	91
6.2	Hypotheses and Aims	93
6.3	Results	94
6.3.1	Derivation of astrocyte from human iPSCs	94
6.3.2	Charaterisation of iPSCs-derived astrocytes	96

6.3.3	Proliferation and metabolic profile of astrocytes	98
6.3.4	Cytokine profiling of astrocytes	100
6.3.5	Gene expression array of astrocytes	105
6.4	Discussion	109
6.4.1	RTT patient's iPSCs can generate astrocytes	109
6.4.2	Use of iPSCs-derived astrocytes for cytokine profiling	110
6.4.3	MT astrocytes show abnormal cytokine profile	111
6.4.4	Gene expression study revealed several genes that are differentially regulated in MT astrocytes	113
6.4.5	MT astrocytes showed abnormalities in proliferation rate	115
6.4.6	Metabolic function of MT astrocytes is altered	116
6.4.7	The roles of astrocytes in neurological diseases	117
6.5	Conclusions	118
6.6	Limitations	118
6.6.1	More patients' samples needed	118
6.6.2	Primary cells as positive controls	119
6.6.3	Expression of meCP2 in iPSC-derived astrocytes	119
6.6.4	Quantification of glucose uptake	119
6.6.5	Identity of the derived cells	119
 Chapter 7: Investigating the role of microglia in RTT using iPSCs		
7.1	Introduction	120
7.2	Hypotheses and Aims	121

7.3	Results	122
7.3.1	Derivation of microglia from RTT patient's isogenic iPSCs	122
7.3.2	MT microglia display reduced motility	124
7.3.3	MT microglia are neurotoxic	126
7.3.4	Gene expression array of microglia	127
7.3.5	Comparison of gene expression of different cell types	131
7.4	Discussion	132
7.4.1	RTT patient's iPSCs can generate microglia	132
7.4.2	MT microglia show motility abnormality	133
7.4.3	Gene expression study revealed several genes differentially regulated in MT microglia	134
7.4.4	MT microglia induce neurotoxicity by an unknown mechanism	135
7.4.5	The role of microglia in neurological diseases	137
7.4.6	Different cell types derived from isogenic clones showed different changes in gene expression	138
7.5	Conclusions	139
7.6	Limitations	139
7.6.1	More patients' samples needed	140
7.6.2	Quantification of phagocytosis	139
7.6.3	Assessment of neurotoxicity	140
7.6.4	Expression of MeCP2 in iPSC-derived microglia	140
7.6.4	Primary cells as positive controls	140

Chapter 8: Conclusions and perspectives	
8.1 Introduction	142
8.2 The use of iPSCs to model RTT	143
8.3 Predictions in RTT patients based on <i>in vitro</i> observations	143
8.4 Future directions	146
8.4.1 The role of RTT astrocytes in BBB maintenance	146
8.4.2 Testing of the lactate shuttle hypothesis	148
8.4.3 Microglia transplantation as a therapeutic for RTT	148
8.4.4 Investigation of MeCP2 targets genes	149
8.4.5 Development of a stem-cell based high-throughput assay	149
8.5 Concluding remarks	150
References	151
Appendices	181

Summary

Rett Syndrome (RTT) is a neurodevelopmental disease affecting mainly females. Neurological diseases are traditionally hard to model in a human context due to inaccessibility of relevant cell types, but induced pluripotent stem cells (iPSCs) offers a viable route of access to neural cells from a human patient. In this thesis, I describe the modelling of RTT using iPSCs reprogrammed from RTT patients carrying mutations in the *Methyl CpG binding Protein 2 (MeCP2)* gene.

First, I derived isogenic wildtype (WT) and mutant (MT) iPSCs from RTT patients. With these isogenic iPSCs, I induced neural precursor cells (NPCs) and found that MT NPCs showed reduced migration compared to WT NPCs, indicating the possible involvement of NPCs in the disease. I also generated astrocytes from isogenic iPSCs and found abnormalities in the proliferation rate and cytokine secretions of MT astrocytes. Finally, I showed that microglia derived from MT iPSCs have reduced mobility and phagocytosis compared to WT microglia. As MeCP2 is a transcriptional regulator, gene expression analysis was carried out in the different cell types (i.e. NPCs, astrocytes and microglia) to determine possible target genes of MeCP2 in each cell type. This work provides evidence of NPCs and glia involvement in RTT and represents a promising tool for disease modelling.

List of Tables

Table 3.1 List of antibodies used in immunostaining	35
Table 3.2 List of primers for RT-PCR	41
Table 3.3 List of primers for qRT-PCR	42
Table 4.1 X-Chromosome status of iPSCs reprogrammed from RTT patients from various groups	64
Table 5.1 Top 15 differentially up regulated genes in MT iPSCs-derived NPCs based on fold change	79
Table 5.2 Top 15 differentially down regulated genes in MT iPSCs-derived NPCs based on fold change	80
Table 5.3 Comparison of microarray and real-time PCR fold changes of selected genes	81
Table 5.4 Top 5 GO terms under biological processes identified among differentially expressed genes based on p-value using DAVID	81
Table 6.1 List of cytokines used in this study	102
Table 6.2 Fold differences of cytokines at 24 hours between WT and MT astrocytes	103
Table 6.3 Fold differences of cytokines at 72 hours between WT and MT astrocytes	104
Table 6.4 Top 15 differentially up regulated genes in MT iPSCs-derived astrocyte based on fold change	106
Table 6.5 Top 15 differentially down regulated genes in MT iPSCs-derived astrocyte based on fold change	107
Table 6.6 Top 10 GO terms under biological processes identified among differentially expressed genes based on p-value using DAVID	108
Table 6.7 Comparison of astrocytes microarray and real-time PCR results of selected genes	108
Table 7.1 Top 15 differentially up regulated genes in MT iPSCs-derived microglia based on fold change	128

Table 7.2 Top 15 differentially down regulated genes in MT iPSCs-derived microglia based on fold change	129
Table 7.3 Top 15 pathways identified among differentially expressed genes based on p-value	130
Table 7.4 Top 15 biological process identified among differentially expressed genes based on p-value	130
Table 7.5 Comparison of microglia microarray and real-time PCR results of selected genes	131

List of Figures

Fig 1.1	Schematic representations of <i>MeCP2</i> transcript variants and respective protein isoforms	5
Fig 1.2	Schematic representation of the MeCP2 protein	7
Fig 1.3	Schematic of early mammalian development	17
Fig 1.4	Key milestones leading to reprogramming of human cells	19
Fig 1.5	Molecular changes during reprogramming	21
Fig 2.1	Graphical representation of project outline	28
Fig 3.1	Measurement of surface area	38
Fig 4.1	Reprogramming of fibroblast into iPSCs	50
Fig 4.2	Derivation of isogenic iPSCs from RTT patients' fibroblasts	52
Fig 4.3	RT-PCR characterisation of iPSCs	54
Fig 4.4	Characterisation of the iPSCs lines	55
Fig 4.5	<i>in vitro</i> differentiation of iPSCs lines	57
Fig 4.6	<i>in vivo</i> differentiation of iPSCs lines	59
Fig 4.7	Cytogenetics analysis of iPSCs lines	60
Fig 4.8	Expression of MeCP2 in PSCs	61
Fig 5.1	Derivation of NPCs from iPSCs	71
Fig 5.2	Characterisation of iPSCs-derived NPCs	72
Fig 5.3	Proliferation rate of WT and MT NPCs	73
Fig 5.4	Migration rate of NPCs	75
Fig 5.5	Coculture of WT and MT NPCs	77
Fig 5.6	Heat map cluster analysis of microarray	79
Fig 5.7	Real-time PCR validation of expression microarray	81

Fig 5.8	Differentiation of NPCs into neurons	82
Fig 5.9	Migration defects in <i>CDKL5</i> mouse model of RTT	86
Fig 5.10	Measurement of migration rate	90
Fig 6.1	Mouse model of RTT astrocytes	91
Fig 6.2	Derivation of astrocytes from iPSCs	95
Fig 6.3	Characterisation of iPSCs-derived astrocytes	97
Fig 6.4	Proliferation assay of astrocytes	98
Fig 6.5	FACS profile of 2-NBDG uptake by astrocytes	100
Fig 6.6	Cytokine profiling of WT and MT iPSCs-derived astrocyte at 24 hours	103
Fig 6.7	Cytokine profiling of WT and MT iPSCs-derived astrocyte at 72 hours	105
Fig 6.8	Heat map cluster analysis showing gene expression levels	106
Fig 6.9	Real-time PCR of selected genes	108
Fig 6.10	Proposed model of dysfunctional astrocytes on the BBB in the RTT brain	114
Fig 6.11	Proposed model of glucose uptake deficiency in RTT astrocytes	117
Fig 7.1	CM from <i>Mecp2</i> -null microglia are neurotoxic	120
Fig 7.2	Derivation and characterisation of iPSCs-derived microglia	123
Fig 7.3	MT microglia showed less phagocytosis of apoptotic bodies	124
Fig 7.4	MT microglia showed decreased motility	125
Fig 7.5	Co-culture of neurons with MT microglia causes neurotoxicity	127
Fig 7.6	Heat map cluster analysis of microarray	128
Fig 7.7	Real-time PCR of selected genes	131

Fig 7.8	Venn diagram show the number of common genes that are differentially expressed between WT and MT cells of the different cell types	132
Fig 7.9	Model of how RTT microglia could contribute to RTT	136
Fig 8.1	Proposed model for how astrocytes and microglia can contribute to the RTT pathology based on findings	145
Fig 8.2	Assays for measuring for BBB permeability	147
Fig 8.3	High-throughput compound screening using stem cells derivatives	150

List of Abbreviations

2NBDG	2-(<i>N</i> -(7-Nitrobenz-2-oxa-1,3-diazol-4-yl)Amino)-2-Deoxyglucose
BBB	Blood-Brain Barrier
BDNF	Brain Derived Neurotrophic Factor
CM	Conditioned Medium
CNS	Central Nervous System
DAVID	Database for Annotation, Visualization and Integrated Discovery
DEG	Differentially Regulated Genes
ESCs	Embryonic Stem Cells
GO	Gene Ontology
hESCs	human Embryonic Stem Cells
hTert	human Telomerase
ICM	Inner Cell Mass
iPSCs	induced Pluripotent Stem Cells
KO	Knock Out
MBD	Methyl-CpG Binding Domain
<i>MeCP2</i>	Human <i>Methyl-CpG binding protein 2</i> gene
MeCP2	Human Methyl-CpG binding protein 2 protein
<i>Mecp2</i>	Mouse <i>Methyl-CpG binding protein 2</i> gene
Mecp2	Mouse Methyl-CpG binding protein 2 protein
MET	Mesenchymal-Epithelial Transition
MT	Mutant
NPCs	Neural Precursor Cells

OSKM	Oct4, Sox2, Klf4, c-Myc
P48	Patient 48
P72	Patient 72
P80	Patient 80
PSCs	Pluripotent Stem Cells
RTT	Rett Syndrome
SCNT	Somatic Cell Nuclear Transfer
shRNA	small hairpin RNA
TRD	Transcriptional Repression Domain
WT	Wildtype
WST-1	Water soluble tetrazolium salt 1

Chapter 1: Introduction

1.1 Rett Syndrome

1.1.1 Introduction to Rett Syndrome

Rett Syndrome (RTT) is a neurological disorder that occurs almost exclusively in females with an incidence of 1 in 10 000 female live births (Chahrour and Zoghbi, 2007). It is one of the most common genetic causes of severe mental retardation in females. Patients with RTT have a seemingly normal post-natal developmental period after which symptoms start to appear in early childhood. These include cognitive impairment, loss of motor, language and social skills, microcephaly and stereotypic hand movements. It was this distinctive hand movement that led to an Austrian pediatrician, Dr Andreas Rett to first document this disorder in 1966. He had observed female patients with similar hand movements and clinical features in his clinic in Vienna and subsequently extended his observations to other parts of Europe. However, it was not until 1983, when a Swedish neurologist, Dr Bengt Hagberg published an article on RTT, that RTT gained widespread recognition in the medical community. The disease was termed “Rett Syndrome” to recognize and honour the work of Dr Andreas Rett.

1.1.2 Stages of the disease and clinical manifestations

The RTT infant from birth first appears healthy, has normal growth, and is able to achieve early developmental milestones. The course of the disease and severity of symptoms vary from patient to patient but in general, RTT can be divided into 4 stages. They are:

Early onset (6-18 months): Symptoms are usually subtle and the child has less eye contact and exhibits deceleration of head growth. Atypical socio-communicative function and speech-language development have also been detected in this early stage (Bartl-Pokorny et al., 2013; Marschik et al., 2013).

Rapid Regression (1-4 years): The patient loses purposeful hand skills and develops stereotypical hand movement such as wringing, washing, clapping or putting the hand to the mouth. General motor functions including walking are also affected (apraxia). The patient now fails to acquire new language skills and may lose previously acquired language skills. Mental retardation and autistic features become apparent now. The patient also has general growth retardation and weight loss (by age 2, most RTT patients are below the 5th percentile of the normal female population) (Percy and Lane, 2005).

Plateau (2-10 years): There is no further significance deterioration and there may be improvement in communication and social skills but most symptoms remain. Many patients remain in this stage for the majority of their lives.

Late Motor Deterioration (10 years onwards): The patient suffers gradual loss of mobility and appearance of parkinsonian features such as shaking and rigidity of movements (FitzGerald et al., 1990).

Some other features of RTT are microcephaly, breath holding, hyperventilation, seizures, teeth grinding (bruxism), curvature of the spine (scoliosis) and cold hands and feet (Chahrour and Zoghbi, 2007; Han et al., 2012; Percy and Lane, 2004). Life expectancy of RTT patients is not well studied but patients surviving into the early thirties have been recorded

(Halbach et al., 2013). There is currently no cure for RTT and most patients require full time care in all aspects of life.

1.1.3 Brain pathology of RTT patients

From post-mortem studies, brain weight of RTT patients was decreased by 12-34%, but not other major organs such as heart, liver, lungs and kidney based on height (Armstrong et al., 1999; Jellinger et al., 1988). Besides a decrease in brain weight, other neuropathological defects observed are reduced neuronal soma size, increased cell packing density (Bauman et al., 1995a, b), reduced dendritic arborisation and reduced dendritic spine numbers especially in the frontal, motor and temporal lobes (Armstrong et al., 1995; Belichenko et al., 1994; Chapleau et al., 2009; Kaufmann and Moser, 2000; Schule et al., 2008). It is generally accepted that there is no obvious neurodegeneration in the RTT brain (Armstrong, 2005).

1.1.4 RTT is caused by mutations in the *MeCP2* gene

As 99% of RTT cases are sporadic, it was difficult to identify the gene/genes responsible for the disorder. However, as RTT occurs mainly in females, it was likely that the gene/genes responsible are X-linked. Using this clue, exclusion mapping of rare familial cases of RTT led to the identification of chromosome region Xq28 to contain the “RTT gene” (Ellison et al., 1992; Sirianni et al., 1998). In 1999, systemic gene screening of this region of RTT patients led to the identification of *Methyl CpG binding protein 2 (MeCP2)* as the causative gene in the majority of RTT cases (Amir et al., 1999).

RTT is primarily caused by mutation in *MeCP2*, but mutations in *cyclin-dependent kinase-like 5 (CDKL5)* and *Forkhead box G1 (FOXP1)* can lead to

neurological symptoms that resemble RTT (Allou et al., 2012; Fehr et al., 2013; Kortum et al., 2011; Maortua et al., 2012). *CDKL5* is located on the X-chromosome and encodes for a serine/threonine kinase protein. One of its targets is MeCP2 though its other targets remain unknown (Bertani et al., 2006; Mari et al., 2005). *FOXG1* is located on 14q12 and encodes for a transcriptional repressor that is important in brain development.

1.1.5 *MeCP2* gene location and transcript variants

The *MeCP2* gene is located at chromosome Xq28. It is flanked by the *interleukin-1 receptor (IRAK1)* and a long-wavelength sensitive *opsin (OPN1LW)* gene which is transcribed in the opposite strand (Singh et al., 2008). *MeCP2* has four exons (exon 1-4) and is alternatively spliced to give two different protein isoforms, MeCP2_e1 and MeCP2_e2 (Kriaucionis and Bird, 2004; Mnatzakanian et al., 2004; Reichwald et al., 2000)(**Fig.1.1**). MeCP2_e1 is 498 amino acid long and is encoded by exons 1,3 and 4 while MeCP2_e2 is 486 amino acid long and encoded by exons 2, 3 and 4 (Kriaucionis and Bird, 2004; Mnatzakanian et al., 2004). In both mouse and human, MeCP2_e1 is the predominant isoform expressed in the post-natal brain (Dragich et al., 2007; Kriaucionis and Bird, 2004; Mnatzakanian et al., 2004; Yasui et al., 2014). It was also reported that *Mecp2_e2* has a later onset of expression than *Mecp2_e1* (Olson et al., 2014). *Mecp2_e1* showed uniform expression across the brain while *Mecp2_e2* has a more regional specific expression with a higher expression in olfactory bulb and cerebellum (Olson et al., 2014). *Mecp2_e1* is more efficiently translated than *Mecp2_e2* (Kriaucionis and Bird, 2004), and has greater stability in neurons (Yasui et al.,

2014). Loss of the *Mecp2_e1*, but not *Mecp2_e2* can lead to RTT symptoms in mice (Itoh et al., 2012; Yasui et al., 2014). In contrast, expression of either isoforms can lead to rescue of symptoms in RTT mouse model though *Mecp2_e1* has a better efficiency (Giacometti et al., 2007; Kerr et al., 2012; Luikenhuis et al., 2004). *Mecp2_e2* is however found to be crucial in placenta development and embryo survival (Itoh et al., 2012). In addition, *Mecp2_e2* is found to be upregulated in dying neurons and overexpression of the *Mecp2_2* can promote neuronal death and this can be inhibited by FoxG1 (Dastidar et al., 2012). Each isoform has its' distinct roles, but there is also partial overlapping functions (i.e *Mecp2_e2* can effect a rescue). So far, no MeCP2-e2 specific mutation has been reported in RTT.

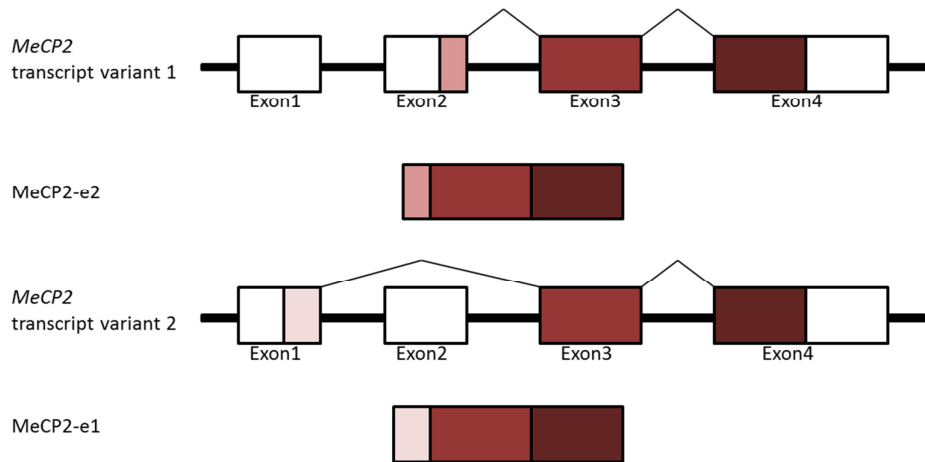


Fig 1.1 Schematic representations of *MeCP2* transcript variants and respective protein isoforms. *MeCP2* has 2 transcripts variants. Transcript variant 1, composed of exons 2, 3 and 4 is translated to give protein isoform MeCP2-e2 (486 aa). Transcript variant 2 is composed of exons 1, 3 and 4 and is translated to give protein isoform MeCP2-e1 (498 aa).

1.1.6 MeCP2 protein structure and functions

The MeCP2 protein was first discovered by Adrian Bird in 1992 as a 53KDa nuclear protein that could bind to methylated CpGs (Lewis et al., 1992). It

belongs to a family of DNA-binding proteins with the Methyl-CpG Binding Domain (MBD) sequence motif. In mammals, the 4 other members of the family are MBD1-4 and all members of the family are expressed ubiquitously (Hendrich and Tweedie, 2003). Incidentally, there is a MeCP1 but it is a complex consisting of multiple proteins rather than a single polypeptide and hence not part of the family (Cross et al., 1997; Feng and Zhang, 2001).

Structural analyses of MeCP2 based on trypsin digestion experiments indicate that it contains 6 biochemically distinct domains (Adams et al., 2007)(**Fig 1.2**). They are the N-terminal domain, the MBD, the inter-domain, the Transcriptional Repression Domain (TRD) and the C-terminal domain α and β (Adams et al., 2007). The 2 most well characterized domains are the MBD and the TRD. The MBD is described as the region that is sufficient to recognize and bind to methylated DNA although it can also bind to non-methylated DNA with a lower affinity (~3 fold lower)(Fraga et al., 2003; Nan et al., 1993). The MBD has been found to be able to bind to higher ordered DNA structures like un-methylated four-way DNA junction and heterochromatin (Galvao and Thomas, 2005; Nan et al., 1996) More recently, the MBD has also been shown to be able to bind specifically to 5-hydroxymethylcytosine, an oxidized form of 5-methylcytosine (Hashimoto et al., 2012; Mellen et al., 2012). The TRD is a segment found to be able to repress transcription through recruitment and interaction of a repressor complex involving histone deacetylase (HDAC) and the corepressor SIN3A (Jones et al., 1998; Nan et al., 1998). The TRD was also found to be able to bind to the NCoR/SMRT corepressors (Lyst et al., 2013). Besides transcriptional repression, the TRD (aa 195-329) has also been found to be able to bind to the YB1 protein which is involved in alternative

splicing (Young et al., 2005). The TRD also contains an AT-hook (regions of a protein that bind to AT-rich DNA) that is necessary for DNA binding and compaction of chromatin (Baker et al., 2013). The C-terminal domain is largely uncharacterized, but it is thought to promote the binding of MeCP2 to DNA and contains a WW domain that is predicted to mediate interactions with proteins (Buschdorf and Stratling, 2004; Chandler et al., 1999). While the functions of the other domains beside MBD and TRD are not established, mutations resulting in RTT have been found throughout the *MeCP2* gene indicating that every domain have important functions.

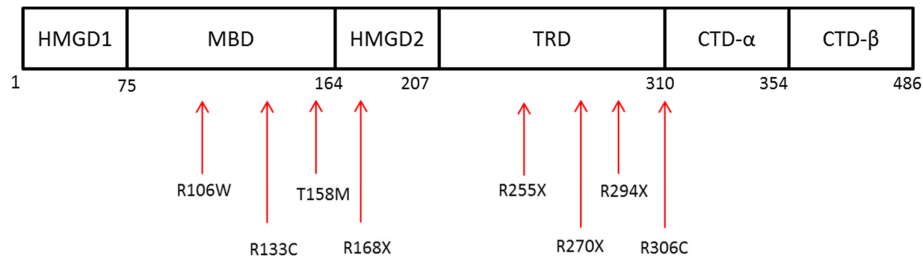


Fig 1.2 Schematic representation of the MeCP2 protein. MeCP2 can be divided into 6 domains, the HMGD1, MBD, HMGD2, TRD, CTD-α and CTD-β. Arrows depict relative position of the 8 most common mutations in RTT and they all are results of C>T substitutions (adapted from (Gonzales et al., 2012)).

1.1.7 *MeCP2* Mutations

Single C >T substitutions at one of a number of sites are the most common mutations reported (RettBASE: IRSF MECP2 Variation Database) (**Fig. 1.2**). RTT patients with multiple mutations in the *MeCP2* gene have been reported though multiple mutations are not reported to increase the severity of the symptoms (Chapleau et al., 2013). It is worth noting that not all individuals with a mutation in *MeCP2* will have a RTT phenotype, possibly due to non-

deleterious effect, X-inactivation status and/or modifier genes (Hoffbuhr et al., 2001; Takahashi et al., 2008). Interestingly, studies investigating the parental origin of *MeCP2* mutations in sporadic cases of RTT found that most de novo mutations of *MeCP2* occur on the paternally derived X-chromosome (71-96%) (Girard et al., 2001; Trappe et al., 2001; Zhang et al., 2012).

1.1.8 *MeCP2* mutations in males

Mutations in *MeCP2* in males usually results in 3 outcomes: prenatal or early infant mortality, males with neurological symptoms not classified as RTT and males with classic RTT.

Males surviving with *MeCP2* mutations but not classified as RTT cases have symptoms that range from severe neonatal encephalopathy to mild mental retardation (Moog et al., 2003; Villard, 2007). In familial cases of RTT, males who have identical *MeCP2* mutation as their RTT sister have severe encephalopathy and often die in the early years (Hoffbuhr et al., 2001; Villard et al., 2000).

In males with classic RTT, 2 unique genetic conditions can lead to male patients having a mixture of WT and MT cells akin to the female patient. Klinefelter Syndrome is a condition in which there is an extra copy of X chromosome (47, XXY). Random X-inactivation occurs such that only one copy of X chromosome is expressed in any one cell. If one of the X-chromosome carries a mutation in the *MeCP2* gene, the male subject can suffer from RTT. In another condition that can lead to RTT in males, diploid males (46, XY) have a normal *MeCP2* gene in some cells and a mutated

MeCP2 gene in other cells (Armstrong et al., 2001; Topcu et al., 2002). This is known as somatic mosaicism and is thought to occur early in development when a cell undergoes mutation in the *MeCP2* gene thus leading to subsequent daughter cells carrying the mutation. A small number of males with mutation in *MeCP2* but seemingly without Klinefelter or somatic mosaicism have also been reported to have symptoms similar to RTT (Dayer et al., 2007; Masuyama et al., 2005).

1.1.9 Duplication of MeCP2

MeCP2 duplication syndrome is a condition in which the patient has early infantile hypotonia, spasticity, developmental delays, mental retardation, dysmorphic features (brachycephaly, large ears and flat nasal bridge), autistic features, seizures and recurrent infection of the respiratory tract (del Gaudio et al., 2006; Friez et al., 2006; Van Esch et al., 2005). The cause of this condition is typically a duplication of the Xq28 region due to abnormal chromosomal duplication. In all cases reported, the duplicated region always contains the *MeCP2* gene, resulting in a gain of *MeCP2* dosage (Ramocki et al., 2010). The majority of *MeCP2* duplication syndrome cases identified are males who inherited the abnormal X-chromosome from their asymptomatic carrier mother. Females with *MeCP2* gene duplication are typically asymptomatic or have mild symptoms due to X-chromosome inactivation skewing towards the abnormal X chromosome (Ramocki et al., 2010; Van Esch, 2012). The effects of increased *MeCP2* dosage show that there need to be a balance of *MeCP2* in the body and have important implications in the treatment of diseases involving *MeCP2*.

1.1.10 Knockout mouse models of RTT

The earliest attempts to create a *Mecp2*-null mouse model from embryonic stem cells (ESC) failed due to embryonic lethality and suggested that *Mecp2* is essential for embryonic development. (Tate et al., 1996) This was disproven when two groups successfully generated *Mecp2*-null mouse models using Cre-Lox technology (Chen et al., 2001; Guy et al., 2001). Mice were first generated from ESC in which part of the *Mecp2* gene was flanked by lox-P sites (*Mecp2^{lox}*). These *Mecp2^{lox}* mice were then crossed with deleter mice in which Cre is expressed. Offsprings carrying both the Cre transgene and *Mecp2^{lox}* would thus have part of the *Mecp2* gene deleted resulting in inactivation of the *Mecp2* gene. The *Mecp2*-null mouse generated by the Bird lab has deletion of exon 3 and 4 while the one generated by the Jaenish Lab contains a deletion of exon 3. In both models, null offsprings (*Mecp2^{-/-}*) were viable and healthy during the first few weeks of life. Between 3-8 weeks, symptoms such as uncoordinated gait, trembling, reduced movement, respiratory problems, weight loss and hindlimb clasping start to show and these *Mecp2*-null mice died at 10-16 weeks. Brains of *Mecp2*-null mice were smaller than wildtypes with an increase in cell packing density and reduction in neuronal size (Chen et al., 2001). *Mecp2* heterozygous females mice (*Mecp2^{+/-}*) were born healthy and only a small percentage start to show any symptoms until a much later age of 3-4 months (Chen et al., 2001; Guy et al., 2001). Symptoms observed were weight gain, reduced activity and ataxic gait similar to those of *Mecp2*-null male mice but were generally milder, i.e they did not rapidly deteriorate and could live beyond a year and some did not show symptoms at all (Guy et al., 2001). For this reason, most mouse studies

of RTT are done using male mice although there have been an interest in the use of the female mouse model in recent years (Garg et al., 2013; Lang et al., 2014; Schaevitz et al., 2013).

1.1.11 Mutant mouse models of RTT

In addition to *Mecp2*-null mice models, mouse models with different *Mecp2* mutations have been generated. Here I will describe some of the mouse models.

T158A. This mutation reduces the binding of *Mecp2* to methylated DNA and decreases *Mecp2* stability (Goffin et al., 2012). Mice with this mutation had normal development in the first 4 weeks followed by hindlimb claspings, reduced weight from week 4, followed by weight gain to WT levels and seizures. Mutant mice also had reduced brain size, reduced locomotion, impaired motor functions, learning and memory deficits and a shortened lifespan of < 16 weeks (Goffin et al., 2012).

R168X. This mutation causes a premature truncation leaving only the MBD. Mice with this mutation showed hypoactivity, forelimb stereotypies, breathing irregularities, weight changes, hind limb atrophy, tremors, scoliosis and reduced lifespan of 12-14 weeks (Lawson-Yuen et al., 2007). Other phenotypes reported in these mice include decreased anxiety and impaired nest building (Wegener et al., 2014).

R270X. This mutation affects the binding of *Mecp2* to chromatin, resulting in a failure of *Mecp2* to maintain chromatin structure (Baker et al., 2013). Mice with this mutation develop normally till 4-6 weeks when symptoms start to

show. These symptoms include weight gain at week 7, tremor, gait abnormalities, motor dysfunction, smaller brain size, and a reduced lifespan of around 12 weeks (Baker et al., 2013).

R306C. This mutation abolishes the interaction between the TRD and the NCoR/SMRT (Lyst et al., 2013). These mice are normal for the first 6 weeks followed by symptoms such as hindlimb clasping, reduced locomotion, impaired motor functions, tremors and with a shortened lifespan of <20 weeks (Lyst et al., 2013).

Premature stop after codon 308. A stop codon was inserted after codon 308 leaving behind intact MBD and TRD but a truncated C-terminal in this mouse model (Shahbazian et al., 2002a). Mice with this mutation have normal development for the first 6 weeks, followed by progressive neurological symptoms such as tremors, motor impairments, hypoactivity, increased anxiety-related behavior, seizures, kyphosis and stereotypic forelimb motions. These mice had normal body and brain weight and were able to survive at least a year (Shahbazian et al., 2002a).

In general, these mouse models recapitulate the human RTT phenotype. For example, a post-natal and progressive onset of symptoms, motor dysfunctions, gait abnormality and cognitive deficits are similar symptoms of RTT patients. Forelimb stereotypies and hindlimb clasping seen in mouse models also mirrors the human RTT phenotype of hand stereotypies. *Mecp2*-null mice show early onset of symptoms (3-8 weeks), have severe phenotypes and have shortened lifespan (10-16 weeks). Mice with mutations affecting the MBD and TRD typically show onset of symptoms at (4-6 weeks), severe phenotypes and

lifespan of 12-20 weeks while C-terminal truncation mouse model show a later onset of symptoms after 6 weeks and can live up to a year. The type of mutations in mouse models also reflects the severity of RTT patients as patients with C-terminal truncations typically have a milder phenotype than those with mutations in the MBD and TRD (Bebbington et al., 2010).

Several other *Mecp2* mouse models have been generated and they include a transgenic mouse in which human *MeCP2* is overexpressed by ~ 2 fold (Collins et al., 2004), inactivation of *Mecp2* in specific cell types such as in neural lineages, GABAergic neurons and aminergic neurons (Chao et al., 2010; Chen et al., 2001; Samaco et al., 2009) or in specific brain regions such as in the hypothalamus and basolateral amygdala (Adachi et al., 2009; Fyffe et al., 2008). Most of these different animal models are reviewed in (Calfa et al., 2011). Later chapters will describe in details inactivation of mouse models of *Mecp2* inactivation in astrocyte and microglia.

1.1.12 Rescue of mouse RTT models

In 2007, it was shown that re-expression of *Mecp2* in symptomatic *Mecp2*-null mice led to phenotypic reversal (Guy et al., 2007). Knock-out mice were first made by silencing of *Mecp2* through insertion of lox-stop cassette in the endogenous *Mecp2* gene. These mice developed symptoms similar to *Mecp2*-null mice. Removal of the lox-stop cassette resulted in reactivation of endogenous *Mecp2* and in mice already showing severe symptoms, reactivation of *Mecp2* showed pronounced reversal of phenotype and enhanced lifespan. Importantly, this showed that absence of *Mecp2* did not

cause irreversible damage, in mice at least, and raised hope that human patients could one day have effective treatment.

Another rescue study was carried out by conditional re-activation of *Mecp2* in only the brain of *Mecp2*-null mice (Giacometti et al., 2007). This was performed through the use of specific promoters regulating the expression of Cre, which in turn facilitates the expression of *Mecp2* in an exogenous lox-stop cassette. In summary, the use of Nestin Cre (targets all neural cell) and Tau Cre (targets post-mitotic neurons) increased the lifespan of null mice from 10-12 weeks to > 8 months while C93 Cre and C159 Cre (both targeting mature neurons) increased lifespan by only 4 weeks. All rescued mice showed significantly increased nocturnal activity compared to *Mecp2*-null mice. These findings showed that restoration of *Mecp2* in the brain was enough to mediate a partial rescue.

To test the concept of gene therapy, the self-complementary adeno-associated virus, scAAV9, was used to deliver *Mecp2* cDNA into the *Mecp2*-null mice (Gadalla et al., 2013). Neonatal mice injected with the scAAV9/*Mecp2* virus showed slightly improved lifespan to 16 weeks and improved motor functions compared with control injected mice. In another study, scAAV9 was also used to deliver *Mecp2* cDNA with increased lifespan of >40weeks and improved overall health (Garg et al., 2013). Importantly, the authors also injected *Mecp2*^{+/-} female mice with the virus and found that scAAV9/*Mecp2* expressed *Mecp2* at levels close to physiological level. Female scAAV9/*Mecp2* injected mice showed improvement of symptoms such as motor functions and seizures and overall better health over their control injected counterparts although there

was no improvement in respiratory symptoms. This work is important clinically as the majority of human RTT patients are female and over-expression of MeCP2 will cause neurological symptoms.

Besides re-expression of MeCP2 to alleviate symptoms, another avenue of therapeutics is through drugs. A promising candidate is aminoglycosides which promotes read-through of premature stop codons, which affects 35 % of RTT patients (Percy et al., 2007). Several studies have found that aminoglycosides have effectiveness of 10-38% in promoting read-through of various MeCP2 premature stop codons (Brendel et al., 2011; Brendel et al., 2009; Popescu et al., 2010; Vecsler et al., 2011).

Brain Derived Neurotrophic Factor (BDNF) is a known MeCP2 target (Wang et al., 2006), but is poor at crossing the blood-brain barrier (BBB). Instead, drugs increasing the expression of BDNF such as cysteamine (increased vesicle secretion of BDNF) and 7,8-dihydroxyflavone (BDNF receptor activation) reportedly improved RTT symptoms in mouse model (Johnson et al., 2012; Roux et al., 2012). Insulin Growth Factor 1 (IGF1), which targets many similar pathways as BDNF, has been shown to be useful in relieving RTT symptoms in mice (Castro et al., 2014; Tropea et al., 2009) and in RTT-patient derived neurons (ref), and has been shown to improve anxiety and breathing abnormalities in RTT patients in a clinical trial (Khwaja et al., 2014).

Another approach is the use of drugs that target various neurotransmitters receptors. Benzodiazepine which enhances the effect of GABA could transiently reverse breathing abnormalities in mice (Voituron and Hilaire, 2011). Pentobarbital which inhibits GABA receptors could restore structural

defects and synaptic activity in *Mecp2*-deficient neurons (Ma et al., 2015). The ampakine CX546 which activates glutamatergic receptor could restore respiratory behavior in *Mecp2*-null mice (Ogier et al., 2007). L-Dopa which increases dopamine levels that targets the dopaminergic system improved motor deficits, tremors and respiratory phenotypes of *Mecp2*-null mice (Panayotis et al., 2011; Szczesna et al., 2014). Overall, these drugs are promising in overcoming defects in RTT.

1.2 Stem cells

1.2.1 Introduction to embryonic stem cells

In a broad sense, stem cells are unspecialized cells that can undergo self-renewal and have the ability to differentiate into specialized cell types. In mammals, development begins when the oocyte is fertilized by the sperm. This results in the formation of the initial diploid cell known as the zygote (**Fig 1.3**). The zygote subsequently undergoes cellular division to form a ball of dividing cells called the morula and later, a more specialized structure called the blastocyst. The blastocyst contains a group of cells called the inner cell mass (ICM) and as the blastocyst matures, the ICM forms into two cell layers, the hypoblast- which forms the yolk sac, and the epiblast which forms the three primordial germ layers (ectoderm, mesoderm and endoderm) from which all fetal cells are derived. It is from the ICM of the early blastocyst that embryonic stem cells (ESCs) are derived (**Fig 1.3**). The first successful attempt to isolate human embryonic stem cells (hESCs) from the inner cell mass was in 1994 (Bongso et al., 1994). These cells however could not be maintained in culture for long. In 1998, hESCs were successfully derived and maintained in culture leading to widespread interest in the field (Thomson et

al., 1998). hESCs are pluripotent stem cells (PSCs) meaning they can differentiate into the three germ layers from which all the cells in the human body derive. Because of this, hESCs are seen as an attractive source for obtaining cells that are difficult to access from the body such as brain or heart cells for studies in both development and diseases. Due to their malleability, hESCs represent a potential source of cellular material in the field of regenerative medicine such as replacing defective insulin-producing cells in diabetes or replacing degenerated dopaminergic neurons in Parkinson's disease. Despite their obvious potential in science and medical applications, the use of hESCs is opposed in some quarters. This is because generating hESCs lines requires the destruction of the blastocyst, which has the potential to become a human. Hence the use of hESCs has been shrouded in ethical controversy.

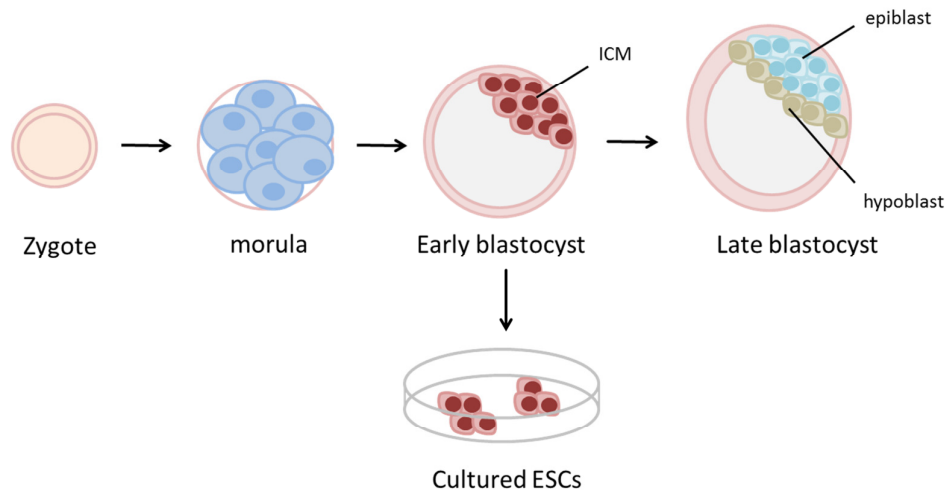


Fig 1.3 Schematic of early mammalian development. Fertilisation produces a zygote which undergoes cleavage division to form the morula. Further division of the morula forms the early blastocyst which contains the ICM. The ICM in the late blastocyst segregates into the epiblast and the hypoblast. ESCs are typically derived from the ICM of the early blastocyst.

1.2.2 The advent of induced pluripotent stem cells

It was long believed that differentiated cells could not change into another cell type nor revert to an undifferentiated state. This paradigm was challenged in 1962 when John Gurdon demonstrated that a frog's egg with its nucleus replaced by that of an intestinal epithelial cell could still fully develop into a tadpole (Gurdon, 1962) (**Fig 1.4A**). This method is known as somatic cell nuclear transfer (SCNT) and in principle, John Gurdon had shown that the nucleus of a differentiated cell retained the capacity of pluripotency. In 1997, the same principle was reenacted in mammals with "Dolly the sheep" (Wilmut et al., 1997). These experiments laid the belief that differentiated human cells too have the potential of pluripotency. In 2006, Kazutoshi Takahashi and Shinya Yamanaka reported that they had managed to coax mouse embryonic fibroblast into an undifferentiated state by viral transduction of a cocktail of transcription factors (Takahashi and Yamanaka, 2006). This technique was termed "reprogramming" and the resultant cells resembled ESCs in many ways including morphology, expression of ESC markers, and ability to form the three lineages. These ESC-like cells were called "induced pluripotent stem cells" (iPSCs). In 2007, the same experiments were successfully reproduced in human cells, thus generating the first human iPSC lines (Takahashi et al., 2007; Yu et al., 2007) (**Fig 1.4B**).

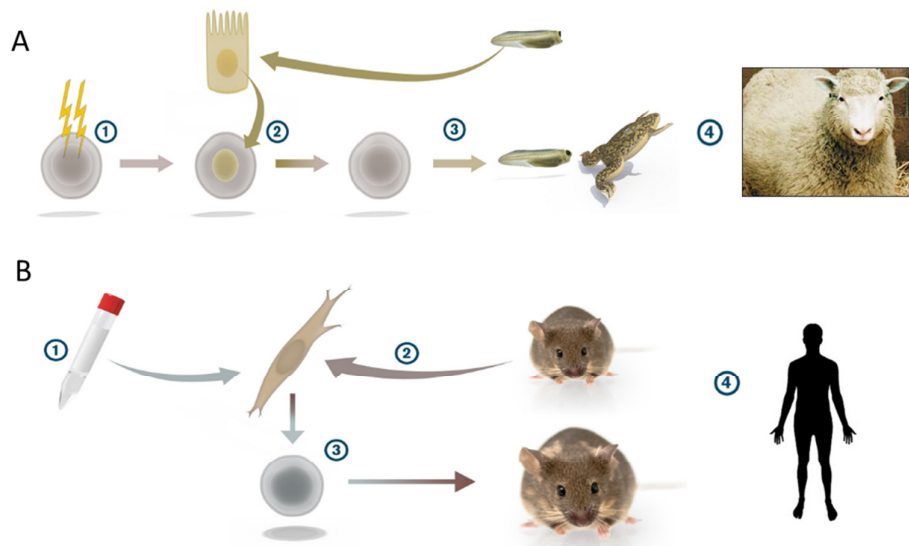


Fig 1.4 Key milestones leading to reprogramming of human cells. (A) SCNT experiments with animal models (1) UV was used to destroy the nucleus in a frog egg and (2) the nucleus of the egg was replaced with a nucleus from an epithelial cell of a tadpole. (3) The manipulated egg was able to develop into an adult frog. (4) SCNT was successfully carried out in mammals. (B) Reprogramming using transcription factors. (1) A set of transcription factors was introduced into (2) mouse fibroblast resulting in (3) pluripotent cells capable of contributing to chimeric mice. (4) Reprogramming was successfully carried out in human cells. Image adapted from (Jonas Frisen, 2012).

1.2.3 The reprogramming process

The initial experiments to generate iPSCs utilised 4 transcription factors. They are Oct4, Sox2, Klf4, c-Myc (OSKM) (Takahashi and Yamanaka, 2006). Oct4, Sox2 and Klf4 are highly expressed in ESCs and are involved in the regulation of other pluripotent and self-renewal genes (Boyer et al., 2005; Chew et al., 2005; Jiang et al., 2008; Rodda et al., 2005). c-Myc is a proto-oncogene best known to be involved in cell cycle regulation and proliferation of tumours but it also plays a role in the maintenance of ESCs (Cartwright et al., 2005; Varlakhanova et al., 2010). Of OSKM, Oct4, Sox2 and Klf4 represent critical

components of reprogramming while c-Myc has been shown to be dispensible (Nakagawa et al., 2008; Wernig et al., 2008b). The addition of c-Myc however served to enhance efficiency of the reprogramming process (Nakagawa et al., 2008; Wernig et al., 2008a).

The molecular mechanism of reprogramming remains to be understood but several studies have shed light as to the role of each factor during reprogramming. For a somatic cell to become an iPSC, it needs to undergo two main phases (**Fig 1.5**). The first is the Mesenchymal-Epithelial Transition (MET) (Sancho-Martinez and Izpisua Belmonte, 2013). For facilitation of MET, Oct4, Sox2 and c-Myc have been found to promote the epithelial state by downregulating mesenchymal genes and TGF-beta receptors (Li et al., 2010a). Klf4 activates epithelial genes including E-cadherin that gives the cell an epithelial identity (Li et al., 2010a). After the MET, the cell undergoes a second phase which is the establishment of the pluripotent circuitry. The individual role of OSKM in this second phase is less well understood but Oct4 and Sox2 target genes were found to be upregulated early in this phase before subsequent activation of target genes by Klf4 to complete the reprogramming process (Polo et al., 2012). c-Myc is not thought to play a major role in the second phase (Polo et al., 2012; Sridharan et al., 2009). However, the role of each factor is highly dependent on context as sequential addition of the factors in the order of OK+M+S instead of simultaneous OSKM addition was found to result in a different gene expression profile, and also resulted in a higher reprogramming efficiency (Liu et al., 2013). Several other changes occur during reprogramming including microRNA expression and chromatin

modifications and these have been reviewed in several articles (Adachi and Scholer, 2012; Apostolou and Hochedlinger, 2013; Liang and Zhang, 2013).

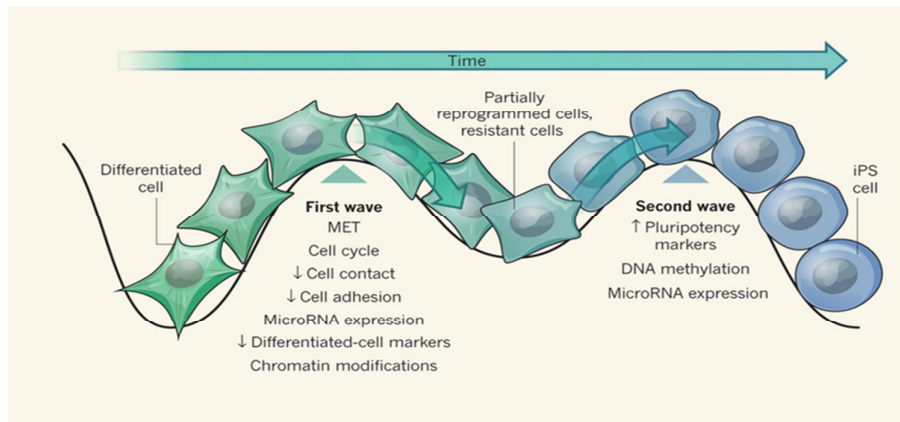


Fig 1.5 Molecular changes during reprogramming. Reprogramming of somatic cells into iPSCs entails two main “waves”. The first wave is the MET which gives the cell an epithelial identity. The second wave establishes pluripotent genes expression and gives the cell an ESC-like identity. Image reproduced with permission from (Sancho-Martinez and Izpisua Belmonte, 2013).

1.2.4 Advantages of iPSCs

Like hESCs, iPSCs have the ability to self-renew and differentiate into the 3 lineages. However, there are many key advantages to using iPSCs over hESCs. First, as iPSCs do not involve the destruction of the blastocyst, there are no ethical issues to overcome. Second, iPSCs derived from patients suffering from a genetic disorder provide a direct disease-related and genetically relevant source of material for research and clinical applications. Third, for regenerative medicine, iPSCs derived from individuals would possibly have a lesser chance of immuno-incompatibility when cells are transplanted into the same individual. While cellular transplantation using hiPSCs derived material still has to overcome many significant challenges (i.e. safety and efficacy) to be of practical use, an obvious impact of iPSCs has been disease modeling.

Like hESCs, iPSCs allows an indirect access to specific cell types like brain or heart cells that have traditionally been difficult to obtain. Using iPSCs, we can now generate cellular models to study genetic diseases with specific human cell types. The attractiveness is apparent and is evident by the large numbers of studies that has generated and studied disease-bearing iPSCs lines (Onder and Daley, 2012; Rajamohan et al., 2012).

1.3 Neural cells

This section gives an introduction to the main cell types investigated in this thesis.

1.3.1 Neural stem cells

The central nervous system originates from the neural plate and neural tube. Both the neural plate and neural tube are composed of neuroepithelial cells that can undergo symmetrical division. These neuroepithelial cells are the first neural stem cells in the developing embryo and are the precursors to the neurons, astrocytes and oligodendrocytes. Besides the developing brain, neural stem cells have also been demonstrated to be present in discrete regions of the mammalian adult brain, including human (Eriksson et al., 1998; Song et al., 2002; van Praag et al., 2002). Neural stem cells from humans can be isolated from post-mortem fetal brain tissue or adult brain tissue but these sources are limited by availability of donor material (Park et al., 2012; Uchida et al., 2000; van Strien et al., 2014). Alternatively, iPSCs represent a useful source for NPC. In line with most publications, the term NPC is used here to refer to a heterogeneous population comprising of neural stem cells and progenitor cells that can be derived from PSC (Reubinoff et al., 2001; Zhang et al., 2001).

1.3.2 Astrocytes

Astrocytes are the most common glia in the CNS and derive from the neural stem cells of the neuroepithelia. Astrocytes perform a wide range of functions. One function of astrocyte is their ability to regulate neurotransmitter homeostasis in the brain. For example, glutamate is released during neuronal transmission as an excitatory neurotransmitter. However, excess glutamate is neurotoxic and astrocytes perform an important role in taking up excess glutamate to prevent neurotoxicity (Schousboe and Waagepetersen, 2005).

Astrocytes are essential for the formation and maintenance of the Blood-Brain barrier (BBB). The BBB is a tightly regulated interface between the CNS and the vascular system that controls the movement of nutrients, ions, hormones and cells into the CNS. Astrocytes together with pericytes and endothelial cells are the 3 cell types that make up the BBB. Astrocytic endfeet are in close contact with endothelial cells and pericytes in the CNS and is thought to almost completely cover the whole blood vessel structure (Mathiisen et al., 2010). Besides forming a physical barrier, astrocytes secrete ECM proteins that serves as attachment factors and signalling components of the BBB. The ECM also make up the basement membrane which forms additional physical barrier and provide physical support for the different cells types (Baeten and Akassoglou, 2011). BBB dysfunction has been associated with many pathological symptoms such as stroke, multiple sclerosis, Alzheimer's disease and Parkinson's (Abbott et al., 2006; Cabezas et al., 2014; Desai et al., 2007).

Astrocytes are known to secrete a variety of cytokines that are related to inflammatory functions. For example, CXCL1, CXCL8 and CXCL10, which

regulate neutrophils and T cells recruitment in the CNS, are induced in astrocytes upon viral infection (Kutsch et al., 2000; Rubio and Sanz-Rodriguez, 2007). Abnormal cytokine levels secreted by astrocytes such as TNF- α could also be a cause of neurodegeneration in Parkinson disease (Hirsch et al., 2003).

Another important astrocyte function is supplying metabolic precursors to the neurons. Accumulating evidence shows that astrocytes release of lactate that is taken up by neurons as a metabolic substrate in times of neuronal activity (Brown and Ransom, 2007; Escartin et al., 2006; Figley, 2011). Disruption of the astrocyte-neuron lactate transport resulted in learning and long-term memory deficits in mice highlighting its importance in cognitive functions (Suzuki et al., 2011).

These examples highlight the importance of astrocytes in brain homeostasis and development. Understanding astrocyte's functions and roles in pathology may lead to prospective therapies in neurological diseases .

1.3.3 Microglia

Microglia are the innate immune cells of the CNS and play important roles in inflammation in response to pathogens and injuries (Streit, 1996). The brain has however harnessed these professional phagocytes for additional purposes— neuronal development and plasticity. For instance, microglia regulate synapse numbers by engulfing immature or weak synapses in a process called synaptic pruning (Paolicelli et al., 2011; Schafer et al., 2012). Removal of these unwanted synapses is important for brain maturation (Paolicelli et al., 2011), and reduced synaptic pruning can result in impaired

social behavior and repetitive behavior in mice (Zhan et al., 2014), much like some of the symptoms of RTT. Microglia also play an important role in clearing away apoptotic cells in the brain by phagocytosis (Ashwell, 1990; Marin-Teva et al., 2004), and this was shown to facilitate neurogenesis in the adult brain (Sierra et al., 2010). In addition, microglia can also secrete cytokines that regulate neurogenesis (Battista et al., 2006{Walton, 2006 #2340). The discovery of microglia's role beyond immunity revealed important ways in which neuronal development and plasticity are regulated. These findings unmask microglia as important contributors to brain pathologies.

Chapter 2: Background and outline of thesis

2.1 Background of thesis

RTT animal models, especially the mouse, have contributed greatly to our knowledge of RTT. However, crucial inter-species differences exist between mice and humans. For instance, heterozygous female *Mecp2*^{+/-} show either no or very mild symptoms (Guy et al., 2001). As such, the male *Mecp2*^{-/y} mouse which shows more severe symptoms is typically used to model RTT despite the disease primarily affecting females in humans. This indicates that findings from mice might not always be translatable to humans. Hence, it is important to reconcile findings from mice model with human based model. It is however not feasible to isolate brain cells from humans, especially from that of an RTT patient. The use of iPSCs is therefore a viable alternative of studying RTT in a human context. My main hypothesis is that human iPSCs can be used to model RTT. To test this hypothesis, I decided to generate iPSCs from patients carrying MeCP2 mutations. Shortly after commencing on the project, several publications reported the modelling of RTT using RTT patients' iPSCs (Ananiev et al., 2011; Cheung et al., 2012; Kim et al., 2011; Marchetto et al., 2011). These studies reported that iPSCs have been generated from RTT patients carrying *MeCP2* mutations and showed that neurons generated from RTT iPSCs display diseased phenotypes such as reduced synapse number and reduced dendrite development (Marchetto et al., 2011). As the mutations I was studying is similar to what has been published (Marchetto et al., 2011), I decided to look into how iPSCs can be used to model other aspects of the disease to complement the existing literature. One area lacking detailed studies

is the role of non-neuronal cells such as the NPCs, astrocytes and microglia in the pathology of RTT. Recent findings from RTT mouse models indicated that other brain cell types might play a role in the disease (Ballas et al., 2009; Maezawa and Jin, 2010; Maezawa et al., 2009; Nguyen et al., 2013). I hypothesize that non-neuronal cells might play a role in the pathology of the RTT in humans. *In vitro* differentiation of glia from RTT patients' iPSCs would allow a system to study the role of glia in the pathology of the disease. Hence I decided to look further into the roles of NPCs, astrocytes and microglia in the pathology of RTT. More specific hypotheses and aims are described in the relevant chapters.

2.2 Outline of thesis

For my project, I aimed to model the role of NPCs, astrocytes and microglia by inducing iPSCs from RTT patients and differentiating these cells into the respective cell types. In the first part of my thesis (Chapter 4), I reprogrammed and characterized isogenic iPSCs from RTT patients carrying *MeCP2*. Chapter 5 describes the induction of NPCs from isogenic iPSCs. The differentiation of neurons from the NPCs is also detailed here. In Chapter 6, I describe the generation of astrocytes from isogenic iPSCs-derived NPCs. The differentiation of microglia from iPSCs is described in chapter 7. With each cell type, comprehensive characterization was carried out to confirm their identity. Phenotypic comparisons were then carried out to identify differences between isogenic WT and MT cells, the results of which are detailed in the respective chapters. The graphical outline of this project is shown in **Fig 2.1**. Chapter 8 summarises the project and includes recommended future directions.

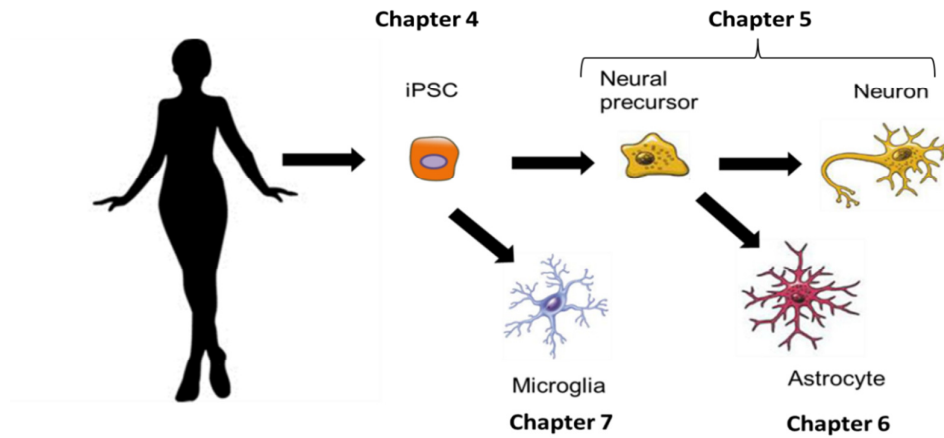


Fig 2.1 Graphical representation of project outline. Fibroblasts are reprogrammed into isogenic iPSCs and subsequently differentiated into several brain cell types. Chapter 4 describes the generation of iPSCs, Chapter 5 describes the differentiation of NPCs and neurons, Chapter 6 describes the work done on astrocytes and Chapter 7 describes the work done on microglia.

Chapter 3: Materials and Methods

3.1 Cell culture medium

Fibroblast medium

DMEM supplemented with 10% FBS, 2mM L-glutamine and 1% Penicillin/Streptomycin (all from Gibco, Life Technologies)

iPSCs medium

KO-DMEM supplemented with 20% KOSR, 2mM L-glutamine, 0.2mM NEAA, 0.1mM 2-mercaptoethanol and 5ng/ml basic Fibroblast Growth Factor (bFGF)

Neural Induction Medium

DMEM/F12 supplemented with 20% KOSR, 2mM L-glutamine, 0.2mM NEAA, 0.1mM 2-mercaptoethanol and 1mM Sodium Pyruvate.

NPCs medium

Neurobasal medium supplemented with 2mM L-glutamine, 1% B27, 1% N2 and 20ng/ml bFGF.

Neural differentiation medium

Neurobasal medium supplemented with 2mM L-glutamine, 1% B27, 1% N2 and 20ng/ml bFGF.

3.2 Cell culture

MEF

Mouse embryonic fibroblast (MEF) were plated onto gelatin coated plate and maintained in fibroblast medium. Cultures were passaged using trypsin at a ratio of 1:4-1:6 to passage 4 after which gamma irradiation was performed at 2000 rad. The inactivated MEF were then cryopreserved. For use as feeder layers, inactivated MEF were plated on gelatin coated dish at a density of 25000cells/cm².

Patients' Fibroblast

RTT patients' fibroblasts were procured from Coriell Cell Repository. Cells were passaged using trypsin at a ratio of 1:2-1:5 and maintained in fibroblast medium.

HEK293T

HEK293T cells were maintained in Fibroblast medium at a density of 5 x 10⁴ cells/cm².

iPSCs and ESCs

iPSCs and ESCs cell lines were all maintained on inactivated MEF in iPSC medium. Medium change was performed every day and cultures were passaged manually at a ratio of 1:6-1:9 every 5-7 days.

Reprogramming of fibroblast

Patient's fibroblasts were plated at a density of 100 000 cells/well of a 6cm plate in fibroblast medium. 24hrs later, reprogramming viruses were added to cells. 48hrs later, fibroblast was trypsinised and plated onto a 100mm plate of MEF in fibroblast medium at a density of 100000 cells/plate. 48hrs later medium was changed to iPSCs medium. Colonies will appear 2 weeks later and were manually isolated for plating onto MEF feeder for maintenance under iPSCs conditions.

***In vitro* embryoid body differentiation**

iPSCs were manually cut out from feeder layer and transferred to low attachment plate in iPSCs medium without bFGF for formation of embryoid bodies. After 2 weeks, EBs were attached on TC plate and cultured further for another 2-4 weeks.

Generation of NPCs from PSCs

iPSCs were manually cut out from feeder layer and dissociated into single cells by accutase. 10 000 cells were plated into one well of a 96-well round bottom low attachment plate in Neural induction medium (NIM) for formation of neurospheres. After 24 hours, cells aggregate into a sphere. ½ vol medium change was performed every 3 days and cells were left in the plate for a total of 7 days. Neurospheres were then attached onto laminin coated plates in NPC medium. Rosettes will be visible in 7-14 days and rosettes are manually cut out and expanded in suspension in low attachment plates. Henceforth they are

known as NPC and maintained in NPC medium with medium change once every 3 days.

Generation of neurons from NPC

NPC were dissociated into single cells and plated onto laminin coated plate at a density of 100000 cells/cm² in NPC medium without bFGF for a period of 2-6 weeks. Medium was changed once every 3 days.

Generation of astrocytes from NPC

NPC were dissociated into single cells and plated onto laminin coated plate at a density of 100000 cells/cm² in NPC medium without bFGF. Cells were passaged and replated every 2 weeks for a period of 90 days. Neurons were gently removed by pipetting.

Generation of microglia from PSC

At the time of writing, the method used for deriving microglia is patent pending.

3.3 Teratoma formation

iPSCs were dissociated into single cells by accutase and cells were harvested and counted. 3 million cells (resuspended in PBS) were injected intramuscularly into one thigh of a 6 week old SCID mice. Teratoma growth was observed every week for up to 12 weeks. Teratoma was harvested between 8-12 weeks by dissection, fixed in formalin and sent for histological processing by a pathology service.

3.4 Karyotyping

Colcemid was added to actively proliferating cells overnight before sending samples for karyotyping analysis. Standard G-banding chromosome analysis was carried out in the Cytogenetics Lab at KK Women's and Children's Hospital of Singapore.

3.5 Plasmids

Reprogramming retrovirus plasmids: pMXs-hOCT3/4 (Addgene #17217), pMXs-hSOX2 (Addgene #17218), pMXs-hKLF4 (Addgene #17219), pMXs-hc-MYC (Addgene #17220), pBABE-neo-hTert (Addgene #1774).

Packaging plasmids for lentivirus: pMDLg/pRRE (Addgene #12251), pRSV-Rev (Addgene # 12253), pMD2.G (Addgene #12259).

A shRNA sequence against MeCP2 was cloned into the pLL 3.7 lentilox vector (Addgene #11795) to form the hairpin loop (5'-GGAGGTCTTCTATCCGATCTGTTCAAGAGTCCAGATCGGATAGAAGACCTCC-3') (Marchetto et al., 2010). Underlined region indicates loop.

A control shRNA sequence against LacZ was cloned into the pLL 3.7 lentilox vector to form the hairpin loop (5'-TGTGGATGGAGCCGATATTGGATTCAAGAGATCCAATATCGGCTCCATCCACT-3'). Underlined region indicates loop.

3.6 Virus preparation

HEK293T cells were seeded at 4.5×10^6 cells/ 100mm plate. 24hrs later, cell density should be at 90-95%. Plasmid and packaging vectors were transfected into HEK293T cells using lipofectamine 2000 (Invitrogen) according to manufacturer's instruction. 48 hours later, medium was collected from plates and spun at 2000rpm for 5min. Supernatant was collected and spun in an ultracentrifuge at 25000rpm for 2 hrs at 8°C. Virus pellets were resuspended in DMEM and frozen into aliquots at -80°C.

3.7 Immunocytochemistry

Cells were fixed in 4% paraformaldehyde for 20 mins. Permeabilisation and blocking was done in blocking buffer consisting of 0.1% Triton-X 100, 4% goat or donkey serum diluted in PBS for 30 min. Primary antibodies were diluted in blocking buffer and incubated overnight at 4°C. Secondary antibodies were diluted in blocking buffer at 1:1000 and incubated for 30 mins at room temperature. The list of primary antibody and dilution is provided in table 3.1

Table 3.1 List of antibodies used in immunostaining

Antibody	Provider and Cat #	Host	Dilution
OCT 3/4	Santa Cruz SC-5279	Mouse	1:200
SOX2	R&D MAB2018	Mouse	1:200
NANOG	R&D AF1997	Goat	1:50
TRA 1-60	Chemicon MAB4360	Mouse	1:100
Alpha Feto Protein	Sigma A8452	mouse	1:1000
Smooth muscle actin	Thermo MS113P	Mouse	1:1000
Vimentin	Chemicon AB5733	Chicken	1:1000
Desmin	Dako M0760	Mouse	1:100
anti-NESTIN	BD 611659	Mouse	1:200
VGUT1	Synaptic Systems 135302	Rabbit	1:1000
MAP2	Synaptic Systems 188004	Guinea Pig	1:1500
β III-TUB	Covance MMS-435P	Mouse	1:3000
GFAP	Dako Z0334	Rabbit	1:1500
S100 β	Sigma S-2532	Mouse	1:1500
MECP2 N-terminal	Sigma HPA000593-100	Rabbit	1:1000
MECP2 C-terminal	Sigma M6818-200	Mouse	1:800

3.8 Flow cytometry

Cells were dissociated into single cells by accutase and fixed using Cytofix/cytoperm reagent (BD Bioscience) for 20mins on ice. Fixed cells were washed with PBS and blocked with 4% goat serum for 20mins on ice. Incubation with primary antibody was carried out for 40mins on ice. Cells were washed 3x with 0.1% PBST before incubation with secondary antibody for 30mins on ice. Cells were washed 3x with 0.1% PBST and resuspended in PBS + 1% goat serum. Samples were ran through a FACScalibur and quantitated using Cellquest Pro software. Normalisation was done using an isotype control or no primary antibody control. Nestin antibody (BD #61159) was used at a dilution of 1:400 and GFAP antibody (Dako #Z0334) was used at a dilution of 1: 2000.

3.9 Live-cell flow cytometry sorting

Cells were dissociated into single cells by accutase and washed twice with PBS and blocked with 1% BSA for 20 mins on ice. Incubation with primary antibody was carried out for 20mins on ice. Cells were washed 2x with PBS before incubation with secondary antibody for 20mins on ice. Cells were washed 2x with PBS and resuspended in PBS + 1% BSA and sent for live cell sorting. Live cell sorting was carried out at the Singapore Immunology Network Flow Cytometry facility.

3.10 Luminex

For collection of conditioned medium, NPC were plated at a density of cells/cm² and astrocytes were plated at a density of 10000 cells/cm². Conditioned medium (CM) was collected at 24 hours and 72 hours. Luminex was carried out at the Singapore Immunology Network Luminex facility.

3.11 Glucose uptake assay

Cells were plated at 8000 cells/cm² overnight. The next day, cells were incubated with low glucose DMEM for 6hrs. Medium was removed and fresh low glucose DMEM with 100µM 2-(N-(7-Nitrobenz-2-oxa-1,3-diazol-4-yl)Amino)-2-Deoxyglucose (2NBDG) (Invitrogen) was added to cells and incubated for the respective time. Medium was removed and cells were detached into single cells for flow cytometry.

3.12 Glutamate determination assay

Glutamate determination assay was carried out using a Glutamate assay kit (Biovision #K629-100) according to manufacturer's instruction. Briefly, 100 000 cells were plated overnight and fresh medium with 100 μ M of L-Glutamic acid was added. CM was collected at the respective times and centrifuged at 2000rpm for 5mins. Supernatant was collected and 50 μ L of sample was added to 1 well of reaction mix and incubated for 30 min at 37°C. Optical density was measured at 450nm in a microplate reader. Readings from triplicate wells were taken and averaged.

3.13 WST-1 Proliferation assay

Cell proliferation assay was carried out using the cell proliferation reagent water soluble tetrazolium salt 1 (WST-1) (Roche #05015944001) according to the manufacturer's instruction. Briefly 2000 cells/ well were plated into a 96 well plate. 10 μ L/well of WST-1 reagent was added and incubated for 0.5 hr in an incubator. Absorbance was measured using a plate reader at 480nm. Readings from triplicate wells were taken and averaged.

3.14 TNF α detection assay

100 000 cells were incubated in one well of a 12 well plate for 24 hours. CM was collected and TNF α detection was carried out using the Human TNF α ELISA Kit (Thermo Scientific #EH3TNFA2) according to manufacturer's instructions. Absorbance was measured using a plate-reader (SpectraMax M5, Molecular Devices). Readings from triplicate wells were taken and averaged.

3.15 Phagocytosis assay

NPCs were dissociated into single cells and stained with 5 μ L/mL of 5-Carboxytetramethylrhodamine (5-TAMRA) (Life Technologies #C-6121) for 5 minutes. Stained NPCs were then treated with ultraviolet light in a laminar flow hood for 15 min and washed with PBS (through centrifugation) before incubation with microglia for 5 hours.

3.16 Migration assay

NPCs were dissociated into single cells by accutase and 8000 cells were plated into one well of a 96-well low-attachment plate for formation of a neurosphere. 24 hours later, single neurospheres were plated into one well of a 24-well plate coated with laminin. 24 hours later, cells were fixed and stained with nestin antibody. To quantify surface area, images were taken with a fluorescent microscope (**Fig 3.1A**) and converted to an 8-bit image (**Fig 3.1B**) using the Image J software. Using the “Analyse particles” function in Image J, the total surface area of all stained object was directly measured (**Fig 3.1C**).

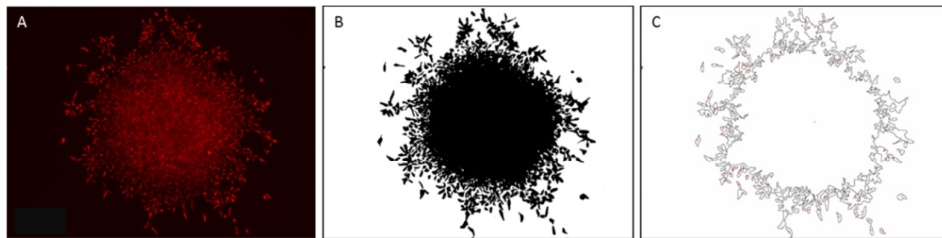


Figure 3.1 Measurement of surface area. Fluorescent image of neurosphere (**A**) is converted into an 8-bit image (**B**) using Image J. The surface area is determined using the “Analyse Particles” function in Image J (**C**).

3.17 Synapse quantification

Neurons were plated at a density of 2000 cells/cm² onto laminin coated glass cover-slips. 6-8 weeks later, neurons were fixed and stained with VGlut1, PSD95 and Map2 antibodies. Images of neurons were taken with a confocal microscope and numbers of synapse were manually counted.

3.18 RNA isolation

Medium was aspirated and cells were washed twice with PBS before addition of lysis buffer. RNA was extracted with RNeasy Mini Kit (Qiagen), according to the manufacturer's instructions. DNase I (Qiagen) was used for all extraction to minimize genomic DNA contamination. RNA quality and quantity was measured using a spectrophotometer (Nanodrop, Thermo Scientific). Only samples with an A260/A280 absorbance ratio greater than 1.9 were analyzed.

3.19 Reverse transcription

1µg of RNA was reverse transcribed to complementary DNA (cDNA) using the iScript Reverse Transcription Supermix (BioRad #170-8840) according to the manufacturer's instructions to a volume of 20µL. Master mixes were prepared for multiple reactions and incubations were carried out on a thermal cycler (Mastercycler, Eppendorf).

3.20 Reverse Transcription-PCR (RT-PCR)

RT-PCR was carried out using Platinum PCR Supermix (Invitrogen) according to the manufacturer's instructions. 2µL of cDNA and 200nM of

primers were used and amplification was carried out on a thermocycler (Mastercycler, Eppendorf). PCR amplifications were performed as follows:

1. Initial denaturation 94 °C 3 min
2. Denaturation 94 °C 30 sec
3. Annealing 55 °C 15 sec
4. Extension 72 °C 1 min per Kb

Repeat step 2 to 4 for 35 cycles

RT-PCR products were ran on a 1% agarose gel made up with 1x TAE buffer and visualized using the BioRad GEL-Doc system.

Table 3.2 List of primers for RT-PCR and sequencing

Target Gene	Primer sequence (5' to 3')
Oct3/4 exo	F: CCC CAG GGC CCC ATT TTG GTA CC R: TTA TCG TCG ACC ACT GTG CTG CTG
Sox2 exo	F: GGC ACC CCT GGC ATG GCT CTT GGC TC R: TTA TCG TCG ACC ACT GTG CTG CTG
KLF4 exo	F: ACG ATC GTG GCC CCG GAA AAG GAC C R: TTA TCG TCG ACC ACT GTG CTG CTG
C-Myc exo	F: CAA CAA CCG AAA ATG CAC CAG CCC CAG R: TTA TCG TCG ACC ACT GTG CTG CTG
hTert exo	F: GCC TCC AGA CGG TGT GCA CC R: ACC CTA ACT GAC ACA CAT TCC
Oct3/4 endo	F: GAC AGG GGG AGG GGA GGA GCT AGG R: CTT CCC TCC AAC CAG TTG CCC CAA AC
Sox2 endo	F: GGG AAA TGG GAG GGG TGC AAA AGA GG R: TTG CGT GAG TGT GGA TGG GAT TGG TG
KLF4 endo	F: ACG ATC GTG GCC CCG GAA AAG GAC C R: TGA TTG TAG TGC TTT CTG GCT GGG CTC C
C-Myc endo	F: GCG TCC TGG GAA GGG AGA TCC GGA GC R: TTG AGG GGC ATC GTC GCG GGA GGC TG
hTert endo	F: GCC TCC AGA CGG TGT GCA CC R: CTT GGC CCC CAG CGA CAT CC
Nanog	F: CAG CCC CGA TTC TTC CAC CAG TCC C R: CGG AAG ATT CCC AGT CGG GTT CAC C
Dnmt3b	F: TGC TGC TCA CAG GGC CCG ATA CTT C R: TCC TTT CGA GCT CAG TGC ACC ACA AAA C
MeCP2-72	F: CAC CAT CAC CAC CAC TCA GA R: TGG GCA TCT TCT CCT CTT TG
MeCP2-80	F: CAC GGA AGC TTA AGC CAA AGG R: CTG GAG CTT TGG GAG ATT TG
MeCP2-48	F: ACC CTA ATG ATT TTG ACT TC R: ATA GAA GAC TCC TTC ACG

3.21 Quantitative RT-PCR (qRT-PCR)

qRT-PCR was carried out using 2µL of cDNA, 200nM of each primer and 2x iQ SYBR Green Mastermix (BioRad) in a 25µL reaction. Amplification and detection was carried out using the iQ5 real-time PCR detection system (Biorad). PCR amplifications were performed as follows:

1. Initial denaturation 96 °C 3 min
2. Denaturation 96 °C 30 sec
3. Annealing 55 °C 15 sec

4. Extension 60 °C 4 min - Repeat step 2 to 4 for 40 cycles

Glyceraldehyde 3-phosphate dehydrogenase (GAPDH) and Beta 2 Microglobulin (B2M) were used as endogenous controls. Relative expression of target genes was calculated using the comparative method ($2^{-\Delta\Delta C_t}$). Melting curves analysis and “no template control” reactions were performed to ensure primer specificity. All reactions were ran in triplicates.

Table 3.3 List of primers for qRT-PCR

Target Gene	Primer sequence (5' to 3')
TMEM132D	F: TCA ATG GGA GGA AGC GTG TC R: GCC CAG CCT TTG AGA GAC AG
CNTN6	F: AAC ACT GGC AGC CTC ATT GT R: TCA ATG GAG GGG TCA TGG GA
SCN2A	F: CCC GCC CTC TAG TGG TAG T R: AGA CCA CAC CTA ACT TCC TGT AA
HOXB8	F: GAC AGA CCT ACA GCC GCT AC R: GAT ACC TCG ATT CGC CGC TT
GAP43	F: CCA ACG GAG ACT GGG GAG AG R: CTT GGT CAG CCT CAG GTT CC
ABAT	F: GGT GGC AGC ACG CAA A R: TTT GGC TGC AGC TTG ACT AAT
PCDHB5	F: TGG GCT TCG TTC TTG TGG AA R: TTT TGC TAG CGC AGT CTC CA
PCDH19	F: CCT TCA AGG ACT TAG AGG GCA R: ATC ACA ATA CAG GCT CCG CT
LYZ	F: AAT AGC CGC TA CTG GTG TAA TG R: ATC ACG GAC AAC CCT CTT TG
DEFA1	F: TCC CAG AAG TGG TTG TTT CC R: CTG GTA GAT GCA GGT TCC ATA G
DEFA3	F: GGA GCC ATT GAG AAT CCA TAG T R: GGT GGG AAG GTG AGG TTA AAG
FCN1	F: ACC TCA CCA GAG GGA GAA TTA R: TGC AAC AGA CAC AGG AAA GT
GAPDH	F: CGA TGC TGG CGC TGA GTA CG R: AGA GGG GGC AGA GAT GAT GAC
B2M	F: GCT GGC GGG CAT TCC TGA AG R: ATC TTT GGA GTA CGC TGG ATA GCC

3.22 Sequencing

PCR was carried out using 3-10ng of DNA, 10 μ M of primer and 8ul of BigDye terminator reaction mix with a volume of 20 μ L. PCR amplifications were performed as follows:

1. Initial denaturation 96 °C 3 min
2. Denaturation 96 °C 30 sec
3. Annealing 50-55 °C 15 sec - Temp depends on Primer T_m, skip if T_m > 60°C
4. Extension 60 °C 4 min - Repeat from step 2 for 35 cycles for >800 bps read, 25 cycles for <500 bps reads

Subsequent sequencing steps were performed by the IMCB sequencing unit.

3.23 Microarray experiments

RNA quality control

RNA was isolated as described in section 3.23. For further quality control, RNA quality was analysed using the Bioanalyzer (Agilent) according to the manufacturer's instruction. Only samples with an RNA integrity number (RIN) above 8 is used for microarray.

RNA amplification

500ng of RNA was amplified using the Illumina TotalPrep- 96 RNA Amplification Kit (Ambion) according to the manufacturer's instructions.

Briefly, 500ng of total RNA was reverse transcribed to cDNA followed by second strand cDNA synthesis. Second strand cDNA was purified followed by *in vitro* transcription to complementary RNA (cRNA). cRNA was purified and quantified with the Nanodrop.

Bead chip hybridization

Briefly, 750 ng of cRNA was prepared according to manufacturer's instructions and added to each sample array of the HumanHT-12 v4 Expression BeadChip (Illumina) which targets more than 47,000 probes derived from the National Center for Biotechnology Information Reference Sequence (NCBI) RefSeq Release 38. The Beadchips was incubated for 20hours at 58°C in a hybridization oven with rocker. Following that, the Beadchips washed, blocked and stained with streptavidin-Cy3 according to manufacturer's instructions. Scanning was done with the Illumina BeadArray Reader.

Analysis of microarray data

The raw image signal was extracted using Illumina BeadStudio software and converted to .CEL files for analysis using GeneSpring GX v11.5 (Agilent). To identify differentially expressed genes (DEG) between 2 conditions, a student's paired T-test with Benjamin-Hochberg false discovery rate (FDR) control (0.05) was performed. Analyses were further performed using the Database for Annotation, Visualisation and Integrated Discover (DAVID) version 6.7 (<http://david.abcc.ncifcrf.gov/>) (Huang da et al., 2009a, b).

Alternatively, additional microarray analyses for microglia data were performed using the Ingenuity iReport (Qiagen).

3.24 Statistical Analysis

The numeric data are presented as mean \pm SEM. The statistical significance of the differences between group means was evaluated using an unpaired Student's t-test. 1 way ANOVA followed by post-hoc Tukey test was performed for all multiple comparisons. All statistics were performed using GraphPad Prism (Version 5, GraphPad Software, Inc. La Jolla, CA).

Chapter 4: Reprogramming of RTT patients' fibroblast

4.1 Introduction

The relatively straight forward and robust method of generating hiPSCs by introduction of a defined set of transcription factors has been achieved by several groups (Lowry et al., 2008; Park et al., 2008a; Takahashi et al., 2007; Yu et al., 2007). The use of hiPSCs in modeling neurological disorder for which brain cells are difficult to access has been a popular choice for many researchers (Han et al., 2011; Wang and Doering, 2012).

However, one of the challenges in using iPSCs for disease modeling is getting suitable control cells. Age matched control from non-affected subjects are typically used but this is not ideal as variability in genetic background and risk factor exposure could lead to confounding results. X-linked genetic disorders offer the possibility of generating isogenic WT and MT iPSCs from the same patient. In humans, females inherit two copies of the X-chromosome from the paternal and maternal gametes. In a phenomenon called X chromosome inactivation (XCI), one copy of the X is inactivated. Both the paternal or maternal copy of the X can be inactivated and this process is thought to be random resulting in a 1:1 mixture of active paternal and maternal copy of the X chromosome (Ozbalkan et al., 2005). Hence it is theoretically possible to obtain isogenic WT and MT iPSCs from an individual with an X-linked mutation.

4.2 Hypotheses and Aims

Female RTT patients have a mosaic of cells in which half expresses the wildtype (WT) copy of *MeCP2* and the other half expresses the mutant (MT) copy of *MeCP2*. Due to this phenomenon, there is a possibility of getting isogenic iPSCs lines from the same patient in which some colonies would express WT MeCP2 and some colonies would express MT MeCP2. This will give us isogenic lines in which both WT and MT iPSCs lines would have identical genetic background with the exception of the viral integration site of the reprogramming factors OSKM and the active copy of X-Chromosome. My hypothesis is that isogenic iPSCs can be generated from individual female RTT patients. To test this hypothesis, I decided to reprogram RTT patients' fibroblast using retroviral OSKM and isolate single colonies. Characterisation of the colonies would be carried out to confirm that the cells are pluripotent and karyotypically normal. Identification of the colony's genotype would be carried out based on the *MeCP2* mutation. These iPSCs would be used to generate the cell types to be studied in later chapters.

At the time this project commenced, one group had reported the generation of iPSCs from RTT patients but without phenotypic investigation (Hotta et al., 2009). During the course of this study, several other groups reported derivation of iPSCs from RTT patients bearing *MeCP2* mutations (Ananiev et al., 2011; Cheung et al., 2011; Kim et al., 2011; Marchetto et al., 2010). The results of these studies will be reviewed in the discussion.

4.3 Results

4.3.1. RTT patients' background

Fibroblasts from female RTT patients were purchased from Coriell Cell bank. GM11272 was derived from a 3 yr female Caucasian and carries a 32 bp deletion in position 1155 of *MeCP2*. This also causes a frameshift downstream of the deletion resulting in putative premature stop codons. This patient is reported to show classic RTT symptoms. Henceforth, cells and derivatives from this patient are referred to as P72.

GM16548 was derived from a 5 yr female Caucasian and carries a C>T transition at position 730 of *MeCP2*. This causes a codon change from glutamine to termination. This patient is reported to be clinically affected with the following symptoms: abnormal sleep patterns; ambulatory with some rigidity/spasticity; slight spine curvature; breath holding; constipation; decelerating head circumference; limited purposeful hand use; nonverbal; poor hand and feet circulation; repetitive hand motions; seldom exhibits self-injurious behavior; small feet; teeth grinding; minor eating difficulties and reflux; tremors; EEG shows minor abnormalities. Henceforth, cells and derivatives from this patient are referred to as P48.

GM17880 was derived from a 5 yr female Caucasian and carries a C>T transition at position 473 of *MeCP2*. This results in the substitution of threonine by methionine at position 158 of the MeCP2 protein. This patient is reported to have growth and developmental delay; can walk only with assistance; nonverbal; no hand use; constant repetitive hand motions; no

seizures, but significantly abnormal EEG; teeth grinding; some sleep difficulties; eating problems with minor reflux; breath holding and hyperventilation; small feet; some tremor. Henceforth, cells and derivatives from this patient are referred to as P80.

4.3.2. Reprogramming of fibroblast through retroviral induction

The most commonly employed method of reprogramming is through viral induction of OSKM (Lowry et al., 2008; Park et al., 2008b). Therefore, we sought to reprogram RTT patients' fibroblasts using retroviral induction of OSKM. Briefly, fibroblasts were expanded and transduced with pooled OSKM retrovirus particles (**Fig 4.1C&D**). Transduced fibroblasts were then trypsinized and plated onto mouse embryonic feeders (MEF) (**Fig 4.1E**). 2 weeks later, iPSC like colonies were manually picked and expanded on MEF (**Fig 4.1F-H**).

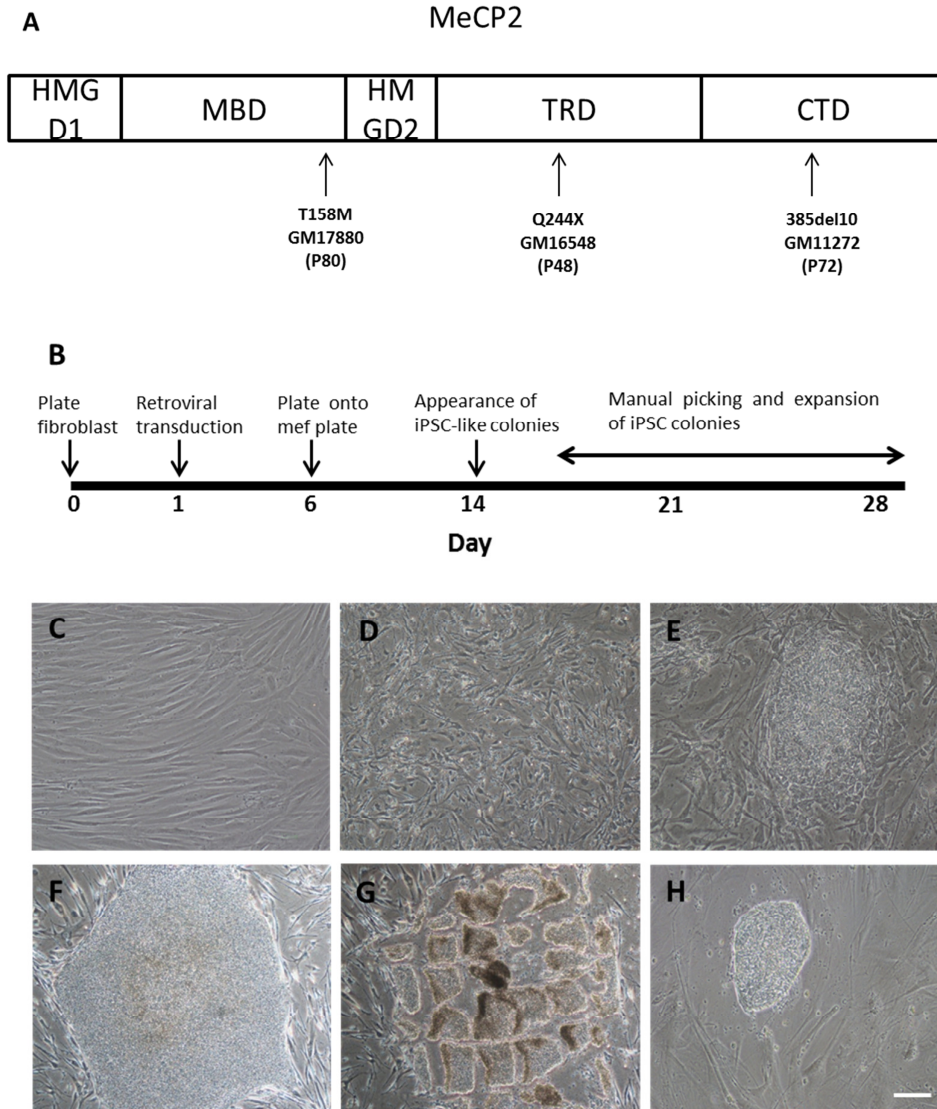


Fig 4.1 Reprogramming of fibroblast into iPSCs. (A) Diagram of the MeCP2 protein showing relative position and type of mutation of the cell lines used in this study. (B) Schematic representation of the reprogramming protocol (C) Morphology of fibroblast at day 1 before transduction. (D) Morphology of fibroblast 3 days after viral transduction (E) Emergence of iPSCs-like colonies at day 14 (F) Morphology of a fully reprogrammed colony at day 21 (G) Chosen colony is manually cut and transferred to new MEF plate (H) Morphology of handpicked colony at day 1 after subculture. Scale bar represents 100 μM.

4.3.3. hTert can overcome skewing of reprogramming

To identify between WT and MT iPSCs clones from P72, we designed primers that flanked the 32 bp deletion of the MT *MeCP2*. Due to a 32 bp deletion of *MeCP2* in MT cells, PCR products were easily distinguishable on an agarose gel between WT and MT iPSCs due to a size difference. For P48 and P80, DNA sequencing was used to distinguish between WT and MT *MeCP2* expressing cells. RT-PCR of the P72 fibroblast population showed that both WT and MT cells are present (**Fig 4.2A**). Unexpectedly, we discovered that all iPSCs clones from P72 expressed the MT allele (**Fig 4.2A**). To further investigate, we subcloned the mixed fibroblasts from P72 and P80 into populations that exclusively express either the WT or MT allele only and reprogrammed the pure population. Alkaline phosphatase staining which is a marker for stem cells is used to identify iPSCs colonies. P72 MT fibroblasts showed a higher reprogramming efficiency than P72 WT fibroblast while on the other hand, P80 WT fibroblasts showed a higher reprogramming efficiency than P80 MT fibroblasts based on alkaline phosphate expression (**Fig 4.2B**). Subsequent experiments to investigate the cause of this unequal reprogramming led to the discovery that P72 WT cells entered senescence earlier and exhibited increased DNA Foci damage (Pomp et al., 2011b), and that this phenotype could be overcome by expression of exogenous human telomerase reverse transcriptase (hTert) (Pomp et al., 2011b). To see if hTert could also overcome the reprogramming roadblock of the P72 WT fibroblast, we used OSKM + hTert as the viral transduction cocktail. Addition of hTert enabled us to generate both WT and MT iPSCs clones (**Fig 4.2C**). For P48, we did not check the reprogramming efficiency for the individual WT and MT

populations as OSKM + hTert was directly used to reprogram a mixed culture of fibroblasts and we managed to get both WT and MT iPSC colonies (**Fig 4.2D**).

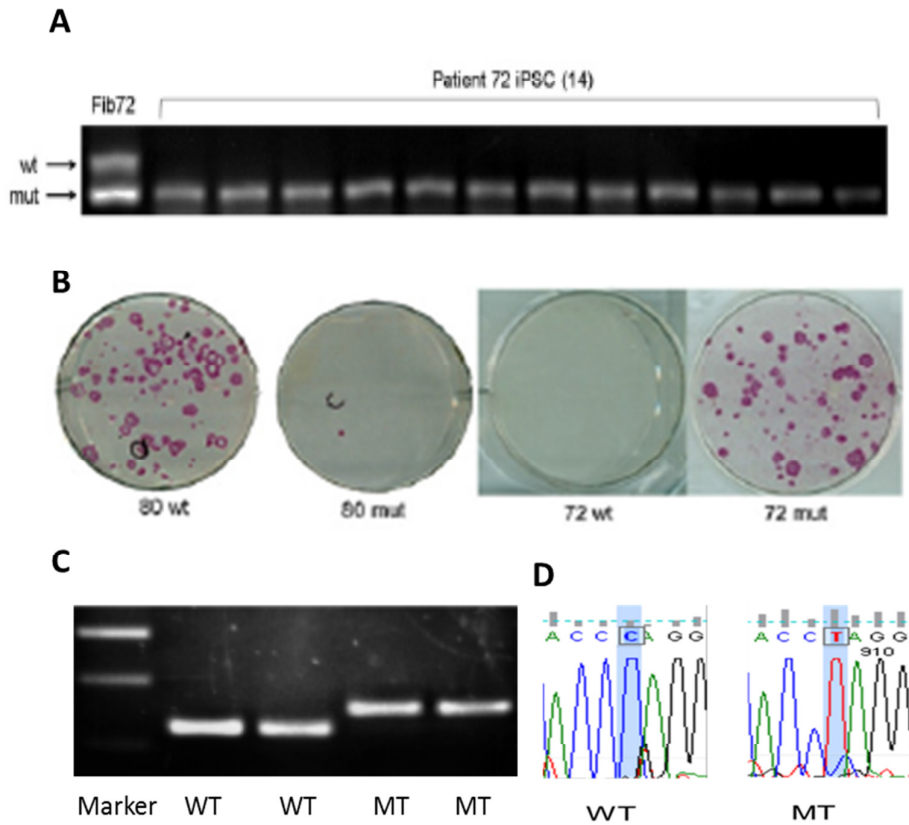


Fig 4.2 Derivation of isogenic iPSCs from RTT patients' fibroblast. (A) RT-PCR results showed reprogramming using OSKM from mixed population of P72 fibroblast gave rise to only MT iPSCs clones. (B) OSKM reprogramming of subcloned fibroblast population showed presence of iPSC colonies as indicated by alkaline phosphatase staining in only WT population from P80 and in only MT population from P72. (C) RT-PCR result from OSKM + hTert reprogramming enabled successful reprogramming of isogenic clones from P72. (D) Sequencing result from OSKM + hTert reprogramming enabled successful reprogramming of isogenic clones from P48.

4.3.4 Pluripotent marker expression and transgene silencing

Characterisation of the generated iPSCs was carried out to check for expression of pluripotent markers and silencing of the transgenes. Several lines were generated but for the purpose of this thesis, only results from iPSCs generated from P72 and P48 are shown. RT-PCR of endogenous expression of pluripotent genes such as *Oct4*, *Sox2*, *Nanog* and *Dnmt3b* was carried out and all iPSCs clones showed up-regulation of pluripotent markers (**Fig 4.3A**). RNA from the hESC line H9 was used as a positive control. To test for silencing of transgenes, RT-PCR of transgenic OSKM + hTert was carried out. The results showed these transgenes were silenced in the mature iPSCs clones (**Fig 4.3B**). The respective plasmid vector used for reprogramming was used as a positive control (1:1000 dilution). To examine if patient's iPSCs express pluripotent markers at the protein level, immunofluorescence staining of Oct4, Sox2 and Tra 1-60 was carried out and all iPSCs clones showed strong expression of the markers used (**Fig 4.4**).

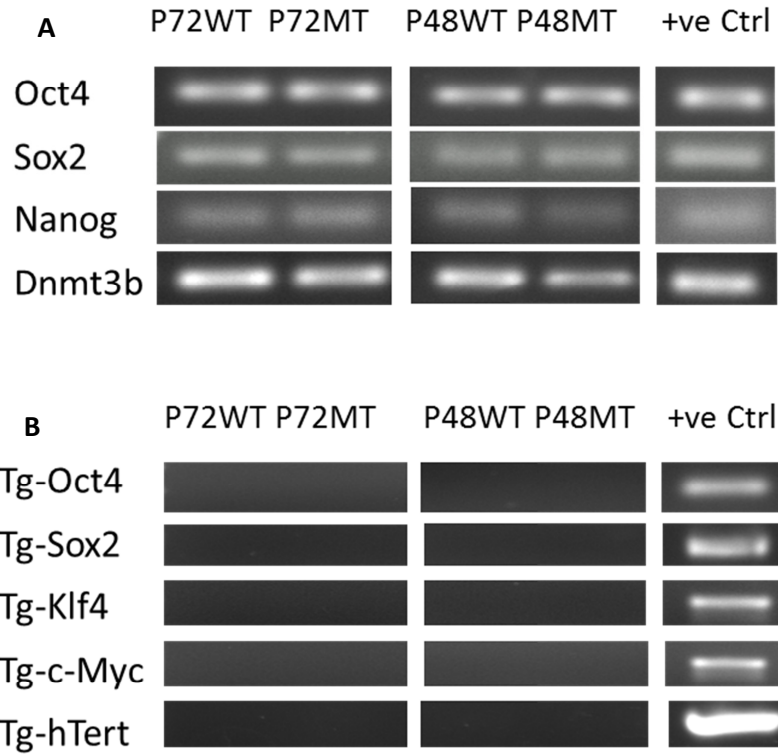


Fig 4.3 RT-PCR characterisation of iPSCs. (A) iPSCs clones generated showed expression of endogenous pluripotent markers. (B) iPSCs clones showed no expression of the OSKM and hTert transgenes.

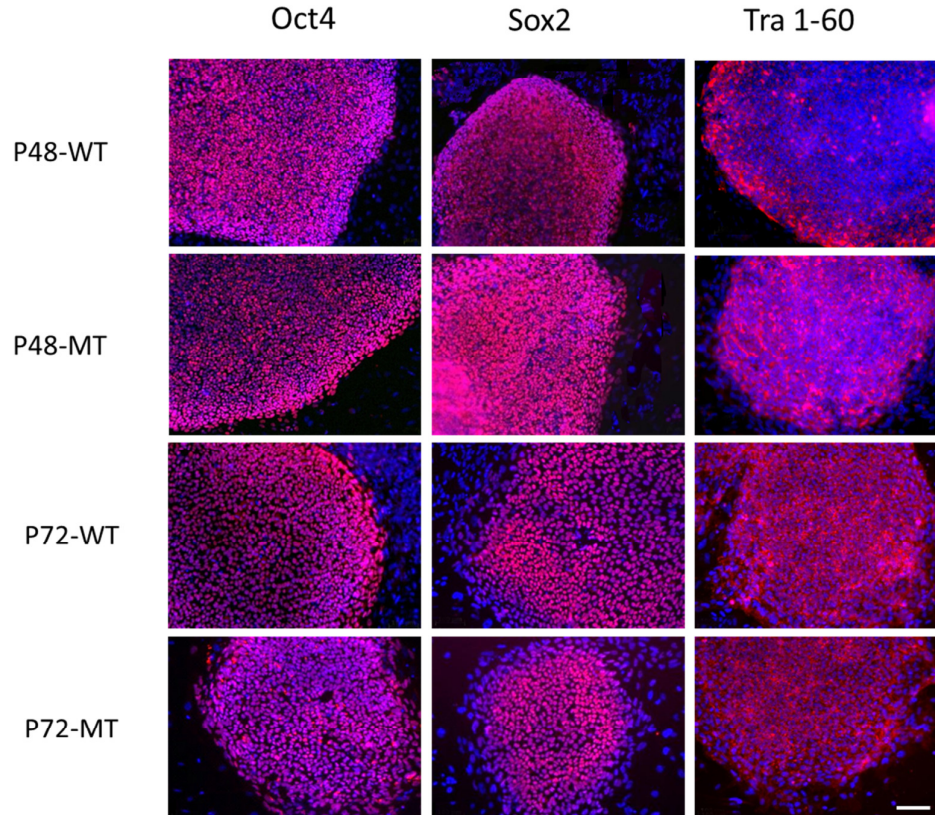
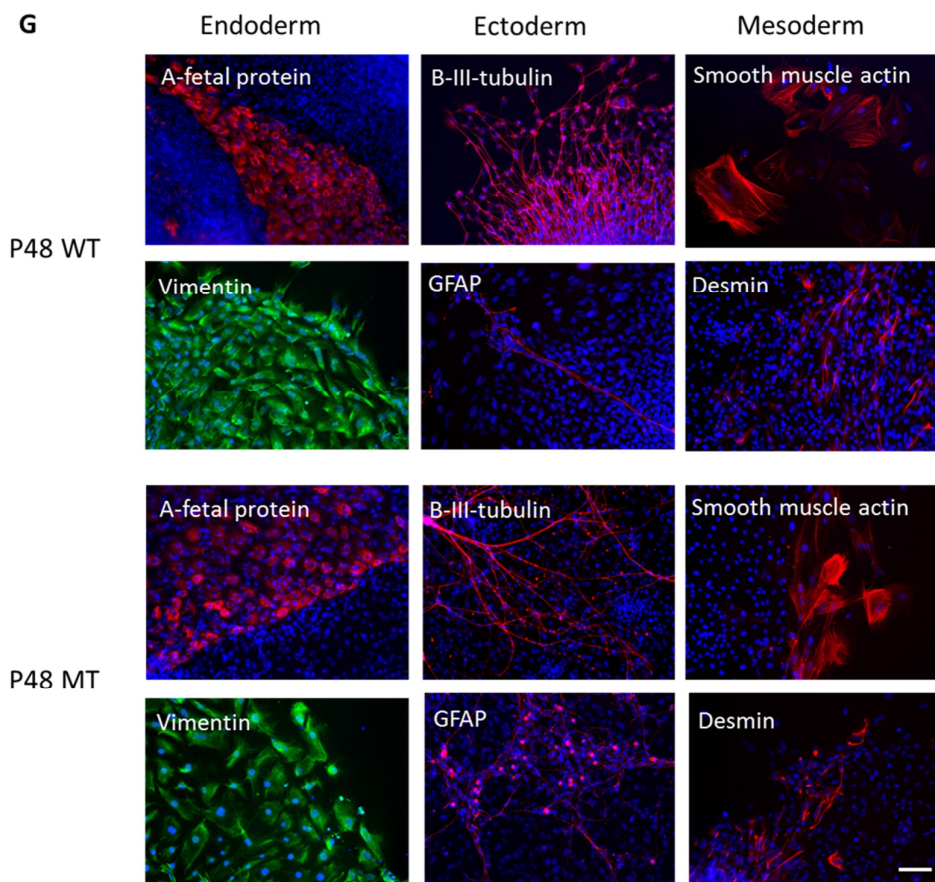
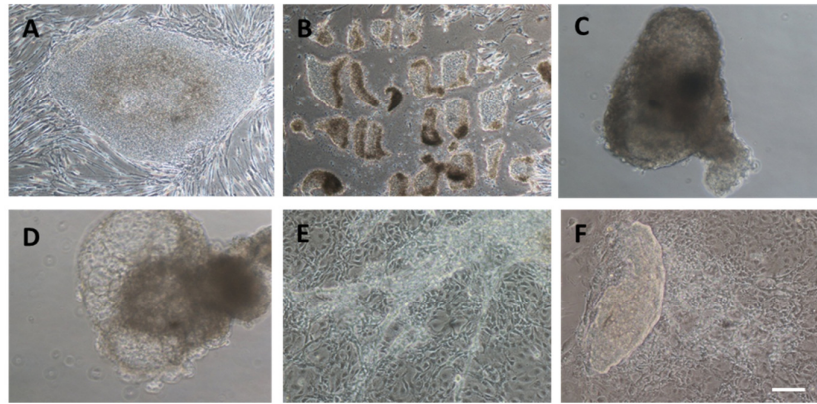


Fig 4.4 Characterisation of the iPSCs lines. Immunofluorescence of iPSCs lines P48 and P72 showing expression of the pluripotent markers Oct4, Sox2 and Tra1-60. Scale bar represents 100 μ M.

4.3.5 *In vitro* differentiation of iPSCs

An important aspect of pluripotency is the ability to generate the three germ layers. To test for this ability in the generated iPSCs, *in vitro* differentiation was carried out. This is done through formation of embryo-like aggregates termed embryoid bodies (EBs). EBs recapitulate several aspects of early development and all three embryonic germ layers are present (Itskovitz-Eldor et al., 2000). Briefly, undifferentiated iPSCs were cut into pieces and cultured in suspension to allow for formation of 3-D spheroid structures (**Fig 4.5A-D**). EBs formed by 3-5 days and cystic EBs formed after 2 weeks of differentiation. Plating of EBs onto gelatin coated plates resulted in attachment and outgrowth of heterogeneous cell types (**Fig 4.5E&F**). Immunofluorescence

of the differentiated cells showed presence of the three germ layers. The presence of each germ layer was confirmed by at least 2 different markers (**Fig 4.5G&H**).



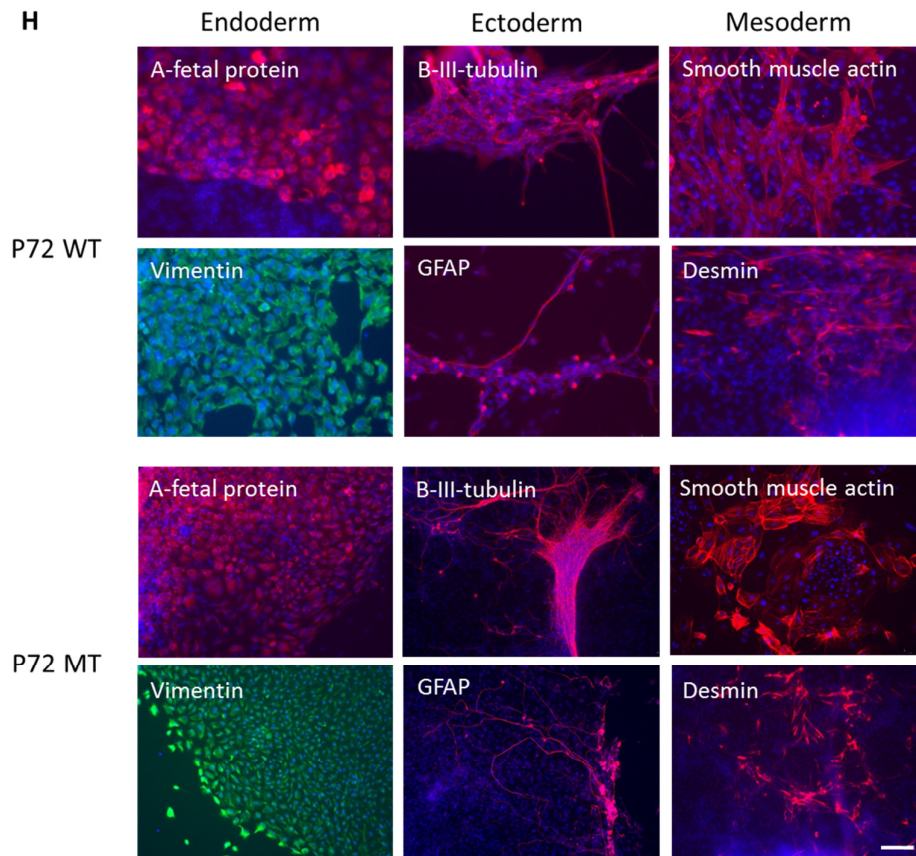


Fig 4.5 *in vitro* differentiation of iPSCs lines. Formation of EBs. (A) Morphology of undifferentiated iPSCs. (B) iPSCs colony is manually cut into pieces. (C) iPSCs in suspension form EBs after 48 hours. (D) EB showing cystic structure. (E) and (F) Spontaneous differentiation of attached EBs showed heterogenous morphology and cystic structures. Immunocytochemistry of EBs from iPSCs of (G) P48 and (H) P72 showed presence of the three germ layers: fetoprotein and vimentin (endoderm), β -III-tubulin and GFAP (ectoderm) smooth muscle actin and desmin (mesoderm). Blue staining represents Hoescht. Scale bars represent 100 μ M.

4.3.6 *in vivo* differentiation of iPSCs

To further confirm the pluripotency of the iPSCs lines, *in vivo* differentiation was carried. This is done through transplantation of undifferentiated iPSCs into immune-compromised mice. This results in the formation of a teratoma which is a benign tumour comprising of differentiated cell types of the three

germ layers (Thomson et al., 1998). Sections of teratomas showed presence of the three germ layers (**Fig 4.6A&B**).

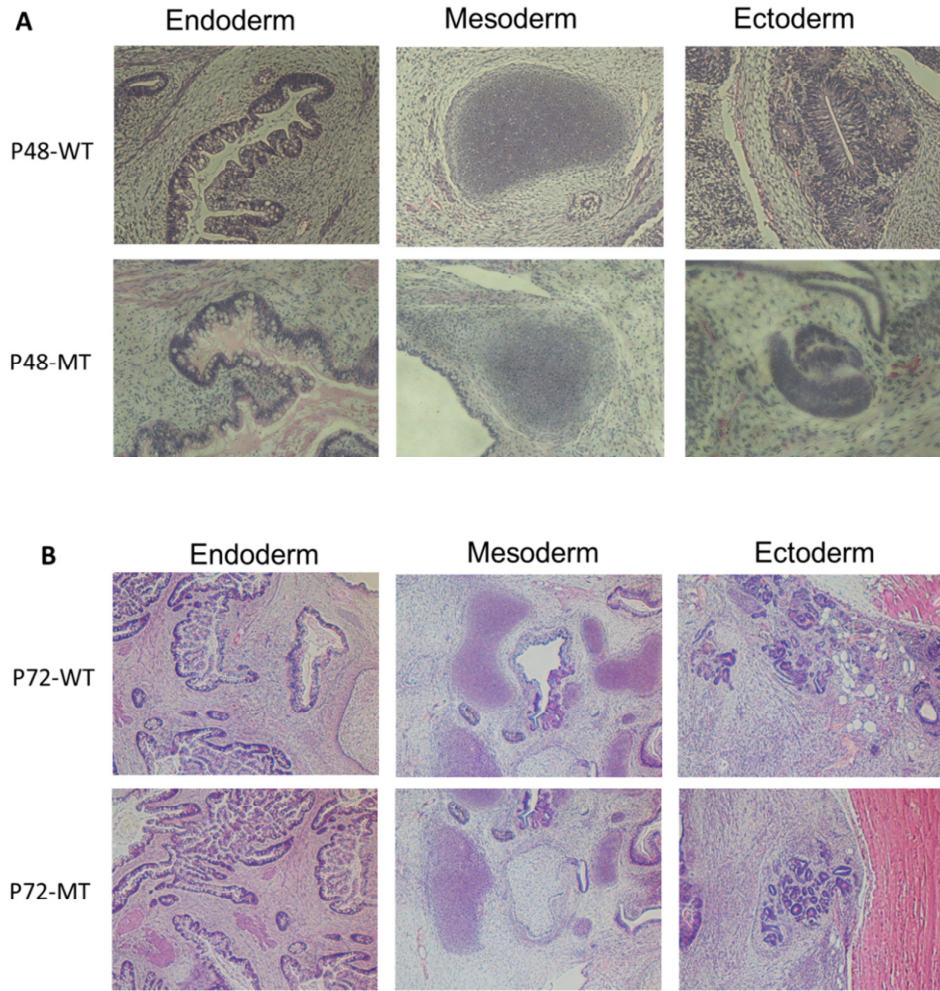


Fig 4.6 *in vivo* differentiation of iPSCs lines. Teratomas from iPSCs of (A) P48 and (B) P72 showed formation of the three germ layers 6-8 weeks after transplantation into SCID mouse.

4.3.7 Karyotypic analysis of iPSCs

Cytogenetics analysis was carried out using karyotype analysis. This technique utilises Giemsa staining following cell arrest in the metaphase stage and any chromosomal abnormalities can be observed under a microscope. All iPSCs generated showed normal karyotype (Fig 4.7).

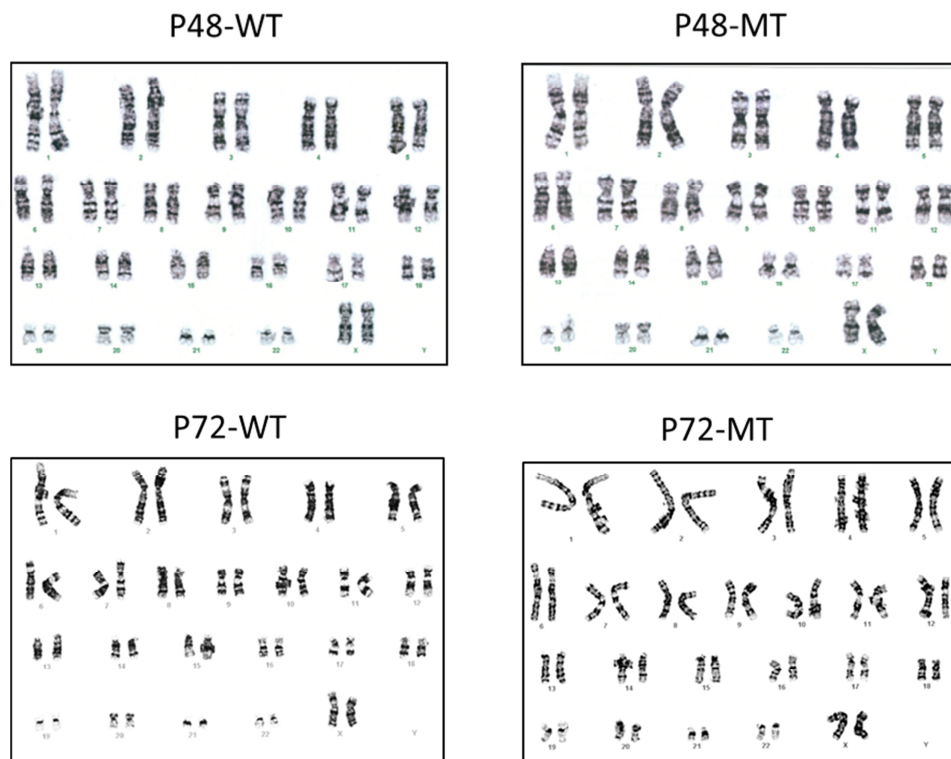


Fig 4.7 Cytogenetics analysis of iPSCs lines. Karyotype analysis of iPSCs lines from P48 and P72 showed normal XX karyotype at passage 10.

4.3.8 Detection of MeCP2 in iPSCs

To examine if iPSCs express MeCP2 protein, immunofluorescence using an antibody able to detect N-terminal MeCP2 was performed. The ESC line H9 was used as a positive control and showed clear nuclear staining of MeCP2

(**Fig 4.8A**). However, both WT and MT iPSCs do not show distinct nuclear MeCP2 staining (**Fig 4.8B&C**). Instead, a diffuse staining pattern was observed on the iPSCs colonies while surrounding MEF showed clear nuclear staining. To further confirm this result, a control iPSCs line from a non-affected subject (a kind gift from a colleague, Zhou Fan) was used and the same non-specific staining was observed (**Fig 4.8D**).

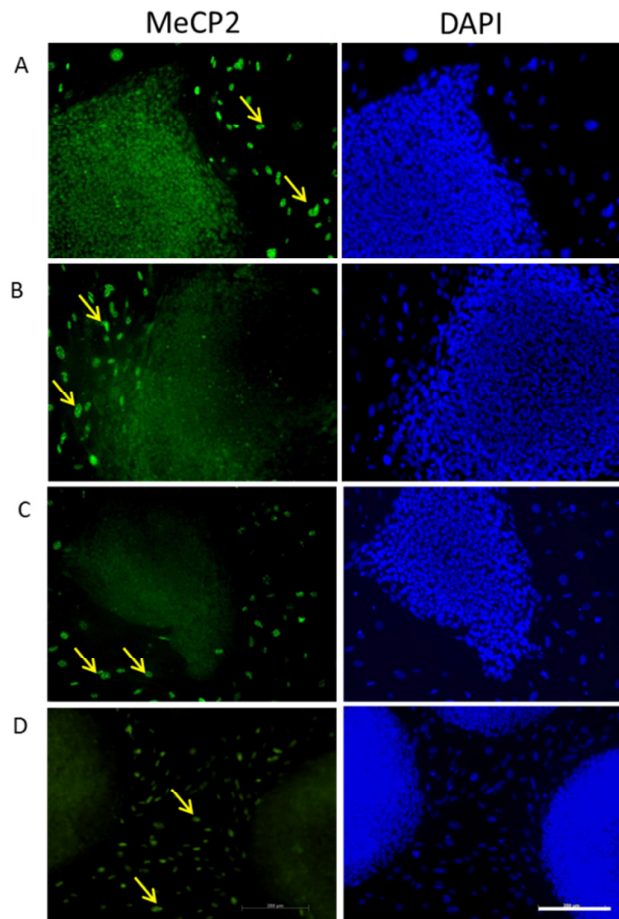


Fig 4.8 Expression of MeCP2 in PSCs. Immunofluorescence of MeCP2 staining in (A) H9 showed distinct nuclear expression while (B) WT and (C) MT iPSCs derived from P72 and (D) control iPSCs do not show expression of MeCP2. Yellow arrows depict MeCP2 staining in MEF. Scale bar represents 200 μ M.

4.4. Discussion

4.4.1. The role of TERT in reprogramming

Telomeres are repetitive nucleotide sequences at the ends of chromosomes that protect chromosomes from deterioration or recombination with neighbouring chromosomes (Blackburn, 2001). However, each cell replication cycle results in shortened telomeres and shortened telomeres is associated with cellular senescence and organismal aging (Allsopp et al., 1995; Blasco, 2005). In mammals, one way of telomere length maintenance is through telomerase- a ribonucleoprotein structure consisting of TERT and TERC (Telomere RNA component). TERT functions as a reverse transcriptase at the ends of chromosomes to add repeat sequences to compensate for telomeres shortening during mitosis (Greider and Blackburn, 1985) while TERC acts as an RNA template for TERT. Telomerase activity is present in indefinitely replicating cells such as ESC and immortal cancer cells (Hiyama and Hiyama, 2007; Kim et al., 1994), but is absent in most somatic cells which eventually leads to shortening of telomeres and cellular senescence (Allsopp et al., 1995; Blasco, 2005). It has been reported that iPSCs have high telomerase activity and cells from telomerase-deficient mice with critically shortened telomeres showed lower reprogramming efficiency and reintroducing of telomerase could restore reprogramming efficiency (Marion et al., 2009).

In this study, we successfully generated isogenic iPSCs from RTT patients' fibroblast. Using the commonly employed virus mix OSKM, we report that only one fibroblast population could be induced into iPSCs. Further investigation into this phenomenon showed that the fibroblast population that

had low reprogramming efficiency showed increased DNA damage and underwent senescence earlier than fibroblasts with normal reprogramming efficiency. As telomeres are involved in cell proliferation and DNA repair, and telomere length has been correlated with reprogramming efficiency (Marion et al., 2009), we hypothesized that addition of exogenous hTert could lead to DNA repairs and restoration of telomere length, which in turn will lead to recovery of reprogramming efficiencies. Hence the cell population with low reprogramming efficiency could be improved. However, cells with normal reprogramming efficiency do not see an improvement possibly because hTert do not improve reprogramming beyond its role of DNA damage and overcoming cell senescence. Introduction of hTert together with OSKM yielded iPSCs expressing either WT MeCP2 or MT MeCP2. At this point, we speculate that the mechanism behind this skewing is X-linked polymorphism (Pomp et al., 2011a). Together, our findings highlight the significance of telomere biology in iPSCs generation.

During the course of this study, several groups reported derivation of iPSCs from RTT patients bearing *MeCP2* mutation (Ananiev et al., 2011; Cheung et al., 2011; Kim et al., 2011; Marchetto et al., 2010). There are however, inconsistencies in the X-Chromosome status of the iPSCs as reported by the various groups (**Table 4.1**). Marchetto et al., 2010 reported getting biallelic iPSCs and that subsequent differentiation of the iPSCs resulted in random XCI of the progeny cell (Marchetto et al., 2011). Kim et al., 2011 reported getting iPSCs that are either biallelic or monoallelic (Kim et al., 2011). Cheung et al., 2011 and Ananiev et al., 2011 reported getting monoallelic iPSCs clones which our supports our data (Ananiev et al., 2011; Cheung et al., 2011). The

cause for the inconsistency remains unknown but one possibility is that the type of feeders used in generating iPSCs could be a factor in determining X-Chromosome status (Tomoda et al., 2012).

Table 4.1. X-Chromosome status of iPSCs reprogrammed from RTT patients from various groups

Reference	X-Chromosome status
Marchetto et al., 2010	Biallelic
Kim et al., 2011	Mixture of biallelic and monoallelic
Cheung et al., 2011	Monallelic
Ananiev et al., 2011	Monoallelic
Our study (Pomp et al., 2011)	Monoallelic

4.4.2. Characterisation of iPSCs

Exhaustive characterization of the iPSCs lines was carried out and both WT and MT iPSCs generated showed similar features to hESC including cell morphology and expression of pluripotent markers. The pluripotency of the iPSCs was demonstrated by both *in vitro* and *in vivo* differentiation through the presence of the three germ layers of endoderm, mesoderm and ectoderm. No difference was detected between WT and MT iPSCs. In addition, OSKM and hTert transgenes expression were silenced and iPSCs showed normal karyotypes. In summary, the iPSCs generated fulfilled the criteria of PSC and there was no difference between WT and MT iPSCs. This is in line with the other reports. As our results showed, *MeCP2* is either not translated or is expressed at very low levels in iPSCs though it has a higher expression in ESCs. Hence, iPSCs properties are not affected by MeCP2 expression.

4.5. Conclusions

In summary, I described the generation of isogenic WT and MT iPSCs lines from RTT patients. Reprogramming of fibroblasts showed bias and this could be overcome by exogenous hTert expression. Isogenic lines are genetically very similar and represent a good model for disease modeling. Later chapters will describe the use of these lines for modeling RTT.

4.6. Limitations

4.6.1 Characterisation of more patients' iPSCs.

The results here showed the characterization of P72 and P48 iPSC WT and MT lines. However, iPSCs from P80 were not completed in time for this thesis due to the length of time needed to carry out the characterization.

4.6.2 Retroviral-based reprogramming

The iPSCs generated in this project were done using integrating viral vectors and is currently the most widely used technique due to its high efficiency. However, this method might introduce mutations at the transgene integration site and other genetic aberrations (Laurent et al., 2011). Several strategies have been developed to generate transgene free iPSCs. These include non-integrating Sendai viruses (Fusaki et al., 2009), episomal vectors (Yu et al., 2009), mRNA based reprogramming (Warren et al., 2010) and protein based reprogramming (Kim et al., 2009; Zhou et al., 2009). These methods will minimize variations due to reprogramming process and create better quality and more consistent iPSCs lines. Another strategy would have been to induce

the mutation in normal stem cells and to correct the mutation in MT cells by molecular gene editing (e.g. using CRISPR-CAS9 system (Hsu et al., 2014)).

4.6.3 MeCP2 expression in iPSCs

In **section 4.3.8**, MeCP2 immunostaining was shown to be present in the hESC line H9 but the staining was weak and diffuse in iPSC lines. Hence, the result is inconclusive and a western blot should be done to further confirm the expression level of MeCP2 in iPSC lines. An iPSCs specific marker such as Tra1-60 should also be used to better distinguish between the iPSC colonies and MEF in **Figure 4.8**. However, these experiments were not conducted in time for this thesis.

Chapter 5: Investigating the role of NPCs in RTT using iPSCs

5.1 Introduction

The majority of early RTT research was focused on neurons as initial studies in mice demonstrated the critical role of *Mecp2* in neurons. Knocking out *Mecp2* in post-mitotic neurons was enough for RTT symptoms to manifest in mouse (Chen et al., 2001), while re-expression of *Mecp2* in post-mitotic neurons of *Mecp2*-null mice was able to effect a rescue of the RTT phenotype (Luikenhuis et al., 2004). Afflicted neurons show several morphological phenotypes including reduced dendritic arbors (Kishi and Macklis, 2004), smaller soma and nucleus size (Chen et al., 2001) and reduced excitatory synapse number (Chao et al., 2007). Afflicted neurons also showed abnormal electrophysiological properties such as abnormal long term potentiation (Asaka et al., 2006; Moretti et al., 2006). These findings and the absence of MeCP2 expression in glia led to the belief that RTT is an exclusively neuronal disorder (Kishi and Macklis, 2004; Shahbazian et al., 2002b). It was only in recent years that new evidences revealed the involvement of the other brain cell types such as astrocytes, microglia and oligodendrocytes in RTT pathology (Ballas et al., 2009; Maezawa and Jin, 2010; Nguyen et al., 2013).

RTT is largely seen as a disorder of post-natal maturation. The age of onset of RTT symptoms in human (6-18 months) and mice (6 weeks) coincides with the period of neuronal maturation, and this is supported by the progressively higher expression of *Mecp2* as neurons mature (Kishi and Macklis, 2004; Shahbazian et al., 2002b). However, the neo-natal fatalities and severe infantile encephalopathy of human males with *MeCP2* mutations suggest an

early brain developmental role of *MeCP2*. Furthermore, in *Xenopus laevis* embryos, silencing of *Mecp2* resulted in early neuronal patterning defects (Stancheva et al., 2003). These evidences suggest MeCP2 may have a role in the early development of the CNS.

5.2 Hypotheses and Aims.

During CNS development, NPCs arising from the neural tube proliferates, migrate and further differentiate into neurons and glia. The main purpose of this study was to test the hypothesis that NPCs may represent a cell type that is affected in RTT. As there are no in-depth studies of the role of NPCs in RTT, I decided to look at how MeCP2 mutations can affect NPCs' properties. One property I wanted to investigate is proliferation. Microcephaly is a symptom associated with RTT and one cause of microcephaly is reduced proliferation of the NPCs. My hypothesis is that NPCs affected by MeCP2 mutations could show reduced proliferation. To test this hypothesis, a proliferation assay will be carried out comparing the growth rate of WT and MT NPCs.

Another aspect I wanted to look at is migration. NPCs are highly migratory cells as shown during both brain development (Doetsch and Alvarez-Buylla, 1996; Halliday and Cepko, 1992; Merkle and Alvarez-Buylla, 2006), and during brain pathology (Imitola et al., 2004; Jeon et al., 2008; Shah et al., 2005). As several neurological disorders including autism and schizophrenia are found to have abnormality in neuronal migration (Wegiel et al., 2010; Yang et al., 2011). I was interested to see if NPCs are affected in their migratory property. To test this hypothesis, a migration assay will be carried out comparing the migration rate between WT and MT NPCs.

The third aspect I wanted to test is the differentiation potential of the NPCs to neurons. As brains of RTT patients and mouse models show immature neuronal development (Chao et al., 2007; Francke, 2006), I wanted to examine whether MeCP2 mutations affect neuronal development. To test this hypothesis, I intend to compare neuronal differentiation between WT and MT NPCs and also the maturity of the respective neurons based on synapse numbers.

5.3 Results

5.3.1 Derivation of NPCs from iPSCs

WT and MT iPSC lines from P72 were used to derive NPCs with the “serum-free embryoid body” (SFEB) method with modifications (Eiraku et al., 2008)(**Fig 5.1A**). This method is based on the default model of neural induction which states that embryonal cells acquire a neural identity in the absence of signaling instructions, hence “by default” (Hemmati-Brivanlou and Melton, 1997) (Tropepe et al., 2001) (Reubinoff et al., 2001). We chose this method as it mimics the *in vivo* development of the neural system and is defined compared to the stromal cell induction system. Briefly, iPSCs were dissociated into single cells and allowed to form EB cell aggregates under defined condition (**Fig 5.1B-D**). Adhesion of EBs to the plastic dish in the presence of FGF2 led to the formation of rosette-like structures after 2-3 weeks of neural induction (**Fig 5.1E**). Neural rosettes are radially organized columnar epithelial cells that resemble the neuroepithelial cells in the neural tube (Zhang et al., 2001). The neural rosettes can then be manually isolated and further expanded as NPCs in the presence of FGF2 (**Fig 5.1F&G**).

To validate that cells generated were NPCs, immunocytochemistry was performed using 2 widely used NPCs markers– nestin and sox2 (Ellis et al., 2004; Reubinoff et al., 2001; Zhang et al., 2001). Immunocytochemistry showed that the iPSCs-derived NPCs stained strongly for these 2 markers (**Fig 5.2A**). These results showed that both WT and MT iPSCs could generate. To see if NPCs express MeCP2, we performed immunocytochemistry using an antibody specific to a sequence at the N-terminal of MeCP2. Both WT and MT NPCs showed positive staining demonstrating that MeCP2 is expressed in NPCs (**Fig 5.2A**). FACS using nestin antibody was carried out to measure the purity of the NPCs and the data show that both WT and MT iPSCs generated NPCs equally well (**Fig 5.2B**). RT-PCR showed that the respective NPCs retained their active X-chromosome expression (**Fig 5.2C**). These results show that MeCP2 does not affect NPCs induction in human iPSCs.

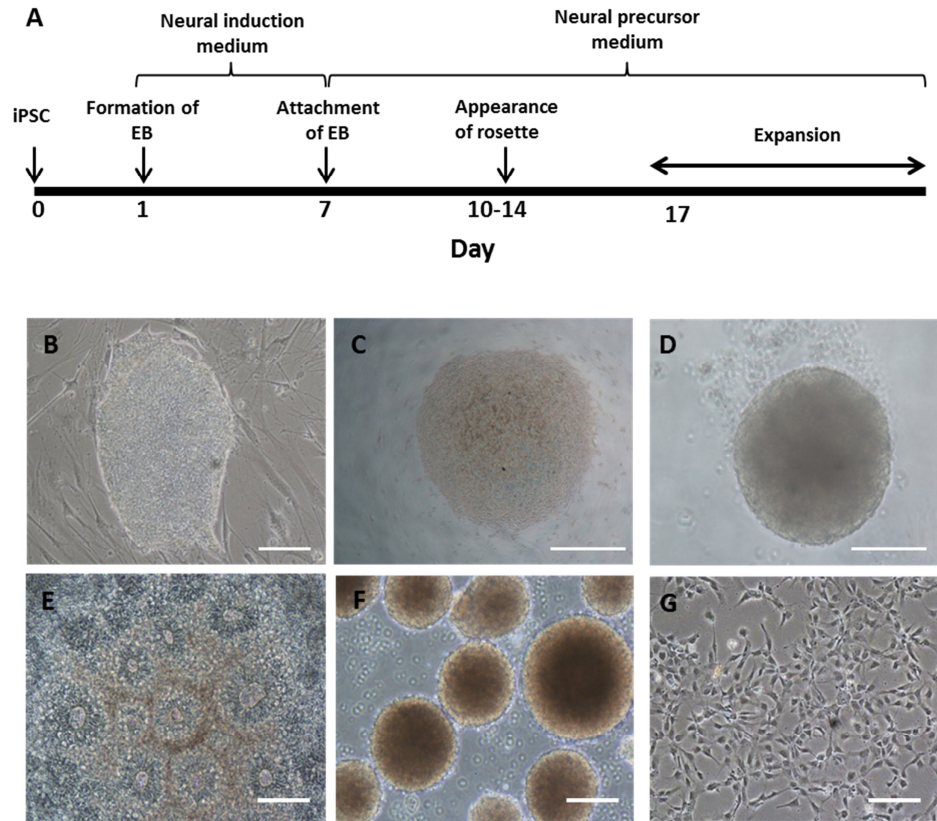


Figure 5.1 Derivation of NPCs from iPSCs (A) Schematic of NPCs induction from iPSCs. (B-G) Representative images of NPC induction protocol at different stages, (B) day 0– iPSCs (C) day 1– aggregation of single cells in round bottom well (D) day 2– formation of embryoid body (E) day 14– formation of rosettes (F) day 17–expansion of NPCs in suspension or (G) expansion in monolayer. Scale bars represents 200 μ M.

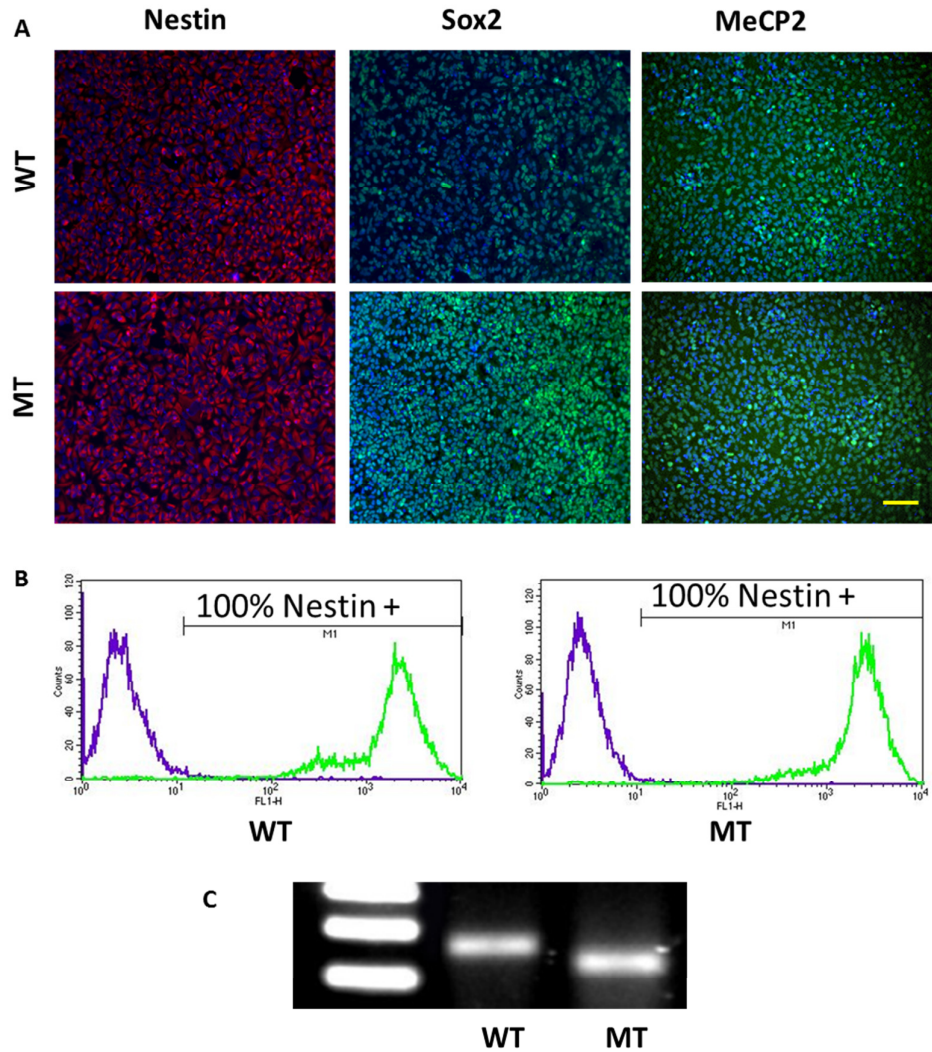


Fig 5.2 Characterisation of iPSCs-derived NPCs. (A) Immunocytochemistry showing positive staining with antibodies targeting Nestin, Sox2 and MeCP2 for both WT and MT NPCs. Scale bar represents 100 μ M. (B) FACS showing high percentage of nestin-positive cells for both WT and MT NPCs. Purple histograms represent no-primary antibody control while green histograms represent cells incubated with antibody. (C) RT-PCR showing respective clones retained their X-inactivation pattern after NPC induction.

5.3.2 Comparison of NPCs proliferation rate

Both human RTT patients and mouse models show microcephaly (Chen et al., 2001; Hagberg, 1995). One main cause of microcephaly in general is reduced proliferation of NPCs (Woods et al., 2005). We wanted to see if MeCP2 deficiency would affect NPCs proliferation. Cell proliferation assays were carried out using water-soluble tetrazolium salt 1 (WST-1) assay. This method is based on the enzymatic cleavage of WST-1 by viable cells to form a colorimetric dye as a proxy of cell number. Our results showed no significant differences in the proliferation rate between WT and MT NPCs (**Fig 5.3**). This suggests proliferation of NPCs is not likely to be the cause of microcephaly in RTT.

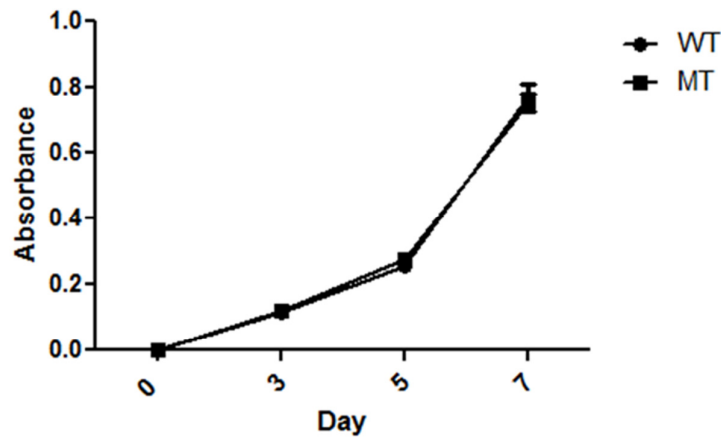


Fig 5.3 Proliferation rate of WT and MT NPCs. WST1 proliferation assay of WT and MT NPCs over 7 days.

5.3.3 iPSCs-derived NPCs show defect in cell migration

As cell migration is an important aspect of NPCs during brain development and abnormal migration is the cause of many brain disorders (Valiente and Marin, 2010), we wanted to determine if cell migration is affected in MT

NPCs. Neurospheres (aggregates of NPCs) of equal size were made and attached onto laminin coated plate. After 24 hours, the amount of migration was measured. We consistently observed a higher rate of distant migration in WT neurospheres compared to MT neurospheres (**Fig 5.4A**).

To confirm this phenotype was caused by deficiency of MeCP2, we performed RNA silencing of *MeCP2* in WT NPCs using a shRNA specific to *MeCP2* (Marchetto et al., 2010). Silencing of *MeCP2* caused a reduction of the migration rate of WT neurosphere compared to a control shRNA with a scrambled sequence (**Fig 5.4B**). We further performed RNA silencing of *MeCP2* in H9-derived NPCs and observed the same phenotype (**Fig 5.4C**). These results indicate that deficiency of MeCP2 causes reduced migration of NPCs.

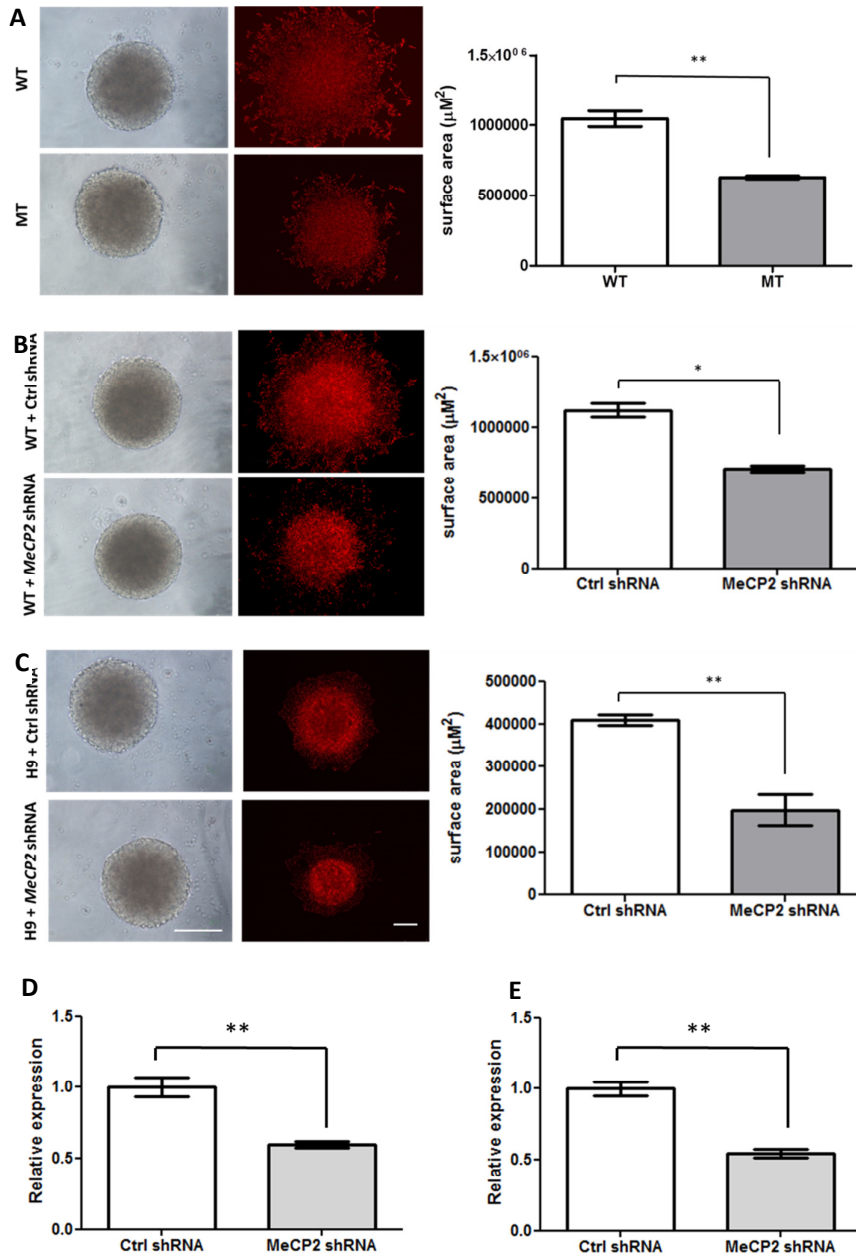


Fig 5.4 Migration rate of NPCs. (A-C) Left panel- Representative images of respective neurospheres before attachment and 24hrs after attachment, Right panel- graphical representation of respective neurospheres of surface area 24hrs after attachment (Mean \pm SEM, n=6, * p-value <0.05, ** p-value <0.01, unpaired t-test) . Efficiency of *MeCP2* silencing in (D) WT iPSCs-derived NPCs and (E) H9-derived NPCs (Mean + SEM, ** p-value <0.01, unpaired t-test). Scale bar represents 100 μM .

5.3.4 Non-cell autonomous effect of NPCs

As the human female RTT brain consists of a mix of WT and MT cells, we wanted to model the physiological cellular make-up by mixing WT NPCs with MT NPCs. We labeled WT NPCs with a red fluorescence protein (m-cherry) and MT NPCs with a green fluorescence protein (GFP), and mixed equal numbers of labeled WT and MT NPCs to form single neurospheres. We wanted to see whether cellular migration rates were affected by the mixing of WT and MT cells. In particular, we wished to see if the presence of the WT or MT NPCs influenced the migration rate of the other population. There could be four possible scenarios— the mixed cells will migrate: 1) similar to the MT cells, 2) have an intermediate migration rate, 3) similar to the WT and 4) the WT cells migrate faster leaving behind the MT cells (**Fig 5.5A**).

Mixing of WT and MT cells resulted in scenario 2 in which there is an intermediate rate of migration demonstrated by both cell types (**Fig 5.5B&C**). We also did not observe WT NPCs showing higher migration rate than MT NPCs in the mixed neurosphere (**Fig 5.5D**). This indicates that there is a non-cell autonomous effect of MT-NPCs on migration.

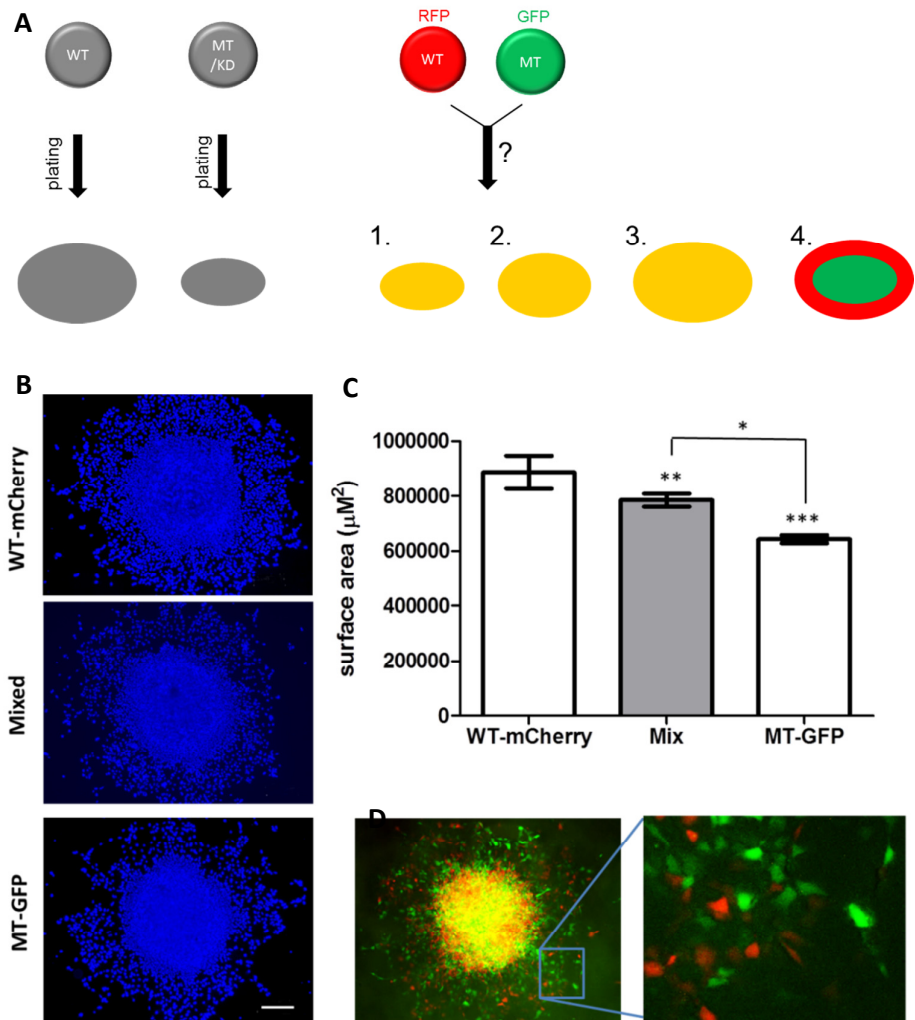


Fig 5.5 Coculture of WT and MT NPCs. (A) Mixture of WT-mCherry (red) and MT-GFP (green) NPCs into single neurospheres could show four different scenarios, 1. same size as MT only, 2. intermediate size between MT and WT, 3. same size as WT only or 4. WT cells moving at a faster rate compared to MT cells. (B) Representative images showing migration rate of WT, mixed and MT NPCs stained with DAPI. (C) Graphical representation of the migration rate of the three cell types (n=6, * p-value <0.05, ** p-value <0.01, *** p-value <0.001, 1-way ANOVA with post-hoc Tukey test). (D) Mixed cells showed equal rate of migration in a mixed population. Scale bar represents 100 μM .

5.3.5 Gene expression array of NPCs

The presence of MeCP2 as seen in immunostaining of NPCs indicates that MeCP2 might have a role in gene regulation (**Fig 5.2A**). Therefore, we carried out gene expression microarray to identify if there was any difference between WT and MT NPCs. The gene expression study of NPCs generated from isogenic iPSCs provided many valuable insights into the possible functions of MeCP2 in human NPCs. Analysis of the microarray signals revealed a list of 598 differentially expressed genes (DEG) (P-value <0.05; absolute fold change >2) (**Appendix 1**). Hierarchical clustering of the 598 DEG was performed to give an overview of relative expression value among the samples (**Fig 5.6**). The heat map generated revealed consistent gene expression patterns in WT NPCs versus MT NPCs, illustrating the reproducibility of the expression data (**Fig 5.6**). Of the 598 DEG, 283 genes were upregulated in MT NPCs while 315 genes were downregulated (**Appendix 1**). The top 15 up-regulated and down-regulated genes are shown in **Table 5.1 and Table 5.2**. The finding of both up- and down-regulation of transcripts support the evidence that MeCP2 can act as both a transcriptional repressor and activator (Yasui et al., 2007).

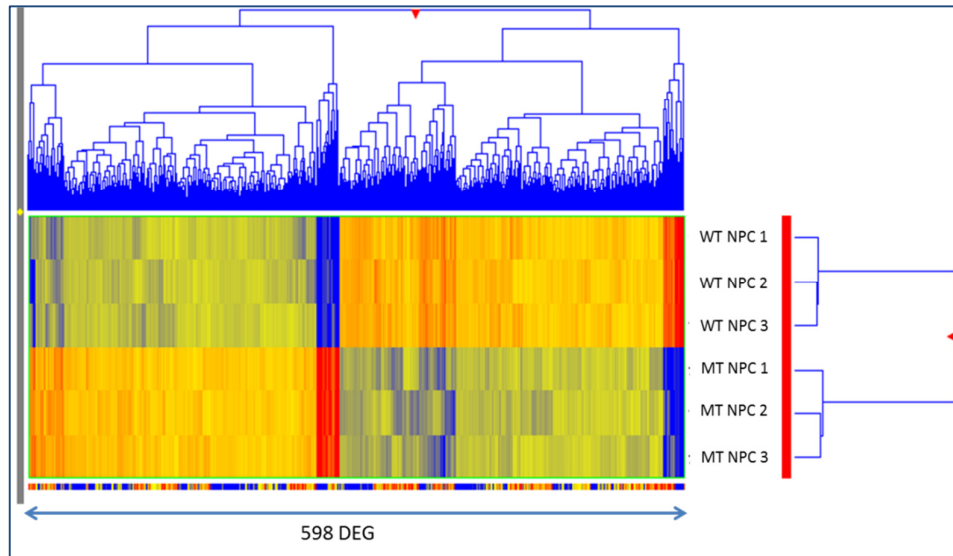


Fig 5.6 Heat map cluster analysis of microarray. 598 DEGs were identified between WT and MT NPCs

Table 5.1 Top 15 differentially up-regulated genes in MT iPSCs-derived NPCs based on fold change.

Symbol: Name	Fold Change
1. LOC647322: PREDICTED: hypothetical protein LOC647322	285.422
2. IRX2: iroquois homeobox 2	165.872
3. LOC100131139: PREDICTED: misc_RNA	139.184
4. TMEM132D: transmembrane protein 132D	118.460
5. CNTN6: contactin 6	96.343
6. FLJ30428: PREDICTED: hypothetical protein A230046P18; cDNA sequence BC055759	83.586
7. ZNF596: zinc finger protein 596	58.759
8. LOC653071: PREDICTED: Homo sapiens similar to CG32820-PA, isoform A	57.613
9. LOC654433: hypothetical LOC654433	49.022
10. FLJ30428: PREDICTED: hypothetical protein A230046P18; cDNA sequence BC055759,	41.580
11. C7orf54: chromosome 7 open reading frame 54 (C7orf54), mRNA.	38.918
12. LOC439936: PREDICTED: hypothetical gene supported by NM_173668	35.681
13. SNORD108: small nucleolar RNA, C/D box 108	28.849
14. EDN3: endothelin 3 (EDN3)	26.927
15. FLJ10246: PREDICTED: Homo sapiens FLJ10246	26.407

Table 5.2 Top 15 differentially down-regulated genes in MT iPSCs-derived NPCs based on fold change.

Symbol: Name	Fold Change
1. HOXB8: homeobox B8	-136.064
2. ZNF558: zinc finger protein 558	-135.323
3. TRIM16L: tripartite motif-containing 16-like	-95.642
4. PCDHB5: protocadherin beta 5	-86.977
5. MIMT1: MER1 repeat containing imprinted transcript 1 (non-protein coding)	-44.510
6. DLX5: distal-less homeobox 5	-43.991
7. ACBD5: acyl-Coenzyme A binding domain containing	-42.699
8. GATA2: GATA binding protein 2	-40.469
9. NTRK3: neurotrophic tyrosine kinase, receptor, type 3	-36.070
10. MARVELD3: MARVEL domain containing 3	-29.024
11. HOXB7: homeobox B7	-28.858
12. RPE65: retinal pigment epithelium-specific protein 65kDa	-27.307
13. GREM1: gremlin 1, cysteine knot superfamily, homolog (Xenopus laevis)	-26.219
14. AKAP14: A kinase (PRKA) anchor protein 14	-22.175
15. MMP9: matrix metalloproteinase 9 (gelatinase B, 92kDa gelatinase, 92kDa type IV collagenase)	-18.990

To validate the results of the microarray, real-time PCR of selected genes of interest including *Transmembrane protein 132D (TMEM132D)*, *Contactin 6 (CNTN6)*, *Sodium Channel, voltage-gated, type II alpha subunit (SCN2A)* and *Homeobox B8 (HOXB8)* was carried out (**Fig 5.7**). The result showed consistency with the microarray results (**Table 5.3**). A gene ontology (GO) analysis using DAVID Functional Annotation was performed (Huang da et al., 2009b). GO analysis (P-value <0.05) showed an enrichment of GO terms relating to neuron differentiation, neuron development and neurogenesis (**Table 5.4**).

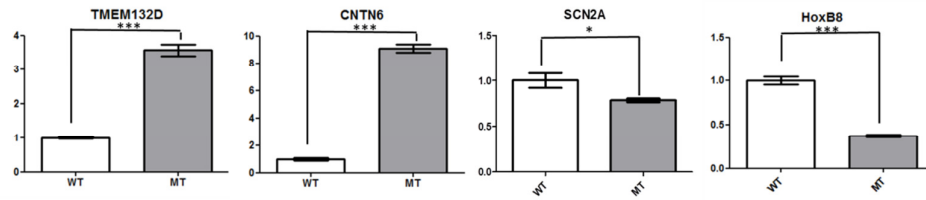


Fig 5.7 Real-time PCR validation of expression microarray. Each graph represents the relative fold difference of MT NPCs compared to WT NPCs (mean+SEM, * p-value<0.01, ***p-value<0.001, unpaired t-test).

Table 5.3 Comparison of microarray and real-time PCR fold changes of selected genes. Values are expressed as MT/WT fold change, with positive value denoting up-regulation and negative value denoting down-regulation in MT NPCs.

Gene	Microarray fold change	Real-time PCR fold change
TMEM132D	118.5	3.6
CNTN6	96.3	9.1
SCN2A	-3.1	-1.25
HOXB8	-136.1	-2.5

Table 5.4 Top 5 GO terms under biological processes identified among differentially expressed genes based on p-value using DAVID.

	GO ACCESSION	Gene Ontology Term (Biological Process)	p-value	No. of genes
1.	GO:0030182	Neuron differentiation	4.14E-08	30
2.	GO:0048666	Neuron development	9.30E-06	22
3.	GO:0050767	Regulation of neurogenesis	1.02E-05	15
4.	GO:0060284	Regulation of cell development	2.73E-05	16
5.	GO:0051960	Regulation of nervous system development	5.24E-05	15

5.3.6 Neuronal differentiation of NPCs

It was reported in the RTT mouse model that *Mecp2* deficient neurons showed reduced excitatory synapse numbers (Chao et al., 2007). We wanted to see if MT neurons could recapitulate this phenotype. To generate neurons, we carried out spontaneous differentiation of the NPCs by withdrawal of bFGF from the culture medium. Under this condition, NPCs generated cells with neuronal morphology with positive β -tubulin III immunostaining (**Fig 5.8A**). Both WT and MT NPCs were able to generate neurons at similar efficiencies

(**Fig 5.8B**). These results demonstrate that both WT and MT NPCs from P72 were able to generate neurons.

To check for synapse numbers, we stained our iPSCs-derived neurons with an excitatory pre-synaptic marker, vGlut1 and a dendritic marker, Map2 and quantified the numbers of vGlut1 puncta. We found that similar to the mouse model, MT neurons displayed reduced synapse numbers (**Fig 5.8C&D**). These results demonstrated that human iPSCs could recapitulate the neuronal phenotype seen in the mouse model. Together with findings from mouse studies (Chao et al., 2007) and human iPSCs models (Marchetto et al., 2010), these results support the evidence that MeCP2 regulates glutamatergic synapse density.

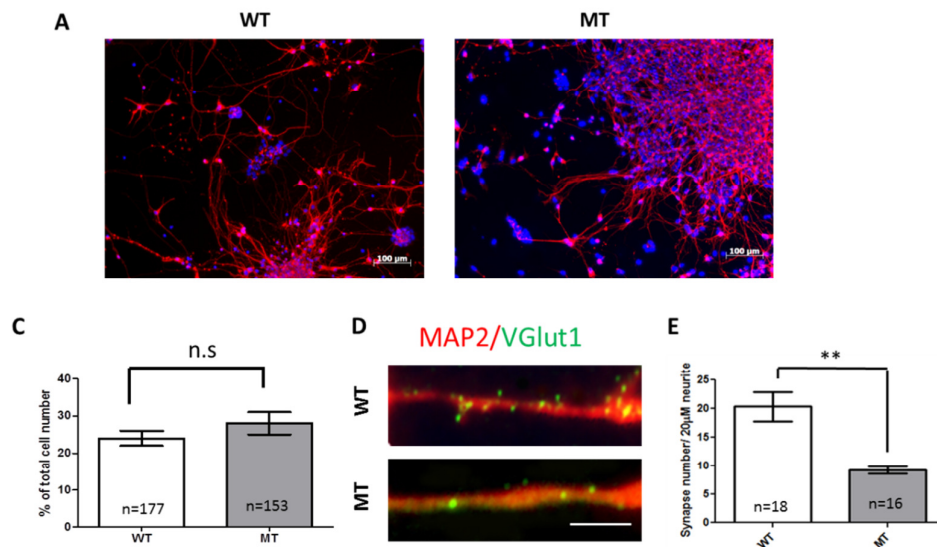


Fig 5.8 Differentiation of NPCs into neurons (A) Representative images β III-tubulin staining of WT and MT neurons. (B) Patch-clamp electrophysiology showed action potential in both WT and MT neurons. (C) Graphical representation of efficiency of differentiation of WT and MT NPCs into neurons (mean \pm SEM, unpaired t-test). (D) Representative images of WT and MT neurons stained with Map2 and vGlut1 (E) Graphical representation of synapse number counted in WT and MT neurons (mean \pm SEM, ** p-value < 0.01, unpaired t-test).

5.4 Discussion

5.4.1 iPSCs from RTT patients can be induced into NPCs and neurons

Disorders affecting brain development have been modeled mainly in mouse due to the difficulty in getting human neuronal cells. However, differences between the mouse and human brain may not lead to faithful recapitulation of development and diseases (Fietz and Huttner, 2011; Lui et al., 2011). To circumvent these hurdles, we attempted to model RTT using iPSCs. However, it was unknown if iPSCs with *MeCP2* deficiency could be induced into NPCs and differentiated into neurons. In this chapter, I describe the generation of NPCs from isogenic WT and MT iPSCs from a RTT patient. We used the SFEB method which is well-defined and follows the in vivo development pattern. Both WT and MT iPSCs can generate NPCs with equal efficiency. During the course of this study, several publications came out detailing the use of iPSCs to study RTT (Ananiev et al., 2011; Cheung et al., 2011; Kim et al., 2011; Marchetto et al., 2010). These studies report the successful generation of NPCs from RTT iPSCs confirming our result that *MeCP2* is not involved in NPCs formation. However, none of these studies examined the NPCs in detail. We therefore took the opportunity to further investigate the effects of *MeCP2* deficiency in NPCs.

5.4.2 MT NPCs show migratory defects

Both WT and MT NPCs proliferated equally well, but we found that MT NPCs did not migrate as well as WT NPCs. During brain development, neural stem/progenitor cells undergo several steps, including migration and

positioning before they establish the proper connections to form the mature brain. Migration is thus an important process of brain development. Our finding that NPCs showed reduced migration demonstrates a cellular mechanism that may occur in RTT NPCs.

While this has not been shown, one possible way migration defects in NPCs could affect RTT patients is through structural malformation of the brain. Structural brain defects are not seen in female RTT patients, but a post-mortem brain study of a male subject with a *MeCP2* mutation, presenting with severe neonatal encephalopathy showed polymicrogyria (Geerdink et al., 2002). In this case, structural defects may be more apparent in males due to our observation that in a mixed culture of WT and MT NPCs, the migration rate of mixed NPCs is increased indicating that non-cell autonomous effects are incurring. This might allow female patients to compensate for the migration defect to a certain extent. This also provides a reasonable explanation of why males with *MeCP2* mutations show early and severe defects in brain functions as they lack this compensatory mechanism. Non-cell autonomous effects in *MeCP2* deficiency cells have been reported in other cell types. For example, mice WT neurons showed abnormal dendritic arborisation when grown in an environment consisting of *Mecp2*-null neurons (Belichenko et al., 2009; Kishi and Macklis, 2010). In female RTT patients, WT neurons were also noted to have lower expression of *MeCP2* compared to non-affected control subjects (Braunschweig et al., 2004). Mice WT astrocytes also showed reduced *Mecp2* levels when co-cultured with *Mecp2*-null astrocytes (Maezawa et al., 2009). These findings and our observation of non-cell autonomous effects in NPCs highlights the significance of X-chromosome skewing ratio.

These evidences suggest that treatment or recovery of a percentage of afflicted cells may be enough to have an effect and have important implications for RTT patients.

It is also not known if defects in NPC migration would lead to defective neuronal migration. As NPCs are precursors to neurons, they represent a different developmental stage to that of neurons. If NPCs' positioning in the brain is affected, then it is reasonable to assume that the neurons position will be affected too. However, there is no evidence of this. But abnormal neuronal migration has been shown to be affected in RTT rodent models of *CDKL5* deficiency (Chen et al., 2010a; Ricciardi et al., 2012). Mutations in *CDKL5* lead to neurological symptoms that resembles RTT suggesting that *CDKL5* and *MeCP2* may have overlaps in the same pathway/s (Archer et al., 2006; Scala et al., 2005; Tao et al., 2004; Weaving et al., 2004). Silencing of *CDKL5* in rodent NPCs has been shown to result in delayed neuronal migration in cortical regions of both embryonic brain and post-natal day 0 pups brain suggesting deficiencies of *CDKL5* affects early brain development (**Fig 5.9**) (Chen et al., 2010a; Ricciardi et al., 2012). In agreement, RTT patients with *CDKL5* mutations typically show early-onset seizures in the first three months after birth indicating early brain dysfunction. Our observations support the evidence that migration abnormalities may be a cellular pathology of RTT.

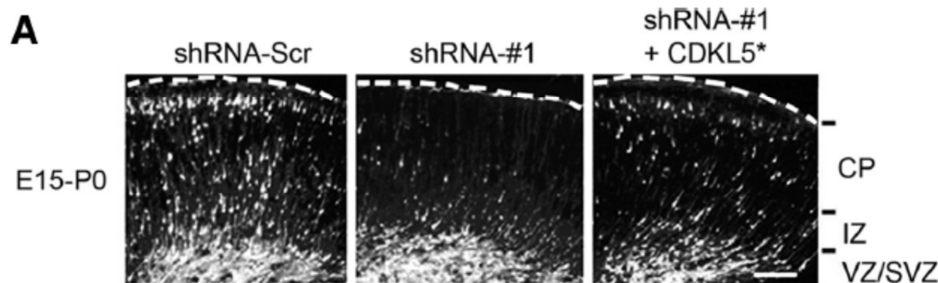


Fig 5.9 Migration defects in *CDKL5* mouse model of RTT. Neural progenitors electroporated with a shRNA against *CDKL5* displayed a delayed migration of neurons from the ventricular zone/ subventricular zone (VZ/SVZ) into the intermediate zone (IZ) and cortical plate (CP). (Right panel) Exogenous expression of WT *CDKL5* was able to partially rescue this phenotype. Image reproduced with permission from (Chen et al., 2010a).

5.4.3 Gene expression study revealed several genes differentially regulated in MT NPCs

Our gene microarray results revealed several differences between WT and MT NPCs and provide a few clues as to what could be behind the migration abnormality observed. For example, the contactin protein, *CNTN6* (up in MT), is a neural cell-adhesion molecules in which a gain of *CNTN6* copy number variation (CNV) was found in ASD patients (van Daalen et al., 2011; Zuko et al., 2013). A mouse model of autism in which the contactin associated protein, *CNTNAP2* was knocked-out displayed neuronal migration abnormality (Penagarikano et al., 2011). This indicates that the contactins and their associated proteins play crucial roles in migration and ASD. Another gene, *DLX5* (down in MT) has been reported to be involved in migration of neurons in which *DLX5/6* double knock-out mouse showed reduced migration of interneurons (Wang et al., 2010). *DLX5/6* has been reported to be regulated by MeCP2 (Horike et al., 2005; Miyano et al., 2008), although there have been conflicting findings (Schule et al., 2007).

Besides genes involved in migration, other genes were identified that have links to autism and/or RTT-related neurological symptoms. *TMEM132D* (up in MT) encodes for a transmembrane protein that has been found to be upregulated in patients with anxiety disorder though the function of the protein remains unknown (Erhardt et al., 2011). Both RTT patients and mouse model have been reported to show heightened anxiety (Mount et al., 2002; Ren et al., 2012; Sansom et al., 1993). Another target identified, *SCN2A* (down in MT), encodes a sodium channel subunit which has been implicated in overlapping RTT symptoms such as epilepsy, ASD and stereotypic behavior (Kearney et al., 2001; Weiss et al., 2003). The *HOXB8* gene has been reported to be expressed in the neural tube (Deschamps and Wijgerde, 1993) and *Hoxb8* mouse knockout has been observed to exhibit self-injurious behavior caused by compulsive grooming (Chen et al., 2010b; Greer and Capecchi, 2002). Self-injurious behavior has been observed in RTT patients (Iwata et al., 1986; Oliver et al., 1993) while compulsive grooming has been observed in a RTT mouse model (Chao et al., 2010). Further investigation of these genes may help us understand the molecular targets of *MeCP2*.

We further performed pathway analysis to identify what biological processes might be affected. The pathway studies show enrichment of pathway relating to neuronal differentiation and development. A closer look at the genes behind these pathways included a number of genes that are involved in neural progenitor movement such as *C-X-C motif chemokine 12 (CXCL12)* (Holgado et al., 2013), *L1 cell adhesion molecule (L1CAM)* (Kishimoto et al., 2013; Tonosaki et al., 2014), *GATA binding protein 2 (GATA2)* (Willett and Greene, 2011) and *Neurogenin 2 (NEUROG2)* (Heng et al., 2008). While these genes

remain to be validated, they support the notion that MeCP2 is involved in the early stages of neuronal development, especially migration. Further studies on these target genes could help us to understand the role of NPCs in RTT.

5.4.4 MT neurons have reduced synapse numbers

We further demonstrated that both WT and MT NPCs can be differentiated into neurons. In the mouse model, neurons showed reduced synapse numbers (Chao et al., 2007). We attempted to recapitulate the phenotype using iPSCs and showed that MT iPSCs-derived neurons display a similar reduction of synapse phenotype. This result supports similar findings from another iPSCs study (Marchetto et al., 2010). In contrast, we did not observe a reduced differentiation to neurons as reported by (Kim et al., 2011). One reason could be the different quality of iPSCs obtained as explained in section 4.4.1.

5.5 Conclusions

In summary, I described the induction of NPCs from isogenic iPSCs from a RTT patient. MT NPCs showed a reduced migration rate. Gene expression array of NPCs identified several novel genes that may be involved in RTT. Neurons differentiated from MT NPCs showed reduced synapse density.

5.6 Limitations

5.6.1 More patients' samples needed

Only iPSC lines from P72 were used here. RTT patients differ from one another in the range and severity of symptoms. These differences partially stem from differing mutations of the *MeCP2* gene and different genetic

backgrounds (i.e. modifier genes). Since the finding in this thesis may represent the disease in one patient, it would be beneficial to reproduce these experiments in iPSCs lines from additional patients. The strategy was to first determine the phenotype to be studied using iPSC lines from one patient before extending the findings to other patients. However, the experiments from more patients (P48 and P80) could not be completed in time for this thesis.

5.6.2 Rescue of migration phenotype

The results in **section 5.3.3** showed that MT NPCs had a slower migration rate. This phenotype was replicated when MeCP2 was silenced in WT NPCs and H9 hESC line. To further confirm that this phenotype is caused by MeCP2, a rescue experiment of MT NPC using exogenous WT MeCP2 should be performed. However, this experiment was not performed in time for this thesis.

5.6.3 Non-cell autonomous effect of NPCs

Section 5.3.4 showed that a mixture of WT and MT NPCs resulted in an intermediate migration rate between that of pure WT and pure MT NPCs. An important control for this experiment is to do a reciprocal experiment to label MT NPCs with mCherry and WT NPCs with GFP. Also, a mix of WT/WT cells and MT/MT cells is important to ensure that the phenotype observed is not due to non-specific effects caused by labelling of the NPCs. However, these controls were not performed in time for this thesis.

As WT and MT NPCs are labeled accordingly with red and green fluorescent tag, we did not observe an accumulation of one colour around the perimeter of

the sphere as depicted in **Figure 5.5A**. Hence, for this part, we did not do an in-depth quantification of the migration rate. However, further quantification of the migration rate is possible by measuring the direct distance of individual WT (blue line) or MT cells (white line) from the center of the sphere (**Fig 5.10**). This would give a more accurate measurement of migration rate of the cell populations.

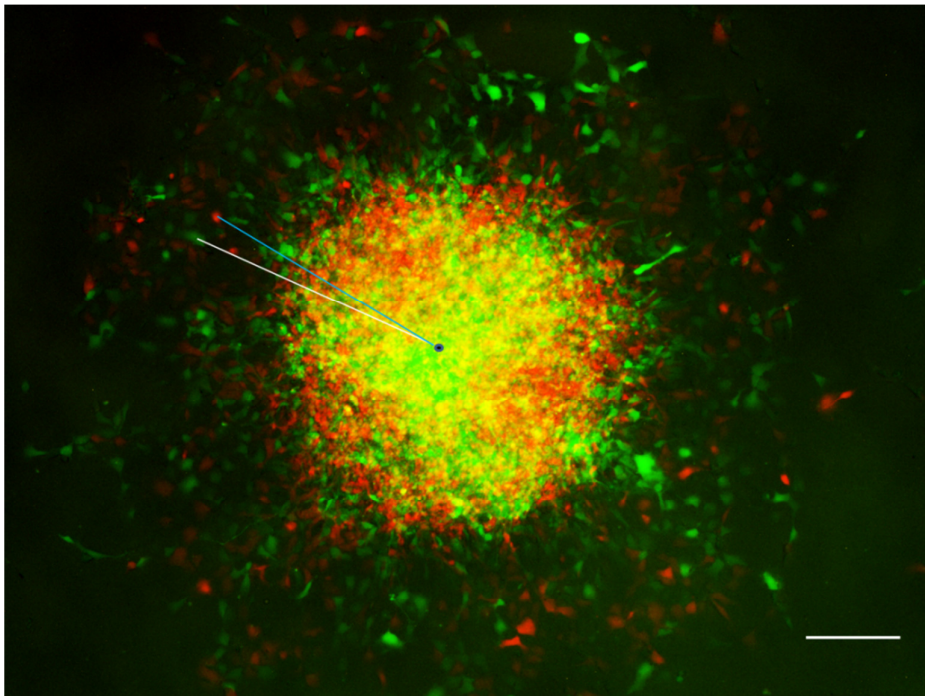


Figure 5.10 Measurement of migration rate. The distance migrated by different cell populations can be measured by measuring the distance of the individual WT (blue line) or MT (white line) cells from the center of the sphere. Scale bar represents 100 μ M.

Chapter 6: Investigating the role of astrocytes in RTT using iPSCs

6.1 Introduction

Early studies of RTT were focused on neurons as astrocytes were not found to express *Mecp2* (Kishi and Macklis, 2004; Shahbazian et al., 2002b). This notion was challenged when improved sensitivity in immunostaining methods detected the presence of *Mecp2* in rodent astrocytes and that they could play a role in RTT pathology (Ballas et al., 2009; Maezawa et al., 2009; Nagai et al., 2005). Ballas et al., 2009 reported neurotoxic effects of astrocytes isolated from *Mecp2*-null mice when co-cultured with WT hippocampal neurons (Fig 6.1A&B)(Ballas et al., 2009). Further investigations revealed that conditioned medium (CM) from *Mecp2*-null astrocytes had the same detrimental effects and that a mixture of CM from *Mecp2*-null and WT astrocytes could not abrogate this effect (Fig 6.1C). This suggested the presence of one or more neurotoxic factors secreted by *Mecp2*-null astrocytes.

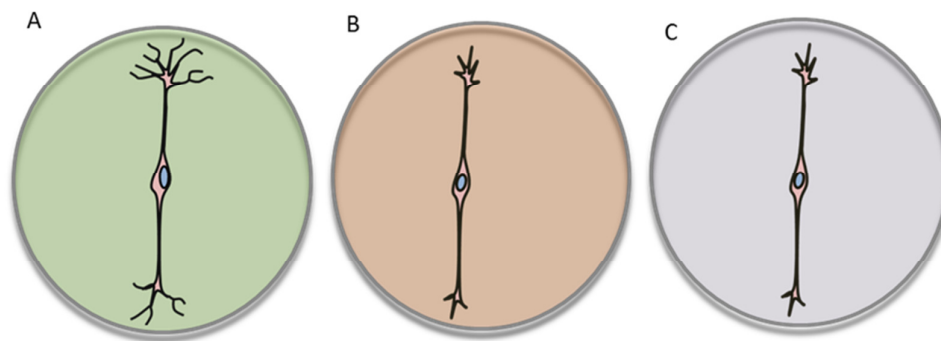


Figure 6.1 Mouse model of RTT astrocytes. (A) WT neurons develop elaborate dendrites in CM from WT astrocytes. (B) WT neurons showed stunted dendritic growth in CM from *Mecp2*-null astrocytes. (C) WT neurons showed stunted dendritic growth in CM mixed from WT and *Mecp2*-null astrocytes.

Maezawa et al., 2009 similarly reported that astrocytes from *Mecp2*-null mice showed less dendritic induction of WT neurons in co-culture experiments.

Mecp2-null astrocytes also showed reduced proliferation, had lower BDNF expression and abnormal cytokine secretions. Curiously, the authors observed that co-culture of WT astrocytes with *Mecp2*-null astrocytes led to reduction of *Mecp2* levels in WT astrocytes. They hypothesized that the presence of *Mecp2*-null astrocytes mediated a reduction of *Mecp2* levels in WT astrocytes and showed that gap junctions played a role in mediating this reduction. This suggested a non-cell autonomous effect of astrocytes in which MT astrocytes reduced the levels of *Mecp2* in WT astrocytes.

The role of astrocytes in the pathology of RTT was further highlighted in a KO mouse model in which *Mecp2* expression was inducible only in astrocytes (using a GFAP promoter) in an otherwise global KO (Lioy et al., 2011). Induction of *Mecp2* expression in astrocytes led to increased longevity (>2.5x longer), better overall health score, increased movement and reversal of respiratory ailments (Lioy et al., 2011). In the same study, the converse mouse model in which *Mecp2* was deficient only in astrocytes resulted in mice with smaller body size, clasped hindlimb phenotype and respiratory abnormalities though other RTT phenotypes such as lifespan, movement and anxiety related behaviours were not affected (Lioy et al., 2011). These findings demonstrated that astrocytes alone can contribute to the RTT pathology in mouse.

6.2 Hypotheses and Aims

The studies in the mouse model suggested that astrocytes play a role in the pathology of RTT. However, due to inter-species differences between mouse and human, it remained unclear if human RTT astrocytes also contribute to disease pathology. My hypothesis is that human astrocytes play a role in the

pathology of the disease. To investigate this further, I decided to develop a protocol to differentiate astrocytes from human iPSCs. To determine the astrocytic identity, markers and functional assay would be carried out.

Studies in mice indicated that medium conditioned from *MeCP2*-null astrocytes resulted in stunted growth of neurons. As astrocytes play important roles in the regulation of the inflammation status of the brain through secretions of cytokines, my hypothesis is that astrocytes could contribute to sub-optimal neuronal health through abnormal secretion of cytokines. To test this hypothesis, I decided to collect conditioned medium from both WT and MT iPSC-derived astrocytes and measured their cytokine levels to determine if cytokine levels are different between the two.

Another important astrocyte function is in the regulation of brain metabolic functions. Astrocytes are known to take up glucose and convert it to lactate as an energy supply to neurons. Hence deficiencies in these functions could result in suboptimal neuronal function. My hypothesis is that MT astrocytes could contribute to RTT pathology through deficiencies in support of brain metabolic functions. To test this hypothesis, I decided to test if glucose uptake is affected in MT astrocytes.

To further shed light on the possible effects of *MeCP2* mutations on astrocytes, I decided to look at the gene expression of WT astrocytes vs MT astrocytes. My hypothesis is that *MeCP2* being a transcriptional regulator, have an effect on astrocytes' gene expression. To test this hypothesis, I decided to carry out a microarray to detect differences in gene expression between WT and MT astrocytes.

6.3 Results

6.3.1 Derivation of astrocytes from human iPSCs

WT and MT iPSC lines from P72 were used to derive astrocytes. Due to the lack of established protocols for deriving astrocytes from iPSCs at the time this project commenced, a novel protocol was developed (**Fig 6.2A**). First, the NPCs described in chapter 5 were allowed to undergo spontaneous differentiation by withdrawal of bFGF. In the early phase, NPCs differentiated mainly into neurons with few astrocytes around (**Fig 6.2B&C**). Due to the fact that neurons are post-mitotic cells and astrocytes are proliferative cells, long term culture of these cells will result in expansion of astrocytes without corresponding increase in neuronal numbers. As neurons are less adhesive than astrocytes, gentle pipetting resulted in detachment of neurons while astrocytes remained attached (**Fig 6.2D-F**). Using this method, homogenous populations of astrocytic-like cells were derived and expanded (**Fig 6.2G**). Both WT and MT NPCs were able to generate astrocytes. This indicated that WT and MT iPSCs from P72 can be differentiated into astrocytes.

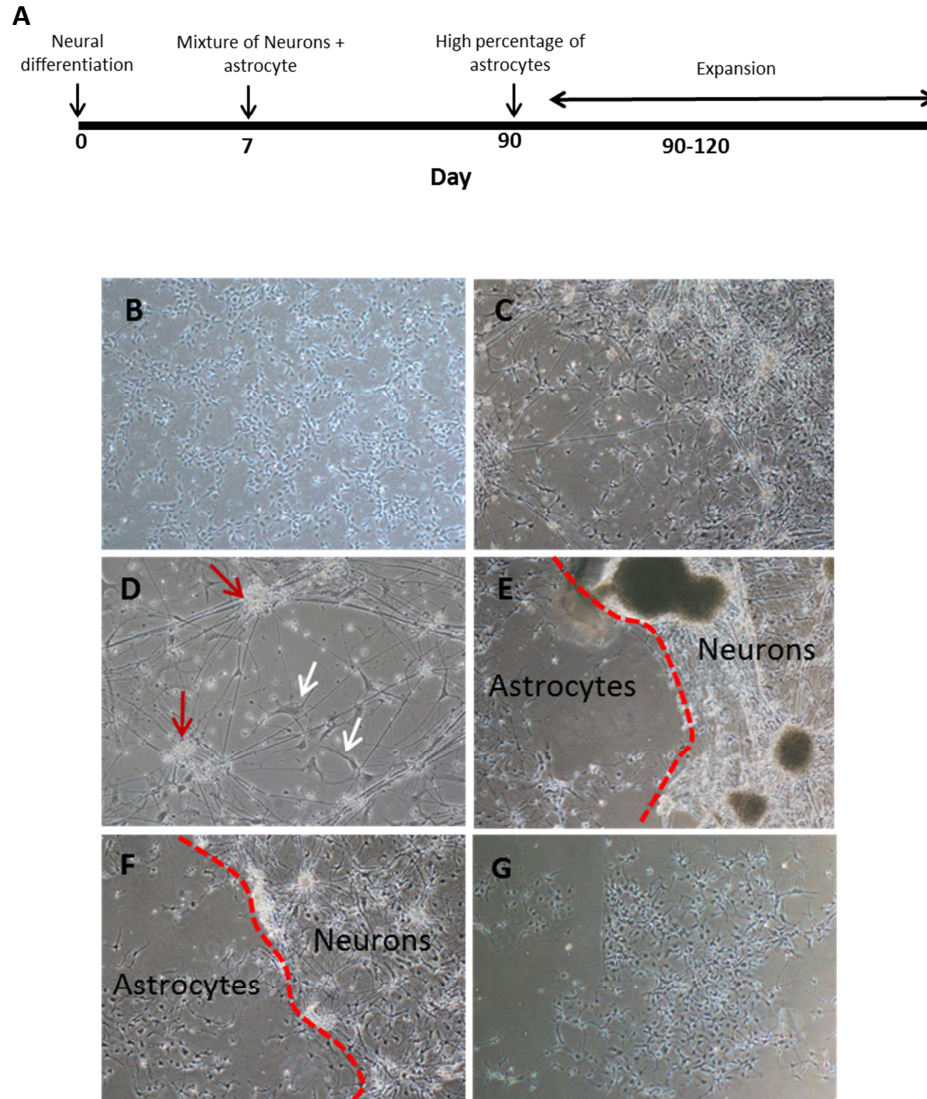


Fig 6.2 Derivation of astrocytes from iPSCs. (A) Schematic of astrocyte differentiation from NPCs. (B-G) Representative pictures of cells at various stages of the protocol with (B) day 0 showing undifferentiated NPCs (C) day 7 showing differentiation of NPCs into mainly neurons, (D) day 90 showing mixture of neurons (red arrows) with astrocytes (yellow arrows). (E) and (F) Neurons can be gently detached leaving behind patches of astrocytes. Red broken line depict border of neuron detachment. (G) Pure population of astrocytes is left behind after detachment of neurons. Scale bar represents 100 μ M.

6.3.2 Characterisation of iPSCs-derived astrocytes

To confirm the astrocytic identity of these cells, immunocytochemistry was carried out using 2 commonly used astrocyte markers, GFAP and S100 β (Brozzi et al., 2009; Raponi et al., 2007; Reubinoff et al., 2001; Zhang et al., 2001). Both WT and MT astrocytes showed strong immuno-reactivity to GFAP and S100 β although MT astrocytes appear to have less GFAP+ve cells (**Fig 6.3A**). However, this could be due to a lower proliferation rate (see **section 6.3.3**) as flow cytometry showed a high percentage of the isolated cell population was GFAP positive (**Fig 6.3B**).

To determine if the iPSC-derived astrocytes are functional, we carried out a glutamate uptake assay as glutamate uptake is a key characteristic of astrocytes (Schousboe and Waagepetersen, 2005). 100 μ M of glutamate was added to astrocyte cultures and the amount of glutamate remaining was measured over a three hour period. Both WT and MT iPSC-derived astrocytes showed an ability to take up glutamate and we did not observe a significant difference between the two (**Fig 6.3C**). This indicates that iPSC-derived astrocytes are functional and MT astrocytes derived from P72 do not show a defect in glutamate uptake.

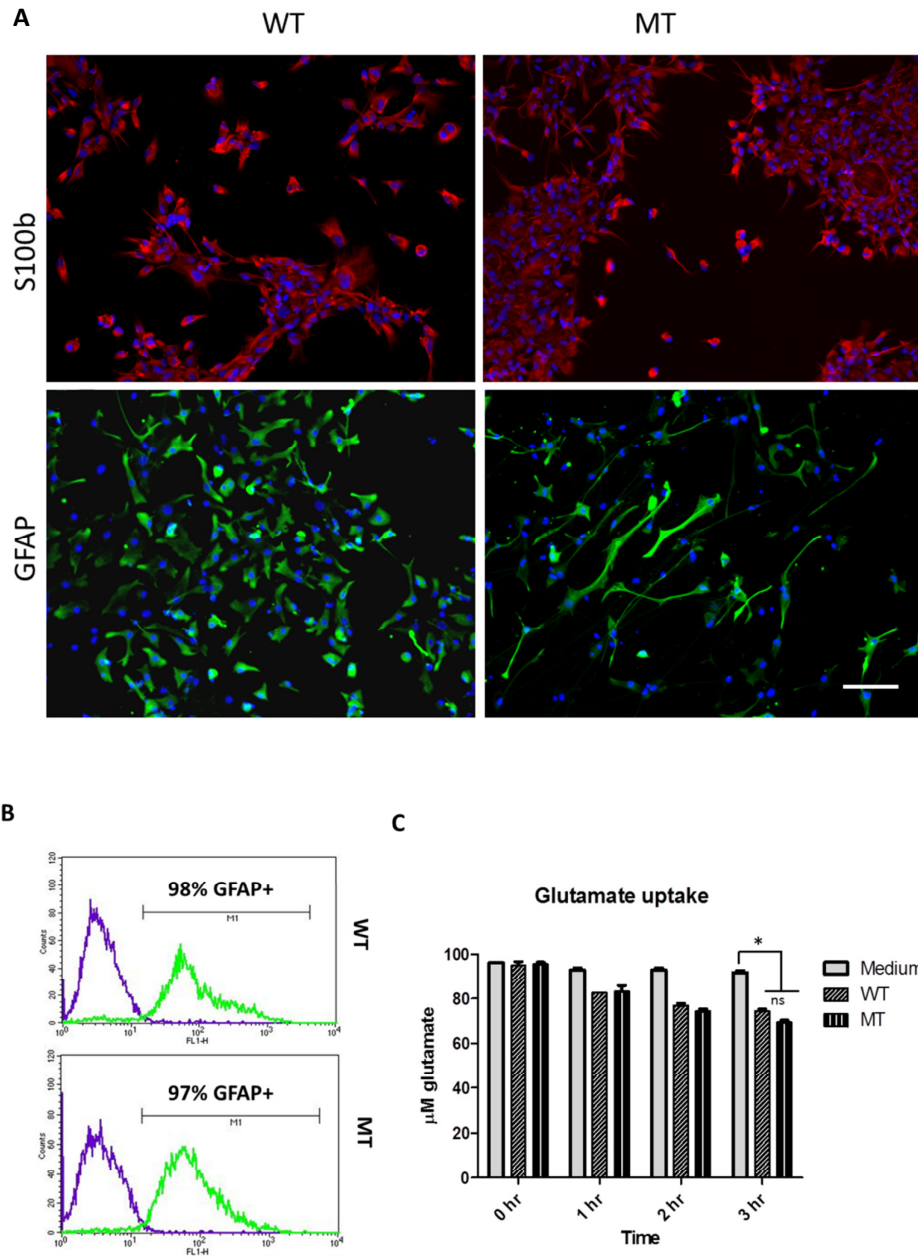


Figure 6.3 Characterisation of iPSCs-derived astrocytes. (A) Immunocytochemistry of WT and MT iPSCs-derived astrocytes showed positive GFAP and S100b staining. (B) FACS showed high percentage of GFAP positive cells (C) Glutamate uptake assay showed both WT and MT iPSCs-derived astrocytes were able to take in glutamate over a 3 hr time period (mean \pm SEM, n= 3, * p-value <0.05, 1-way ANOVA with post-hoc Tukey test). Scale bar represents 100 μM .

6.3.3 Proliferation and metabolic profile of iPSCs-derived astrocytes

During the course of maintaining the astrocytes, it was observed that MT astrocytes proliferated at a slower rate compared to WT astrocytes. To investigate further, a WST-1 proliferation assay was performed. This assay is based on the cleavage of the stable tetrazolium salt WST-1 by metabolically active cells to form a colourimetric reaction. The results showed that MT astrocytes proliferated at a slower rate compared to WT astrocytes (**Fig 6.4**). This appeared to be an astrocyte specific phenotype as no differences were observed in the respective NPCs (see chapter 5).

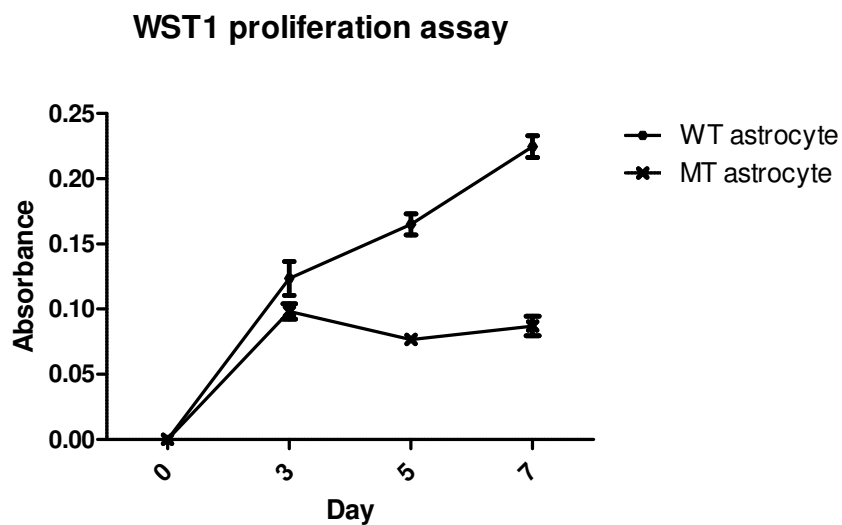


Fig 6.4 Proliferation assay of astrocytes. MT astrocytes showed reduced proliferation compared to WT astrocytes.

We next looked at astrocyte energy metabolism. The brain is a high energy-consuming organ. It takes up 20% of total body energy in a resting state despite being only 2% of total body weight. Glucose is regarded as the main energy source for the brain (Sokoloff, 1977), and increasing evidence show that glucose is taken up by astrocytes which then provide neurons with lactate

as a metabolite substrate in times of neuronal activity (Chuquet et al., 2010; Pellerin et al., 1998; Rouach et al., 2008). As astrocytes play an important role in neuronal metabolism, we wanted to see if MT astrocytes are abnormal in this aspect.

We looked at the glucose uptake capability of the astrocytes. To compare glucose uptake between WT and MT astrocytes, a fluorescent glucose analog 2-(*N*-(7-Nitrobenz-2-oxa-1,3-diazol-4-yl)Amino)-2-Deoxyglucose (2-NBDG) was used. 2-NBDG was added to astrocyte culture and incubated for ½ - 2 hours before performing flow cytometry. Fluorescence intensity corresponds directly to uptake of 2-NBDG levels in this assay. ½ hour incubation showed WT astrocytes displaying higher fluorescence intensity compared to MT astrocytes (**Fig 6.5A**). This indicates that WT astrocytes internalized a higher amount of 2-NBDG in that time. A longer incubation time 1 and 2 hours showed overlapping FACS histogram profiles indicating that both WT and MT astrocytes took in an equal amount of 2-NBDG (**Fig 6.5B**). These results showed that both WT and MT astrocytes could take in glucose but MT astrocytes displayed an initial delayed response compared to WT astrocytes. This result suggests MT astrocytes might be deficient in brain energy metabolism.

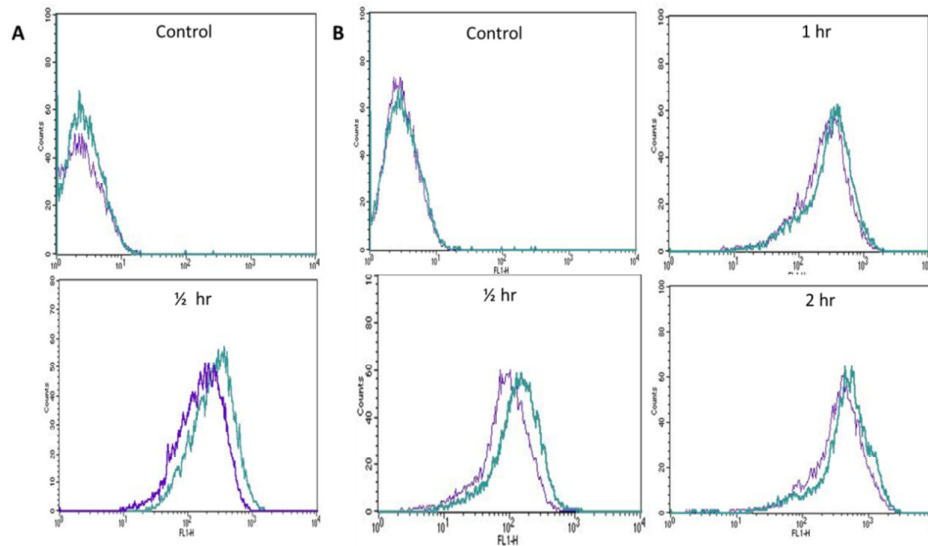


Fig 6.5 FACS profile of 2-NBDG uptake by astrocytes. (A) Experiment 1; Control shows WT astrocytes (green) and MT astrocytes (purple) having same amount of background fluorescence before addition of 2-NBDG , 1/2 hr incubation with 2-NBDG resulted in WT astrocytes showing higher fluorescence compared to MT astrocytes. (B) Experiment 2; Incubation of 2-NBDG for 1/2 hour reproduced the same result as in experiment 1. Further incubation for 1 hour and 2 hours showed WT and MT astrocyte having almost over-lapping fluorescence profile.

6.3.4 Cytokine profiling of astrocyte

Astrocytes play a key role in neuroinflammation through secretions of cytokines (Aloisi et al., 1995; Lieberman et al., 1989). Hence, we decided to carry out cytokine profiling of the iPSCs-derived astrocytes to see if MT astrocytes are abnormal in cytokine secretions. Cytokine detection typically relies on the ELISA method but the Luminex platform offers several advantages such as improved sensitivity, multiplexing and comparatively higher throughput (Burkert et al., 2012; Elshal and McCoy, 2006). We therefore decided to assess the cytokine profiles of astrocytes using the Luminex platform. To determine the levels of cytokines secreted by astrocytes, CM from astrocyte culture was collected after 24 hours of culture. To ensure

equal cell numbers, cell number was determined before and after medium collection. Non-conditioned medium was used to normalize for background levels.

The secretion levels of 14 cytokines were investigated (**Table 6.1**). These cytokines were selected based on whether they are known to be secreted by primary astrocytes. Of the cytokines, MCP-1, M-CSF and PDGF-AA were found to highly secreted (>100 pg/mL) (**Table 6.2**). Fractalkine, GRO, IL-8, IP-10, Lif, SCF and VEGF were moderately secreted (1-30 pg/mL). The rest of the cytokines (IL-10, IL-17, MIP-1A and TNF- α) were undetectable. This could be due to the conditioning time being too short or that the iPSCs-derived astrocytes do not secrete these cytokines.

Table 6.1. List of cytokines used in this study

Cytokine	Gene name	Produced by astrocyte	Ref
Fractalkine	CX3CL1	Yes	Maciejewski-Lenoir, Chen et al. 1999; Mizuno, Kawanokuchi et al. 2003
GRO	CXCL1	Yes	Rubio and Sanz-Rodriguez 2007
IL-8	CXCL8	Yes	Kutsch, Oh et al. 2000; Burkert, Moodley et al. 2012
IL-10	IL10	Yes	Burkert, Moodley et al. 2012
IL-17	IL17A	Yes	Tzartos, Friese et al. 2008
IP-10	CXCL10	Yes	Bhowmick, Duseja et al. 2007; Burkert, Moodley et al. 2012
Lif	LIF	Yes	Aloisi, Rosa et al. 1994
M-CSF	CSF1	Yes	Fischer and Bielinsky 1999; Schilling, Nitsch et al. 2001
MCP-1	CCL2	Yes	Burkert, Moodley et al. 2012
MIP-1A	CCL3	Yes	Burkert, Moodley et al. 2012
PDGF-AA	PDGFA	Yes	Pringle, Collarini et al. 1989
SCF	SCF	Yes	Genis, Davila et al. 2014
TNF-a	TNF	Yes	Maezawa, Swanberg et al. 2009; Burkert, Moodley et al. 2012
VEGF	VEGF	Yes	Argaw, Asp et al. 2012

Among the secreted cytokines analysed, M-CSF showed lower levels in MT astrocyte (p-value 0.005) (**Fig 6.6**). Other notable differences included iL-8, Fractalkine, SCF and VEGF (**Table 6.2**). However, as the detected levels were quite low (<10 pg/mL), these differences were not considered meaningful. We therefore decided to increase the amount of time for conditioning the medium to 72 hours to see if the previously undetected cytokines would be detected and if a longer conditioning time might reveal further differences.

Table 6.2. Fold differences of cytokines at 24 hours between WT and MT astrocytes. ND (Not Detected) * (statistical significance).

Cytokine	WT iPSC-derived astrocyte (pg/mL)	MT iPSC-derived astrocyte (pg/mL)	WT/MT ratio
Fractalkine	3.405	4.51	0.75
GRO	1.225	1.35	0.90
IL-8	2.41	1.645	1.47
IL-10	ND	ND	-
IL-17	ND	ND	-
IP-10	7.16	7.865	0.91
Lif	19.94	26.42	0.75
M-CSF	2911.81	2015.175	1.44**
MIP-1	ND	ND	-
MCP-1A	11769.975	10355.075	1.14
PDGF-AA	165.915	152.615	1.09
SCF	0.51	2.19	0.23
TNF- α	ND	ND	-
VEGF	4.83	9.925	0.49

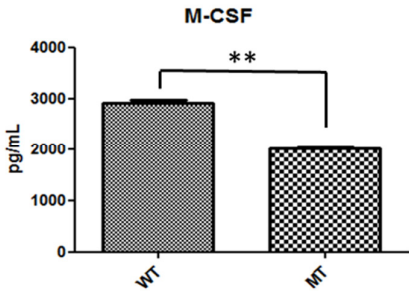


Fig 6.6 Cytokine profiling of WT and MT iPSCs-derived astrocyte at 24 hours. MT astrocyte showed significantly lower M-CSF level (mean \pm SD, n= 2, ** p-value <0.01, unpaired t-test).

At 72 hours, cytokines that were not detected at 24 hours remained undetected (IL-10, IL-17, MIP-1A and TNF- α) (**Table 6.3**). This could mean that either the iPSCs-derived astrocytes do not secrete these cytokines under the condition used or that the detection method is incompatible with this assay. Comparatively, MCP-1, M-CSF and PDGF-AA again showed high levels (>300 pg/mL) and the rest of the detectable cytokines (Fractalkine, GRO, IL-8, IP-10, Lif, SCF and VEGF) showing moderate levels (<100 pg/mL) (**Table 6.3**). At 72 hours, MT astrocytes showed significantly higher PDGF-AA levels (p-value 0.007) while fractalkine level was lower (p-value 0.02) (**Fig 6.7**). Although some other cytokines showed differences in MT astrocyte, they either did not reach statistical significance (IP-10, M-CSF, VEGF), or the levels detected were too low (<20 pg/mL) (GRO, iL-8, SCF) and not considered meaningful. The higher level of PDGF-AA (pro-inflammatory) and lower level of fractalkine (anti-inflammatory) suggest that MT astrocyte might contribute to pro-inflammatory conditions in the brain.

Table 6.3. Fold differences of cytokines at 72 hours between WT and MT astrocytes. ND (Not Detected) * (statistical significance).

Cytokine	WT iPSC-derived astrocyte (pg/mL)	MT iPSC-derived astrocyte (pg/mL)	WT/MT ratio
Fractalkine	21.70	13.7	1.58*
GRO	3.78	0.86	4.40
iL-8	11.73	1.28	9.16
IL-10	ND	ND	-
IL-17	ND	ND	-
IP-10	28.33	3.68	7.70
Lif	65.24	83.85	0.78
M-CSF	3736.40	2305.85	1.62
MIP-1	ND	ND	-
MCP-1	11248.87	9832.79	1.14
PDGF-AA	314.63	2672.53	0.12**
SCF	2.33	5.22	0.44
TNF- α	ND	ND	-
VEGF	7.83	18.79	0.42

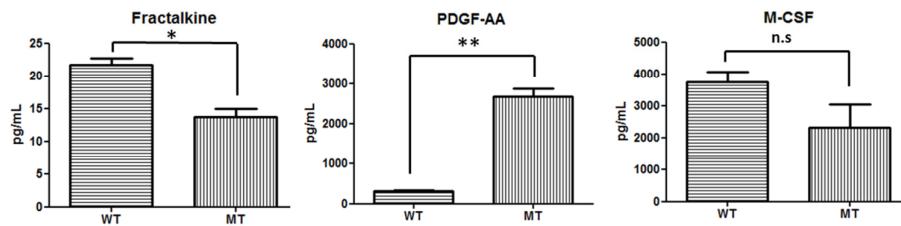


Fig 6.7 Cytokine profiling of WT and MT iPSCs-derived astrocyte at 72 hours. MT astrocytes showed abnormal levels of Fractalkine and PDGF-AA but not M-CSF (mean \pm SD, n= 2,* p-value <0.05, ** p-value <0.01, unpaired t-test).

6.3.5 Gene expression array of astrocytes

Previous gene expression studies have been performed on the astrocytes of RTT mouse model due to the lack of human material (Okabe et al., 2012; Yasui et al., 2013). These studies identified differences in gene transcript expression of astrocytes from the RTT mouse model indicating that at least in mouse, *Mecp2* has a role in astrocyte's transcription. Here, we performed

microarray expression analysis on pure population of human astrocytes comparing isogenic WT and MT cells. The gene expression study of astrocyte generated from RTT iPSCs-derived astrocytes provided many valuable insights into the possible functions of *MeCP2* in human astrocytes.

Analysis of the microarray signals revealed a list of 590 differentially expressed genes (DEG) (P-value <0.05; absolute fold change >2) (Appendix 2). Hierarchical clustering of the 590 DEG was performed to give an overview of relative expression value among the samples (**Fig 6.8**). The heat map generated revealed consistent gene expression patterns in WT astrocytes versus MT astrocytes, illustrating the reproducibility of the expression data. Of the 590 DEG, 325 genes were upregulated in MT while 265 genes were downregulated (Appendix). The top 15 up-regulated and down-regulated genes are shown in **Table 6.4 and 6.5**. Both up- and down-regulation of transcripts were observed supporting the finding that MeCP2 can act as both a transcriptional repressor and activator (Yasui et al., 2007; Yasui et al., 2013).

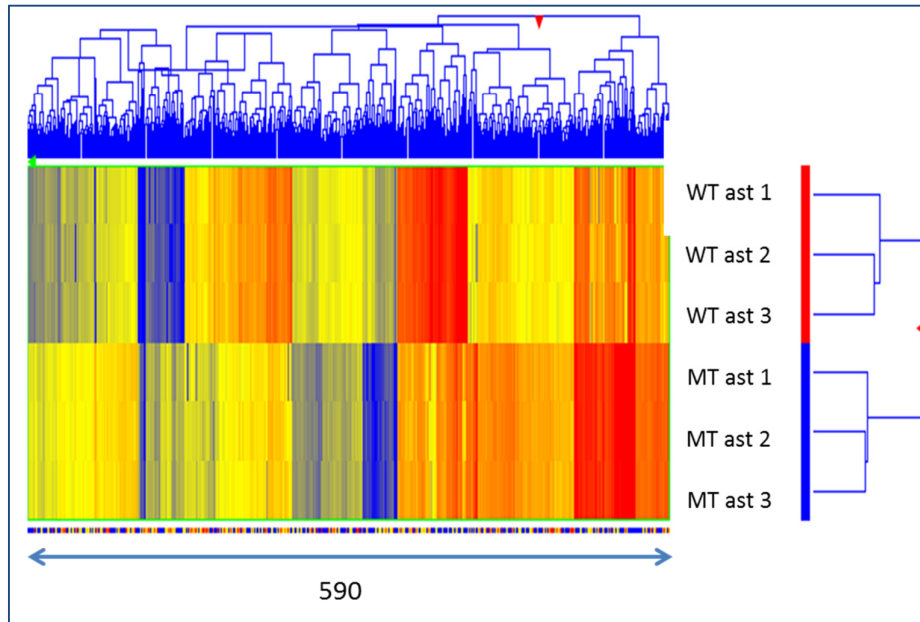


Fig 6.8. 6 Heat map cluster analysis of microarray. 590 DEGs were identified between WT and MT astrocytes

Table 6.4 Top 15 differentially up regulated genes in MT iPSCs-derived astrocyte based on fold change.

Symbol: Name	Fold Change
1. TMEM132D: transmembrane protein 132D	311.242
2. IRX2: iroquois homeobox 2	162.489
3. LOC647322: PREDICTED: hypothetical protein LOC 647322	99.070
4. SYNPR: synaptoporin	68.209
5. C18orf51: chromosome 18 open reading frame 51	33.497
6. LOC644128: PREDICTED: hypothetical protein LOC644128	33.405
7. MAL: T-cell differentiation protein, transcript variant a	32.574
8. LOC400879: PREDICTED: hypothetical LOC400879, transcript variant 2	32.083
9. C1orf61: chromosome 1 open reading frame 61	31.944
10. MSC: musculin	29.753
11. LOC642477: PREDICTED: hypothetical protein LOC642477	29.631
12. RPL23AP53: ribosomal protein L23a pseudogene 53, non-coding RNA	29.135
13. LGALS8: galactoside-binding, soluble, 8, transcript variant 4	27.377
14. LOC654433: PREDICTED: hypothetical LOC654433, non-coding RNA	25.865
15. TOX3: TOX high mobility group box family member 3	25.229

Table 6.5 Top 15 differentially down regulated genes in MT iPSCs-derived astrocyte based on fold change.

Symbol: Name	Fold Change
1. C5orf23: chromosome 5 open reading frame 23	-226.75
2. PCDHB5: protocadherin beta 5	-143.579
3. EFEMP1: EGF-containing fibulin-like ECM protein 1, transcript variant 1,	-78.5408
4. CSRP1: cysteine and glycine-rich protein 1	-68.9403
5. CDH13: cadherin 13, H-cadherin (heart)	-65.819
6. COL10A1: collagen, type X, alpha 1	-45.0631
7. LOC644348: PREDICTED: hypothetical protein LOC644348,	-45.0442
8. SFRP2: secreted frizzled-related protein 2	-37.7507
9. PEG3: paternally expressed 3	-33.9225
10. HP: haptoglobin	-31.4574
11. GRIK1: glutamate receptor, ionotropic, kainate 1, transcript variant 2	-29.8528
12. PLAC9: placenta-specific 9	-29.7104
13. CDH3: cadherin 3, type 1, P-cadherin (placental)	-25.8302
14. LRRTM1: leucine rich repeat transmembrane neuronal 1	-24.3527
15. LOC652097: PREDICTED: hypothetical protein LOC652097	-23.5402

A gene ontology (GO) analysis using DAVID was performed (Huang da et al., 2009b). GO analysis (P-value <0.01) showed an enrichment of GO terms relating to cell adhesion and blood vessel development (**Table 6.6**). To validate the results of the microarray, Real-time PCR of selected genes including *TMEM132D*, *Growth Associated Protein 43 (GAP43)*, *4-aminobutyrate aminotransferase (ABAT)*, *Protocadherin 5 and 19 (PCDHB5 and PCDH19)* was carried out. Real-time PCR results showed consistency with the microarray results in terms of up or down-regulation. Through this microarray experiment, we identified a number of candidate genes with a potential relevance for regulating astrocyte functions, which provide new insight into the role of MeCP2 in astrocytes.

Table 6.6 Top 10 GO terms under biological processes identified among differentially expressed genes based on p-value using DAVID.

	GO ACCESSION	Gene Ontology Term (Biological Process)	p-value	No. of genes
1.	GO:0007155	Cell adhesion	8.19E-09	44
2.	GO:0022610	Biological adhesion	8.39E-09	44
3.	GO:0001568	Blood vessel development	8.49E-08	23
4.	GO:0001944	Vasculature development	1.30E-07	23
5.	GO:0048514	Blood vessel morphogenesis	1.11E-05	18

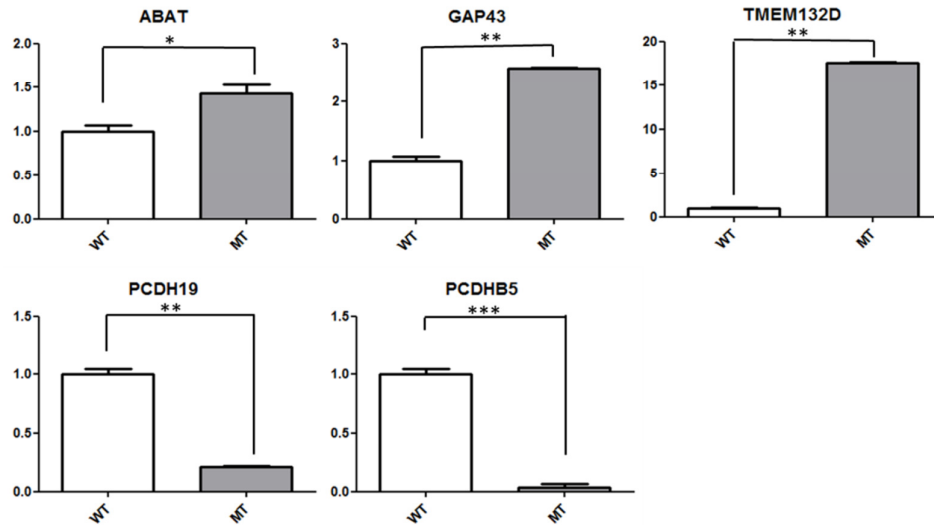


Fig 6.9 Real-time PCR of selected genes. Each graph represents the relative fold difference of MT astrocytes compared to WT astrocytes (normalized to 1). (mean+SEM, * p-value<0.01,*p-value<0.001 ***p-value<0.0001, unpaired t-test)

Table 6.7 Comparison of microarray and Real-time PCR results of selected genes. Values are expressed as MT/WT fold change, with positive value denoting up-regulation and negative value denoting down-regulation in MT astrocytes.

Gene	Microarray fold change	Real-time PCR fold change
TMEM132D	311.2	17.6
GAP43	2.2	2.6
ABAT	2.0	1.4
PCDHB5	-143.6	-28.5
PCDH19	-4.6	-4.8

6.4 Discussion

6.4.1 RTT patient's iPSCs can generate astrocytes

Once thought of as nothing more than “glue”, astrocytes have emerged as an important cell type that plays multiple roles in the CNS. Our understanding of astrocyte functions have mainly come from rodent as human astrocytes are hard to access. However, human astrocytes have been shown to have distinct properties from rodent astrocytes such as a higher propagation rate of calcium signaling (Han et al., 2013). iPSCs represents a potential unlimited source for generating human astrocytes and one aim of this study was to assess the usefulness of human iPSCs as a tool for getting human astrocytes. In this chapter, I described a robust and reproducible protocol to generate astrocytes from iPSCs. A unique feature of deriving astrocytes using this method is that it recapitulates the developmental sequence of astrogenesis in the human brain. In the developing brain, astrogenesis follows neurogenesis which means that the majority of astrocytes are formed in the presence of neurons (Kanski et al., 2014; Liu and Zhang, 2011; Molofsky et al., 2012). The protocol developed in this thesis mirrors the *in vivo* development of the brain, in which neurons are first generated followed by astrocytes. Importantly, iPSCs-derived astrocytes showed typical astrocytic morphology, had strong expression of astrocyte markers, exhibit secretions of cytokines known to be secreted by astrocyte and were functional in terms of glutamate uptake. These results indicate iPSCs represents a viable way to get astrocytes from human. Furthermore, we found that iPSCs from P72 can be differentiated to astrocytes. Together with reports from another study in which astrocytes are derived from RTT iPSCs (Williams

et al., 2014), this indicates that iPSCs from RTT patients represents a viable method for obtaining astrocytes for the study of RTT.

A recent study reported the generation of astrocytes from RTT patients' iPSCs (Williams et al., 2014). In that study, the authors generated astrocyte progenitor through prolonged culture (up to 300 days) of the NPCs using EGF and FGF as growth factors before differentiation of the progenitor into astrocytes. High numbers of s100 β and GFAP positive cells were reported. They found MT iPSCs-derived astrocytes and their CM had adverse effects on neuronal morphology and electrophysiological functions in co-culture, supporting what was uncovered in the RTT mouse model (Ballas et al., 2009; Maezawa et al., 2009). Our findings corroborate the finding that RTT iPSCs can generate astrocytes. We went on to study several aspects of astrocyte functions including proliferation, metabolism, maintenance of glutamate homeostasis, cytokine secretions and gene expression in a bid to uncover possible mechanisms behind astrocyte pathology in RTT.

6.4.2 Use of iPSCs-derived astrocytes for cytokine profiling

Astrocytes are important modulators of the CNS homeostasis through secretions of cytokines (Aloisi et al., 1995; Lieberman et al., 1989). Recent studies investigating human astrocyte cytokine secretions have used astrocytes isolated from human fetal brain tissue which is an extremely limited source (Choi et al., 2014), or astrocytes derived from Ntera2, an embryonal carcinoma cell line that is karyotypically abnormal (Burkert et al., 2012). In this study, we showed that iPSCs-derived astrocytes secrete high levels of MCP-1, M-CSF and PDGF-AA, and moderate levels of fractalkine, GRO, IL-

8, IP-10, Lif, SCF and VEGF. These results indicate that iPSCs-derived astrocyte are functional in terms of cytokine secretion and are a useful tool for studying cytokine secretions. This is the first study looking at cytokine profiling of human iPSCs-derived astrocytes to the best of my knowledge.

6.4.3 MT astrocytes show abnormal cytokine profile

We investigated the levels of 14 cytokines and found MT astrocytes secreted abnormal levels of 2 cytokines. One of them is PDGF-AA with MT astrocytes showing ~8-fold increase. PDGFs are growth factors that play significant roles in cell growth and blood vessel formation. PDGFs exist as homo- or heterodimers of disulfide-linked polypeptide chains and the four PDGF family members include PDGF-A, PDGF-B, PDGF-C and PDGF-D (Andrae et al., 2008). Two PDGF receptors (PDGFR) are known, PDGFR- α , of which is the receptor for PDGF-AA (Shim et al., 2010), and PDGFR- β . Both PDGFRs can activate several signaling pathways including RAS-MAPK, PI3K and PLC- γ (Andrae et al., 2008).

One known consequence of increased PDGF levels in the brain is the disruption of the BBB through activation of PDGFR- α (Ma et al., 2011; Su et al., 2008; Yao et al., 2011). Disruption of the BBB results in uncontrolled flux of molecules, ions and immune cells across the BBB and has been implicated in neuroinflammation, seizures and autism (Cabezas et al., 2014; Theoharides and Zhang, 2011). Studies have shown that interference of PDGFR signaling with neutralizing antibodies or with an inhibiting compound, imatinib, has been shown to enhance BBB integrity and reduce neuroinflammation in mouse models of brain haemorrhage and multiple sclerosis (Adzemovic et al., 2013;

Ma et al., 2011). Interestingly, PDGF-B was found to be increased at the transcript level of RTT mouse astrocyte (Yasui et al., 2013), and in humans, PDGF-BB levels have been shown to be increased in serum levels of autism patients (Kajizuka et al., 2010). These findings suggest regulation of PDGF level or PDGFR- α activation could be a potential therapeutic for RTT.

The other cytokine with abnormal levels is fractalkine (1.6x down in MT). Fractalkine is a transmembrane protein in which the extracellular domain is digested by protease to produce a soluble form. The sole receptor for fractalkine in the CNS is CX3CR1, and is reported to be expressed exclusively on microglia (Cardona et al., 2006; Harrison et al., 1998; Liang et al., 2009), although others report that CX3CR1 is also expressed in neurons (Deiva et al., 2004; Meucci et al., 2000). In neurons, fractalkine has been reported to have a direct neuroprotective effect through inhibition of NMDA-mediated apoptosis (Deiva et al., 2004; Meucci et al., 2000). In microglia, lack of CX3CR1 led to increased microglia-mediated neurotoxicity in mouse model of ALS and Parkinson's disease indicating that fractalkine acts to suppress microglia mediated neurotoxicity (Cardona et al., 2006; Pabon et al., 2011). Microglia lacking CX3CR1 also showed less process dynamic and migration, and decreased synaptic pruning (Liang et al., 2009; Paolicelli et al., 2011). These evidences suggest fractalkine have important anti-inflammatory and neurodevelopmental roles. Here, MT astrocytes secreting less fractalkine suggests that in RTT, there may be a reduction of direct neuroprotective effect, and increased microglia induced neurotoxicity and reduced synaptic pruning. The implications of abnormal microglia activity are further discussed in chapter 7.

6.4.4 Gene expression study revealed several genes that are differentially expressed in MT astrocytes

The microarray results presented here is the first genome wide gene expression screen for *MeCP2* target genes in human astrocytes. A previous microarray study identified *Mecp2* target genes in mouse astrocytes but not in human (Yasui et al., 2013). Between the mouse and human studies, several related genes were found to be differentially expressed. In the mouse, APOC2, C3, FZD5, IGFBP4, ITGA1 were up-regulated while we found up-regulation of similar class of genes such as APOBEC, C5, FZD6, IGFBP7, ITGA4 in our iPSCs model. In the mouse, PCDH17, TM4SF1 and TSPAN13 were down-regulated while PCDH17, TM4SF1, TM4SF18 AND TSPAN2 were down-regulated in our iPSCs model. These findings imply that similar pathways may be affected in both mouse and human astrocytes and it will be of further interest to pursue these genes.

Furthermore, the microarray data identified several genes of interest that are implicated in neurological disorders. For example, *GAP-43* (up in MT) is a cytoplasmic protein involved in neurite formation and neurotransmission, and has been implicated in autism (Allen-Brady et al., 2009; Zaccaria et al., 2010). *ABAT* (up in MT) is an enzyme involved in catabolism of GABA and has been implicated in mental retardation and reported as autism candidate genes (Barnby et al., 2005; Szatmari et al., 2007). *PCDHB5* and *PCDH19* (both down in MT) belong to the protocadherin family which are important proteins involved in cell adhesion and signaling pathways of the nervous system (Chen and Maniatis, 2013; Ye and Jan, 2005). Several of the protocadherin genes including *PCDH19* have implicated in ASD and epilepsy (Anitha et al., 2013;

Dibbens et al., 2008; Tsai et al., 2012). These genes however are not well studied in astrocytes and the finding that these genes are differentially expressed in MT astrocytes implies that astrocytes play important roles in ASD. Further studies on these set of genes in astrocytes could help us understand how astrocytes influence RTT.

We further performed pathway analysis between WT and MT astrocytes and found that the pathways enriched are those involved in blood vessel function, cell adhesion and ECM. Astrocytes play important roles in the formation and maintenance of the BBB. Loss of cell adhesion and ECM components in astrocytes could lead to loss of close contact with blood vessels and a breakdown of the BBB (Baeten and Akassoglou, 2011; Baumann et al., 2009; Scholler et al., 2007). These findings further support our hypothesis that BBB could be affected in RTT (**Fig 6.10**).

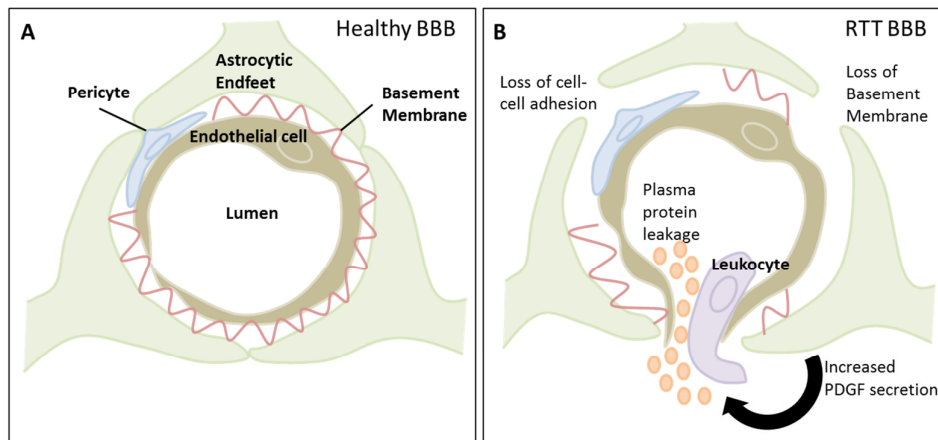


Fig 6.10 Proposed model of dysfunctional astrocytes on the BBB in the RTT brain. (A) In a healthy brain, astrocytic endfeet completely surround the blood vessel and form tight cell-cell adhesion with each other, with pericytes and with the BM thus forming an effective barrier. (B) In the RTT brain, loss of cell-cell and cell-ECM adhesion and loss of BM lead to breakdown of the BBB. Increased PDGF secretion by astrocytes further contributes to BBB leakiness. Image adapted from (Baeten and Akassoglou, 2011).

6.4.5 MT astrocytes showed abnormalities in proliferation rate

In our study, we observed proliferation difference between isogenic WT and MT astrocytes but not in isogenic iPSCs lines (chapter 4) or NPCs lines (chapter 5). This could indicate that MeCP2 affect proliferation in specific cell types, and in this case, astrocytes. MeCP2 has previously been reported to reduce proliferation in lymphocytes from RTT patients (Balmer et al., 2002), and mesenchymal stem cells isolated from a RTT patient (Squillaro et al., 2012; Squillaro et al., 2008). Silencing of *MeCP2* has also been observed to cause a decrease in cell proliferation in the neuroblastoma line, SK-N-BE(2)-C (Squillaro et al., 2012), murine fibroblast line, NIH-3T3 and transformed human prostate cell lines, PC-3 and LNCaP (Babbio et al., 2012). Furthermore, a reduced proliferation rate was also reported in astrocytes isolated from *Mecp2-null* mice (Maezawa et al., 2009). However, another mouse study did not observe astrocyte growth retardation (Okabe et al., 2012) and differences in astrocytic proliferation were not reported by (Williams et al., 2014) in their iPSCs-derived astrocytes. One reason for the differing results between Williams et al., 2014 and ours could be the different strategy used in generating astrocytes. (Williams et al., 2014) generated astroglia progenitors from NPCs while we made use of the astrocytes innate proliferative capacity and bypassed the progenitor stage. This could result in our astrocytes having undergone more cell cycles and having a more “mature” phenotype and hence manifestation of premature senescence. Another possible reason could be that the iPSCs used carried different mutations (Williams et al., 2014).

6.4.6 Metabolic function of MT astrocytes is altered

Here, we report that MT astrocytes displayed an initial delayed response towards glucose uptake when exposed to a glucose analog. Over a prolonged time however, MT astrocytes showed similar glucose uptake capacity as WT astrocytes. An initial delay in the glucose uptake capacity of MT astrocytes may mean that MT astrocytes are unable to respond quickly to support high neuronal energy demand during times of neuronal activity (**Fig 6.11**). In the literature, RTT patients have been reported to show both increased and decreased glucose metabolism depending on brain region (Villemagne et al., 2002). However, this study was performed in sedated patients and may not reflect the true brain glucose utilization during neuronal activity. This work is preliminary and further studies need to be done (see future experiments).

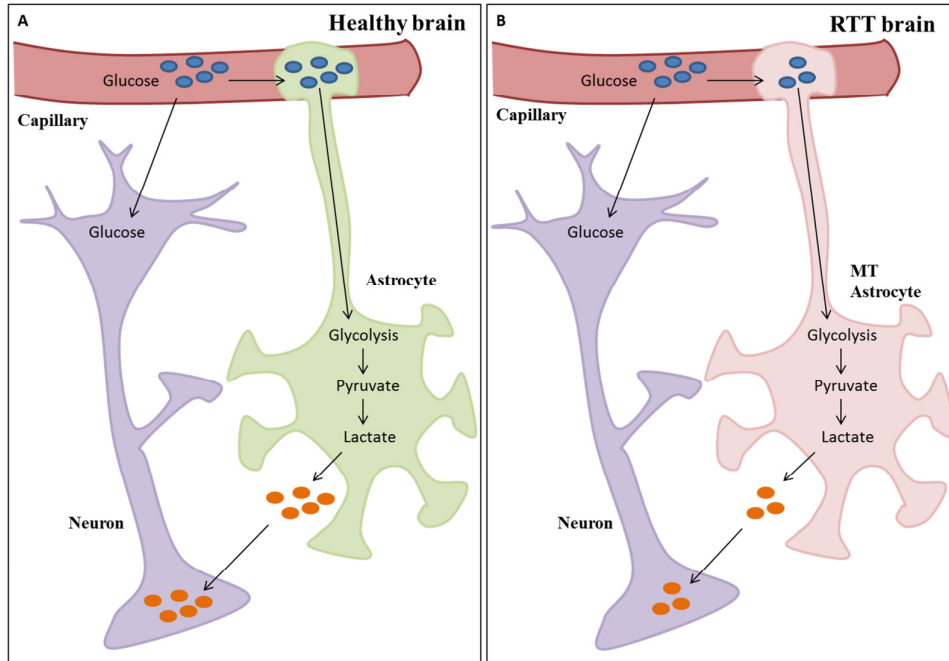


Fig 6.11 Proposed model of glucose uptake deficiency in RTT astrocytes. (A) In a healthy brain, glucose is taken up by astrocyte and converted to lactate as a form of metabolic substrate taken up by neurons according to the lactate shuttle hypothesis. (B) In the RTT brain, delay in glucose uptake leads to reduced production of lactate and reduced energy supply to neurons (picture modified from Felipe et al., 2012).

6.4.7 Role of astrocytes in RTT and neurological diseases

Astrocytes fulfill several functions in the CNS and disruptions in any astrocytic functions can cause neurological symptoms. For example, excess glutamate released from astrocytes was found to induce seizure in a rodent epilepsy model (Perez et al., 2012), and astrocytes from Huntington's disease mice models were found to be deficient in regulating K^+ homeostasis (Tong et al., 2014). In our RTT model, we found MT astrocytes have abnormal cytokine secretion, retarded energy metabolics, reduced proliferation and abnormal gene expression. We proposed that MT astrocytes lead to disruption of the BBB, increase neuroinflammation and negatively impact brain energy

metabolics. As astrocytes are important players in regulating brain homeostasis, we propose that regulation of astrocyte function would be a promising approach to treating neuropathology and RTT. Future work to investigate and prove these hypotheses may lead to novel strategies in targeting RTT.

6.5 Conclusions

In summary, I have described the generation of astrocytes from isogenic iPSCs from a RTT patient. MT astrocyte showed reduced proliferation and delayed glucose uptake. Cytokine profiling demonstrated cytokines dysregulation in PDGF-AA and fractalkine and gene expression array identified blood vessel, cell adhesion and ECM functions are affected in MT astrocytes.

6.6 Limitations

6.6.1 More patients' samples needed

Only iPSC lines from P72 were used here. RTT patients differ from one another in the range and severity of symptoms. These differences partially stem from differing mutations of the *MeCP2* gene and different genetic backgrounds (i.e. modifier genes). Since the finding in this thesis may represent the disease in one patient, it would be beneficial to reproduce these experiments in iPSCs lines from additional patients. The strategy was to first determine the phenotype to be studied using iPSC lines from one patient before extending the findings to other patients. However, the experiments from more patients (P48 and P80) could not be completed in time for this thesis.

6.6.2 Primary cells as positive controls

While the cells derived show expression of astrocyte markers and is able to take up glutamate, a positive control using primary cells is needed for important measurements such as glutamate and glucose uptake. Primary astrocytes could be isolated from mouse brain as a control (Kim and Magrane, 2011; Schildge et al., 2013).

6.6.3 Expression of MeCP2 in iPSC-derived astrocytes

While mouse astrocytes have been shown to express *Mecp2* (Ballas et al., 2009; Maezawa et al., 2009), it is important to show that iPSC-derived astrocytes express MeCP2. An immunostain or western blot should be performed. However, this experiment was not completed in time for this thesis.

6.6.4 Quantification of glucose uptake

MT astrocytes showed a slower rate of glucose uptake. Using FACS, I was unable to quantify the rate of uptake. A better assay would be to plate equal numbers of WT and MT astrocytes into 24 well plates and add 2-NBDG. Readings of fluorescent intensity could be taken at various time points such as 0 min, 10 min, 20 min, 30 min, 60 min using a plate reader. This will provide a more accurate quantification of the rate of glucose uptake.

6.6.5 Identity of the derived cells

While various specific markers and functional assay was used to determine the astrocytic identity of the cells, the data gene expression array could be used to further ascertain the identity by checking for cell-type specific genes. This will further confirm the lineage of the derived cells.

Chapter 7: Investigating the role of microglia in RTT using iPSCs

7.1 Introduction

Before 2010, it was generally believed that the cellular culprits in RTT were neurons and astrocytes. Then in 2010, a report implicating microglia was published (Maezawa and Jin, 2010). In this study, CM from microglia isolated from *Mecp2*-null mice showed neurotoxicity and resulted in WT neurons having stunted dendritic development and dendritic beading (**Fig 7.1**). Further investigations found that *Mecp2*-null microglia released a five-fold higher level of glutamate compared to WT microglia and inhibition of both glutamate production and glutamate release from *Mecp2*-null microglia rendered the CM less neurotoxic. Inhibition of glutamate receptors in WT neurons also decreased the toxic effect of the *Mecp2*-null microglia, further demonstrating that the neurotoxic effect of *Mecp2*-null microglia was from excessive glutamate release.

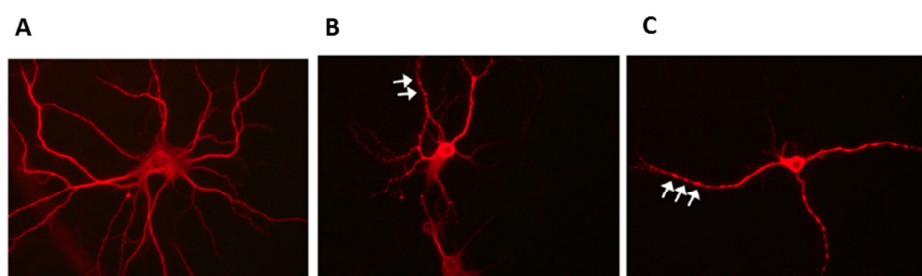


Fig 7.1 CM from *Mecp2*-null microglia are neurotoxic. (A) WT neurons cultured in WT microglia CM showed normal morphology. (B) and (C) WT neurons cultured in CM from *Mecp2*-null microglia showed signs of neurotoxicity such as dendritic beading (arrows) Image reproduced with permission from (Maezawa and Jin, 2010).

The role of microglia in RTT was further demonstrated when transplantation of WT bone marrow was able to arrest disease progression in *Mecp2*-null mice

(Derecki et al., 2012). Repopulation of microglia in the brain from donor bone-marrow was shown to be essential for the rescue as prevention of donor microglia repopulation in the brain resulted in no arrest of pathology. To further verify the role of myeloid cells in RTT, *Mecp2*^{lox-stop/y}*Lysm*^{cre} mice were crossed, resulting in only myeloid cells expressing *Mecp2* in an otherwise global *Mecp2* KO mouse. *Mecp2*^{lox-stop/y}*Lysm*^{cre} mice showed better appearance and growth, and had increased lifespan and reduced respiratory symptoms. *in vitro* investigation of *Mecp2*-null microglia revealed they have reduced phagocytic capacity. Pharmacological treatment of *Mecp2*^{lox-stop/y}*Lysm*^{cre} mice with a phagocytosis inhibitor, annexin V blocked phagocytotic activity of microglia/macrophage and abolished the amelioration of disease showing that phagocytosis activity is needed for rescue of RTT symptoms in those mice.

7.2 Hypotheses and Aims

The above studies highlighted the role of microglia in the mouse model of RTT. It was unclear, however, if microglia would have a role in the human RTT. My hypothesis is that human microglia could be a cell type that is affected by MeCP2 mutations. To test my hypothesis, I decided to generate microglia from a RTT patient's iPSCs using a novel protocol developed by a collaborator. To determine the microglia identity, several microglia markers would be used and functional assay would be carried out.

Due to evidence from the mouse model showing a defect in microglia phagocytosis, my hypothesis is that human MT microglia are abnormal in

phagocytosis. To investigate this, I aimed to carry out a phagocytosis assay to see if MT microglia are abnormal in this aspect.

Besides abnormal phagocytosis, studies from the mouse model showed that *Mecp2*-null microglia are neurotoxic. My hypothesis is that human MT microglia are neurotoxic. To test this hypothesis, I decided to mix the microglia with WT human neurons to see if MT microglia have neurotoxic effects. The mouse model also demonstrated that the source of neurotoxicity is excessive glutamate secretion from *Mecp2*-null microglia. Hence, I decided to test for glutamate secretion to see if this was also true in human MT microglia.

Furthermore, as MeCP2 is a transcriptional factor, I decided to carry out a gene expression study to see if any changes in gene expression between WT and MT microglia can be detected.

7.3 Results

7.3.1 Derivation of microglia from RTT patient's isogenic iPSCs

WT and MT iPSCs from P72 were differentiated to microglia using a novel protocol. As microglia originates from the hematopoietic progenitors of the yolk sac during embryogenesis (Ginhoux et al., 2013), iPSCs were first induced into the mesodermal lineage for 5 days before specification to the haematopoietic lineage at day 8. Haematopoietic cells were allowed to mature for 7 days before addition of factors to expand the cell population. Cells were harvested at day 22 (**Fig 7.2A**).

To purify the microglia-like cells, live-cell sorting was carried out. CD45, CD11b and CD14 are cell surface markers used to identify microglia

(Beschorner et al., 2002; Cosenza-Nashat et al., 2006; Wu et al., 2014). The cell populations underwent sequentially sorting first using CD45 followed by CD11b and then CD14. Both WT and MT iPSCs were able to generate microglia at efficiencies of 7-15% based on FACS data (Fig 7.2B&C). To further confirm microglia identity, we carried out immunocytochemistry for the commonly used microglia markers, Iba1 and CD68 (Ito et al., 1998; Kozłowski and Weimer, 2012). All microglia purified by FACS were positive for Iba1 and CD68 (Fig 7.2D&E).

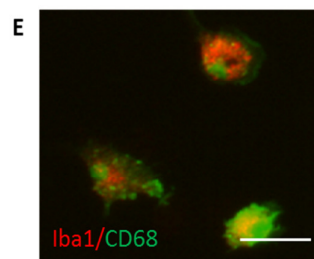
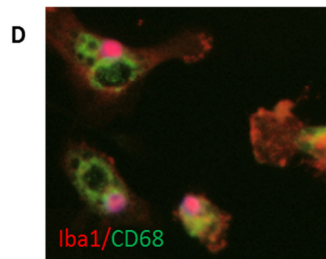
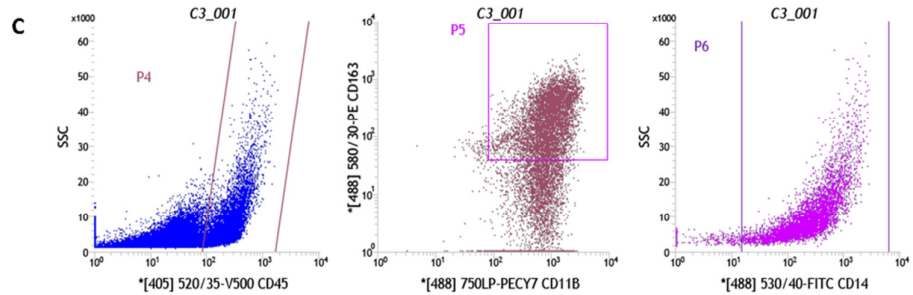
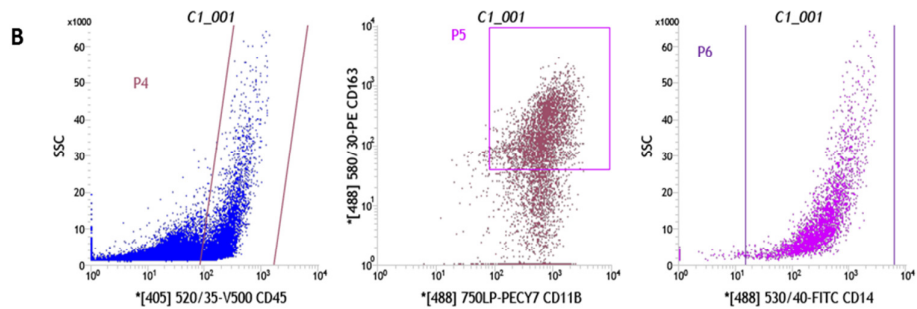
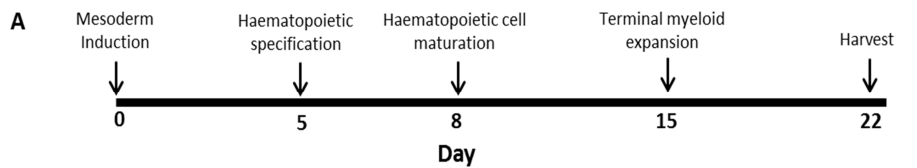


Fig 7.2 Derivation and characterisation of iPSCs-derived microglia. (A) Schematic of microglia differentiation protocol from iPSCs. Live cell FACS using CD-45, CD11B and CD14 of (B) WT iPSCs-derived microglia and (C) MT iPSCs-derived microglia. Immunocytochemistry staining of Iba1 and CD68 on (D) WT iPSCs-derived and (E) MT iPSCs-derived microglia. Scale bar indicates 50µM. Images D & E courtesy of Oz Pomp.

7.3.2 MT microglia display reduced motility

Phagocytosis is an innate function of microglia especially in the clearance of dead cells and debris. To determine the phagocytic ability of the iPSCs-derived microglia, we conducted phagocytosis assays. NPCs were irradiated under UV lamp in the hood to induce apoptosis and added to microglia culture as apoptotic bodies (Derecki et al., 2012). Time lapse microscopy indicates both WT and MT microglia have phagocytic ability (**Fig 7.3A**). However, MT microglia was observed to show less phagocytosis of apoptotic bodies (**Fig 7.3B&C**).

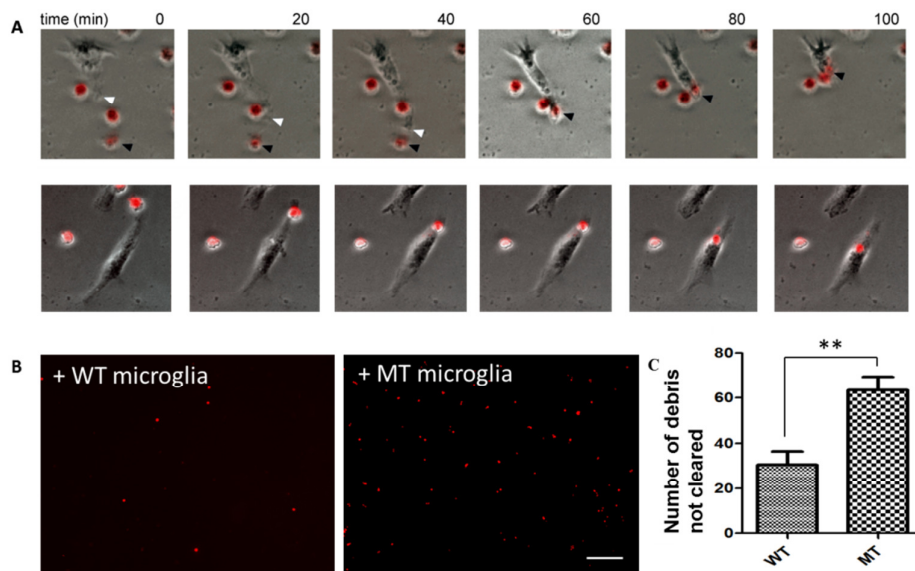


Fig 7.3 MT microglia showed less phagocytosis of apoptotic bodies. (A) Representative images of phagocytosis by iPSCs-derived microglia at 20 minutes interval. White arrowhead show leading edge of microglia, black arrowhead show a labelled apoptotic NPC being phagocytosed (B) Representative images of apoptotic body 8 hrs after addition of WT microglia and MT microglia. Scale bar represents 100µM. (C) Graphical representation

of apoptotic bodies clearance (mean \pm SEM, n=3 ** p value<0.01, unpaired t-test). Images courtesy of Oz Pomp.

Microglia are highly motile cells and constantly survey their environment with frequent filopodia extensions and retractions even while in a resting state (Nimmerjahn et al., 2005; Wake et al., 2009). Time lapse microscopy was performed on both WT and MT microglia to track their motility over 15 hours. MT microglia was observed to display less filopodia process dynamics than WT microglia (**Fig 7.4A**). We further tracked the movement of microglia over a 15 hour time period and found that MT microglia were significantly less locomotory (**Fig 7.4B&C**). These findings suggest that motility is impeded in MT microglia and reduced motility could be the reason behind a reduced phagocytosis.

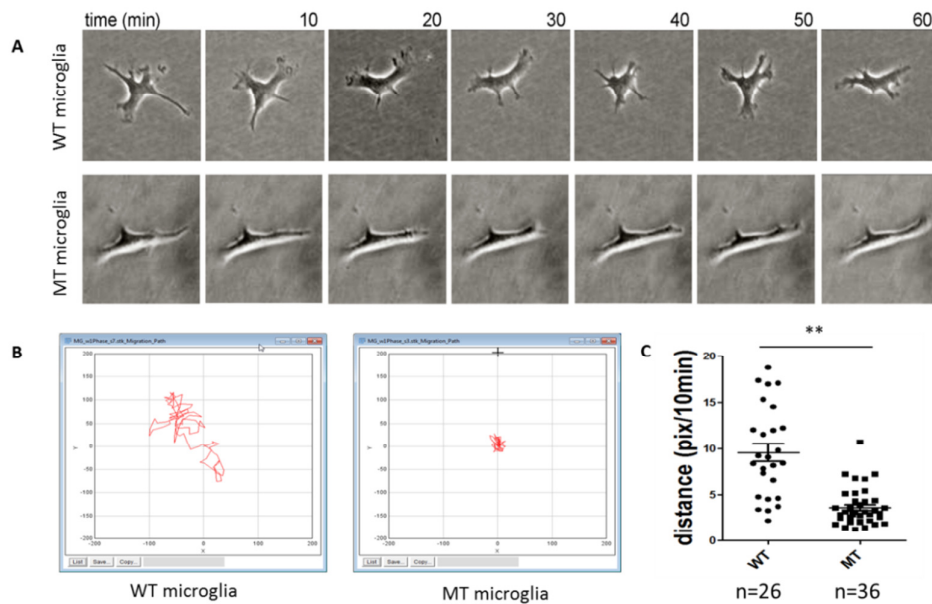


Fig 7.4 MT microglia showed decreased motility. (A) Photos taken at 10 minutes intervals showing process dynamics of iPSCs-derived microglia. (B) Representative charts showing extent of movement within a 15 hour time frame of WT (left) and MT (right) microglia. (C) Graphical representation of microglia movement (mean + SEM, ** p-value <0.05, unpaired t-test). Images courtesy of Oz Pomp.

7.3.3 MT microglia are neurotoxic

It was reported in the mouse model that *Mecp2*-null microglia are neurotoxic (Maezawa and Jin, 2010). To test for neurotoxicity of MT microglia, we set up a co-culture system comprising of WT iPSCs-derived neurons and astrocytes with the addition of either WT or MT microglia (**Fig 7.5A**). The unique feature of this system is that all cell types are derived from the same patient. 10 days after co-culture, we observed neuronal beading in co-cultures of neurons with MT microglia but not with WT microglia (**Fig 7.5A**).

Neuronal beading is an indication of neurotoxicity and it was reported in the RTT mouse model that *Mecp2*-null microglia secreted excessive levels of glutamate to cause dendritic beading (Maezawa and Jin, 2010). We therefore investigated the levels of glutamate secreted by the iPSCs-derived microglia but we did not find significantly increased levels of glutamate secretion by MT microglia (**Fig 7.5B**). We next looked at tumor necrosis factor- α (TNF α) secretion levels as it has been reported to induce neurotoxicity by inducing glutamate release in microglia (Takeuchi et al., 2006). Both WT and MT microglia released TNF α but we did not find elevated levels of TNF α in MT iPSCs-derived microglia (**Fig 7.5C**). These findings suggest that in our iPSC model, MT microglia do not secrete excess levels of glutamate or TNF α that could be the cause of neuronal beading. Further investigation is necessary to unveil the mechanism of neuronal beading.

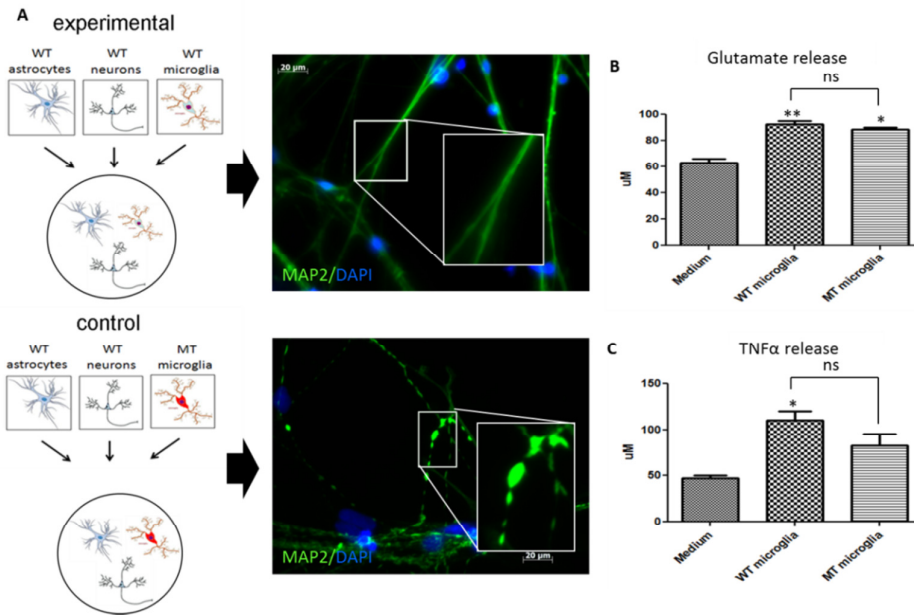


Fig 7.5 Co-culture of neurons with MT microglia causes neurotoxicity. (A) Schematics showing co-culture setup of multiple cell types with “Control” setup comprising of WT neurons, astrocytes and microglia and “Experimental” setup comprising of WT neurons and astrocytes with MT microglia. Experimental setup resulted in neurons showing beading morphology. Scale bar represents 20 μ M. CM from both WT and MT microglia do not show significant differences in (B) glutamate levels or (C) TNF α levels (mean \pm SEM, n=3, *p-value <0.05, ** p-value <0.01, 1-way ANOVA with post-hoc Tukey test). Images courtesy of Oz Pomp.

7.3.4 Gene expression study of microglia

To uncover possible gene targets of MeCP2 in iPSCs-derived microglia, a gene expression microarray study comparing WT and MT microglia was carried out. 126 differentially expressed genes (DEG) were identified (P-value < 0.05; absolute fold change > 1.5) (Appendix 3). Of the 126 genes, 74 were up-regulated while 52 were down-regulated in MT microglia. Heat-map hierarchical clustering analysis of the 126 genes revealed consistent gene expression patterns in WT microglia that were distinct from MT microglia

(Fig 7.7) The top 15 up and down regulated genes are shown in **Table 7.1** and **Table 7.2**.

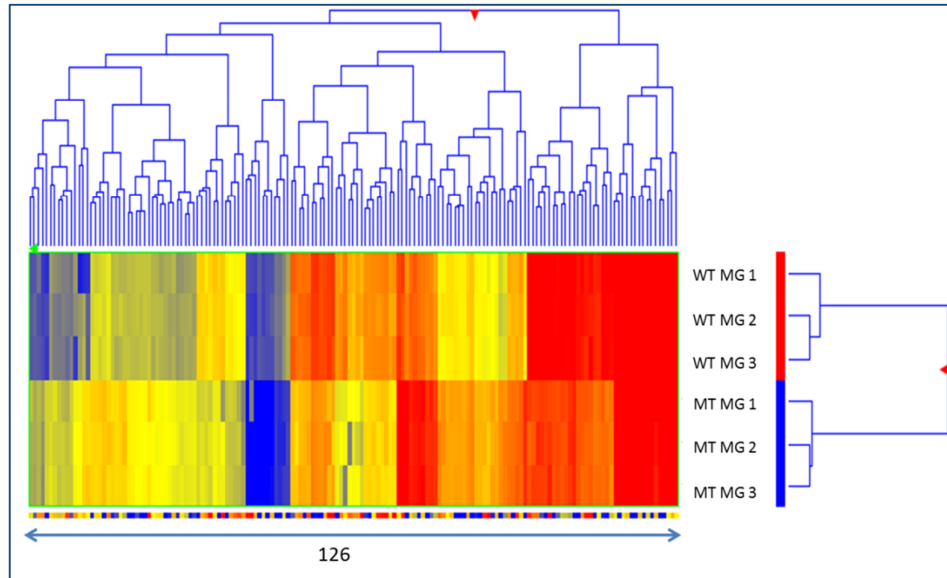


Fig 7.6 Heat map cluster analysis of microarray. 121 DEGs were identified between WT and MT microglia.

Table 7.1 Top 15 differentially up regulated genes in MT iPSCs-derived microglia based on fold change.

Symbol: Name	Fold Change
1 SLC15A4: solute carrier family 15, member 4	2.857
2 CH25H: cholesterol 25-hydroxylase	2.668
3 CCL2: chemokine (C-C motif) ligand 2	2.661
4 SQLE: squalene epoxidase	2.46
5 ACAT2: acetyl-CoA acetyltransferase 2	2.223
6 ETV5: ets variant 5	2.119
7 ALDOC: aldolase C, fructose-bisphosphate	2.034
8 TSPAN7: tetraspanin 7	1.988
9 SNRPN: small nuclear ribonucleoprotein polypeptide N	1.971
10 EGR2: early growth response 2	1.963
11 TNF: tumor necrosis factor	1.951
12 LYVE1: lymphatic vessel endothelial hyaluronan receptor 1	1.932
13 NDN: necdin, melanoma antigen (MAGE) family member	1.904
14 DKK3: dickkopf 3 homolog (<i>Xenopus laevis</i>)	1.902
15 HK2: hexokinase 2	1.901

Table 7.2 Top 15 differentially down regulated genes in MT iPSCs-derived microglia based on fold change.

Symbol: Name	Fold Change
1 HLA-DRA: major histocompatibility complex, class II, DR alpha	-2.712
2 DEFA1 (includes others): defensin, alpha 1	-2.678
3 CRABP1: cellular retinoic acid binding protein 1	-2.617
4 HLA-DPA1: major histocompatibility complex, class II, DP alpha 1	-2.372
5 LYZ: lysozyme	-2.326
6 FCER1A: Fc fragment of IgE, high affinity I, receptor for; alpha polypeptide	-2.299
CD74: CD74 molecule, major histocompatibility complex, class II invariant chain	-2.086
7 HLA-DRB6: major histocompatibility complex, class II, DR beta 6 (pseudogene)	-2.08
8 SYT11: synaptotagmin XI	-2.056
9 FCN1: ficolin (collagen/fibrinogen domain containing) 1	-2.018
10 PEG3: paternally expressed 3	-1.952
11 SNORD13: small nucleolar RNA, C/D box 13	-1.947
12 HLA-DRB4: major histocompatibility complex, class II, DR beta 4	-1.927
13 VTRNA2-1: vault RNA 2-1	-1.916
14 PDK4: pyruvate dehydrogenase kinase, isozyme 4	-1.879

Grouping of the DEG into biological processes which refers to the cellular events which the genes contributes revealed enrichment of cholesterol metabolism, (i.e metabolism of cholesterol, synthesis of sterol) and motility of myeloid cells (i.e chemotaxis of macrophage, cell movement of macrophage) (**Table 7.3**). To look further, pathway analysis of the DEG which looks at the metabolic, signaling and regulatory pathways revealed an enrichment of pathways involved in cholesterol metabolism (i.e Superpathway of cholesterol biosynthesis, cholesterol biosynthesis III) and immune cell functions (antigen presentation pathway, granulocyte adhesion and diapedesis) (**Table 7.4**). Taken together, the results suggest that in human microglia, MeCP2 could be a regulator of genes involved in cholesterol metabolism, immune cell function and cell motility.

Table 7.3 Top 15 biological process identified among differentially expressed genes based on p-value.

Biological Process (Ingenuity)	p-value
1 Inflammation of organ	4.4E-11
2 Formation of osteoclasts	6.04E-11
3 Synthesis of lipid	1.14E-10
4 Inflammation of respiratory system component	2.03E-10
5 Chemotaxis of antigen presenting cells	5.48E-10
6 Inflammation of lung	5.98E-10
7 Chemotaxis of macrophages	1.34E-09
8 Metabolism of cholesterol	2.2E-09
9 Inflammatory response	2.66E-09
10 Synthesis of sterol	3.36E-09
11 Chemotaxis of myeloid cells	3.59E-09
12 Cell movement of macrophages	3.61E-09
13 Chemotaxis of phagocytes	6.02E-09
14 Steroid metabolism	7.72E-09
15 Metabolism of terpenoid	8.75E-09

Table 7.4 Top 15 pathway identified among differentially expressed genes based on p-value.

Pathways (Ingenuity)	p-value
1 Superpathway of Cholesterol Biosynthesis	2.18E-11
2 LXR/RXR Activation	4.4E-11
3 Cholesterol Biosynthesis III (via Desmosterol)	1.82E-08
4 Cholesterol Biosynthesis II (via 24,25-dihydrolanosterol)	1.82E-08
5 Cholesterol Biosynthesis I	1.82E-08
6 Antigen Presentation Pathway	1.92E-07
7 Glycolysis I	5.66E-07
8 Granulocyte Adhesion and Diapedesis	3.29E-06
9 Dendritic Cell Maturation	4.15E-06
10 Differential Regulation of Cytokine Production in Macrophages and T Helper cells	6.26E-06
11 Allograft Rejection Signaling	2.4E-05
12 Communication between Innate and Adaptive Immune Cells	4.06E-05
13 Agranulocyte Adhesion and Diapedesis	4.29E-05
14 Epoxysqualene Biosynthesis	4.78E-05
15 TREM1 Signaling	5.49E-05

To validate the results of the microarray, real-time PCR of selected genes including *Lysozyme (Lyz)*; *Defensin 1 and 3 (DEFA1 and DEFA3)*, and *Ficolin1 (FCN1)* was carried out (**Fig 7.7**). The results showed consistency with the microarray results (**Table 7.5**).

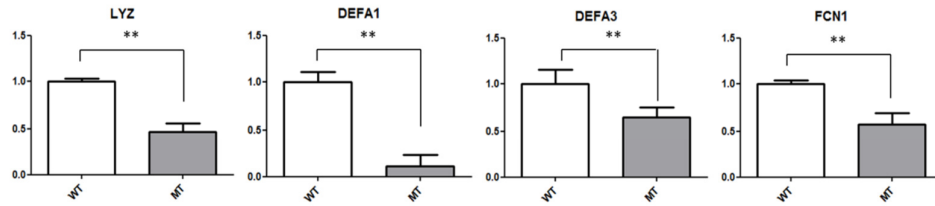


Fig 7.7 Real-time PCR of selected genes. Each graph represents the relative fold difference of WT microglia compared to MT microglia (normalized to 1). (mean+SEM, **p-value<0.001, unpaired t-test).

Table 7.5 Comparison of microglia microarray and real-time PCR results of selected genes. Values are expressed as MT/WT absolute fold change, with positive value denoting up-regulation and negative value denoting down-regulation in MT microglia.

Gene	Microarray fold change	Real-time PCR fold change
LYZ	-2.02	-2.16
DEFA1	-3.59	-9.38
DEFA3	-3.53	-1.53
FCN1	-2.29	-1.75

7.3.5 Comparison of gene expression of different cell types

Having performed gene expression microarray on NPCs, astrocytes and microglia, we wanted to see if there are overlapping genes that are differentially expressed across the different cell lines. We compared the list of differentially expressed genes in each cell type (**Fig 7.8**). In summary, 53 common genes were differentially expressed between NPC and astrocytes, 13 common genes were differentially expressed between NPC and microglia and 18 common genes were differentially expressed between astrocytes and microglia only. 4 genes were found to be differentially expressed between WT and MT cells of all three cell types. The 4 genes are *LOC644128*, *LOC730024*, *Ribosomal Protein L23a Pseudogene 53 (RPL23AP53)* and *Sex Comb on Midleg-Like 1 (SCML1)*. Moreover, we found that common genes that are differentially regulated do not necessarily show the same directional changes. For example, of the 13 genes differentially expressed between NPC and

microglia, only 8 genes showed the same pattern of expression in terms of up or down-regulation. This indicates that MeCP2 regulates the same genes differently in different cell types. This could be the reason why whole brain microarray between WT and *Mecp2*-null mouse showed little changes in gene expression (Tudor et al., 2002). The list of overlapping genes can be found in **Appendix 4**.

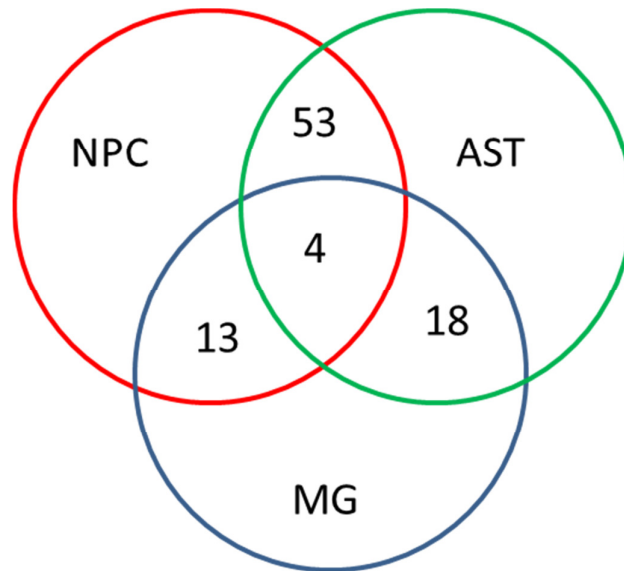


Fig 7.8 Venn diagram show the number of common genes that are differentially expressed between WT and MT cells of the different cell types.

7.4 Discussion

7.4.1 RTT patient's iPSCs can generate microglia

The study of microglia has often been dependent on their isolation from rodent and human brain but the numbers obtained are typically low (Ford et al., 1995; Giulian and Baker, 1986). Immortalized microglia cell lines exist (Bocchini et al., 1992) but their properties have been reported to be different from those of primary microglia (Horvath et al., 2008). iPSC-derived microglia represents a

useful approach towards acquiring microglia for research and potentially for use in regenerative medicine. Here, I described a novel protocol for generating microglia from iPSCs. To confirm microglia identity, a panel of microglia markers such as CD45, CD11B and CD14 was used to perform live-cell flow cytometry. Immunocytochemistry of Iba1 and CD68 further confirmed the microglia identity of the purified cells. Motility and phagocytosis assays demonstrate that iPSCs-derived microglia display key microglia characteristics. These findings demonstrate the usefulness of iPSCs for generating microglia for research and potentially, clinical purpose. The added advantage we have here is having isogenic WT and MT microglia from the same RTT patient (Pomp et al., 2011b).

7.4.2 MT microglia show motility abnormality

Microglia are highly motile cells and constantly extend and retract their processes (Nimmerjahn et al., 2005). It was reported that microglia from *Mecp2*-null mouse exhibit reduced phagocytosis compared to microglia from WT mouse (Derecki et al., 2012). In agreement, our results showed that MT microglia had reduced phagocytosis. Time lapse microscopy further revealed that MT microglia have less process dynamics and locomotion compared to WT microglia.

How could deficiencies of microglial motility and phagocytosis lead to neurological or RTT symptoms? One possibility is that microglia are highly motile cells that constantly survey their environment. This surveying activity is needed to remodel neuronal network through synaptic pruning and phagocytosis of apoptotic cells. Reduction of microglia motility and

phagocytosis therefore results in deficits in neuronal development. As there is a time window for synaptic maturation, this might also be the reason why bone marrow transplantation were most effective when carried out early in mice (Derecki et al., 2012). Transplantation at a later stage could have missed the time window and thus had limited impact. Indeed, a lack of microglia synaptic pruning has been found to lead to abnormal brain development in mice (Paolicelli et al., 2011; Zhan et al., 2014), and there are evidence that impaired microglial phagocytosis might be a cause of neurological symptoms in Nasu-Hakola disease (Takahashi et al., 2005).

7.4.3 Gene expression study reveals several genes differentially regulated in MT microglia

Our findings suggest MeCP2 could be a regulator of genes involved in microglia motility. In support of this theory, our gene expression array identified genes and pathways that are involved in cell movement and chemotaxis of the myeloid lineage. These genes include *DEFA1*, *CD74* and *S100A4* all of which are involved in macrophage motility (Frolich et al., 2012; Furman et al., 2002; Li et al., 2010b). These genes represent potential genes of interest for further investigations.

In addition to cell movement, our microarray analysis also unexpectedly showed an enrichment of pathways involved in cholesterol metabolism as being affected in MT microglia. Intriguingly, a recent publication showed that modulating cholesterol levels ameliorated some RTT symptoms in the mouse model (Buchovecky et al., 2013). In that study, mutation of a gene involved in

cholesterol synthesis, *squalene epoxidase* (*Sqle*) improved some RTT symptoms such as motor dysfunction and longevity. Further investigations by the authors uncovered previously unknown abnormal cholesterol levels in *Mecp2*-null mice. Our gene expression screen showed that MT microglia had higher expression of genes involved in cholesterol biosynthesis including *SQLE*, *CH25H* and *ACAT2*, supporting the evidence that MeCP2 might be a regulator of genes involved in cholesterol pathways. It is not known how these genes could affect microglia function. One possibility is that abnormal cholesterol levels could alter the phagocytic capability and neurotoxicity of microglia (Rackova, 2013). Microglia are also known to be a cholesterol supply source for young neurons (Funfschilling et al., 2012) and for axon growth (Hayashi et al., 2004). Hence any disruption in cholesterol metabolism in microglia could affect the development of neurons. Further investigations are needed to understand the role of cholesterol metabolism in microglia and in RTT.

7.4.4. MT microglia induce neurotoxicity by an unknown mechanism

We observed MT microglia induced neurotoxicity when co-cultured with WT neurons and astrocytes. We investigated glutamate levels and contrary to the mouse system, did not find elevated levels of glutamate secretion from MT microglia. We also looked at TNF α , a cytokine secreted by microglia that could cause neurotoxicity, but found no differences in secretion levels of MT microglia. One possible molecule which we have not looked into at this point is Interferon- γ (IFN- γ) which has been reported to cause neuronal beading and

is secreted by microglia (Mizuno et al., 2008). The cause of neurotoxicity of MeCP2 deficient microglia in human remains to be investigated.

Based on our findings, we propose a model in which deficiencies in microglia function contributes to RTT. In a normal brain, microglia are able to carry out its normal function such as debris clearance and contribute to synaptic maturation through synaptic pruning (**Fig 7.9A**). In the RTT brain, microglia are unable to carry out its role due to reduced motility and phagocytosis (**Fig 7.9B**). Hence, there is an accumulation of debris which can contribute to inflammation (Kettenmann et al., 2011; Liu et al., 2006; Majumdar et al., 2007). Furthermore, microglia are unable to carry out synaptic pruning efficiency leading to stunted synaptic maturity (Paolicelli et al., 2011; Zhan et al., 2014).

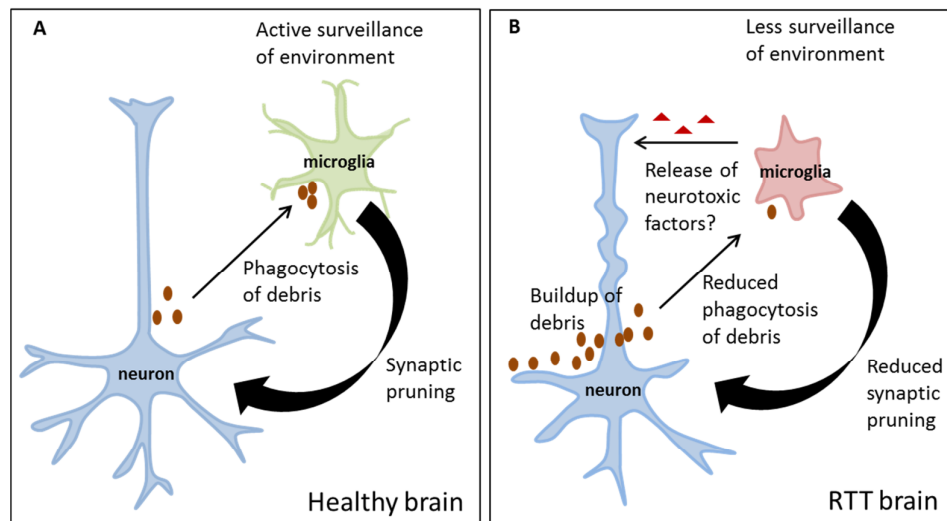


Fig 7.9 Model of how RTT microglia could contribute to RTT. (A) In the healthy brain, microglia actively performs surveillance to carry out essential duties such as debris clearance and synaptic pruning in accordance to the neuronal environment. Neurons are healthy and neuronal transmission occurs optimally. (B) In the RTT brain, microglia is less active in surveying of neuronal environment. In addition, the reduced phagocytosis ability leads to less clearance of cellular debris and less synaptic pruning impeding neuronal

development. RTT microglia may also secrete neurotoxic factor that leads to neurotoxicity. All these factors contribute to poor neuronal health and exacerbate the RTT phenotype.

7.4.5 The role of microglia in neurological diseases

Microglia are increasingly being implicated as one of many causes behind the pathology of neuro-degenerative diseases such as Alzheimer's disease and Parkinson's disease (Perry et al., 2010), and also in neuro-psychiatric diseases such as depression and schizophrenia (Frick et al., 2013). One example however stands out with microglia dysfunction being implicated as the primary cause of neuronal symptoms. Nasu-Hakola disease is a disorder in which mutations of the *Triggering receptor expressed on myeloid cells 2 (TREM2)* gene causes presenile dementia and systemic bone cysts (Bianchin et al., 2004; Paloneva et al., 2001). In the CNS, *TREM2* is expressed only by the microglia and a study showed that impaired phagocytosis and increased inflammatory response of microglia could be the cause of neurodegeneration in the disease (Takahashi et al., 2005). Much about microglia's role in neurological diseases remains unknown and it is therefore important to develop cellular models to gain insight into microglial disease mechanisms. Here, we developed a human stem-cell based model to uncover the abnormalities of *MeCP2* deficient microglia. These work and data provide a foundation for further investigation of microglia's role during development and RTT.

7.4.6 Different cell types derived from isogenic clones showed different changes in gene expression

From this project, different brain cell types were differentiated from the same parental isogenic WT and MT iPSCs lineage. This represents a good opportunity to compare gene expression among different cell types. The transcriptional profiling done in the different cell types identified several genes that are differentially regulated. Comparison of the different gene lists showed that different cell types had different changes in gene expression and there is no consistent pattern of changes between the cell types (**App 4**). Of the 4 genes that appear in all three cell types, *LOC644128* and *LOC730024* are putative proteins and their function remain unknown. *RPL23AP53* stands for *Ribosomal Protein L23a Pseudogene 53* and is a pseudogene of the *Ribosomal Protein L23A* gene (*RPL23A*). *RPL23A* encodes a ribosomal protein that is a component of the 60S subunit of ribosomes involved in protein synthesis. However, *RPL23AP53* has no known function. *SCML1* is an X-linked gene and hence differences seen here might be due to differing copy of X-Chromosome expression. The lack of a clear set common differentially expressed genes between the cell types raise the possibility that MeCP2 regulates genes differently in different cell types. This finding might also explain why whole brain gene expression studies between WT and *Mecp2*-null mice showed little changes in gene expression due to a mixture of cells in the brain confounding the results (Tudor et al., 2002). Hence it might be more meaningful to compare gene expression of pure populations of cells, rather than of a mixed population such as in whole brain, due to differing changes in

different cell types. Further studies are needed to understand the role of MeCP2 amongst different cell types.

7.5 Conclusions

In conclusion, I report the successful generation of microglia from RTT iPSCs that could recapitulate several microglia characteristics. We found key differences between isogenic WT and MT microglia in area of phagocytosis, motility and locomotion. MT microglia also have neurotoxic effects not seen in WT microglia. Gene expression analysis also uncovered potential targets of MeCP2 in microglia.

7.6 Limitations

7.6.1 More patients' samples needed

Only iPSC lines from P72 were used here. RTT patients differ from one another in the range and severity of symptoms. These differences partially stem from differing mutations of the MeCP2 gene and different genetic backgrounds (i.e. modifier genes). Since the finding in this thesis may represent the disease in one patient, it would be beneficial to reproduce these experiments in iPSCs lines from additional patients. The strategy was to first determine the phenotype to be studied using iPSC lines from one patient before extending the findings to other patients. However, the experiments from more patients (P48 and P80) could not be completed in time for this thesis.

7.6.2 Quantification of phagocytosis

Section 7.3.2 show that MT microglia has reduced phagocytosis in number of apoptotic bodies. For a more accurate quantification of phagocytosis rate, images of T=0 should be taken to show the number of apoptotic bodies at the beginning of the experiment. A larger magnification of the field should be also be taken.

7.6.3 Assessment of neurotoxicity

Due to the low survival rate of neurons when sparsely plated, we could only assess neurotoxicity in denser cultures. While we observed neuronal beading in the co-culture with MT microglia, we could not quantify the dendritic beading frequency in dense cultures. BDNF (a survival factor) could be used when plating neurons at low density and withdrawn before conducting the assay. Besides neuronal beading, other methods such as measurement of dendritic length and quantification of acetylated Tubulin intensity could also be used to assess for neurotoxicity (Maezawa and Jin, 2010).

7.6.3 Expression of MeCP2 in iPSC-derived microglia

While mouse microglia have been shown to express *Mecp2* (Maezawa and Jin, 2010), it is important to show that iPSC-derived microglia express MeCP2. An immunostain or western blot should be performed. However, this experiment was not completed in time for this thesis.

7.6.4 Primary cells as positive controls

While the iPSC-derived microglia show expression of microglia markers and demonstrate phagocytosis, a positive control using primary cells is needed for

assays such as phagocytosis assay, glutamate release and TNF α release. Primary microglia could be isolated from mouse brain as a control (Lee and Tansey, 2013; Moussaud and Draheim, 2010).

Chapter 8: Conclusions and perspectives

8.1 Introduction

The absence of neuronal degeneration in RTT raised hopes that the disease may be treatable. Indeed, expression of *Mecp2* led to the rescue of RTT symptoms in the *Mecp2*-null mouse (Guy et al., 2007). Follow-up studies further identified compounds that improved or rescued specific RTT symptoms (e.g. insulin-like growth factor 1 (Tropea et al., 2009), the ampakine CX546 (Ogier et al., 2007), fingolimod (Deogracias et al., 2012), and statin drugs (Buchovecky et al., 2013). These encouraging findings motivated scientists all over the world to further explore the disease. As more data accumulated, additional complexities of RTT emerged. For example, the traditional belief that RTT is exclusively a neuronal disease was replaced by the concept that other brain cell types are also involved and contribute significantly to the pathology of the disease (e.g. astrocytes, microglia and oligodendrocytes (Ballas et al., 2009; Maezawa and Jin, 2010; Maezawa et al., 2009; Nguyen et al., 2013). This knowledge in turn led to novel potential therapeutic strategies including bone marrow transplantation as a means of supplementing the brain with WT monocyte that could play the role of microglia (Derecki et al., 2012). The focus of my thesis was to investigate the impact of *MeCP2* mutations on less explored features of brain development such as neural progenitor migration as well as contributions from other neuronal and non-neuronal cell types like astrocytes and microglia respectively. Through reprogramming of female patient fibroblasts, I was able to prepare isogenic iPSC lines, which either expressed WT or MT MeCP2. Using the isogenic lines from a patient with a 1155del32bp mutation in

MeCP2, I identified novel phenotypes in resident brain cells, some of which have never been implicated in the disease before (e.g. NPCs).

8.2 The use of iPSCs to model RTT

“If our brains were simple enough for us to understand them, we'd be so simple that we couldn't” - Ian Stewart (professor, writer). The lack of understanding of our own brains makes it particularly challenging for us to understand diseases which result from complex interactions between different brain cells. Thus, although it is an over-simplification, disease modeling in a dish is a good strategy to isolate and address questions regarding to brain diseases. In this thesis I demonstrated the generation of pure populations of different types of RTT afflicted cells. Importantly, for each cell type, I generated both experimental MT cells, and as a perfect control, WT cells from the same patient. This allowed me to get new insights regarding the effects of loss of function of *MeCP2* on a specific cell type (e.g. reduced motility in mutant microglia, deficient in proliferation potential in astrocytes) and also to predict potential phenotypes *in vivo* (see next section). Examining *MeCP2* transcriptional regulation in specific cell types is a classic example of one of the advantages of iPSCs technology. While microarray analysis for brain samples which are composed of different cell types may produce confounding information, comparison of homogeneous and isogenic populations of iPSCs derived cells produced informative results.

8.3 Predictions in the patient based on *in vitro* observations

In vitro models are vastly simplified. They give an indication of the phenotype but may not be relevant to the *in vivo* condition. Based on my results in this

work, I will attempt to link how these observations can affect the RTT patient. For example, mutations in MeCP2 can cause migration deficiencies in NPCs, and that the presence of WT NPCs partially alleviates this phenotype. Thus, this data may explain a later onset of the disease in females compared to an early onset of the disease in male. However, there is so far no evidence that NPCs are affected in RTT patients.

The finding of increased PDGF secretion by MT astrocytes and results from gene expression microarray suggest that MT astrocytes may cause leakiness of the BBB. This could be relevant to RTT patients as disruption of BBB is thought to be a major cause of epilepsy (Marchi et al., 2011; Oby and Janigro, 2006), and may be a cause of seizures in RTT patients. However, there is so far no evidence showing that BBB is affected in RTT patients.

In addition, I found that MT microglia are less motile and have less phagocytosis *in vitro*. If this is the situation in the RTT brain, there could be insufficient debris clearance and synaptic pruning which have the potential to contribute to symptoms as seen in the mouse model (Derecki et al., 2012). I also observed MT microglia are neurotoxic. This can lead to damages of neuronal axons and dendrites (Maezawa and Jin, 2010) (Takeuchi et al., 2005). Preliminary studies of microglia dysfunction have been shown in mice *in vivo* model (Derecki et al., 2012), but have not been shown in RTT patients.

Figure 8.1 illustrates some of the findings and predictions based on this work. Astrocytes through increased PDGF-AA secretion (**Fig 8.1A**) can cause leakiness of the BBB (**Fig 8.1B**). Astrocytes also increase activation of microglia due to reduced secretion of fractalkine (**Fig 8.1C**). Microglia are

deficient in phagocytosis (**Fig 8.1D**) which could cause accumulation of debris (**Fig 8.1E**) which in turn leads to poor neuronal health.

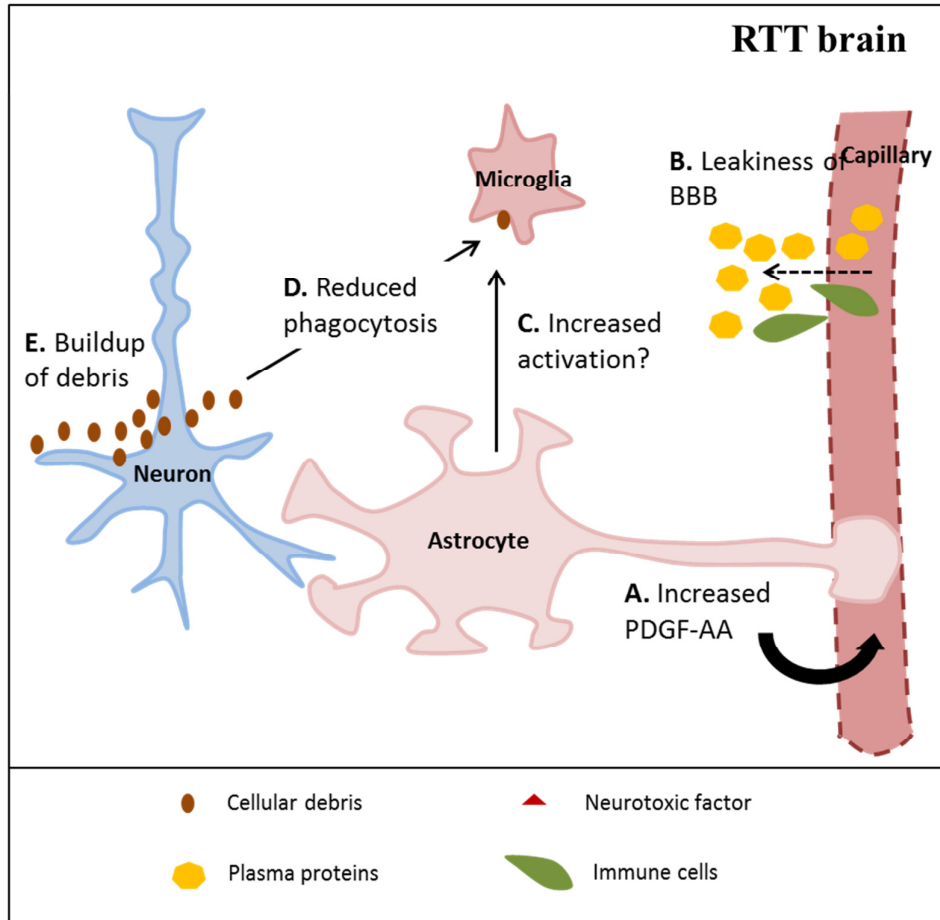


Fig 8.1 Proposed model for how astrocytes and microglia can contribute to the RTT pathology based on findings. MT neurons are dysfunctional in terms of neurotransmission due to reduced synapse numbers and dendritic arbors. This is further exacerbated by several deficiency in glia functions. (A) Over-secretion of PDGF from MT astrocytes could lead to leaky BBB thus enabling (B) infiltration of plasma proteins and immune cells from the peripheral circulation. This leads to the imbalance of the CNS environment homeostasis. (C) MT astrocyte releases less fractalkine which increases activation of microglia. (D) Reduced phagocytosis by MT microglia leads to (E) buildup of debris and causes reduced neuronal health. Note that the RTT brain contains a mixture of WT and MT cells but only MT cells are depicted here for simplicity. All of these predictions should be investigated *in vivo*.

8.4 Future directions

8.4.1 The role of RTT astrocytes in BBB maintenance

The BBB is a specialised structure comprising of three main cell types- the endothelial cells lining the brain vasculature, the astrocytes whose endfeet surround the blood vessel, and the pericytes which are embedded between the endothelial cells and astrocytes. One important function of the BBB is to control the transport of substances between the blood and brain. The tight junctions that forms between the endothelial cells are essential in regulating the transport of many molecules and ions. In addition to the cellular component, ECM proteins in the basement membrane between the endothelial cells and astrocytes are involved in BBB functions.

Astrocytes play an important role in inducing endothelial cells to form tight junctions (Janzer and Raff, 1987; Kuchler-Bopp et al., 1999). As microarray results revealed that blood vessel function and cell adhesion as pathways that are affected in MT astrocytes, I propose that MT astrocytes could cause BBB leakiness due to a reduction of cell to cell contact between astrocytes-astrocyte and astrocytes with the other cell types such as endothelial cells and pericytes. The transwell assay is an *in vitro* method used to assay the permeability of the BBB (**Fig 8.2A**) (Lippmann et al., 2014; Urich et al., 2013; Wong et al., 2013). In this assay, a confluent layer of endothelial cells is plated onto a porous membrane that separates two chambers. Astrocytes and pericytes can be seeded onto the opposite side of the membrane or in the bottom of the chamber. A dye or ions can be introduced into the apical side of the insert and the medium on the basolateral side can then be spectroscopically measured for

leakiness of the dye or a conductivity probe can be used to detect changes in conductivity.

Another way which MT astrocytes could affect BBB leakiness is through excessive PDGF-AA. Though the mechanism is unknown, it is possible that pericytes play an important role in mediating PDGF effects as pericytes are known to express PDGF receptors (Arimura et al., 2012; Quaegebeur et al., 2010; Winkler et al., 2010). The transwell assay could also be used to test for the effects of PDGF-AA on BBB leakiness by addition of varying levels of PDGF-AA or PDGFR inhibitors. Investigation of BBB integrity can also be done in a *Mecp2*-null mouse model by injecting a dye which binds to plasma protein (i.e Evans Blue), and checking for infiltration of the dye in the brain using optical imaging (**Fig 8.2B**) (Jaffer et al., 2013).

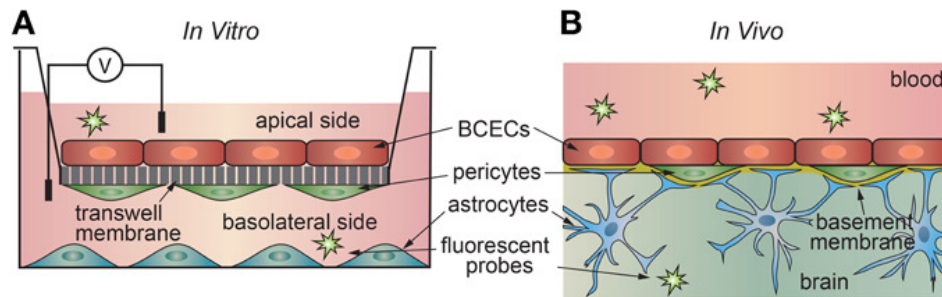


Fig 8.2 Assays for measuring BBB permeability. (A) The transwell in vitro assay consists of endothelial cell plated on the apical side of a microporous membrane and pericytes/astrocytes plated on the basolateral side. Fluorescent probes or ions can be introduced to the apical side and the movement of the probe or ions can be determined on the basolateral side. (B) In vivo assay is performed by injecting a probe into the blood of an animal model. Imaging technique can then be used to detect presence of the probe in the brain of the animal. Image reproduced with permission from (Wong et al., 2013).

8.4.2 Testing of the lactate shuttle hypothesis

Preliminary evidence from this project suggests that the astrocytes have deficit in taking up glucose. If this is the case, it is possible that astrocytes are unable to provide enough metabolites in times of high neuronal demand. According to the astrocyte-neuron lactate shuttle hypothesis, glucose is taken up by astrocytes and converted to lactate to be used as an energy source for neurons (Escartin et al., 2006; Figley, 2011; Pellerin et al., 1998). When the lactate shuttle is affected in mice, cognitive functions and working memory were found to be impaired (Newman et al., 2011; Suzuki et al., 2011) . To further find out the effects of delayed glucose consumption in MT astrocytes, lactate production of iPSC-derived astrocytes can be measured to see if it is affected. The astrocytes could also be stimulated by electrical stimulation or glutamate to see if glucose uptake and lactate production is affected. Another important component is to check glycogen levels as astrocytes are known to have a glycogen storage and convert it into lactate for release in times of neuronal activity (Brown and Ransom, 2014; Brown et al., 2005; Tarczyluk et al., 2013). Together, this series of studies will provide a better idea of how astrocytic metabolics are affected in RTT.

8.4.3 Microglia transplantation as a therapeutic for RTT

In the mouse study, WT bone marrow transplant ameliorated RTT symptoms in mice. This raised the possibility that bone marrow transplant could be used as a treatment for RTT. However, donor bone marrows are in short supply and the chance of finding a bone marrow match is slim. As a validation of the mouse study, WT-iPSCs derived microglia can be transplanted into RTT

mouse model to test if RTT symptoms can be ameliorated. As microglia are highly motile cells, they are able to migrate from the site of transplantation as demonstrated in microglia transplantation studies carried out in mouse models of Alzheimer's disease and cerebral ischemia (Narantuya et al., 2010; Takata et al., 2007). This makes microglia a more suitable cell type for transplantation in RTT than other neural cell types. This will be a proof of concept study and could lead to development of a potential therapeutic strategy for RTT.

8.4.4 Investigation of MeCP2 target genes

The microarray analyses revealed several genes that might be targets of MeCP2 for each cell type. More in-depth study should be done to study these pathways. For example, the cholesterol pathway was highly enriched in the pathway analysis between WT and MT microglia. Further work should be done to determine how cholesterol synthesis is affected in microglia, and how disruption of this process could lead to neurological symptoms. Next, if it is determined that cholesterol synthesis is affected, cholesterol level modulating drugs could be used to see if any MT microglia phenotype could be rescued.

8.4.5 Development of a stem-cell based high-throughput assay

The lack of a cell based system for high-throughput compound screening has been a challenge for neurological disorders (Jain and Heutink, 2010). Stem cells offer an unlimited source of material for drug-screening due to their unlimited proliferation and potential for differentiation. An excellent example of a stem cell based model was presented by Scholer et al., 2012. In this study, the authors co-cultured astrocytes, motor neurons and microglia to screen 10

000 small molecule compounds that can inhibit microglia-mediated toxicity (Fig 8.3). The study was done mainly with rodent ESC derivatives, but in this thesis, I have demonstrated that it is possible to get the cellular derivatives from human iPSCs and this could be a more clinically relevant model when doing drug screening.

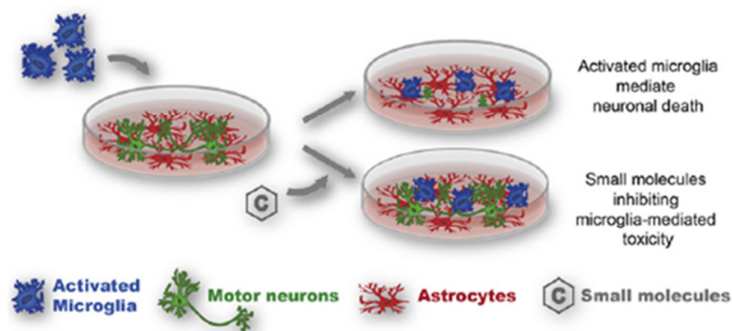


Fig 8.3 High-throughput compound screening using stem cells derivatives. A co-culture system consisting of microglia, motor neurons and astrocytes from mouse. Image reproduced with permission from (Hoing et al., 2012)

8.5 Concluding remarks

Much has been uncovered since the identification of *MeCP2* as the main cause of RTT. While *in vitro* disease modeling at present is limited in its ability to reveal the complex interactions between different cells in the brain, it provides a simplified system to identify cell specific phenotypes and to reveal molecular and biochemical pathways. This technology is just making its first ‘proof of principle’ infant steps. I set out on this project to better understand how RTT happens. By submitting this work I feel privileged to add a step to this exciting journey.

References

- Abbott, N.J., Ronnback, L., and Hansson, E. (2006). Astrocyte-endothelial interactions at the blood-brain barrier. *Nat Rev Neurosci* 7, 41-53.
- Adachi, K., and Scholer, H.R. (2012). Directing reprogramming to pluripotency by transcription factors. *Curr Opin Genet Dev* 22, 416-422.
- Adachi, M., Autry, A.E., Covington, H.E., 3rd, and Monteggia, L.M. (2009). MeCP2-mediated transcription repression in the basolateral amygdala may underlie heightened anxiety in a mouse model of Rett syndrome. *J Neurosci* 29, 4218-4227.
- Adams, V.H., McBryant, S.J., Wade, P.A., Woodcock, C.L., and Hansen, J.C. (2007). Intrinsic disorder and autonomous domain function in the multifunctional nuclear protein, MeCP2. *J Biol Chem* 282, 15057-15064.
- Adzemovic, M.V., Zeitelhofer, M., Eriksson, U., Olsson, T., and Nilsson, I. (2013). Imatinib ameliorates neuroinflammation in a rat model of multiple sclerosis by enhancing blood-brain barrier integrity and by modulating the peripheral immune response. *PLoS One* 8, e56586.
- Allen-Brady, K., Miller, J., Matsunami, N., Stevens, J., Block, H., Farley, M., Krasny, L., Pingree, C., Lainhart, J., Leppert, M., *et al.* (2009). A high-density SNP genome-wide linkage scan in a large autism extended pedigree. *Mol Psychiatry* 14, 590-600.
- Allou, L., Lambert, L., Amsellem, D., Bieth, E., Edery, P., Destree, A., Rivier, F., Amor, D., Thompson, E., Nicholl, J., *et al.* (2012). 14q12 and severe Rett-like phenotypes: new clinical insights and physical mapping of FOXP1-regulatory elements. *Eur J Hum Genet* 20, 1216-1223.
- Allsopp, R.C., Chang, E., Kashefi-Azam, M., Rogaev, E.I., Piatyszek, M.A., Shay, J.W., and Harley, C.B. (1995). Telomere shortening is associated with cell division in vitro and in vivo. *Experimental cell research* 220, 194-200.
- Aloisi, F., Borsellino, G., Care, A., Testa, U., Gallo, P., Russo, G., Peschle, C., and Levi, G. (1995). Cytokine regulation of astrocyte function: in-vitro studies using cells from the human brain. *Int J Dev Neurosci* 13, 265-274.
- Amir, R.E., Van den Veyver, I.B., Wan, M., Tran, C.Q., Francke, U., and Zoghbi, H.Y. (1999). Rett syndrome is caused by mutations in X-linked MECP2, encoding methyl-CpG-binding protein 2. *Nat Genet* 23, 185-188.
- Ananiev, G., Williams, E.C., Li, H., and Chang, Q. (2011). Isogenic pairs of wild type and mutant induced pluripotent stem cell (iPSC) lines from Rett syndrome patients as in vitro disease model. *PLoS One* 6, e25255.
- Andrae, J., Gallini, R., and Betsholtz, C. (2008). Role of platelet-derived growth factors in physiology and medicine. *Genes Dev* 22, 1276-1312.

Anitha, A., Thanseem, I., Nakamura, K., Yamada, K., Iwayama, Y., Toyota, T., Iwata, Y., Suzuki, K., Sugiyama, T., Tsujii, M., *et al.* (2013). Protocadherin alpha (PCDHA) as a novel susceptibility gene for autism. *J Psychiatry Neurosci* 38, 192-198.

Apostolou, E., and Hochedlinger, K. (2013). Chromatin dynamics during cellular reprogramming. *Nature* 502, 462-471.

Archer, H.L., Evans, J., Edwards, S., Colley, J., Newbury-Ecob, R., O'Callaghan, F., Huyton, M., O'Regan, M., Tolmie, J., Sampson, J., *et al.* (2006). CDKL5 mutations cause infantile spasms, early onset seizures, and severe mental retardation in female patients. *J Med Genet* 43, 729-734.

Arimura, K., Ago, T., Kamouchi, M., Nakamura, K., Ishitsuka, K., Kuroda, J., Sugimori, H., Ooboshi, H., Sasaki, T., and Kitazono, T. (2012). PDGF receptor beta signaling in pericytes following ischemic brain injury. *Curr Neurovasc Res* 9, 1-9.

Armstrong, D., Dunn, J.K., Antalffy, B., and Trivedi, R. (1995). Selective dendritic alterations in the cortex of Rett syndrome. *J Neuropathol Exp Neurol* 54, 195-201.

Armstrong, D.D. (2005). Neuropathology of Rett syndrome. *J Child Neurol* 20, 747-753.

Armstrong, D.D., Dunn, J.K., Schultz, R.J., Herbert, D.A., Glaze, D.G., and Motil, K.J. (1999). Organ growth in Rett syndrome: a postmortem examination analysis. *Pediatr Neurol* 20, 125-129.

Armstrong, J., Pineda, M., Aibar, E., Gean, E., and Monros, E. (2001). Classic Rett syndrome in a boy as a result of somatic mosaicism for a MECP2 mutation. *Ann Neurol* 50, 692.

Asaka, Y., Jugloff, D.G., Zhang, L., Eubanks, J.H., and Fitzsimonds, R.M. (2006). Hippocampal synaptic plasticity is impaired in the *Mecp2*-null mouse model of Rett syndrome. *Neurobiol Dis* 21, 217-227.

Ashwell, K. (1990). Microglia and cell death in the developing mouse cerebellum. *Brain Res Dev Brain Res* 55, 219-230.

Babbio, F., Castiglioni, I., Cassina, C., Gariboldi, M.B., Pistore, C., Magnani, E., Badaracco, G., Monti, E., and Bonapace, I.M. (2012). Knock-down of methyl CpG-binding protein 2 (MeCP2) causes alterations in cell proliferation and nuclear lamins expression in mammalian cells. *BMC Cell Biol* 13, 19.

Baeten, K.M., and Akassoglou, K. (2011). Extracellular matrix and matrix receptors in blood-brain barrier formation and stroke. *Dev Neurobiol* 71, 1018-1039.

Baker, S.A., Chen, L., Wilkins, A.D., Yu, P., Lichtarge, O., and Zoghbi, H.Y. (2013). An AT-hook domain in MeCP2 determines the clinical course of Rett syndrome and related disorders. *Cell* 152, 984-996.

Ballas, N., Liroy, D.T., Grunseich, C., and Mandel, G. (2009). Non-cell autonomous influence of MeCP2-deficient glia on neuronal dendritic morphology. *Nat Neurosci* 12, 311-317.

Balmer, D., Arredondo, J., Samaco, R.C., and LaSalle, J.M. (2002). MECP2 mutations in Rett syndrome adversely affect lymphocyte growth, but do not affect imprinted gene expression in blood or brain. *Hum Genet* 110, 545-552.

Barnby, G., Abbott, A., Sykes, N., Morris, A., Weeks, D.E., Mott, R., Lamb, J., Bailey, A.J., and Monaco, A.P. (2005). Candidate-gene screening and association analysis at the autism-susceptibility locus on chromosome 16p: evidence of association at GRIN2A and ABAT. *Am J Hum Genet* 76, 950-966.

Bartl-Pokorny, K.D., Marschik, P.B., Sigafos, J., Tager-Flusberg, H., Kaufmann, W.E., Grossmann, T., and Einspieler, C. (2013). Early socio-communicative forms and functions in typical Rett syndrome. *Res Dev Disabil* 34, 3133-3138.

Battista, D., Ferrari, C.C., Gage, F.H., and Pitossi, F.J. (2006). Neurogenic niche modulation by activated microglia: transforming growth factor beta increases neurogenesis in the adult dentate gyrus. *Eur J Neurosci* 23, 83-93.

Bauman, M.L., Kemper, T.L., and Arin, D.M. (1995a). Microscopic observations of the brain in Rett syndrome. *Neuropediatrics* 26, 105-108.

Bauman, M.L., Kemper, T.L., and Arin, D.M. (1995b). Pervasive neuroanatomic abnormalities of the brain in three cases of Rett's syndrome. *Neurology* 45, 1581-1586.

Baumann, E., Preston, E., Slinn, J., and Stanimirovic, D. (2009). Post-ischemic hypothermia attenuates loss of the vascular basement membrane proteins, agrin and SPARC, and the blood-brain barrier disruption after global cerebral ischemia. *Brain Res* 1269, 185-197.

Bebbington, A., Percy, A., Christodoulou, J., Ravine, D., Ho, G., Jacoby, P., Anderson, A., Pineda, M., Ben Zeev, B., Bahi-Buisson, N., *et al.* (2010). Updating the profile of C-terminal MECP2 deletions in Rett syndrome. *J Med Genet* 47, 242-248.

Belichenko, N.P., Belichenko, P.V., and Mobley, W.C. (2009). Evidence for both neuronal cell autonomous and nonautonomous effects of methyl-CpG-binding protein 2 in the cerebral cortex of female mice with Mecp2 mutation. *Neurobiol Dis* 34, 71-77.

Belichenko, P.V., Oldfors, A., Hagberg, B., and Dahlstrom, A. (1994). Rett syndrome: 3-D confocal microscopy of cortical pyramidal dendrites and afferents. *Neuroreport* 5, 1509-1513.

Bertani, I., Rusconi, L., Bolognese, F., Forlani, G., Conca, B., De Monte, L., Badaracco, G., Landsberger, N., and Kilstrup-Nielsen, C. (2006). Functional consequences of mutations in CDKL5, an X-linked gene involved in infantile spasms and mental retardation. *J Biol Chem* 281, 32048-32056.

Beschorner, R., Nguyen, T.D., Gozalan, F., Pedal, I., Mattern, R., Schluesener, H.J., Meyermann, R., and Schwab, J.M. (2002). CD14 expression by activated parenchymal microglia/macrophages and infiltrating monocytes following human traumatic brain injury. *Acta Neuropathol* 103, 541-549.

Bianchin, M.M., Capella, H.M., Chaves, D.L., Steindel, M., Grisard, E.C., Ganev, G.G., da Silva Junior, J.P., Neto Evaldo, S., Poffo, M.A., Walz, R., *et al.* (2004). Nasu-Hakola disease (polycystic lipomembranous osteodysplasia with sclerosing leukoencephalopathy--PLOS): a dementia associated with bone cystic lesions. From clinical to genetic and molecular aspects. *Cell Mol Neurobiol* 24, 1-24.

Blasco, M.A. (2005). Telomeres and human disease: ageing, cancer and beyond. *Nature reviews Genetics* 6, 611-622.

Bocchini, V., Mazzolla, R., Barluzzi, R., Blasi, E., Sick, P., and Kettenmann, H. (1992). An immortalized cell line expresses properties of activated microglial cells. *J Neurosci Res* 31, 616-621.

Bongso, A., Fong, C.Y., Ng, S.C., and Ratnam, S. (1994). Isolation and culture of inner cell mass cells from human blastocysts. *Hum Reprod* 9, 2110-2117.

Boyer, L.A., Lee, T.I., Cole, M.F., Johnstone, S.E., Levine, S.S., Zucker, J.P., Guenther, M.G., Kumar, R.M., Murray, H.L., Jenner, R.G., *et al.* (2005). Core transcriptional regulatory circuitry in human embryonic stem cells. *Cell* 122, 947-956.

Braunschweig, D., Simcox, T., Samaco, R.C., and LaSalle, J.M. (2004). X-Chromosome inactivation ratios affect wild-type MeCP2 expression within mosaic Rett syndrome and *Mecp2*^{-/+} mouse brain. *Hum Mol Genet* 13, 1275-1286.

Brendel, C., Belakhov, V., Werner, H., Wegener, E., Gartner, J., Nudelman, I., Baasov, T., and Huppke, P. (2011). Readthrough of nonsense mutations in Rett syndrome: evaluation of novel aminoglycosides and generation of a new mouse model. *J Mol Med (Berl)* 89, 389-398.

Brendel, C., Klahold, E., Gartner, J., and Huppke, P. (2009). Suppression of nonsense mutations in Rett syndrome by aminoglycoside antibiotics. *Pediatr Res* 65, 520-523.

Brown, A.M., and Ransom, B.R. (2007). Astrocyte glycogen and brain energy metabolism. *Glia* 55, 1263-1271.

Brown, A.M., and Ransom, B.R. (2014). Astrocyte glycogen as an emergency fuel under conditions of glucose deprivation or intense neural activity. *Metab Brain Dis*.

Brown, A.M., Sickmann, H.M., Fosgerau, K., Lund, T.M., Schousboe, A., Waagepetersen, H.S., and Ransom, B.R. (2005). Astrocyte glycogen metabolism is required for neural activity during aglycemia or intense stimulation in mouse white matter. *J Neurosci Res* 79, 74-80.

Brozzi, F., Arcuri, C., Giambanco, I., and Donato, R. (2009). S100B Protein Regulates Astrocyte Shape and Migration via Interaction with Src Kinase: IMPLICATIONS FOR

ASTROCYTE DEVELOPMENT, ACTIVATION, AND TUMOR GROWTH. *J Biol Chem* 284, 8797-8811.

Buchovecky, C.M., Turley, S.D., Brown, H.M., Kyle, S.M., McDonald, J.G., Liu, B., Pieper, A.A., Huang, W., Katz, D.M., Russell, D.W., *et al.* (2013). A suppressor screen in *Mecp2* mutant mice implicates cholesterol metabolism in Rett syndrome. *Nat Genet* 45, 1013-1020.

Burkert, K., Moodley, K., Angel, C.E., Brooks, A., and Graham, E.S. (2012). Detailed analysis of inflammatory and neuromodulatory cytokine secretion from human NT2 astrocytes using multiplex bead array. *Neurochem Int* 60, 573-580.

Buschdorf, J.P., and Stratling, W.H. (2004). A WW domain binding region in methyl-CpG-binding protein MeCP2: impact on Rett syndrome. *J Mol Med (Berl)* 82, 135-143.

Cabezas, R., Avila, M., Gonzalez, J., El-Bacha, R.S., Baez, E., Garcia-Segura, L.M., Jurado Coronel, J.C., Capani, F., Cardona-Gomez, G.P., and Barreto, G.E. (2014). Astrocytic modulation of blood brain barrier: perspectives on Parkinson's disease. *Front Cell Neurosci* 8, 211.

Calfa, G., Percy, A.K., and Pozzo-Miller, L. (2011). Experimental models of Rett syndrome based on *Mecp2* dysfunction. *Exp Biol Med (Maywood)* 236, 3-19.

Cardona, A.E., Pioro, E.P., Sasse, M.E., Kostenko, V., Cardona, S.M., Dijkstra, I.M., Huang, D., Kidd, G., Dombrowski, S., Dutta, R., *et al.* (2006). Control of microglial neurotoxicity by the fractalkine receptor. *Nat Neurosci* 9, 917-924.

Cartwright, P., McLean, C., Sheppard, A., Rivett, D., Jones, K., and Dalton, S. (2005). LIF/STAT3 controls ES cell self-renewal and pluripotency by a Myc-dependent mechanism. *Development* 132, 885-896.

Castro, J., Garcia, R.I., Kwok, S., Banerjee, A., Petravic, J., Woodson, J., Mellios, N., Tropea, D., and Sur, M. (2014). Functional recovery with recombinant human IGF1 treatment in a mouse model of Rett Syndrome. *Proc Natl Acad Sci U S A* 111, 9941-9946.

Chahrour, M., and Zoghbi, H.Y. (2007). The story of Rett syndrome: from clinic to neurobiology. *Neuron* 56, 422-437.

Chandler, S.P., Guschin, D., Landsberger, N., and Wolffe, A.P. (1999). The methyl-CpG binding transcriptional repressor MeCP2 stably associates with nucleosomal DNA. *Biochemistry* 38, 7008-7018.

Chao, H.T., Chen, H., Samaco, R.C., Xue, M., Chahrour, M., Yoo, J., Neul, J.L., Gong, S., Lu, H.C., Heintz, N., *et al.* (2010). Dysfunction in GABA signalling mediates autism-like stereotypies and Rett syndrome phenotypes. *Nature* 468, 263-269.

Chao, H.T., Zoghbi, H.Y., and Rosenmund, C. (2007). MeCP2 controls excitatory synaptic strength by regulating glutamatergic synapse number. *Neuron* 56, 58-65.

Chapleau, C.A., Calfa, G.D., Lane, M.C., Albertson, A.J., Larimore, J.L., Kudo, S., Armstrong, D.L., Percy, A.K., and Pozzo-Miller, L. (2009). Dendritic spine pathologies in hippocampal pyramidal neurons from Rett syndrome brain and after expression of Rett-associated MECP2 mutations. *Neurobiol Dis*.

Chapleau, C.A., Lane, J., Kirwin, S.M., Schanen, C., Vinette, K.M., Stubbolo, D., Macleod, P., and Percy, A.K. (2013). Detection of rarely identified multiple mutations in MECP2 gene do not contribute to enhanced severity in rett syndrome. *Am J Med Genet A* *161*, 1638-1646.

Chen, Q., Zhu, Y.C., Yu, J., Miao, S., Zheng, J., Xu, L., Zhou, Y., Li, D., Zhang, C., Tao, J., *et al.* (2010a). CDKL5, a protein associated with rett syndrome, regulates neuronal morphogenesis via Rac1 signaling. *J Neurosci* *30*, 12777-12786.

Chen, R.Z., Akbarian, S., Tudor, M., and Jaenisch, R. (2001). Deficiency of methyl-CpG binding protein-2 in CNS neurons results in a Rett-like phenotype in mice. *Nat Genet* *27*, 327-331.

Chen, S.K., Tvrdik, P., Peden, E., Cho, S., Wu, S., Spangrude, G., and Capecchi, M.R. (2010b). Hematopoietic origin of pathological grooming in Hoxb8 mutant mice. *Cell* *141*, 775-785.

Chen, W.V., and Maniatis, T. (2013). Clustered protocadherins. *Development* *140*, 3297-3302.

Cheung, A.Y., Horvath, L.M., Carrel, L., and Ellis, J. (2012). X-chromosome inactivation in rett syndrome human induced pluripotent stem cells. *Frontiers in psychiatry* *3*, 24.

Cheung, A.Y., Horvath, L.M., Grafodatskaya, D., Pasceri, P., Weksberg, R., Hotta, A., Carrel, L., and Ellis, J. (2011). Isolation of MECP2-null Rett Syndrome patient hiPS cells and isogenic controls through X-chromosome inactivation. *Hum Mol Genet*.

Chew, J.L., Loh, Y.H., Zhang, W., Chen, X., Tam, W.L., Yeap, L.S., Li, P., Ang, Y.S., Lim, B., Robson, P., *et al.* (2005). Reciprocal transcriptional regulation of Pou5f1 and Sox2 via the Oct4/Sox2 complex in embryonic stem cells. *Mol Cell Biol* *25*, 6031-6046.

Choi, S.S., Lee, H.J., Lim, I., Satoh, J., and Kim, S.U. (2014). Human astrocytes: secretome profiles of cytokines and chemokines. *PLoS One* *9*, e92325.

Chuquet, J., Quilichini, P., Nimchinsky, E.A., and Buzsaki, G. (2010). Predominant enhancement of glucose uptake in astrocytes versus neurons during activation of the somatosensory cortex. *J Neurosci* *30*, 15298-15303.

Collins, A.L., Levenson, J.M., Vilaythong, A.P., Richman, R., Armstrong, D.L., Noebels, J.L., David Sweatt, J., and Zoghbi, H.Y. (2004). Mild overexpression of MeCP2 causes a progressive neurological disorder in mice. *Hum Mol Genet* *13*, 2679-2689.

Cosenza-Nashat, M.A., Kim, M.O., Zhao, M.L., Suh, H.S., and Lee, S.C. (2006). CD45 isoform expression in microglia and inflammatory cells in HIV-1 encephalitis. *Brain Pathol* *16*, 256-265.

Cross, S.H., Meehan, R.R., Nan, X., and Bird, A. (1997). A component of the transcriptional repressor MeCP1 shares a motif with DNA methyltransferase and HRX proteins. *Nat Genet* *16*, 256-259.

Dastidar, S.G., Bardai, F.H., Ma, C., Price, V., Rawat, V., Verma, P., Narayanan, V., and D'Mello, S.R. (2012). Isoform-specific toxicity of Mecp2 in postmitotic neurons: suppression of neurotoxicity by FoxG1. *J Neurosci* *32*, 2846-2855.

Dayer, A.G., Bottani, A., Bouchardy, I., Fluss, J., Antonarakis, S.E., Haenggeli, C.A., and Morris, M.A. (2007). MECP2 mutant allele in a boy with Rett syndrome and his unaffected heterozygous mother. *Brain Dev* *29*, 47-50.

Deiva, K., Geeraerts, T., Salim, H., Leclerc, P., Hery, C., Hugel, B., Freyssinet, J.M., and Tardieu, M. (2004). Fractalkine reduces N-methyl-d-aspartate-induced calcium flux and apoptosis in human neurons through extracellular signal-regulated kinase activation. *Eur J Neurosci* *20*, 3222-3232.

del Gaudio, D., Fang, P., Scaglia, F., Ward, P.A., Craigen, W.J., Glaze, D.G., Neul, J.L., Patel, A., Lee, J.A., Irons, M., *et al.* (2006). Increased MECP2 gene copy number as the result of genomic duplication in neurodevelopmentally delayed males. *Genet Med* *8*, 784-792.

Deogracias, R., Yazdani, M., Dekkers, M.P., Guy, J., Ionescu, M.C., Vogt, K.E., and Barde, Y.A. (2012). Fingolimod, a sphingosine-1 phosphate receptor modulator, increases BDNF levels and improves symptoms of a mouse model of Rett syndrome. *Proc Natl Acad Sci U S A* *109*, 14230-14235.

Derecki, N.C., Cronk, J.C., Lu, Z., Xu, E., Abbott, S.B., Guyenet, P.G., and Kipnis, J. (2012). Wild-type microglia arrest pathology in a mouse model of Rett syndrome. *Nature* *484*, 105-109.

Desai, B.S., Monahan, A.J., Carvey, P.M., and Hendey, B. (2007). Blood-brain barrier pathology in Alzheimer's and Parkinson's disease: implications for drug therapy. *Cell Transplant* *16*, 285-299.

Deschamps, J., and Wijgerde, M. (1993). Two phases in the establishment of HOX expression domains. *Dev Biol* *156*, 473-480.

Dibbens, L.M., Tarpey, P.S., Hynes, K., Bayly, M.A., Scheffer, I.E., Smith, R., Bomar, J., Sutton, E., Vandeleur, L., Shoubridge, C., *et al.* (2008). X-linked protocadherin 19 mutations cause female-limited epilepsy and cognitive impairment. *Nat Genet* *40*, 776-781.

Doetsch, F., and Alvarez-Buylla, A. (1996). Network of tangential pathways for neuronal migration in adult mammalian brain. *Proc Natl Acad Sci U S A* *93*, 14895-14900.

Dragich, J.M., Kim, Y.H., Arnold, A.P., and Schanen, N.C. (2007). Differential distribution of the MeCP2 splice variants in the postnatal mouse brain. *J Comp Neurol* *501*, 526-542.

Eiraku, M., Watanabe, K., Matsuo-Takasaki, M., Kawada, M., Yonemura, S., Matsumura, M., Wataya, T., Nishiyama, A., Muguruma, K., and Sasai, Y. (2008). Self-organized formation of polarized cortical tissues from ESCs and its active manipulation by extrinsic signals. *Cell Stem Cell* 3, 519-532.

Ellis, P., Fagan, B.M., Magness, S.T., Hutton, S., Taranova, O., Hayashi, S., McMahon, A., Rao, M., and Pevny, L. (2004). SOX2, a persistent marker for multipotential neural stem cells derived from embryonic stem cells, the embryo or the adult. *Dev Neurosci* 26, 148-165.

Ellison, K.A., Fill, C.P., Terwilliger, J., DeGennaro, L.J., Martin-Gallardo, A., Anvret, M., Percy, A.K., Ott, J., and Zoghbi, H. (1992). Examination of X chromosome markers in Rett syndrome: exclusion mapping with a novel variation on multilocus linkage analysis. *Am J Hum Genet* 50, 278-287.

Elshal, M.F., and McCoy, J.P. (2006). Multiplex bead array assays: performance evaluation and comparison of sensitivity to ELISA. *Methods* 38, 317-323.

Erhardt, A., Czibere, L., Roeske, D., Lucae, S., Unschuld, P.G., Ripke, S., Specht, M., Kohli, M.A., Kloiber, S., Ising, M., *et al.* (2011). TMEM132D, a new candidate for anxiety phenotypes: evidence from human and mouse studies. *Mol Psychiatry* 16, 647-663.

Eriksson, P.S., Perfilieva, E., Bjork-Eriksson, T., Alborn, A.M., Nordborg, C., Peterson, D.A., and Gage, F.H. (1998). Neurogenesis in the adult human hippocampus. *Nat Med* 4, 1313-1317.

Escartin, C., Valette, J., Lebon, V., and Bonvento, G. (2006). Neuron-astrocyte interactions in the regulation of brain energy metabolism: a focus on NMR spectroscopy. *J Neurochem* 99, 393-401.

Fehr, S., Wilson, M., Downs, J., Williams, S., Murgia, A., Sartori, S., Vecchi, M., Ho, G., Polli, R., Psoni, S., *et al.* (2013). The CDKL5 disorder is an independent clinical entity associated with early-onset encephalopathy. *Eur J Hum Genet* 21, 266-273.

Feng, Q., and Zhang, Y. (2001). The MeCP1 complex represses transcription through preferential binding, remodeling, and deacetylating methylated nucleosomes. *Genes Dev* 15, 827-832.

Fietz, S.A., and Huttner, W.B. (2011). Cortical progenitor expansion, self-renewal and neurogenesis-a polarized perspective. *Curr Opin Neurobiol* 21, 23-35.

Figley, C.R. (2011). Lactate transport and metabolism in the human brain: implications for the astrocyte-neuron lactate shuttle hypothesis. *J Neurosci* 31, 4768-4770.

FitzGerald, P.M., Jankovic, J., and Percy, A.K. (1990). Rett syndrome and associated movement disorders. *Mov Disord* 5, 195-202.

Ford, A.L., Goodsall, A.L., Hickey, W.F., and Sedgwick, J.D. (1995). Normal adult ramified microglia separated from other central nervous system macrophages by

flow cytometric sorting. Phenotypic differences defined and direct ex vivo antigen presentation to myelin basic protein-reactive CD4+ T cells compared. *J Immunol* *154*, 4309-4321.

Fraga, M.F., Ballestar, E., Montoya, G., Taysavang, P., Wade, P.A., and Esteller, M. (2003). The affinity of different MBD proteins for a specific methylated locus depends on their intrinsic binding properties. *Nucleic Acids Res* *31*, 1765-1774.

Francke, U. (2006). Mechanisms of disease: neurogenetics of MeCP2 deficiency. *Nat Clin Pract Neurol* *2*, 212-221.

Frick, L.R., Williams, K., and Pittenger, C. (2013). Microglial dysregulation in psychiatric disease. *Clin Dev Immunol* *2013*, 608654.

Friez, M.J., Jones, J.R., Clarkson, K., Lubs, H., Abuelo, D., Bier, J.A., Pai, S., Simensen, R., Williams, C., Giampietro, P.F., *et al.* (2006). Recurrent infections, hypotonia, and mental retardation caused by duplication of MECP2 and adjacent region in Xq28. *Pediatrics* *118*, e1687-1695.

Frolich, D., Blassfeld, D., Reiter, K., Giesecke, C., Daridon, C., Mei, H.E., Burmester, G.R., Goldenberg, D.M., Salama, A., and Dorner, T. (2012). The anti-CD74 humanized monoclonal antibody, milatuzumab, which targets the invariant chain of MHC II complexes, alters B-cell proliferation, migration, and adhesion molecule expression. *Arthritis Res Ther* *14*, R54.

Funfschilling, U., Jockusch, W.J., Sivakumar, N., Mobius, W., Corthals, K., Li, S., Quintes, S., Kim, Y., Schaap, I.A., Rhee, J.S., *et al.* (2012). Critical time window of neuronal cholesterol synthesis during neurite outgrowth. *J Neurosci* *32*, 7632-7645.

Furman, C., Short, S.M., Subramanian, R.R., Zetter, B.R., and Roberts, T.M. (2002). DEF-1/ASAP1 is a GTPase-activating protein (GAP) for ARF1 that enhances cell motility through a GAP-dependent mechanism. *J Biol Chem* *277*, 7962-7969.

Fusaki, N., Ban, H., Nishiyama, A., Saeki, K., and Hasegawa, M. (2009). Efficient induction of transgene-free human pluripotent stem cells using a vector based on Sendai virus, an RNA virus that does not integrate into the host genome. *Proc Jpn Acad Ser B Phys Biol Sci* *85*, 348-362.

Fyffe, S.L., Neul, J.L., Samaco, R.C., Chao, H.T., Ben-Shachar, S., Moretti, P., McGill, B.E., Goulding, E.H., Sullivan, E., Tecott, L.H., *et al.* (2008). Deletion of *Mecp2* in *Sim1*-expressing neurons reveals a critical role for MeCP2 in feeding behavior, aggression, and the response to stress. *Neuron* *59*, 947-958.

Gadalla, K.K., Bailey, M.E., Spike, R.C., Ross, P.D., Woodard, K.T., Kalburgi, S.N., Bachaboina, L., Deng, J.V., West, A.E., Samulski, R.J., *et al.* (2013). Improved survival and reduced phenotypic severity following AAV9/MECP2 gene transfer to neonatal and juvenile male *Mecp2* knockout mice. *Mol Ther* *21*, 18-30.

Galvao, T.C., and Thomas, J.O. (2005). Structure-specific binding of MeCP2 to four-way junction DNA through its methyl CpG-binding domain. *Nucleic Acids Res* *33*, 6603-6609.

Garg, S.K., Lioy, D.T., Cheval, H., McGann, J.C., Bissonnette, J.M., Murtha, M.J., Foust, K.D., Kaspar, B.K., Bird, A., and Mandel, G. (2013). Systemic delivery of MeCP2 rescues behavioral and cellular deficits in female mouse models of Rett syndrome. *J Neurosci* 33, 13612-13620.

Geerdink, N., Rotteveel, J.J., Lammens, M., Sistermans, E.A., Heikens, G.T., Gabreels, F.J., Mullaart, R.A., and Hamel, B.C. (2002). MECP2 mutation in a boy with severe neonatal encephalopathy: clinical, neuropathological and molecular findings. *Neuropediatrics* 33, 33-36.

Giacometti, E., Luikenhuis, S., Beard, C., and Jaenisch, R. (2007). Partial rescue of MeCP2 deficiency by postnatal activation of MeCP2. *Proc Natl Acad Sci U S A* 104, 1931-1936.

Ginhoux, F., Lim, S., Hoeffel, G., Low, D., and Huber, T. (2013). Origin and differentiation of microglia. *Front Cell Neurosci* 7, 45.

Girard, M., Couvert, P., Carrie, A., Tardieu, M., Chelly, J., Beldjord, C., and Bienvenu, T. (2001). Parental origin of de novo MECP2 mutations in Rett syndrome. *Eur J Hum Genet* 9, 231-236.

Giulian, D., and Baker, T.J. (1986). Characterization of amoeboid microglia isolated from developing mammalian brain. *J Neurosci* 6, 2163-2178.

Goffin, D., Allen, M., Zhang, L., Amorim, M., Wang, I.T., Reyes, A.R., Mercado-Berton, A., Ong, C., Cohen, S., Hu, L., *et al.* (2012). Rett syndrome mutation MeCP2 T158A disrupts DNA binding, protein stability and ERP responses. *Nat Neurosci* 15, 274-283.

Gonzales, M.L., Adams, S., Dunaway, K.W., and LaSalle, J.M. (2012). Phosphorylation of distinct sites in MeCP2 modifies cofactor associations and the dynamics of transcriptional regulation. *Mol Cell Biol* 32, 2894-2903.

Greer, J.M., and Capecchi, M.R. (2002). Hoxb8 is required for normal grooming behavior in mice. *Neuron* 33, 23-34.

Greider, C.W., and Blackburn, E.H. (1985). Identification of a specific telomere terminal transferase activity in Tetrahymena extracts. *Cell* 43, 405-413.

Gurdon, J.B. (1962). The developmental capacity of nuclei taken from intestinal epithelium cells of feeding tadpoles. *Journal of embryology and experimental morphology* 10, 622-640.

Guy, J., Gan, J., Selfridge, J., Cobb, S., and Bird, A. (2007). Reversal of neurological defects in a mouse model of Rett syndrome. *Science* 315, 1143-1147.

Guy, J., Hendrich, B., Holmes, M., Martin, J.E., and Bird, A. (2001). A mouse *Mecp2*-null mutation causes neurological symptoms that mimic Rett syndrome. *Nat Genet* 27, 322-326.

Hagberg, B. (1995). Rett syndrome: clinical peculiarities and biological mysteries. *Acta Paediatr* 84, 971-976.

Halbach, N.S., Smeets, E.E., Steinbusch, C., Maaskant, M.A., van Waardenburg, D., and Curfs, L.M. (2013). Aging in Rett syndrome: a longitudinal study. *Clin Genet* *84*, 223-229.

Halliday, A.L., and Cepko, C.L. (1992). Generation and migration of cells in the developing striatum. *Neuron* *9*, 15-26.

Han, S.S., Williams, L.A., and Eggan, K.C. (2011). Constructing and deconstructing stem cell models of neurological disease. *Neuron* *70*, 626-644.

Han, X., Chen, M., Wang, F., Windrem, M., Wang, S., Shanz, S., Xu, Q., Oberheim, N.A., Bekar, L., Betstadt, S., *et al.* (2013). Forebrain engraftment by human glial progenitor cells enhances synaptic plasticity and learning in adult mice. *Cell Stem Cell* *12*, 342-353.

Han, Z.A., Jeon, H.R., Kim, S.W., Park, J.Y., and Chung, H.J. (2012). Clinical characteristics of children with rett syndrome. *Ann Rehabil Med* *36*, 334-339.

Harrison, J.K., Jiang, Y., Chen, S., Xia, Y., Maciejewski, D., McNamara, R.K., Streit, W.J., Salafranca, M.N., Adhikari, S., Thompson, D.A., *et al.* (1998). Role for neuronally derived fractalkine in mediating interactions between neurons and CX3CR1-expressing microglia. *Proc Natl Acad Sci U S A* *95*, 10896-10901.

Hashimoto, H., Liu, Y., Upadhyay, A.K., Chang, Y., Howerton, S.B., Vertino, P.M., Zhang, X., and Cheng, X. (2012). Recognition and potential mechanisms for replication and erasure of cytosine hydroxymethylation. *Nucleic Acids Res* *40*, 4841-4849.

Hayashi, H., Campenot, R.B., Vance, D.E., and Vance, J.E. (2004). Glial lipoproteins stimulate axon growth of central nervous system neurons in compartmented cultures. *J Biol Chem* *279*, 14009-14015.

Hemmati-Brivanlou, A., and Melton, D. (1997). Vertebrate embryonic cells will become nerve cells unless told otherwise. *Cell* *88*, 13-17.

Hendrich, B., and Tweedie, S. (2003). The methyl-CpG binding domain and the evolving role of DNA methylation in animals. *Trends Genet* *19*, 269-277.

Heng, J.I., Nguyen, L., Castro, D.S., Zimmer, C., Wildner, H., Armant, O., Skowronska-Krawczyk, D., Bedogni, F., Matter, J.M., Hevner, R., *et al.* (2008). Neurogenin 2 controls cortical neuron migration through regulation of Rnd2. *Nature* *455*, 114-118.

Hirsch, E.C., Breidert, T., Rousset, E., Hunot, S., Hartmann, A., and Michel, P.P. (2003). The role of glial reaction and inflammation in Parkinson's disease. *Ann N Y Acad Sci* *991*, 214-228.

Hiyama, E., and Hiyama, K. (2007). Telomere and telomerase in stem cells. *British journal of cancer* *96*, 1020-1024.

Hoffbuhr, K., Devaney, J.M., LaFleur, B., Sirianni, N., Scacheri, C., Giron, J., Schuette, J., Innis, J., Marino, M., Philippart, M., *et al.* (2001). MeCP2 mutations in children with and without the phenotype of Rett syndrome. *Neurology* *56*, 1486-1495.

Hoing, S., Rudhard, Y., Reinhardt, P., Glatza, M., Stehling, M., Wu, G., Peiker, C., Bocker, A., Parga, J.A., Bunk, E., *et al.* (2012). Discovery of inhibitors of microglial neurotoxicity acting through multiple mechanisms using a stem-cell-based phenotypic assay. *Cell Stem Cell* *11*, 620-632.

Holgado, B.L., Martinez-Munoz, L., Sanchez-Alcaniz, J.A., Lucas, P., Perez-Garcia, V., Perez, G., Rodriguez-Frade, J.M., Nieto, M., Marin, O., Carrasco, Y.R., *et al.* (2013). CXCL12-mediated murine neural progenitor cell movement requires PI3Kbeta activation. *Mol Neurobiol* *48*, 217-231.

Horike, S., Cai, S., Miyano, M., Cheng, J.F., and Kohwi-Shigematsu, T. (2005). Loss of silent-chromatin looping and impaired imprinting of DLX5 in Rett syndrome. *Nat Genet* *37*, 31-40.

Horvath, R.J., Natile-McMenemy, N., Alkaitis, M.S., and Deleo, J.A. (2008). Differential migration, LPS-induced cytokine, chemokine, and NO expression in immortalized BV-2 and HAPI cell lines and primary microglial cultures. *J Neurochem* *107*, 557-569.

Hotta, A., Cheung, A.Y., Farra, N., Vijayaragavan, K., Seguin, C.A., Draper, J.S., Pasceri, P., Maksakova, I.A., Mager, D.L., Rossant, J., *et al.* (2009). Isolation of human iPS cells using EOS lentiviral vectors to select for pluripotency. *Nat Methods* *6*, 370-376.

Hsu, P.D., Lander, E.S., and Zhang, F. (2014). Development and applications of CRISPR-Cas9 for genome engineering. *Cell* *157*, 1262-1278.

Huang da, W., Sherman, B.T., and Lempicki, R.A. (2009a). Bioinformatics enrichment tools: paths toward the comprehensive functional analysis of large gene lists. *Nucleic Acids Res* *37*, 1-13.

Huang da, W., Sherman, B.T., and Lempicki, R.A. (2009b). Systematic and integrative analysis of large gene lists using DAVID bioinformatics resources. *Nat Protoc* *4*, 44-57.

Imitola, J., Raddassi, K., Park, K.I., Mueller, F.J., Nieto, M., Teng, Y.D., Frenkel, D., Li, J., Sidman, R.L., Walsh, C.A., *et al.* (2004). Directed migration of neural stem cells to sites of CNS injury by the stromal cell-derived factor 1alpha/CXC chemokine receptor 4 pathway. *Proc Natl Acad Sci U S A* *101*, 18117-18122.

Ito, D., Imai, Y., Ohsawa, K., Nakajima, K., Fukuuchi, Y., and Kohsaka, S. (1998). Microglia-specific localisation of a novel calcium binding protein, Iba1. *Brain Res Mol Brain Res* *57*, 1-9.

Itoh, M., Tahimic, C.G., Ide, S., Otsuki, A., Sasaoka, T., Noguchi, S., Oshimura, M., Goto, Y., and Kurimasa, A. (2012). Methyl CpG-binding protein isoform MeCP2_e2 is dispensable for Rett syndrome phenotypes but essential for embryo viability and placenta development. *J Biol Chem* *287*, 13859-13867.

Itskovitz-Eldor, J., Schuldiner, M., Karsenti, D., Eden, A., Yanuka, O., Amit, M., Soreq, H., and Benvenisty, N. (2000). Differentiation of human embryonic stem cells into embryoid bodies compromising the three embryonic germ layers. *Mol Med* 6, 88-95.

Iwata, B.A., Pace, G.M., Willis, K.D., Gamache, T.B., and Hyman, S.L. (1986). Operant studies of self-injurious hand biting in the Rett syndrome. *Am J Med Genet Suppl* 1, 157-166.

Jaffer, H., Adjei, I.M., and Labhasetwar, V. (2013). Optical imaging to map blood-brain barrier leakage. *Sci Rep* 3, 3117.

Jain, S., and Heutink, P. (2010). From single genes to gene networks: high-throughput-high-content screening for neurological disease. *Neuron* 68, 207-217.

Janzer, R.C., and Raff, M.C. (1987). Astrocytes induce blood-brain barrier properties in endothelial cells. *Nature* 325, 253-257.

Jellinger, K., Armstrong, D., Zoghbi, H.Y., and Percy, A.K. (1988). Neuropathology of Rett syndrome. *Acta Neuropathol* 76, 142-158.

Jeon, J.Y., An, J.H., Kim, S.U., Park, H.G., and Lee, M.A. (2008). Migration of human neural stem cells toward an intracranial glioma. *Exp Mol Med* 40, 84-91.

Jiang, J., Chan, Y.S., Loh, Y.H., Cai, J., Tong, G.Q., Lim, C.A., Robson, P., Zhong, S., and Ng, H.H. (2008). A core Klf circuitry regulates self-renewal of embryonic stem cells. *Nat Cell Biol* 10, 353-360.

Johnson, R.A., Lam, M., Punzo, A.M., Li, H., Lin, B.R., Ye, K., Mitchell, G.S., and Chang, Q. (2012). 7,8-dihydroxyflavone exhibits therapeutic efficacy in a mouse model of Rett syndrome. *J Appl Physiol* (1985) 112, 704-710.

Jonas Frisen, U.L.a.T.P. (2012). Mature cells can be reprogrammed to become pluripotent. Nobel Webpage.

Jones, P.L., Veenstra, G.J., Wade, P.A., Vermaak, D., Kass, S.U., Landsberger, N., Strouboulis, J., and Wolffe, A.P. (1998). Methylated DNA and MeCP2 recruit histone deacetylase to repress transcription. *Nat Genet* 19, 187-191.

Kajizuka, M., Miyachi, T., Matsuzaki, H., Iwata, K., Shinmura, C., Suzuki, K., Suda, S., Tsuchiya, K.J., Matsumoto, K., Iwata, Y., *et al.* (2010). Serum levels of platelet-derived growth factor BB homodimers are increased in male children with autism. *Prog Neuropsychopharmacol Biol Psychiatry* 34, 154-158.

Kanski, R., van Strien, M.E., van Tijn, P., and Hol, E.M. (2014). A star is born: new insights into the mechanism of astrogenesis. *Cell Mol Life Sci* 71, 433-447.

Kaufmann, W.E., and Moser, H.W. (2000). Dendritic anomalies in disorders associated with mental retardation. *Cerebral cortex* 10, 981-991.

Kearney, J.A., Plummer, N.W., Smith, M.R., Kapur, J., Cummins, T.R., Waxman, S.G., Goldin, A.L., and Meisler, M.H. (2001). A gain-of-function mutation in the sodium

channel gene *Scn2a* results in seizures and behavioral abnormalities. *Neuroscience* 102, 307-317.

Kerr, B., Soto, C.J., Saez, M., Abrams, A., Walz, K., and Young, J.I. (2012). Transgenic complementation of *MeCP2* deficiency: phenotypic rescue of *Mecp2*-null mice by isoform-specific transgenes. *Eur J Hum Genet* 20, 69-76.

Kettenmann, H., Hanisch, U.K., Noda, M., and Verkhratsky, A. (2011). Physiology of microglia. *Physiol Rev* 91, 461-553.

Khwaja, O.S., Ho, E., Barnes, K.V., O'Leary, H.M., Pereira, L.M., Finkelstein, Y., Nelson, C.A., 3rd, Vogel-Farley, V., DeGregorio, G., Holm, I.A., *et al.* (2014). Safety, pharmacokinetics, and preliminary assessment of efficacy of mecamsermin (recombinant human IGF-1) for the treatment of Rett syndrome. *Proc Natl Acad Sci U S A* 111, 4596-4601.

Kim, D., Kim, C.H., Moon, J.I., Chung, Y.G., Chang, M.Y., Han, B.S., Ko, S., Yang, E., Cha, K.Y., Lanza, R., *et al.* (2009). Generation of human induced pluripotent stem cells by direct delivery of reprogramming proteins. *Cell Stem Cell* 4, 472-476.

Kim, H.J., and Magrane, J. (2011). Isolation and culture of neurons and astrocytes from the mouse brain cortex. *Methods Mol Biol* 793, 63-75.

Kim, K.Y., Hysolli, E., and Park, I.H. (2011). Neuronal maturation defect in induced pluripotent stem cells from patients with Rett syndrome. *Proc Natl Acad Sci U S A* 108, 14169-14174.

Kim, N.W., Piatyszek, M.A., Prowse, K.R., Harley, C.B., West, M.D., Ho, P.L., Coviello, G.M., Wright, W.E., Weinrich, S.L., and Shay, J.W. (1994). Specific association of human telomerase activity with immortal cells and cancer. *Science* 266, 2011-2015.

Kishi, N., and Macklis, J.D. (2004). *MECP2* is progressively expressed in post-migratory neurons and is involved in neuronal maturation rather than cell fate decisions. *Mol Cell Neurosci* 27, 306-321.

Kishi, N., and Macklis, J.D. (2010). *MeCP2* functions largely cell-autonomously, but also non-cell-autonomously, in neuronal maturation and dendritic arborization of cortical pyramidal neurons. *Exp Neurol* 222, 51-58.

Kishimoto, T., Itoh, K., Umekage, M., Tonosaki, M., Yaoi, T., Fukui, K., Lemmon, V.P., and Fushiki, S. (2013). Downregulation of *L1* perturbs neuronal migration and alters the expression of transcription factors in murine neocortex. *J Neurosci Res* 91, 42-50.

Kortum, F., Das, S., Flindt, M., Morris-Rosendahl, D.J., Stefanova, I., Goldstein, A., Horn, D., Klopocki, E., Kluger, G., Martin, P., *et al.* (2011). The core *FOXG1* syndrome phenotype consists of postnatal microcephaly, severe mental retardation, absent language, dyskinesia, and corpus callosum hypogenesis. *J Med Genet* 48, 396-406.

Kozlowski, C., and Weimer, R.M. (2012). An automated method to quantify microglia morphology and application to monitor activation state longitudinally in vivo. *PLoS One* 7, e31814.

Kriaucionis, S., and Bird, A. (2004). The major form of MeCP2 has a novel N-terminus generated by alternative splicing. *Nucleic Acids Res* 32, 1818-1823.

Kuchler-Bopp, S., Delaunoy, J.P., Artault, J.C., Zaepfel, M., and Dietrich, J.B. (1999). Astrocytes induce several blood-brain barrier properties in non-neural endothelial cells. *Neuroreport* 10, 1347-1353.

Kutsch, O., Oh, J., Nath, A., and Benveniste, E.N. (2000). Induction of the chemokines interleukin-8 and IP-10 by human immunodeficiency virus type 1 tat in astrocytes. *J Virol* 74, 9214-9221.

Lang, M., Wither, R.G., Colic, S., Wu, C., Monnier, P.P., Bardakjian, B.L., Zhang, L., and Eubanks, J.H. (2014). Rescue of behavioral and EEG deficits in male and female *Mecp2*-deficient mice by delayed *Mecp2* gene reactivation. *Hum Mol Genet* 23, 303-318.

Laurent, L.C., Ulitsky, I., Slavin, I., Tran, H., Schork, A., Morey, R., Lynch, C., Harness, J.V., Lee, S., Barrero, M.J., *et al.* (2011). Dynamic changes in the copy number of pluripotency and cell proliferation genes in human ESCs and iPSCs during reprogramming and time in culture. *Cell Stem Cell* 8, 106-118.

Lawson-Yuen, A., Liu, D., Han, L., Jiang, Z.I., Tsai, G.E., Basu, A.C., Picker, J., Feng, J., and Coyle, J.T. (2007). *Ube3a* mRNA and protein expression are not decreased in *Mecp2*R168X mutant mice. *Brain Res* 1180, 1-6.

Lee, J.K., and Tansey, M.G. (2013). Microglia isolation from adult mouse brain. *Methods Mol Biol* 1041, 17-23.

Lewis, J.D., Meehan, R.R., Henzel, W.J., Maurer-Fogy, I., Jeppesen, P., Klein, F., and Bird, A. (1992). Purification, sequence, and cellular localization of a novel chromosomal protein that binds to methylated DNA. *Cell* 69, 905-914.

Li, R., Liang, J., Ni, S., Zhou, T., Qing, X., Li, H., He, W., Chen, J., Li, F., Zhuang, Q., *et al.* (2010a). A mesenchymal-to-epithelial transition initiates and is required for the nuclear reprogramming of mouse fibroblasts. *Cell Stem Cell* 7, 51-63.

Li, Z.H., Dulyaninova, N.G., House, R.P., Almo, S.C., and Bresnick, A.R. (2010b). *S100A4* regulates macrophage chemotaxis. *Mol Biol Cell* 21, 2598-2610.

Liang, G., and Zhang, Y. (2013). Embryonic stem cell and induced pluripotent stem cell: an epigenetic perspective. *Cell Res* 23, 49-69.

Liang, K.J., Lee, J.E., Wang, Y.D., Ma, W., Fontainhas, A.M., Fariss, R.N., and Wong, W.T. (2009). Regulation of dynamic behavior of retinal microglia by CX3CR1 signaling. *Invest Ophthalmol Vis Sci* 50, 4444-4451.

Lieberman, A.P., Pitha, P.M., Shin, H.S., and Shin, M.L. (1989). Production of tumor necrosis factor and other cytokines by astrocytes stimulated with lipopolysaccharide or a neurotropic virus. *Proc Natl Acad Sci U S A* 86, 6348-6352.

Lioy, D.T., Garg, S.K., Monaghan, C.E., Raber, J., Foust, K.D., Kaspar, B.K., Hirrlinger, P.G., Kirchhoff, F., Bissonnette, J.M., Ballas, N., *et al.* (2011). A role for glia in the progression of Rett's syndrome. *Nature* **475**, 497-500.

Lippmann, E.S., Al-Ahmad, A., Azarin, S.M., Palecek, S.P., and Shusta, E.V. (2014). A retinoic acid-enhanced, multicellular human blood-brain barrier model derived from stem cell sources. *Sci Rep* **4**, 4160.

Liu, H., and Zhang, S.C. (2011). Specification of neuronal and glial subtypes from human pluripotent stem cells. *Cell Mol Life Sci* **68**, 3995-4008.

Liu, X., Sun, H., Qi, J., Wang, L., He, S., Liu, J., Feng, C., Chen, C., Li, W., Guo, Y., *et al.* (2013). Sequential introduction of reprogramming factors reveals a time-sensitive requirement for individual factors and a sequential EMT-MET mechanism for optimal reprogramming. *Nat Cell Biol* **15**, 829-838.

Liu, Y., Hao, W., Letiembre, M., Walter, S., Kulanga, M., Neumann, H., and Fassbender, K. (2006). Suppression of microglial inflammatory activity by myelin phagocytosis: role of p47-PHOX-mediated generation of reactive oxygen species. *J Neurosci* **26**, 12904-12913.

Lowry, W.E., Richter, L., Yachechko, R., Pyle, A.D., Tchieu, J., Sridharan, R., Clark, A.T., and Plath, K. (2008). Generation of human induced pluripotent stem cells from dermal fibroblasts. *Proc Natl Acad Sci U S A* **105**, 2883-2888.

Lui, J.H., Hansen, D.V., and Kriegstein, A.R. (2011). Development and evolution of the human neocortex. *Cell* **146**, 18-36.

Luikenhuis, S., Giacometti, E., Beard, C.F., and Jaenisch, R. (2004). Expression of MeCP2 in postmitotic neurons rescues Rett syndrome in mice. *Proc Natl Acad Sci U S A* **101**, 6033-6038.

Lyst, M.J., Ekiert, R., Ebert, D.H., Merusi, C., Nowak, J., Selfridge, J., Guy, J., Kastan, N.R., Robinson, N.D., de Lima Alves, F., *et al.* (2013). Rett syndrome mutations abolish the interaction of MeCP2 with the NCoR/SMRT co-repressor. *Nat Neurosci* **16**, 898-902.

Ma, D., Yoon, S.I., Yang, C.H., Marcy, G., Zhao, N., Leong, W.Y., Ganapathy, V., Han, J., Van Dongen, A.M., Hsu, K.S., *et al.* (2015). Rescue of Methyl-CpG Binding Protein 2 Dysfunction-induced Defects in Newborn Neurons by Pentobarbital. *Neurotherapeutics* **12**, 477-490.

Ma, Q., Huang, B., Khatibi, N., Rolland, W., 2nd, Suzuki, H., Zhang, J.H., and Tang, J. (2011). PDGFR-alpha inhibition preserves blood-brain barrier after intracerebral hemorrhage. *Ann Neurol* **70**, 920-931.

Maezawa, I., and Jin, L.W. (2010). Rett syndrome microglia damage dendrites and synapses by the elevated release of glutamate. *J Neurosci* **30**, 5346-5356.

Maezawa, I., Swanberg, S., Harvey, D., LaSalle, J.M., and Jin, L.W. (2009). Rett syndrome astrocytes are abnormal and spread MeCP2 deficiency through gap junctions. *J Neurosci* 29, 5051-5061.

Majumdar, A., Cruz, D., Asamoah, N., Buxbaum, A., Sohar, I., Lobel, P., and Maxfield, F.R. (2007). Activation of microglia acidifies lysosomes and leads to degradation of Alzheimer amyloid fibrils. *Mol Biol Cell* 18, 1490-1496.

Maortua, H., Martinez-Bouzas, C., Calvo, M.T., Domingo, M.R., Ramos, F., Garcia-Ribes, A., Martinez, M.J., Lopez-Ariztegui, M.A., Puente, N., Rubio, I., *et al.* (2012). CDKL5 gene status in female patients with epilepsy and Rett-like features: two new mutations in the catalytic domain. *BMC Med Genet* 13, 68.

Marchetto, M.C., Brennand, K.J., Boyer, L.F., and Gage, F.H. (2011). Induced pluripotent stem cells (iPSCs) and neurological disease modeling: progress and promises. *Hum Mol Genet* 20, R109-115.

Marchetto, M.C., Carromeu, C., Acab, A., Yu, D., Yeo, G.W., Mu, Y., Chen, G., Gage, F.H., and Muotri, A.R. (2010). A model for neural development and treatment of Rett syndrome using human induced pluripotent stem cells. *Cell* 143, 527-539.

Marchi, N., Tierney, W., Alexopoulos, A.V., Puvenna, V., Granata, T., and Janigro, D. (2011). The etiological role of blood-brain barrier dysfunction in seizure disorders. *Cardiovasc Psychiatry Neurol* 2011, 482415.

Mari, F., Azimonti, S., Bertani, I., Bolognese, F., Colombo, E., Caselli, R., Scala, E., Longo, I., Grosso, S., Pescucci, C., *et al.* (2005). CDKL5 belongs to the same molecular pathway of MeCP2 and it is responsible for the early-onset seizure variant of Rett syndrome. *Hum Mol Genet* 14, 1935-1946.

Marin-Teva, J.L., Dusart, I., Colin, C., Gervais, A., van Rooijen, N., and Mallat, M. (2004). Microglia promote the death of developing Purkinje cells. *Neuron* 41, 535-547.

Marion, R.M., Strati, K., Li, H., Tejera, A., Schoeftner, S., Ortega, S., Serrano, M., and Blasco, M.A. (2009). Telomeres acquire embryonic stem cell characteristics in induced pluripotent stem cells. *Cell stem cell* 4, 141-154.

Marschik, P.B., Kaufmann, W.E., Sigafos, J., Wolin, T., Zhang, D., Bartl-Pokorny, K.D., Pini, G., Zappella, M., Tager-Flusberg, H., Einspieler, C., *et al.* (2013). Changing the perspective on early development of Rett syndrome. *Res Dev Disabil* 34, 1236-1239.

Masuyama, T., Matsuo, M., Jing, J.J., Tabara, Y., Kitsuki, K., Yamagata, H., Kan, Y., Miki, T., Ishii, K., and Kondo, I. (2005). Classic Rett syndrome in a boy with R133C mutation of MECP2. *Brain Dev* 27, 439-442.

Mathiisen, T.M., Lehre, K.P., Danbolt, N.C., and Ottersen, O.P. (2010). The perivascular astroglial sheath provides a complete covering of the brain microvessels: an electron microscopic 3D reconstruction. *Glia* 58, 1094-1103.

Mellen, M., Ayata, P., Dewell, S., Kriaucionis, S., and Heintz, N. (2012). MeCP2 binds to 5hmC enriched within active genes and accessible chromatin in the nervous system. *Cell* *151*, 1417-1430.

Merkle, F.T., and Alvarez-Buylla, A. (2006). Neural stem cells in mammalian development. *Curr Opin Cell Biol* *18*, 704-709.

Meucci, O., Fatatis, A., Simen, A.A., and Miller, R.J. (2000). Expression of CX3CR1 chemokine receptors on neurons and their role in neuronal survival. *Proc Natl Acad Sci U S A* *97*, 8075-8080.

Miyano, M., Horike, S., Cai, S., Oshimura, M., and Kohwi-Shigematsu, T. (2008). DLX5 expression is monoallelic and *Dlx5* is up-regulated in the *Mecp2*-null frontal cortex. *J Cell Mol Med* *12*, 1188-1191.

Mizuno, T., Zhang, G., Takeuchi, H., Kawanokuchi, J., Wang, J., Sonobe, Y., Jin, S., Takada, N., Komatsu, Y., and Suzumura, A. (2008). Interferon-gamma directly induces neurotoxicity through a neuron specific, calcium-permeable complex of IFN-gamma receptor and AMPA GluR1 receptor. *FASEB J* *22*, 1797-1806.

Mnatzakanian, G.N., Lohi, H., Munteanu, I., Alfred, S.E., Yamada, T., MacLeod, P.J., Jones, J.R., Scherer, S.W., Schanen, N.C., Friez, M.J., *et al.* (2004). A previously unidentified MECP2 open reading frame defines a new protein isoform relevant to Rett syndrome. *Nat Genet* *36*, 339-341.

Molofsky, A.V., Krencik, R., Ullian, E.M., Tsai, H.H., Deneen, B., Richardson, W.D., Barres, B.A., and Rowitch, D.H. (2012). Astrocytes and disease: a neurodevelopmental perspective. *Genes Dev* *26*, 891-907.

Moog, U., Smeets, E.E., van Roozendaal, K.E., Schoenmakers, S., Herbergs, J., Schoonbrood-Lenssen, A.M., and Schrandt-Stumpel, C.T. (2003). Neurodevelopmental disorders in males related to the gene causing Rett syndrome in females (*MECP2*). *Eur J Paediatr Neurol* *7*, 5-12.

Moretti, P., Levenson, J.M., Battaglia, F., Atkinson, R., Teague, R., Antalffy, B., Armstrong, D., Arancio, O., Sweatt, J.D., and Zoghbi, H.Y. (2006). Learning and memory and synaptic plasticity are impaired in a mouse model of Rett syndrome. *J Neurosci* *26*, 319-327.

Mount, R.H., Charman, T., Hastings, R.P., Reilly, S., and Cass, H. (2002). The Rett Syndrome Behaviour Questionnaire (RSBQ): refining the behavioural phenotype of Rett syndrome. *J Child Psychol Psychiatry* *43*, 1099-1110.

Moussaud, S., and Draheim, H.J. (2010). A new method to isolate microglia from adult mice and culture them for an extended period of time. *J Neurosci Methods* *187*, 243-253.

Nagai, K., Miyake, K., and Kubota, T. (2005). A transcriptional repressor MeCP2 causing Rett syndrome is expressed in embryonic non-neuronal cells and controls their growth. *Brain Res Dev Brain Res* *157*, 103-106.

Nakagawa, M., Koyanagi, M., Tanabe, K., Takahashi, K., Ichisaka, T., Aoi, T., Okita, K., Mochizuki, Y., Takizawa, N., and Yamanaka, S. (2008). Generation of induced pluripotent stem cells without Myc from mouse and human fibroblasts. *Nat Biotechnol* 26, 101-106.

Nan, X., Meehan, R.R., and Bird, A. (1993). Dissection of the methyl-CpG binding domain from the chromosomal protein MeCP2. *Nucleic Acids Res* 21, 4886-4892.

Nan, X., Ng, H.H., Johnson, C.A., Laherty, C.D., Turner, B.M., Eisenman, R.N., and Bird, A. (1998). Transcriptional repression by the methyl-CpG-binding protein MeCP2 involves a histone deacetylase complex. *Nature* 393, 386-389.

Nan, X., Tate, P., Li, E., and Bird, A. (1996). DNA methylation specifies chromosomal localization of MeCP2. *Mol Cell Biol* 16, 414-421.

Narantuya, D., Nagai, A., Sheikh, A.M., Masuda, J., Kobayashi, S., Yamaguchi, S., and Kim, S.U. (2010). Human microglia transplanted in rat focal ischemia brain induce neuroprotection and behavioral improvement. *PLoS One* 5, e11746.

Newman, L.A., Korol, D.L., and Gold, P.E. (2011). Lactate produced by glycogenolysis in astrocytes regulates memory processing. *PLoS One* 6, e28427.

Nguyen, M.V., Felice, C.A., Du, F., Covey, M.V., Robinson, J.K., Mandel, G., and Ballas, N. (2013). Oligodendrocyte lineage cells contribute unique features to Rett syndrome neuropathology. *J Neurosci* 33, 18764-18774.

Nimmerjahn, A., Kirchhoff, F., and Helmchen, F. (2005). Resting microglial cells are highly dynamic surveillants of brain parenchyma in vivo. *Science* 308, 1314-1318.

Oby, E., and Janigro, D. (2006). The blood-brain barrier and epilepsy. *Epilepsia* 47, 1761-1774.

Ogier, M., Wang, H., Hong, E., Wang, Q., Greenberg, M.E., and Katz, D.M. (2007). Brain-derived neurotrophic factor expression and respiratory function improve after ampakine treatment in a mouse model of Rett syndrome. *J Neurosci* 27, 10912-10917.

Okabe, Y., Takahashi, T., Mitsumasu, C., Kosai, K., Tanaka, E., and Matsuishi, T. (2012). Alterations of gene expression and glutamate clearance in astrocytes derived from an MeCP2-null mouse model of Rett syndrome. *PLoS One* 7, e35354.

Oliver, C., Murphy, G., Crayton, L., and Corbett, J. (1993). Self-injurious behavior in Rett syndrome: interactions between features of Rett syndrome and operant conditioning. *J Autism Dev Disord* 23, 91-109.

Olson, C.O., Zachariah, R.M., Ezeonwuka, C.D., Liyanage, V.R., and Rastegar, M. (2014). Brain region-specific expression of MeCP2 isoforms correlates with DNA methylation within *Mecp2* regulatory elements. *PLoS One* 9, e90645.

Onder, T.T., and Daley, G.Q. (2012). New lessons learned from disease modeling with induced pluripotent stem cells. *Curr Opin Genet Dev* 22, 500-508.

Ozbalkan, Z., Bagislar, S., Kiraz, S., Akyerli, C.B., Ozer, H.T., Yavuz, S., Birlik, A.M., Calguneri, M., and Ozcelik, T. (2005). Skewed X chromosome inactivation in blood cells of women with scleroderma. *Arthritis and rheumatism* 52, 1564-1570.

Pabon, M.M., Bachstetter, A.D., Hudson, C.E., Gemma, C., and Bickford, P.C. (2011). CX3CL1 reduces neurotoxicity and microglial activation in a rat model of Parkinson's disease. *J Neuroinflammation* 8, 9.

Paloneva, J., Autti, T., Raininko, R., Partanen, J., Salonen, O., Puranen, M., Hakola, P., and Haltia, M. (2001). CNS manifestations of Nasu-Hakola disease: a frontal dementia with bone cysts. *Neurology* 56, 1552-1558.

Panayotis, N., Pratte, M., Borges-Correia, A., Ghata, A., Villard, L., and Roux, J.C. (2011). Morphological and functional alterations in the substantia nigra pars compacta of the *Mecp2*-null mouse. *Neurobiol Dis* 41, 385-397.

Paolicelli, R.C., Bolasco, G., Pagani, F., Maggi, L., Scianni, M., Panzanelli, P., Giustetto, M., Ferreira, T.A., Guiducci, E., Dumas, L., *et al.* (2011). Synaptic pruning by microglia is necessary for normal brain development. *Science* 333, 1456-1458.

Park, I.H., Arora, N., Huo, H., Maherali, N., Ahfeldt, T., Shimamura, A., Lensch, M.W., Cowan, C., Hochedlinger, K., and Daley, G.Q. (2008a). Disease-specific induced pluripotent stem cells. *Cell* 134, 877-886.

Park, I.H., Zhao, R., West, J.A., Yabuuchi, A., Huo, H., Ince, T.A., Lerou, P.H., Lensch, M.W., and Daley, G.Q. (2008b). Reprogramming of human somatic cells to pluripotency with defined factors. *Nature* 451, 141-146.

Park, T.I., Monzo, H., Mee, E.W., Bergin, P.S., Teoh, H.H., Montgomery, J.M., Faull, R.L., Curtis, M.A., and Dragunow, M. (2012). Adult human brain neural progenitor cells (NPCs) and fibroblast-like cells have similar properties in vitro but only NPCs differentiate into neurons. *PLoS One* 7, e37742.

Pellerin, L., Pellegrini, G., Bittar, P.G., Charnay, Y., Bouras, C., Martin, J.L., Stella, N., and Magistretti, P.J. (1998). Evidence supporting the existence of an activity-dependent astrocyte-neuron lactate shuttle. *Dev Neurosci* 20, 291-299.

Penagarikano, O., Abrahams, B.S., Herman, E.I., Winden, K.D., Gdalyahu, A., Dong, H., Sonnenblick, L.I., Gruver, R., Almajano, J., Bragin, A., *et al.* (2011). Absence of *CNTNAP2* leads to epilepsy, neuronal migration abnormalities, and core autism-related deficits. *Cell* 147, 235-246.

Percy, A.K., and Lane, J.B. (2004). Rett syndrome: clinical and molecular update. *Curr Opin Pediatr* 16, 670-677.

Percy, A.K., and Lane, J.B. (2005). Rett syndrome: model of neurodevelopmental disorders. *J Child Neurol* 20, 718-721.

Percy, A.K., Lane, J.B., Childers, J., Skinner, S., Annese, F., Barrish, J., Caeg, E., Glaze, D.G., and MacLeod, P. (2007). Rett syndrome: North American database. *J Child Neurol* 22, 1338-1341.

Perez, E.L., Lauritzen, F., Wang, Y., Lee, T.S., Kang, D., Zaveri, H.P., Chaudhry, F.A., Ottersen, O.P., Bergersen, L.H., and Eid, T. (2012). Evidence for astrocytes as a potential source of the glutamate excess in temporal lobe epilepsy. *Neurobiol Dis* 47, 331-337.

Perry, V.H., Nicoll, J.A., and Holmes, C. (2010). Microglia in neurodegenerative disease. *Nat Rev Neurol* 6, 193-201.

Polo, J.M., Anderssen, E., Walsh, R.M., Schwarz, B.A., Nefzger, C.M., Lim, S.M., Borkent, M., Apostolou, E., Alaei, S., Cloutier, J., *et al.* (2012). A molecular roadmap of reprogramming somatic cells into iPS cells. *Cell* 151, 1617-1632.

Pomp, O., Dreesen, O., and Colman, A. (2011a). The "X factor" in cellular reprogramming and proliferation. *Cell Cycle* 10, 3992-3993.

Pomp, O., Dreesen, O., Leong, D.F., Meller-Pomp, O., Tan, T.T., Zhou, F., and Colman, A. (2011b). Unexpected X chromosome skewing during culture and reprogramming of human somatic cells can be alleviated by exogenous telomerase. *Cell Stem Cell* 9, 156-165.

Popescu, A.C., Sidorova, E., Zhang, G., and Eubanks, J.H. (2010). Aminoglycoside-mediated partial suppression of MECP2 nonsense mutations responsible for Rett syndrome in vitro. *J Neurosci Res* 88, 2316-2324.

Quaegebeur, A., Segura, I., and Carmeliet, P. (2010). Pericytes: blood-brain barrier safeguards against neurodegeneration? *Neuron* 68, 321-323.

Rackova, L. (2013). Cholesterol load of microglia: contribution of membrane architecture changes to neurotoxic power? *Arch Biochem Biophys* 537, 91-103.

Rajamohan, D., Matsa, E., Kalra, S., Crutchley, J., Patel, A., George, V., and Denning, C. (2012). Current status of drug screening and disease modelling in human pluripotent stem cells. *Bioessays* 35, 281-298.

Ramocki, M.B., Tavyev, Y.J., and Peters, S.U. (2010). The MECP2 duplication syndrome. *Am J Med Genet A* 152A, 1079-1088.

Raponi, E., Agenes, F., Delphin, C., Assard, N., Baudier, J., Legraverend, C., and Deloulme, J.C. (2007). S100B expression defines a state in which GFAP-expressing cells lose their neural stem cell potential and acquire a more mature developmental stage. *Glia* 55, 165-177.

Reichwald, K., Thiesen, J., Wiehe, T., Weitzel, J., Poustka, W.A., Rosenthal, A., Platzer, M., Stratling, W.H., and Kioschis, P. (2000). Comparative sequence analysis of the MECP2-locus in human and mouse reveals new transcribed regions. *Mamm Genome* 11, 182-190.

Ren, J., Ding, X., Funk, G.D., and Greer, J.J. (2012). Anxiety-related mechanisms of respiratory dysfunction in a mouse model of Rett syndrome. *J Neurosci* 32, 17230-17240.

Reubinoff, B.E., Itsykson, P., Turetsky, T., Pera, M.F., Reinhartz, E., Itzik, A., and Ben-Hur, T. (2001). Neural progenitors from human embryonic stem cells. *Nat Biotechnol* 19, 1134-1140.

Ricciardi, S., Ungaro, F., Hambrock, M., Rademacher, N., Stefanelli, G., Brambilla, D., Sessa, A., Magagnotti, C., Bachi, A., Giarda, E., *et al.* (2012). CDKL5 ensures excitatory synapse stability by reinforcing NGL-1-PSD95 interaction in the postsynaptic compartment and is impaired in patient iPSC-derived neurons. *Nat Cell Biol* 14, 911-923.

Rodda, D.J., Chew, J.L., Lim, L.H., Loh, Y.H., Wang, B., Ng, H.H., and Robson, P. (2005). Transcriptional regulation of nanog by OCT4 and SOX2. *J Biol Chem* 280, 24731-24737.

Rouach, N., Koulakoff, A., Abudara, V., Willecke, K., and Giaume, C. (2008). Astroglial metabolic networks sustain hippocampal synaptic transmission. *Science* 322, 1551-1555.

Roux, J.C., Zala, D., Panayotis, N., Borges-Correia, A., Saudou, F., and Villard, L. (2012). Modification of Mecp2 dosage alters axonal transport through the Huntingtin/Hap1 pathway. *Neurobiol Dis* 45, 786-795.

Rubio, N., and Sanz-Rodriguez, F. (2007). Induction of the CXCL1 (KC) chemokine in mouse astrocytes by infection with the murine encephalomyelitis virus of Theiler. *Virology* 358, 98-108.

Samaco, R.C., Mandel-Brehm, C., Chao, H.T., Ward, C.S., Fyffe-Maricich, S.L., Ren, J., Hyland, K., Thaller, C., Maricich, S.M., Humphreys, P., *et al.* (2009). Loss of MeCP2 in aminergic neurons causes cell-autonomous defects in neurotransmitter synthesis and specific behavioral abnormalities. *Proc Natl Acad Sci U S A* 106, 21966-21971.

Sancho-Martinez, I., and Izpisua Belmonte, J.C. (2013). Stem cells: Surf the waves of reprogramming. *Nature* 493, 310-311.

Sansom, D., Krishnan, V.H., Corbett, J., and Kerr, A. (1993). Emotional and behavioural aspects of Rett syndrome. *Dev Med Child Neurol* 35, 340-345.

Scala, E., Ariani, F., Mari, F., Caselli, R., Pescucci, C., Longo, I., Meloni, I., Giachino, D., Bruttini, M., Hayek, G., *et al.* (2005). CDKL5/STK9 is mutated in Rett syndrome variant with infantile spasms. *J Med Genet* 42, 103-107.

Schaevez, L.R., Gomez, N.B., Zhen, D.P., and Berger-Sweeney, J.E. (2013). MeCP2 R168X male and female mutant mice exhibit Rett-like behavioral deficits. *Genes Brain Behav* 12, 732-740.

Schafer, D.P., Lehrman, E.K., Kautzman, A.G., Koyama, R., Mardinly, A.R., Yamasaki, R., Ransohoff, R.M., Greenberg, M.E., Barres, B.A., and Stevens, B. (2012). Microglia sculpt postnatal neural circuits in an activity and complement-dependent manner. *Neuron* 74, 691-705.

Schildge, S., Bohrer, C., Beck, K., and Schachtrup, C. (2013). Isolation and culture of mouse cortical astrocytes. *J Vis Exp*.

Scholler, K., Trinkl, A., Klotowski, M., Thal, S.C., Plesnila, N., Trabold, R., Hamann, G.F., Schmid-Elsaesser, R., and Zausinger, S. (2007). Characterization of microvascular basal lamina damage and blood-brain barrier dysfunction following subarachnoid hemorrhage in rats. *Brain Res* 1142, 237-246.

Schousboe, A., and Waagepetersen, H.S. (2005). Role of astrocytes in glutamate homeostasis: implications for excitotoxicity. *Neurotox Res* 8, 221-225.

Schule, B., Armstrong, D.D., Vogel, H., Oviedo, A., and Francke, U. (2008). Severe congenital encephalopathy caused by MECP2 null mutations in males: central hypoxia and reduced neuronal dendritic structure. *Clin Genet* 74, 116-126.

Schule, B., Li, H.H., Fisch-Kohl, C., Purmann, C., and Francke, U. (2007). DLX5 and DLX6 expression is biallelic and not modulated by MeCP2 deficiency. *Am J Hum Genet* 81, 492-506.

Shah, K., Bureau, E., Kim, D.E., Yang, K., Tang, Y., Weissleder, R., and Breakefield, X.O. (2005). Glioma therapy and real-time imaging of neural precursor cell migration and tumor regression. *Ann Neurol* 57, 34-41.

Shahbazian, M., Young, J., Yuva-Paylor, L., Spencer, C., Antalffy, B., Noebels, J., Armstrong, D., Paylor, R., and Zoghbi, H. (2002a). Mice with truncated MeCP2 recapitulate many Rett syndrome features and display hyperacetylation of histone H3. *Neuron* 35, 243-254.

Shahbazian, M.D., Antalffy, B., Armstrong, D.L., and Zoghbi, H.Y. (2002b). Insight into Rett syndrome: MeCP2 levels display tissue- and cell-specific differences and correlate with neuronal maturation. *Hum Mol Genet* 11, 115-124.

Shim, A.H., Liu, H., Focia, P.J., Chen, X., Lin, P.C., and He, X. (2010). Structures of a platelet-derived growth factor/propeptide complex and a platelet-derived growth factor/receptor complex. *Proc Natl Acad Sci U S A* 107, 11307-11312.

Sierra, A., Encinas, J.M., Deudero, J.J., Chancey, J.H., Enikolopov, G., Overstreet-Wadiche, L.S., Tsrka, S.E., and Maletic-Savatic, M. (2010). Microglia shape adult hippocampal neurogenesis through apoptosis-coupled phagocytosis. *Cell Stem Cell* 7, 483-495.

Singh, J., Saxena, A., Christodoulou, J., and Ravine, D. (2008). MECP2 genomic structure and function: insights from ENCODE. *Nucleic Acids Res* 36, 6035-6047.

Sirianni, N., Naidu, S., Pereira, J., Pillotto, R.F., and Hoffman, E.P. (1998). Rett syndrome: confirmation of X-linked dominant inheritance, and localization of the gene to Xq28. *Am J Hum Genet* 63, 1552-1558.

Sokoloff, L. (1977). Relation between physiological function and energy metabolism in the central nervous system. *J Neurochem* 29, 13-26.

Song, H.J., Stevens, C.F., and Gage, F.H. (2002). Neural stem cells from adult hippocampus develop essential properties of functional CNS neurons. *Nat Neurosci* 5, 438-445.

Squillaro, T., Alessio, N., Cipollaro, M., Melone, M.A., Hayek, G., Renieri, A., Giordano, A., and Galderisi, U. (2012). Reduced expression of MECP2 affects cell commitment and maintenance in neurons by triggering senescence: new perspective for Rett syndrome. *Mol Biol Cell* 23, 1435-1445.

Squillaro, T., Hayek, G., Farina, E., Cipollaro, M., Renieri, A., and Galderisi, U. (2008). A case report: bone marrow mesenchymal stem cells from a Rett syndrome patient are prone to senescence and show a lower degree of apoptosis. *J Cell Biochem* 103, 1877-1885.

Sridharan, R., Tchieu, J., Mason, M.J., Yachechko, R., Kuoy, E., Horvath, S., Zhou, Q., and Plath, K. (2009). Role of the murine reprogramming factors in the induction of pluripotency. *Cell* 136, 364-377.

Stancheva, I., Collins, A.L., Van den Veyver, I.B., Zoghbi, H., and Meehan, R.R. (2003). A mutant form of MeCP2 protein associated with human Rett syndrome cannot be displaced from methylated DNA by notch in *Xenopus* embryos. *Mol Cell* 12, 425-435.

Streit, W.J. (1996). The role of microglia in brain injury. *Neurotoxicology* 17, 671-678.

Su, E.J., Fredriksson, L., Geyer, M., Folestad, E., Cale, J., Andrae, J., Gao, Y., Pietras, K., Mann, K., Yepes, M., *et al.* (2008). Activation of PDGF-CC by tissue plasminogen activator impairs blood-brain barrier integrity during ischemic stroke. *Nat Med* 14, 731-737.

Suzuki, A., Stern, S.A., Bozdagi, O., Huntley, G.W., Walker, R.H., Magistretti, P.J., and Alberini, C.M. (2011). Astrocyte-neuron lactate transport is required for long-term memory formation. *Cell* 144, 810-823.

Szatmari, P., Paterson, A.D., Zwaigenbaum, L., Roberts, W., Brian, J., Liu, X.Q., Vincent, J.B., Skaug, J.L., Thompson, A.P., Senman, L., *et al.* (2007). Mapping autism risk loci using genetic linkage and chromosomal rearrangements. *Nat Genet* 39, 319-328.

Szczesna, K., de la Caridad, O., Petazzi, P., Soler, M., Roa, L., Saez, M.A., Fourcade, S., Pujol, A., Artuch-Iriberry, R., Molero-Luis, M., *et al.* (2014). Improvement of the Rett syndrome phenotype in a MeCP2 mouse model upon treatment with levodopa and a dopa-decarboxylase inhibitor. *Neuropsychopharmacology* 39, 2846-2856.

Takahashi, K., Rochford, C.D., and Neumann, H. (2005). Clearance of apoptotic neurons without inflammation by microglial triggering receptor expressed on myeloid cells-2. *J Exp Med* 201, 647-657.

Takahashi, K., Tanabe, K., Ohnuki, M., Narita, M., Ichisaka, T., Tomoda, K., and Yamanaka, S. (2007). Induction of pluripotent stem cells from adult human fibroblasts by defined factors. *Cell* 131, 861-872.

Takahashi, K., and Yamanaka, S. (2006). Induction of pluripotent stem cells from mouse embryonic and adult fibroblast cultures by defined factors. *Cell* 126, 663-676.

Takahashi, S., Ohinata, J., Makita, Y., Suzuki, N., Araki, A., Sasaki, A., Murono, K., Tanaka, H., and Fujieda, K. (2008). Skewed X chromosome inactivation failed to explain the normal phenotype of a carrier female with MECP2 mutation resulting in Rett syndrome. *Clin Genet* 73, 257-261.

Takata, K., Kitamura, Y., Yanagisawa, D., Morikawa, S., Morita, M., Inubushi, T., Tsuchiya, D., Chishiro, S., Saeki, M., Taniguchi, T., *et al.* (2007). Microglial transplantation increases amyloid-beta clearance in Alzheimer model rats. *FEBS Lett* 581, 475-478.

Takeuchi, H., Jin, S., Wang, J., Zhang, G., Kawanokuchi, J., Kuno, R., Sonobe, Y., Mizuno, T., and Suzumura, A. (2006). Tumor necrosis factor-alpha induces neurotoxicity via glutamate release from hemichannels of activated microglia in an autocrine manner. *J Biol Chem* 281, 21362-21368.

Takeuchi, H., Mizuno, T., Zhang, G., Wang, J., Kawanokuchi, J., Kuno, R., and Suzumura, A. (2005). Neuritic beading induced by activated microglia is an early feature of neuronal dysfunction toward neuronal death by inhibition of mitochondrial respiration and axonal transport. *J Biol Chem* 280, 10444-10454.

Tao, J., Van Esch, H., Hagedorn-Greiwe, M., Hoffmann, K., Moser, B., Raynaud, M., Sperner, J., Fryns, J.P., Schwinger, E., Gecz, J., *et al.* (2004). Mutations in the X-linked cyclin-dependent kinase-like 5 (CDKL5/STK9) gene are associated with severe neurodevelopmental retardation. *Am J Hum Genet* 75, 1149-1154.

Tarczyluk, M.A., Nagel, D.A., O'Neil, J.D., Parri, H.R., Tse, E.H., Coleman, M.D., and Hill, E.J. (2013). Functional astrocyte-neuron lactate shuttle in a human stem cell-derived neuronal network. *J Cereb Blood Flow Metab* 33, 1386-1393.

Tate, P., Skarnes, W., and Bird, A. (1996). The methyl-CpG binding protein MeCP2 is essential for embryonic development in the mouse. *Nat Genet* 12, 205-208.

Theoharides, T.C., and Zhang, B. (2011). Neuro-inflammation, blood-brain barrier, seizures and autism. *J Neuroinflammation* 8, 168.

Thomson, J.A., Itskovitz-Eldor, J., Shapiro, S.S., Waknitz, M.A., Swiergiel, J.J., Marshall, V.S., and Jones, J.M. (1998). Embryonic stem cell lines derived from human blastocysts. *Science* 282, 1145-1147.

Tomoda, K., Takahashi, K., Leung, K., Okada, A., Narita, M., Yamada, N.A., Eilertson, K.E., Tsang, P., Baba, S., White, M.P., *et al.* (2012). Derivation conditions impact X-inactivation status in female human induced pluripotent stem cells. *Cell Stem Cell* 11, 91-99.

Tong, X., Ao, Y., Faas, G.C., Nwaobi, S.E., Xu, J., Haustein, M.D., Anderson, M.A., Mody, I., Olsen, M.L., Sofroniew, M.V., *et al.* (2014). Astrocyte Kir4.1 ion channel deficits contribute to neuronal dysfunction in Huntington's disease model mice. *Nat Neurosci* 17, 694-703.

Tonosaki, M., Itoh, K., Umekage, M., Kishimoto, T., Yaoi, T., Lemmon, V.P., and Fushiki, S. (2014). L1cam is crucial for cell locomotion and terminal translocation of the Soma in radial migration during murine corticogenesis. *PLoS One* *9*, e86186.

Topcu, M., Akyerli, C., Sayi, A., Toruner, G.A., Kocoglu, S.R., Cimbis, M., and Ozcelik, T. (2002). Somatic mosaicism for a MECP2 mutation associated with classic Rett syndrome in a boy. *Eur J Hum Genet* *10*, 77-81.

Trappe, R., Laccone, F., Cobilanschi, J., Meins, M., Huppke, P., Hanefeld, F., and Engel, W. (2001). MECP2 mutations in sporadic cases of Rett syndrome are almost exclusively of paternal origin. *Am J Hum Genet* *68*, 1093-1101.

Tropea, D., Giacometti, E., Wilson, N.R., Beard, C., McCurry, C., Fu, D.D., Flannery, R., Jaenisch, R., and Sur, M. (2009). Partial reversal of Rett Syndrome-like symptoms in MeCP2 mutant mice. *Proc Natl Acad Sci U S A* *106*, 2029-2034.

Tropepe, V., Hitoshi, S., Sirard, C., Mak, T.W., Rossant, J., and van der Kooy, D. (2001). Direct neural fate specification from embryonic stem cells: a primitive mammalian neural stem cell stage acquired through a default mechanism. *Neuron* *30*, 65-78.

Tsai, N.P., Wilkerson, J.R., Guo, W., Maksimova, M.A., DeMartino, G.N., Cowan, C.W., and Huber, K.M. (2012). Multiple autism-linked genes mediate synapse elimination via proteasomal degradation of a synaptic scaffold PSD-95. *Cell* *151*, 1581-1594.

Tudor, M., Akbarian, S., Chen, R.Z., and Jaenisch, R. (2002). Transcriptional profiling of a mouse model for Rett syndrome reveals subtle transcriptional changes in the brain. *Proc Natl Acad Sci U S A* *99*, 15536-15541.

Uchida, N., Buck, D.W., He, D., Reitsma, M.J., Masek, M., Phan, T.V., Tsukamoto, A.S., Gage, F.H., and Weissman, I.L. (2000). Direct isolation of human central nervous system stem cells. *Proc Natl Acad Sci U S A* *97*, 14720-14725.

Urich, E., Patsch, C., Aigner, S., Graf, M., Iacone, R., and Freskgard, P.O. (2013). Multicellular self-assembled spheroidal model of the blood brain barrier. *Sci Rep* *3*, 1500.

Valiente, M., and Marin, O. (2010). Neuronal migration mechanisms in development and disease. *Curr Opin Neurobiol* *20*, 68-78.

van Daalen, E., Kemner, C., Verbeek, N.E., van der Zwaag, B., Dijkhuizen, T., Rump, P., Houben, R., van 't Slot, R., de Jonge, M.V., Staal, W.G., *et al.* (2011). Social Responsiveness Scale-aided analysis of the clinical impact of copy number variations in autism. *Neurogenetics* *12*, 315-323.

Van Esch, H. (2012). MECP2 Duplication Syndrome. *Mol Syndromol* *2*, 128-136.

Van Esch, H., Bauters, M., Ignatius, J., Jansen, M., Raynaud, M., Hollanders, K., Lugtenberg, D., Bienvenu, T., Jensen, L.R., Gecz, J., *et al.* (2005). Duplication of the MECP2 region is a frequent cause of severe mental retardation and progressive neurological symptoms in males. *Am J Hum Genet* *77*, 442-453.

van Praag, H., Schinder, A.F., Christie, B.R., Toni, N., Palmer, T.D., and Gage, F.H. (2002). Functional neurogenesis in the adult hippocampus. *Nature* *415*, 1030-1034.

van Strien, M.E., Sluijs, J.A., Reynolds, B.A., Steindler, D.A., Aronica, E., and Hol, E.M. (2014). Isolation of neural progenitor cells from the human adult subventricular zone based on expression of the cell surface marker CD271. *Stem Cells Transl Med* *3*, 470-480.

Varlakhanova, N.V., Cotterman, R.F., deVries, W.N., Morgan, J., Donahue, L.R., Murray, S., Knowles, B.B., and Knoepfler, P.S. (2010). *myc* maintains embryonic stem cell pluripotency and self-renewal. *Differentiation* *80*, 9-19.

Vecsler, M., Ben Zeev, B., Nudelman, I., Anikster, Y., Simon, A.J., Amariglio, N., Rechavi, G., Baasov, T., and Gak, E. (2011). Ex vivo treatment with a novel synthetic aminoglycoside NB54 in primary fibroblasts from Rett syndrome patients suppresses MECP2 nonsense mutations. *PLoS One* *6*, e20733.

Villard, L. (2007). MECP2 mutations in males. *J Med Genet* *44*, 417-423.

Villard, L., Kpebe, A., Cardoso, C., Chelly, P.J., Tardieu, P.M., and Fontes, M. (2000). Two affected boys in a Rett syndrome family: clinical and molecular findings. *Neurology* *55*, 1188-1193.

Villemagne, P.M., Naidu, S., Villemagne, V.L., Yaster, M., Wagner, H.N., Jr., Harris, J.C., Moser, H.W., Johnston, M.V., Dannals, R.F., and Wong, D.F. (2002). Brain glucose metabolism in Rett Syndrome. *Pediatr Neurol* *27*, 117-122.

Voituron, N., and Hilaire, G. (2011). The benzodiazepine Midazolam mitigates the breathing defects of *Mecp2*-deficient mice. *Respir Physiol Neurobiol* *177*, 56-60.

Wake, H., Moorhouse, A.J., Jinno, S., Kohsaka, S., and Nabekura, J. (2009). Resting microglia directly monitor the functional state of synapses in vivo and determine the fate of ischemic terminals. *J Neurosci* *29*, 3974-3980.

Wang, H., Chan, S.A., Ogier, M., Hellard, D., Wang, Q., Smith, C., and Katz, D.M. (2006). Dysregulation of brain-derived neurotrophic factor expression and neurosecretory function in *Mecp2* null mice. *J Neurosci* *26*, 10911-10915.

Wang, H., and Doering, L.C. (2012). Induced pluripotent stem cells to model and treat neurogenetic disorders. *Neural Plast* *2012*, 346053.

Wang, Y., Dye, C.A., Sohal, V., Long, J.E., Estrada, R.C., Roztocil, T., Lufkin, T., Deisseroth, K., Baraban, S.C., and Rubenstein, J.L. (2010). *Dlx5* and *Dlx6* regulate the development of parvalbumin-expressing cortical interneurons. *J Neurosci* *30*, 5334-5345.

Warren, L., Manos, P.D., Ahfeldt, T., Loh, Y.H., Li, H., Lau, F., Ebina, W., Mandal, P.K., Smith, Z.D., Meissner, A., *et al.* (2010). Highly efficient reprogramming to pluripotency and directed differentiation of human cells with synthetic modified mRNA. *Cell Stem Cell* *7*, 618-630.

Weaving, L.S., Christodoulou, J., Williamson, S.L., Friend, K.L., McKenzie, O.L., Archer, H., Evans, J., Clarke, A., Pelka, G.J., Tam, P.P., *et al.* (2004). Mutations of CDKL5 cause a severe neurodevelopmental disorder with infantile spasms and mental retardation. *Am J Hum Genet* 75, 1079-1093.

Wegener, E., Brendel, C., Fischer, A., Hulsmann, S., Gartner, J., and Huppke, P. (2014). Characterization of the MeCP2R168X knockin mouse model for Rett syndrome. *PLoS One* 9, e115444.

Wegiel, J., Kuchna, I., Nowicki, K., Imaki, H., Marchi, E., Ma, S.Y., Chauhan, A., Chauhan, V., Bobrowicz, T.W., de Leon, M., *et al.* (2010). The neuropathology of autism: defects of neurogenesis and neuronal migration, and dysplastic changes. *Acta Neuropathol* 119, 755-770.

Weiss, L.A., Escayg, A., Kearney, J.A., Trudeau, M., MacDonald, B.T., Mori, M., Reichert, J., Buxbaum, J.D., and Meisler, M.H. (2003). Sodium channels SCN1A, SCN2A and SCN3A in familial autism. *Mol Psychiatry* 8, 186-194.

Wernig, M., Lengner, C.J., Hanna, J., Lodato, M.A., Steine, E., Foreman, R., Staerk, J., Markoulaki, S., and Jaenisch, R. (2008a). A drug-inducible transgenic system for direct reprogramming of multiple somatic cell types. *Nat Biotechnol* 26, 916-924.

Wernig, M., Meissner, A., Cassady, J.P., and Jaenisch, R. (2008b). c-Myc is dispensable for direct reprogramming of mouse fibroblasts. *Cell Stem Cell* 2, 10-12.

Willett, R.T., and Greene, L.A. (2011). Gata2 is required for migration and differentiation of retinorecipient neurons in the superior colliculus. *J Neurosci* 31, 4444-4455.

Williams, E.C., Zhong, X., Mohamed, A., Li, R., Liu, Y., Dong, Q., Ananiev, G.E., Mok, J.C., Lin, B.R., Lu, J., *et al.* (2014). Mutant astrocytes differentiated from Rett syndrome patients-specific iPSCs have adverse effects on wild-type neurons. *Hum Mol Genet* 23, 2968-2980.

Wilmot, I., Schnieke, A.E., McWhir, J., Kind, A.J., and Campbell, K.H. (1997). Viable offspring derived from fetal and adult mammalian cells. *Nature* 385, 810-813.

Winkler, E.A., Bell, R.D., and Zlokovic, B.V. (2010). Pericyte-specific expression of PDGF beta receptor in mouse models with normal and deficient PDGF beta receptor signaling. *Mol Neurodegener* 5, 32.

Wong, A.D., Ye, M., Levy, A.F., Rothstein, J.D., Bergles, D.E., and Searson, P.C. (2013). The blood-brain barrier: an engineering perspective. *Front Neuroeng* 6, 7.

Woods, C.G., Bond, J., and Enard, W. (2005). Autosomal recessive primary microcephaly (MCPH): a review of clinical, molecular, and evolutionary findings. *Am J Hum Genet* 76, 717-728.

Wu, H.J., Liu, Y.J., Li, H.Q., Chen, C., Dou, Y., Lou, H.F., Ho, M.S., Li, X.M., Gao, Z., and Duan, S. (2014). Analysis of microglial migration by a micropipette assay. *Nat Protoc* 9, 491-500.

Yang, Y., Fung, S.J., Rothwell, A., Tianmei, S., and Weickert, C.S. (2011). Increased interstitial white matter neuron density in the dorsolateral prefrontal cortex of people with schizophrenia. *Biol Psychiatry* 69, 63-70.

Yao, H., Duan, M., and Buch, S. (2011). Cocaine-mediated induction of platelet-derived growth factor: implication for increased vascular permeability. *Blood* 117, 2538-2547.

Yasui, D.H., Gonzales, M.L., Aflatooni, J.O., Crary, F.K., Hu, D.J., Gavino, B.J., Golub, M.S., Vincent, J.B., Carolyn Schanen, N., Olson, C.O., *et al.* (2014). Mice with an isoform-ablating *Mecp2* exon 1 mutation recapitulate the neurologic deficits of Rett syndrome. *Hum Mol Genet* 23, 2447-2458.

Yasui, D.H., Peddada, S., Bieda, M.C., Vallero, R.O., Hogart, A., Nagarajan, R.P., Thatcher, K.N., Farnham, P.J., and Lasalle, J.M. (2007). Integrated epigenomic analyses of neuronal MeCP2 reveal a role for long-range interaction with active genes. *Proc Natl Acad Sci U S A* 104, 19416-19421.

Yasui, D.H., Xu, H., Dunaway, K.W., Lasalle, J.M., Jin, L.W., and Maezawa, I. (2013). MeCP2 modulates gene expression pathways in astrocytes. *Mol Autism* 4, 3.

Ye, B., and Jan, Y.N. (2005). The cadherin superfamily and dendrite development. *Trends Cell Biol* 15, 64-67.

Young, J.I., Hong, E.P., Castle, J.C., Crespo-Barreto, J., Bowman, A.B., Rose, M.F., Kang, D., Richman, R., Johnson, J.M., Berget, S., *et al.* (2005). Regulation of RNA splicing by the methylation-dependent transcriptional repressor methyl-CpG binding protein 2. *Proc Natl Acad Sci U S A* 102, 17551-17558.

Yu, J., Hu, K., Smuga-Otto, K., Tian, S., Stewart, R., Slukvin, II, and Thomson, J.A. (2009). Human induced pluripotent stem cells free of vector and transgene sequences. *Science* 324, 797-801.

Yu, J., Vodyanik, M.A., Smuga-Otto, K., Antosiewicz-Bourget, J., Frane, J.L., Tian, S., Nie, J., Jonsdottir, G.A., Ruotti, V., Stewart, R., *et al.* (2007). Induced pluripotent stem cell lines derived from human somatic cells. *Science* 318, 1917-1920.

Zaccaria, K.J., Lagace, D.C., Eisch, A.J., and McCasland, J.S. (2010). Resistance to change and vulnerability to stress: autistic-like features of GAP43-deficient mice. *Genes Brain Behav* 9, 985-996.

Zhan, Y., Paolicelli, R.C., Sforzini, F., Weinhard, L., Bolasco, G., Pagani, F., Vyssotski, A.L., Bifone, A., Gozzi, A., Ragozzino, D., *et al.* (2014). Deficient neuron-microglia signaling results in impaired functional brain connectivity and social behavior. *Nat Neurosci* 17, 400-406.

Zhang, S.C., Wernig, M., Duncan, I.D., Brustle, O., and Thomson, J.A. (2001). In vitro differentiation of transplantable neural precursors from human embryonic stem cells. *Nat Biotechnol* 19, 1129-1133.

Zhang, X., Bao, X., Zhang, J., Zhao, Y., Cao, G., Pan, H., Wei, L., and Wu, X. (2012). Molecular characteristics of Chinese patients with Rett syndrome. *Eur J Med Genet* 55, 677-681.

Zhou, H., Wu, S., Joo, J.Y., Zhu, S., Han, D.W., Lin, T., Trauger, S., Bien, G., Yao, S., Zhu, Y., *et al.* (2009). Generation of induced pluripotent stem cells using recombinant proteins. *Cell Stem Cell* 4, 381-384.

Zuko, A., Kleijer, K.T., Oguro-Ando, A., Kas, M.J., van Daalen, E., van der Zwaag, B., and Burbach, J.P. (2013). Contactins in the neurobiology of autism. *Eur J Pharmacol* 719, 63-74.

Appendix 1: List of DEGs in NPCs

Symbol	Absolute fold change (WT vs MT)
LOC647322	285.4228
IRX2	165.872
LOC100131139	139.1847
TMEM132D	118.4605
CNTN6	96.34345
FLJ30428	83.58686
ZNF596	58.75916
LOC653071	57.61366
LOC654433	49.02255
FLJ30428	41.58001
C7orf54	38.91885
LOC439936	35.68179
SNORD108	28.8498
EDN3	26.92701
FLJ10246	26.40798
HBE1	25.1198
ERCC8	24.08973
LOC729137	22.73577
BRCA2	22.27036
KCNK6	19.72389
POLR2J4	18.64822
MIR221	9.684649
LOC653483	7.734237
MBTD1	6.949907
LOC730024	6.500651
SPOCK1	6.355283
LOC649546	6.073271
MYOM2	6.067147
VGLL3	5.514755
CRYGS	5.466109
RPL23AP53	5.13234
LOC644128	5.046595
KIAA0492	4.857983
LOC729513	4.616625
PSMA7	4.569947
BMP8B	4.377826
LOC650144	4.239611

PAR5	4.186035
VPS13B	4.082658
LOC644949	4.078494
DPPA4	3.932496
ZNF728	3.857054
FAM82B	3.805552
LOC728806	3.765827
LOC389174	3.708581
C11orf63	3.698073
LHX2	3.651245
SNORD56	3.531907
LOC440157	3.502651
LOC731789	3.33945
LOC647050	3.338559
LOC730291	3.295048
INSIG1	3.253868
GRM3	3.253389
SF1	3.195138
C13orf25	3.185126
ZBTB20	3.182732
LOC727762	3.156503
LOC643396	3.107172
MAFF	3.079971
SFRS14	3.042061
LOC729660	3.032971
FUT6	3.004695
RNPC2	2.973207
LOC644640	2.943617
LOC100128274	2.938427
SLITRK4	2.932797
INPP5F	2.922678
LOC729389	2.916689
LOC100133840	2.90004
ZNF682	2.885229
CCDC152	2.869734
GRM3	2.849333
ADM	2.838582
LOC100130276	2.816175
LOC158301	2.811933
FKBP14	2.805185
LOC100134053	2.775836

ERGIC1	2.764662
LOC644852	2.758443
C8orf45	2.74242
MBOAT2	2.740415
LOC100132585	2.73265
CYP26A1	2.697989
LOC649841	2.694833
LOC123688	2.685614
LOC648852	2.671471
PTX3	2.668906
TMEM17	2.65487
PLCG1	2.648556
BLZF1	2.647256
PTGR2	2.620394
KIAA1751	2.616056
ZNF69	2.603344
GALNT3	2.601637
EFCAB3	2.599712
SNORA28	2.590662
XRCC2	2.573218
CHRNA5	2.569027
LOC100128098	2.562665
LOC100128510	2.560616
SCARNA8	2.553532
LOC100133516	2.543737
LOC729260	2.542445
LOC389765	2.53491
CYP26A1	2.533059
HIATL2	2.523781
LOC645166	2.521895
LOC100131165	2.511801
TDRD1	2.50142
MYO3B	2.490503
PCDHB9	2.489118
ZNF483	2.48766
ZNF14	2.486754
CDKN2AIPNL	2.472957
LOC132241	2.471113
LOC730313	2.468427
LRRFIP1	2.463968
CYP26A1	2.458009

LOC645452	2.452785
RASSF6	2.45028
NLRP8	2.434631
ZNF549	2.433697
LOC727962	2.432772
LOC401098	2.42887
TNFSF15	2.428864
LOC653458	2.426869
KCNK12	2.42088
LOC100129211	2.417542
SNORD30	2.416911
LOC100132391	2.412619
HCG2P7	2.412254
HNRNPU	2.406359
SHROOM4	2.404698
SNORD14A	2.404045
ACVR2B	2.401555
SNORD52	2.398984
MIAT	2.39748
LOC100133923	2.388923
LMOD3	2.387428
LOC642062	2.387012
KCNJ14	2.385386
HSPC268	2.378881
FLJ36131	2.369709
FCAR	2.368066
SMCR5	2.355167
FAM46B	2.348779
LOC728127	2.345393
LOC100129269	2.344526
MGC16121	2.325567
FAM73A	2.32488
CATSPER2	2.3198
LOC90586	2.3067
ZNF394	2.29879
QRFPR	2.297653
C19orf39	2.29712
DUSP19	2.296163
RHBDL2	2.294298
LOC255167	2.287372
LOC400986	2.280851

C13orf15	2.275922
LEP	2.269837
EED	2.266666
LOC441087	2.263056
COL9A1	2.258154
LOC100129502	2.255601
LOC388279	2.243632
LOC645452	2.243296
DEM1	2.242164
LOC100131718	2.241721
GRIPAP1	2.238225
LOC441124	2.225345
PRO1853	2.21655
DUXAP3	2.215603
CCBE1	2.212555
BIRC3	2.209313
YRDC	2.208207
LOC728903	2.204916
SRGAP1	2.203693
C20orf72	2.201947
BACE2	2.19764
FAM175A	2.196328
C14orf85	2.195067
FAM119A	2.193598
DDX12	2.190368
SLC35E1	2.19009
CCDC125	2.188864
COL7A1	2.187424
LOC100128084	2.177133
BMS1P5	2.176427
C14orf153	2.174032
TMEM106A	2.17209
ZNF681	2.171756
FLJ39653	2.171357
L1TD1	2.169413
SEMA3E	2.169169
HSD17B7	2.165938
CYCSL1	2.162225
C4orf29	2.161268
LOC644632	2.15687
LRRC37B2	2.152531

DDX51	2.152474
CEP152	2.152444
SNORD31	2.151333
TEK	2.150794
DENR	2.150654
LOC100128460	2.150488
LOC100190938	2.150086
KISS1R	2.140794
PABPC1L	2.139369
PHAX	2.136152
MBD4	2.132927
SNORA41	2.132597
MBTD1	2.130245
EID2B	2.129863
TRIM13	2.128735
IL17RD	2.125292
FLJ40722	2.115813
DMC1	2.115658
GALC	2.113465
LOC100190986	2.110532
NR2F1	2.107329
IPW	2.106074
SCARNA9	2.105387
MAGT1	2.1053
LOC100128288	2.103777
KCNH6	2.100259
LOC653105	2.096429
HNRNPA2B1	2.092088
MKRN3	2.090918
LOC100131541	2.090564
ARL16	2.0897
LOC649853	2.084618
ZNF248	2.068261
CXorf24	2.068032
BLZF1	2.0674
XIST	2.065747
SEMA3A	2.059877
FAM63A	2.059745
RNY3	2.057644
KLHL28	2.05402
LIN28	2.053981

LOC648059	2.051742
SULT1A1	2.051316
POFUT1	2.050032
LOC100129362	2.046165
ELMOD1	2.045597
LRCH4	2.044485
PDE7A	2.035621
LOC644860	2.033703
TMEM137	2.029217
STAG3L3	2.024292
HSD17B7P2	2.024281
LOC730993	2.020463
C21orf24	2.018812
UTP23	2.017382
SLC5A8	2.017227
PNPT1	2.014331
LOC196752	2.00857
COG5	2.004133
LOC730060	2.003629
PEG3	-957.219
HOXB8	-136.065
ZNF558	-135.324
TRIM16L	-95.6429
PCDHB5	-86.9776
MIMT1	-44.5107
DLX5	-43.9916
ACBD5	-42.6991
GATA2	-40.4691
NTRK3	-36.0701
MARVELD3	-29.0244
HOXB7	-28.8585
RPE65	-27.3078
GREM1	-26.2191
AKAP14	-22.1752
MMP9	-18.9905
NTS	-18.1385
ADAMTS4	-17.8904
SERPINI1	-16.2791
PLEKHA2	-14.6821
OGN	-9.40158
DLX1	-9.39767

LOC100133565	-8.81125
MASP1	-7.74608
PLA2G4E	-6.87693
DLX1	-6.85457
CA12	-6.52777
MASP1	-6.25095
BCL11B	-6.06753
MPPED2	-6.06387
COX16	-5.83927
EPPK1	-5.58226
LOC441763	-5.55416
BRD9	-5.41967
GABBR2	-5.28742
LOC644743	-5.24939
LOC100008589	-5.21464
DMRT2	-5.06259
COL22A1	-5.0517
PRKCB	-4.99754
ATP1A2	-4.98369
C1orf210	-4.97104
TH	-4.96264
SNHG10	-4.84921
TCEAL2	-4.84141
CLTB	-4.80627
TH	-4.74807
ATP9A	-4.72633
GSN	-4.69314
BHLHB2	-4.67347
C1QTNF5	-4.61257
FLJ40504	-4.5698
HOXD3	-4.53038
CXCL12	-4.36147
SPON1	-4.30736
PGM5	-4.21485
C1orf61	-4.21154
SCG2	-4.13319
LBX1	-4.11661
CYP26B1	-4.09677
HRK	-4.08322
EGFL6	-4.08215
PHOX2B	-4.0814

LGALS3	-4.08081
ITGA3	-3.97785
SPARCL1	-3.90375
PRKCB1	-3.88913
TTC9B	-3.84503
RNF144B	-3.82519
MASP1	-3.82033
CD44	-3.79621
LOC729629	-3.77848
CD44	-3.72282
GABRA5	-3.71172
NGEF	-3.70811
RASGRP1	-3.70143
FAM134B	-3.70013
HOXB3	-3.64551
LY6H	-3.64513
SLITRK3	-3.62788
LY6H	-3.58599
SPARCL1	-3.5567
LOC646723	-3.55156
NT5E	-3.51948
PDE7B	-3.51632
MGAT4C	-3.51012
NMNAT2	-3.48673
PHOX2B	-3.46964
LOC100132761	-3.45755
THRA	-3.44892
FAM134B	-3.43337
NEUROG2	-3.41512
FABP7	-3.40734
TFAP2C	-3.40502
HOXA5	-3.3463
NXPH1	-3.33621
MASP1	-3.29538
ARRDC4	-3.28649
NTM	-3.21974
ST8SIA5	-3.21932
GREM1	-3.20936
SYP	-3.20574
KILLIN	-3.18104
CXCL14	-3.16875

TGFB2	-3.16579
HMP19	-3.12837
SCN2A	-3.10007
LOC100129445	-3.07353
SLC24A3	-3.07342
LOC100130123	-3.06195
LOC641522	-3.04429
LOC285943	-3.01872
BNC2	-3.00183
TMEM68	-2.97944
EPR1	-2.96991
EGFL6	-2.93536
CALCRL	-2.93227
DNM3	-2.90587
KCNIP1	-2.90447
IAH1	-2.90065
DPF3	-2.89961
KCNMA1	-2.89309
TP53BP2	-2.89027
CABP7	-2.88196
FAM20C	-2.87453
TNC	-2.87369
LOC100129543	-2.87301
RGPD1	-2.85536
CA12	-2.85365
GABRA5	-2.85061
TMEM200A	-2.84068
PLD5	-2.83402
TRAF1	-2.82405
KLHL4	-2.82143
PPID	-2.79461
TMEM166	-2.77121
SMOC2	-2.76852
ISL1	-2.76279
LRRC4B	-2.74478
RHOJ	-2.72738
MOXD1	-2.71196
PCSK1N	-2.71061
SEZ6	-2.68646
GSDM1	-2.67724
LGALS3BP	-2.67448

LOC650909	-2.67098
LRRC3B	-2.66079
NFIA	-2.66037
NFIX	-2.65884
NPPC	-2.642
NHLH2	-2.64038
LOC731007	-2.63065
LOC100134073	-2.62659
FZD6	-2.62135
LYPD1	-2.60552
DPP10	-2.6001
LEMD1	-2.59974
LOC100008589	-2.58559
NTM	-2.55777
CSDC2	-2.55435
LOC100132394	-2.55355
SKIL	-2.55346
BDNF	-2.55007
MIR1974	-2.54127
HTRA1	-2.5314
CCRL1	-2.5234
FBLN5	-2.52071
GHR	-2.5109
LOC100008588	-2.50985
NOD1	-2.50482
MGAT4C	-2.49385
NDP	-2.49381
ZCCHC12	-2.48945
ASTN1	-2.47442
C20orf103	-2.47181
HS3ST1	-2.47087
DNASE2	-2.4651
PPID	-2.4621
BMP4	-2.45754
SOX9	-2.45532
LSM14B	-2.44112
LOC100132402	-2.43833
UNC5B	-2.43567
IFITM1	-2.43464
LTBP3	-2.43392
SCML1	-2.43033

DACT1	-2.4249
BCL11A	-2.42487
ARRDC4	-2.40979
PCTK1	-2.39894
BCL11A	-2.39391
CBLN1	-2.39197
ZNF503	-2.37719
LOC254559	-2.3744
RGS6	-2.36886
LAMA4	-2.3616
TAF8	-2.35718
PTGER4	-2.35673
SH2D3C	-2.35152
OLFML2A	-2.34555
KLHL4	-2.34541
LOC387763	-2.34369
FAS	-2.34014
OLFM1	-2.33943
ZFP64	-2.33701
KLF9	-2.31401
TUBB4	-2.30978
ENO2	-2.30456
LOC100133667	-2.3036
GFRA2	-2.29759
PPARGC1A	-2.2928
FAM107A	-2.29256
NAV2	-2.28968
AFMID	-2.28835
LOC643389	-2.28175
HSPA12B	-2.28107
MAPT	-2.27652
ID1	-2.26931
FAM110B	-2.26396
PRIM2	-2.26062
GPC3	-2.26051
DKK3	-2.26026
INHBB	-2.25682
DKK3	-2.2565
LOC729623	-2.2535
SLC4A4	-2.25306
PRODH	-2.25271

FAIM2	-2.2508
CDC14B	-2.25036
MT3	-2.24983
RSPO3	-2.24654
FLJ23152	-2.24398
L1CAM	-2.24221
NCAM2	-2.23966
TIMP2	-2.23825
FLJ30375	-2.23312
EEF1A2	-2.22859
OGDHL	-2.22619
SVOP	-2.2234
VSTM2L	-2.22132
C21orf56	-2.20562
RTN1	-2.20326
FBLN5	-2.19795
LRAT	-2.19552
LRRN2	-2.19369
DEFB106B	-2.19241
ALPK2	-2.19211
AK3L1	-2.19142
S100A10	-2.19
KRT18	-2.1856
TNC	-2.18074
SEZ6L2	-2.17949
SOST	-2.17429
LRFN5	-2.17149
RETSAT	-2.16959
DBC1	-2.16389
TSPO	-2.16228
C1orf88	-2.16098
RTN1	-2.15432
PTCHD2	-2.1507
FSTL5	-2.14986
MAST1	-2.14812
NTRK2	-2.1421
GPR56	-2.13697
NMNAT2	-2.13526
PTPRO	-2.1342
PACRG	-2.13161
AP2B1	-2.12902

PTGFRN	-2.127
ZADH2	-2.12422
C6orf48	-2.12382
PKN1	-2.12313
PTRF	-2.12154
APEG1	-2.11775
MAB21L2	-2.11653
IL18BP	-2.11265
PCSK6	-2.10393
LOC285943	-2.09865
C22orf40	-2.09825
TMEM42	-2.09574
MEOX1	-2.0951
GPR124	-2.09508
FAR2	-2.09299
RARB	-2.08149
VCAM1	-2.08001
SEPP1	-2.07387
RERG	-2.07098
ZDHHC22	-2.06905
DACT1	-2.06809
S100A10	-2.06121
CYBA	-2.05224
PENK	-2.04225
SNORD38A	-2.03555
MOXD1	-2.03548
NPY	-2.03394
NTRK2	-2.03049
IL11RA	-2.02958
IFIT1	-2.02371
WNT3A	-2.02266
ANKS1B	-2.02172
RHOJ	-2.02088
RAB6B	-2.0191
LYZ	-2.01733
VEGFB	-2.01456
CHRNA3	-2.01233
FBLN1	-2.00919
SCG5	-2.00453

Appendix 2: List of DEGs in astrocytes

Symbol	Absolute fold change (WT vs MT)
TMEM132D	311.242
IRX2	162.4896
LOC647322	99.07013
SYNPR	68.20955
C18orf51	33.4977
LOC644128	33.40583
MAL	32.57475
LOC400879	32.08357
C1orf61	31.94461
MSC	29.75386
LOC642477	29.63125
RPL23AP53	29.13584
LGALS8	27.37703
LOC654433	25.86594
TOX3	25.22947
ME3	25.16961
LOC100131139	20.5496
COL3A1	20.22473
C18orf51	19.02918
LOC387647	17.84308
S100A6	16.70805
SERPINA3	16.5265
GPR19	14.93009
PNOC	14.65767
B3GALNT1	13.55535
UBD	13.16675
FBXO17	13.04681
IFIH1	12.20252
SNAP91	10.76434
ARMCX1	10.58287
PGM5	10.49443
GCNT2	9.82992
HERC5	9.815037
ARMCX1	9.735718
LGALS8	9.486291
MAOB	9.347251

PGM5	9.094896
IGFBP7	9.087318
AQP4	9.015766
COL8A1	8.798182
LAMA2	8.430301
MOCOS	8.253597
PGM5	8.197868
AFAP1L2	7.831661
VCAM1	7.312584
VCAM1	7.238391
COL8A1	7.004925
AQP4	6.86842
IL13RA2	6.85
HEY1	6.812132
LAMA2	6.59602
MAL	6.499601
IRAK1	6.366007
FBXO17	6.229609
VAT1L	6.027394
ZNF519	5.717021
FZD6	5.689452
DPPA4	5.625546
TSHR	5.594229
CHRNA9	5.448719
CTSC	5.336096
CTSO	5.303316
RUNX1T1	5.211953
EFEMP2	5.207798
KREMEN2	5.086092
HAND2	5.04306
NMRAL1	4.957916
MOXD1	4.892002
PLCXD3	4.777097
NEFM	4.723506
APCDD1L	4.62497
HEPACAM	4.622224
MIR886	4.554885
LOC730024	4.511426
PHF11	4.433146
NRP1	4.283435
MOXD1	4.172741

LOC100129681	4.141345
ARSD	4.112756
DYNLT3	4.093515
CNR1	4.067045
CTSC	4.014461
TMEM132B	3.995428
NPTX2	3.946412
SLC16A3	3.944453
IL32	3.941504
GPR19	3.849523
MX1	3.746757
NFE2L3	3.743264
LOC440160	3.735513
PSMB9	3.720757
LOC653458	3.703381
GAS8	3.678264
NIPAL4	3.676189
JPH4	3.628537
LOC644632	3.604688
NEFL	3.592026
C1orf85	3.560798
PRTFDC1	3.542991
MAP1LC3A	3.504093
XIST	3.495602
CPNE4	3.477242
LOC442597	3.457218
MYLC2PL	3.450306
BST2	3.412099
CXorf57	3.40641
WNT2B	3.403603
CABP7	3.388955
TMSB15A	3.382271
MYOZ3	3.301633
CPZ	3.291342
CTSC	3.235843
GABBR2	3.188288
CDH11	3.165911
LOC644322	3.156961
KCNQ2	3.150564
CBS	3.13147
TRIM9	3.114787

CXCR7	3.104968
CSPG4	3.084212
HEY1	3.083431
PEG10	3.043618
HLA-A29.1	3.038624
OCIAD2	3.025113
LOC645362	2.997446
FABP7	2.987616
C1QL4	2.9767
APOBEC3G	2.975094
NOV	2.965895
GBX2	2.959206
CYP27A1	2.958008
ADM2	2.944753
PODXL	2.938259
RASL11B	2.916364
LOC255130	2.909535
CDH4	2.897546
IL32	2.89163
EFHC2	2.854384
PARP10	2.830062
MKX	2.825374
MAMDC2	2.824748
LOC387856	2.816387
IHPK3	2.811707
PODXL	2.799325
TCEAL2	2.798232
C11orf70	2.796496
STON1	2.790808
C3orf70	2.729802
SOX13	2.728033
SLCO2A1	2.712802
GJB2	2.683755
CXCR7	2.677081
LOC728034	2.674946
CECR7	2.669404
C20orf103	2.661955
PPP2R2B	2.650025
SERPINE2	2.632125
LOC644689	2.632078
GHDC	2.607459

REC8	2.599418
TMEFF2	2.594419
SORCS3	2.5943
TRIM9	2.588832
HIST1H2BH	2.570052
C3orf70	2.563467
BCL11A	2.563101
LOC100133005	2.551272
NTRK2	2.550379
INSM1	2.547705
SNAP25	2.546993
MGC16121	2.533304
LY6E	2.528217
LOC283547	2.516444
GNG2	2.515802
LOC387763	2.514657
PLP2	2.510287
ITGA4	2.507666
GCA	2.499318
GDF10	2.48598
FGF12	2.483877
PCOLCE	2.473357
RAMP1	2.472275
KCNJ4	2.463367
KIAA1524	2.461269
LOC728715	2.460874
DKK1	2.450936
CD34	2.4504
FBLN7	2.44282
LOC285016	2.441327
HLA-G	2.438368
EIF4EBP1	2.434775
C11orf70	2.433851
KCNJ13	2.427966
GSTK1	2.426614
SEL1L2	2.422664
Sep-05	2.417292
APH1B	2.41582
CPE	2.414869
LMO2	2.410156
COL11A1	2.408092

MCM10	2.405896
CRISPLD1	2.404773
PANX2	2.40043
VGLL3	2.40016
C19orf4	2.395937
PPP2R2B	2.388751
LOC650909	2.379838
DOCK10	2.378101
RNF217	2.358763
C9orf140	2.351435
GATM	2.344808
TPK1	2.339788
EMP1	2.335271
FAM150B	2.32087
COL11A1	2.319156
SAMD9	2.317748
PEG10	2.312586
NTRK2	2.305579
CHST15	2.297019
RGS20	2.293021
C8orf4	2.292099
NRP1	2.287889
PTPRZ1	2.286917
MIAT	2.286443
GAP43	2.284361
SP110	2.281901
CDCA7	2.281861
CLIP1	2.275351
DBNDD1	2.272403
NR3C2	2.263839
LOC653184	2.263028
C3orf36	2.262231
RPL39L	2.261417
SLC15A4	2.257205
ULBP1	2.255653
GRIK2	2.255614
SLC15A3	2.255071
SLC15A4	2.25496
CD34	2.254448
ETNK2	2.242156
LOC401317	2.240891

CXCR4	2.240187
RHBDF2	2.239867
ENO3	2.237693
TTYH1	2.237571
MATN2	2.230369
ADCY1	2.228108
C20orf72	2.223217
LOC729366	2.221735
UGT2B7	2.22
DUSP10	2.21969
FBXW4	2.215394
MKRN3	2.20472
ASNS	2.203774
GAL3ST4	2.202665
RAD51C	2.197314
BLM	2.197167
C2orf27A	2.191093
HDAC9	2.188172
RRM2	2.187558
LMNB1	2.186055
CRYAB	2.18499
SOX8	2.183122
ID4	2.176283
LOC647859	2.172748
SLC10A4	2.166806
NES	2.161212
LEF1	2.15434
JAG1	2.150142
BTN3A2	2.149623
STOX1	2.149244
CORO1A	2.147789
SLAIN1	2.147776
TRIM61	2.141057
RNF144A	2.135656
ELAVL3	2.133909
CENPA	2.125065
RNF144	2.121431
C13orf15	2.115532
GPM6A	2.106387
TTYH1	2.100128
KIF18A	2.093161

GRAMD3	2.087271
C1QL1	2.086668
HLA-A	2.085314
RARRES2	2.074639
MGC39900	2.073624
CREB5	2.07012
STOX1	2.063767
C7orf57	2.062354
TMEM54	2.058528
PTX3	2.054652
INHBE	2.054277
LOC91431	2.052005
PLAT	2.051799
SFRP4	2.046924
ADM	2.045152
PMP22	2.044816
HSP90AA1	2.040808
LEF1	2.040014
UBE4B	2.030624
SP110	2.028277
NFKBIE	2.027337
VASH2	2.026547
MGC39900	2.026091
LGI2	2.025113
TFPI	2.02474
PRPH	2.021878
C5	2.021109
KIF4A	2.020763
ABAT	2.02009
CRISPLD1	2.01848
SNTB1	2.017871
COL1A1	2.015989
CDT1	2.015051
KIFC1	2.008473
LOC100129268	2.005908
TRIB3	2.005661
MMP23B	2.003752
C5orf23	-226.75
PCDHB5	-143.579
EFEMP1	-78.5408
CSRP1	-68.9403

CDH13	-65.819
EFEMP1	-58.0384
COL10A1	-45.0631
LOC644348	-45.0442
SFRP2	-37.7507
PEG3	-33.9225
HP	-31.4574
GRIK1	-29.8528
PLAC9	-29.7104
CDH3	-25.8302
LRRTM1	-24.3527
LOC652097	-23.5402
CDH1	-22.8521
TM4SF18	-22.4371
ANXA2P3	-21.1283
EFEMP1	-20.7778
TSPAN2	-20.4162
IGFL3	-17.1503
C4orf26	-17.0078
LOC390427	-16.7854
CHI3L1	-16.4046
NPR3	-15.8904
NPAS2	-14.9452
ANKRD30A	-14.9242
FNDC1	-14.8173
FNDC1	-14.4528
TSPAN2	-13.0061
ANXA2	-12.9995
RGPD1	-12.1798
ANXA2	-11.9547
CNTNAP3B	-9.72038
GRIK1	-9.70556
ANXA2P1	-9.65583
ANXA2P1	-8.83264
COMP	-8.12132
SERPINB1	-8.03093
LOC440934	-8.02092
LOC645553	-7.79967
DBC1	-7.67148
ACTA1	-7.64358
LOC648987	-7.47447

MYL9	-7.46148
PLA2G3	-7.24993
MYL9	-6.59117
CXCL12	-6.55194
ANXA2	-6.14024
TGM2	-6.0721
OGDHL	-6.02345
TGM2	-5.92941
TMEM200A	-5.90445
CHRD1	-5.70665
EPHA3	-5.70449
KCNMB1	-5.66889
THBS4	-5.59679
SCN1B	-5.21673
CTNNA2	-5.21372
SLC47A1	-5.20874
TM4SF1	-5.14658
MYCN	-5.10796
FLI1	-4.96757
HAVCR2	-4.94917
RPRML	-4.92563
MYCN	-4.89598
C13orf27	-4.79195
SCML1	-4.77355
PPARGC1A	-4.7715
SIRPA	-4.76956
PCDH19	-4.60571
CLCNKA	-4.56727
EDN2	-4.55615
CXCL14	-4.53377
STK32B	-4.515
MGC27348	-4.47812
RPESP	-4.31248
GPR64	-4.15611
PCDHA12	-4.1442
OLFM1	-4.1184
GPR64	-4.09324
PCP4	-4.08283
SHE	-4.00563
PTP4A3	-3.97431
FLRT3	-3.93458

PERP	-3.91939
LOC646332	-3.90432
MFAP2	-3.89261
HS3ST1	-3.82689
LOC644760	-3.73484
LTC4S	-3.69005
CHRD1	-3.663
SNORA68	-3.60547
EVI2A	-3.59781
ADRA1B	-3.5961
C6orf15	-3.49903
TWIST1	-3.49264
LOC100129195	-3.42885
ICAM3	-3.39031
MYH11	-3.36978
LPL	-3.35628
LTBP2	-3.34546
KANK1	-3.34143
ADAMTSL2	-3.32895
SERPINF1	-3.32313
STAMBPL1	-3.32299
PAPPA	-3.31966
MAB21L2	-3.2936
PTP4A3	-3.28678
LOC647718	-3.24874
CTSH	-3.24116
JUP	-3.22749
PKP2	-3.18973
PSMD5	-3.1888
HSPB7	-3.16834
SGPP2	-3.14678
CTSH	-3.1241
MBNL3	-3.1066
TPM2	-3.09279
LOC100192378	-3.08381
C1orf133	-3.04134
PCDHA3	-3.03678
ITGA11	-3.03556
FAM127C	-3.03474
TIMP3	-3.02265
NWD1	-3.00408

LGALS3	-2.99381
TNNT2	-2.96267
CLSTN2	-2.95399
SERTAD4	-2.9423
GLT8D2	-2.93777
MARCH4	-2.90673
MARCH1	-2.89983
F3	-2.86645
LY96	-2.85996
INHBB	-2.83017
FLJ41603	-2.78224
C1orf9	-2.77872
ELMOD1	-2.76852
HSD17B6	-2.76747
ABCA4	-2.76362
PCDHA1	-2.76249
HS6ST2	-2.73989
CEND1	-2.72948
F3	-2.70851
OLFM1	-2.69777
PTP4A3	-2.69671
BMP2	-2.68385
TMEM173	-2.65385
LOC650494	-2.64039
LOC647886	-2.63367
C3orf64	-2.61853
PPP2R3B	-2.60727
AHR	-2.60511
JMJD8	-2.59427
SIK1	-2.59413
KLHL4	-2.58969
LOC440498	-2.57292
ITGA11	-2.56297
HS6ST2	-2.56269
NKX2-5	-2.55405
TPM2	-2.5239
ARL4D	-2.50738
LMOD1	-2.50705
NELL2	-2.50306
SCGB3A1	-2.4967
INPP4B	-2.47646

KLF5	-2.4662
PHACTR2	-2.46441
LOC646345	-2.46432
SMAGP	-2.4579
CYGB	-2.45684
LOC100132475	-2.4543
JMJD8	-2.44064
C3orf72	-2.41953
NMU	-2.41474
DPP7	-2.40291
RUNX1	-2.40283
CDCP1	-2.40033
FAM43A	-2.38377
LOC100134265	-2.38278
OTUD7B	-2.38114
CHRNA1	-2.37972
TMTC2	-2.37838
RIMBP3B	-2.37671
RIN2	-2.30829
LAMA4	-2.30436
PXDN	-2.29689
MFAP5	-2.2963
GAS6	-2.27835
EPB49	-2.27728
FZD1	-2.27422
ZNF580	-2.274
LPHN3	-2.27161
NR2E1	-2.26473
NR2E1	-2.26062
SLC46A3	-2.26044
TFPT	-2.24612
NBL1	-2.24149
ACSL1	-2.24095
DKFZp434K191	-2.24072
IFITM1	-2.23856
LOC401093	-2.2088
MFAP2	-2.20647
SLC22A4	-2.20612
SPOCK1	-2.18659
HPS1	-2.18248
KLHL4	-2.18241

CALB2	-2.16704
GLS	-2.16601
CCND1	-2.16368
MFSD6	-2.16334
PLXDC2	-2.15494
ALDH1B1	-2.15427
ABCD1	-2.14432
MBP	-2.13607
RCAN2	-2.12762
ZXDC	-2.1266
SLC25A6	-2.12372
HSPB3	-2.12233
GPNMB	-2.11814
ABHD7	-2.11736
MAF	-2.11098
GFAP	-2.09954
STXBP6	-2.0931
TAF7	-2.08253
GAS6	-2.08019
NBL1	-2.07628
C9orf41	-2.07524
LOC653354	-2.07211
TPM2	-2.06185
ACAT2	-2.06158
ABLIM1	-2.05987
TSPYL3	-2.05958
LYN	-2.05636
LOC100134134	-2.05054
ATP13A2	-2.05016
RECK	-2.04812
NNMT	-2.04745
FAM80A	-2.04359
SEMA3C	-2.03723
PDXK	-2.03681
GAS6	-2.0285
APCDD1	-2.02775
PAPLN	-2.02769
PCDH7	-2.02531
PORCN	-2.01888
C14orf169	-2.01721
CENPV	-2.01541

MID1IP1	-2.01522
GPNMB	-2.0108
RTN2	-2.00963
C1orf53	-2.00697
ESPN	-2.0007

Appendix 3 : List of DEGs in Microglia

Symbol	Absolute fold change (WT vs MT)
RPL23AP53	9.220812
CH25H	8.06556
EGR3	7.473522
SLC15A4	5.695623
SLC15A4	5.581945
VAT1L	5.32119
PNCK	3.660303
LOC644128	3.65873
TSPAN7	3.299751
KCNQ3	3.214652
ACVRL1	3.20172
LOC645313	3.159544
TSPAN7	3.150803
IFI27	2.975922
CCDC46	2.964623
ETV5	2.889563
CXCR7	2.815706
ATP8B3	2.799402
FLJ41603	2.796368
PCDH12	2.756953
FGF13	2.751034
TDO2	2.711936
KBTBD11	2.609129
ETV5	2.597316
TNF	2.578798
PPP1R3C	2.567748
CCL2	2.555638
DHCR24	2.537556
CCNE2	2.527951
ACAT2	2.522731
LOC400120	2.517643
LOC440160	2.51232
SQLE	2.483067
DHCR7	2.466732
SQLE	2.465854
EGFL6	2.46241

DKK3	2.432633
AK3L1	2.431236
LOC645166	2.398337
ALDOC	2.38749
MMP12	2.36977
TDO2	2.358436
DKK3	2.337556
ASAP2	2.266928
CCND1	2.259888
MMP12	2.233945
GP9	2.226241
MOSC1	2.21986
APOO	2.213879
ASAP2	2.213328
DENND1A	2.199217
ISG15	2.166457
IFI44L	2.130709
PFKP	2.120615
LOC727963	2.11897
EGR2	2.117864
TMEM45A	2.110484
FANCE	2.103659
MGC87042	2.098701
CXCR7	2.092832
PMAIP1	2.078637
DHCR7	2.066229
LOC389342	2.060702
SIK1	2.047207
SNRPN	2.045398
TMEM2	2.044194
LYVE1	2.03253
CABYR	2.029841
BIN1	2.021359
FLJ30428	2.012406
HK2	2.011509
LOC730024	2.00854
PLOD2	2.008316
IL21R	2.007582
CRABP1	-7.77266
CTSF	-5.29279
TBX15	-4.24624

MGC72104	-3.95318
DEFA1B	-3.9506
NCALD	-3.83163
ZIC2	-3.80157
CES1	-3.75211
DEFA1B	-3.74964
DEFA4	-3.74028
DEFA1	-3.59228
DEFA3	-3.53017
LOC731682	-3.46363
LOC100133893	-3.41066
TNRC6B	-3.4096
SCML1	-3.39624
HLA-DQA1	-3.35762
HLA-DPB1	-3.28965
FAM50B	-3.28539
CAMP	-3.25032
SYT11	-3.16403
NMU	-3.09156
LOC100133583	-2.97916
LOC642073	-2.9769
LOC100133678	-2.95761
C9orf64	-2.94788
DEFA1B	-2.93548
MAPK10	-2.68779
HLA-DRA	-2.68651
CSRP1	-2.67771
OR8U9	-2.66573
LOC649143	-2.59964
HLA-DRB6	-2.59662
NEFM	-2.55799
CD74	-2.55642
CKB	-2.52816
HLA-DPA1	-2.51856
FCER1A	-2.45673
SLC7A8	-2.43903
ACRBP	-2.42078
MPO	-2.37437
FLJ39639	-2.36818
LOC730415	-2.36381
LYZ	-2.35367

S100A12	-2.34391
SLAMF7	-2.33123
PRTN3	-2.32552
C19orf59	-2.31529
PGLYRP1	-2.2978
GIGYF1	-2.29713
FCN1	-2.28672
CTSK	-2.28609
ABCC3	-2.28005
KCNQ2	-2.27969
TIFAB	2.262441
ORM1	2.235252
HLA-DRB4	-2.22565
SNORD13	-2.22318
CLEC4D	-2.21181
CTXN1	-2.2049
TYW3	-2.19396
NR1H3	-2.19244
PADI2	-2.18152
C5orf20	-2.17209
HP	-2.16947
PDK4	-2.16551
RN7SK	-2.16351
KIAA1324L	-2.15971
LOC728181	-2.15561
CYP26B1	-2.135
C10orf27	-2.1178
CD74	-2.11551
CD74	-2.10513
HLA-DRA	-2.08906
TAF7	-2.07148
TUBB2B	-2.03588
ZNF681	-2.0356
PPP2R3A	-2.033252
BIRC3	-2.03065
LOC642236	-2.014
ACP5	-2.00521
THBS1	-2.00349

Appendix 4: Similar DEGs between cell types

Microglia/ NPCs	Microglia	NPCs
AK3L1	2.431236	-2.19142
BIRC3	-2.030648	2.209313
CYP26B1	-2.134999	4.096772
DKK3	2.432633	2.260261
EGFL6	2.46241	-4.08214
FLJ30428	2.012406	83.58686
LOC644128	3.65873	5.046595
LOC645166	2.398337	2.521895
LOC730024	2.00854	6.500651
LYZ	-2.353674	-2.01732
RPL23AP53	9.220812	5.13234
SCML1	-3.396236	-2.43032
ZNF681	-2.035604	2.171756

Microglia/ Astrocyte	Microglia	Astrocytes
ACAT2	2.5227	-2.0615
CCND1	2.2598	-2.1637
CSRP1	-2.6777	-68.9403
CXCR7	2.8157	3.1050
FLJ41603	2.7963	-2.7822
HP	-2.169	-31.4574
KCNQ2	-2.2796	3.1506
LOC440160	2.5123	3.7355
LOC644128	3.6587	33.4058
LOC730024	2.0085	4.5114
NEFM	-2.5579	4.7235
NMU	-3.0915	-2.4147
RPL23AP53	9.2208	29.1358
SCML1	-3.3962	-4.7735
SIK1	2.0472	-2.5941
SLC15A4	5.6956	2.2572
TAF7	-2.0714	-2.0825
VAT1L	5.3211	6.0274

NPCs/ Astrocytes	NPCs	Astrocytes
ADM	2.838582	2.0452
BCL11A	-2.4249	2.5631
C13orf15	2.2759	2.1155
C1orf61	-4.2115	31.9446
C20orf103	-2.4718	2.6620
C20orf72	2.2019	2.2232
CABP7	-2.8820	3.3890
CXCL12	-4.3615	-6.5519
DBC1	-2.1639	-7.6715
DPPA4	3.9325	5.6255
ELMOD1	2.0456	-2.7685
FABP7	-3.4073	2.9876
FZD6	-2.6213	5.6895
GABBR2	-5.2874	3.1883
HS3ST1	-2.4709	-3.8269
IFITM1	-2.4346	-2.2386
INHBB	-2.2568	-2.8302
IRX2	165.8720	162.4895
KLHL4	2.0540	-2.5897
LAMA4	-2.0540	-2.3044
LGALS3	-4.0808	-2.9938
LOC100131139	139.1847	20.5496
LOC295943		
LOC285943	-3.0187	
LOC387763	-2.3437	2.5147
LOC644128	5.0466	33.4058
LOC644632	2.1569	3.6047
LOC647322	2.1569	99.0702
LOC650909	-2.1569	-2.6404
LOC653458	2.4269	3.7034
LOC654433	49.0226	25.8659
MAB21L2	-2.1165	-3.2936
MGC16121	2.3256	2.5333
MIAT	2.3975	2.2864
MKRN3	2.0909	2.2047
MOXD1	-2.0355	4.1727
NTRK2	-2.0305	2.5504
OGDHL	-2.2262	-6.0235
OLFM1	-2.3394	-4.1184

PCDHB5	-86.9776	-143.5786
PEG3	-957.219	-33.9225
PGM5	-4.2148	9.0949
PPARGC1A	-2.2928	-4.7715
PTX3	2.6689	2.0547
RGPD1	-2.8554	-12.1798
SPOCK1	6.3553	-2.1866
TCEAL2	-4.8414	2.7982
TMEM132D	118.4605	311.2420
TMEM200A	-2.8407	-5.9045
VCAM1	-2.0800	7.3126
VGLL3	5.5148	2.4002
XIST	2.0657	3.4956